

The Catalytic Control of Flavocytochrome P450 BM3

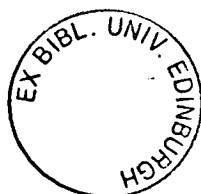
Tobias W. B. Ost



Thesis presented for the degree of Doctor of Philosophy

University of Edinburgh

2002



To my Mum, thank you

Declaration

I declare that this thesis was composed by myself and that I carried out the work presented here, except where indicated in the text. It has not been submitted in part, or in whole, for any other degree. Some of the results have already been published.

Tobias W. B. Ost

October 2001

Acknowledgements

I would like to thank, in particular, Professors Chapman and Reid for the opportunity to conduct my research within their laboratories and for their input and support. I thank Dr. A.W. Munro for introducing me to the field P450 biochemistry and I am indebted to Dr. C. S. Miles (mutagenesis), Dr. C. G. Mowat (crystallography) and Dr. S. N. Daff (criticism and discussion) for their invaluable assistance. I am also grateful to Dr. A. J. Fulco and Dr. M. R. Cheesman for their help with product characterisation and EPR spectroscopy. Lastly, but by no means leastly, thanks is long overdue to all members of the Chapman/Reid empire who have made the tenure of my PhD a happy and enjoyable one – your patience and tolerance is greatly appreciated (well, at least to the same extent as my ‘jokes’ are!), thank you.

Abstract

Substitutions of the phylogenetically conserved phenylalanine residue F393 were constructed in flavocytochrome P450 BM3 from *Bacillus megaterium*. The high degree of conservation of this residue in the P450 superfamily and its proximity to the heme (and its ligand Cys400) implies an essential role in P450 activity. Extensive kinetic and thermodynamic characterization of mutant enzymes F393A, F393H and F393Y highlighted significant differences from wild-type P450 BM3. All enzymes expressed to high levels and contained their full complement of heme. Whilst the reduction and subsequent treatment of the mutant P450s with carbon monoxide led to the formation of the characteristic P450 spectra in all cases, the absolute position of the Soret absorption varied across the series WT/F393Y (449 nm), F393H (445 nm) and F393A (444 nm). Steady-state turnover rates with both laurate and arachidonate showed the trend WT>F393Y>>F393H>F393A. Conversely, the trend in the pre-steady-state flavin-to-heme electron transfer was the reverse of the steady-state scenario, with rates varying F393A>F393H>>F393Y~wild-type. These data are consistent with the more positive substrate-free (-312 mV (F393A), -332 mV (F393H)) and substrate-bound (-151 mV (F393A), -176 mV (F393H)) reduction potentials of F393A and F393H heme domains, favouring the stabilization of the ferrous-form in the mutant P450s relative to wild-type. Elevation of the heme iron reduction potential in the F393A and F393H mutants facilitates faster electron transfer to the heme. This results in an increase in the stability of the oxy-ferrous intermediate, which retards the rate of second electron transfer to the heme, and slows the rate of turnover of the mutant P450s. We postulate that the nature of the residue at position 393 is important in controlling the delicate equilibrium observed in P450s, whereby a trade-off is established between the rate of heme reduction and the rate at which the ferrous heme can bind and, subsequently, activate molecular oxygen. The structural and spectroscopic characterisation of the mutants reveals the probable role of the phenylalanine residue to be to preserve the hydrophobic environment of the heme. This prevents unfavourable inter- and intra-molecular

interactions with the heme or heme-ligand, which have been demonstrated to perturb this delicate thermodynamic balance. This study highlights the electronic influence the cysteine ligand has in dictating the characteristic reactivity of P450s, and its sensitivity to its chemical environment. Modulating the electron density of the Fe-S bond (introduction of intramolecular hydrogen bonds) has a direct effect on the ability of P450s to bind and activate molecular oxygen. This point is key to the high degree of conservation of this residue throughout the P450 superfamily – monooxygenation requires oxygen activation. This phenylalanine is conserved in every member which needs to perform this activation, for the small number that do not, the nature of this residue varies.

The nitrogenous π -acceptor ligand 4-cyanopyridine (4CNPy) exhibits reversible ligation, exclusively to ferrous-heme ($K_d = 12 \mu\text{M}$ for P450 BM3 and $1.0 \mu\text{M}$ for P450cam) *via* its pyridine-ring nitrogen. The ferrous-4CNPy adduct displays unusual spectral properties which provides a useful spectroscopic handle to probe features of the P450 mechanism. 4CNPy is competitively displaced upon substrate binding, and allows a convenient route to the determination of substrate dissociation constants for ferrous P450 – a previously unquantified property. For P450 BM3, $K_d(\text{red})$ (laurate) = $36 \mu\text{M}$ ($K_d(\text{ox}) = 241 \mu\text{M}$); for P450 cam, $K_d(\text{red})$ (fenchone) = $1.5 \mu\text{M}$ ($K_d(\text{ox}) = 52 \mu\text{M}$). This result confirms the previously unsubstantiated assumption that reduction of substrate-bound P450 decreases the magnitude of the substrate dissociation constant, resulting in an increase in the stability of the Michaelis-complex (by 4.2 kJmol^{-1} for P450 BM3 with laurate and 8.9 kJmol^{-1} for P450cam with fenchone). An unusual spectral feature in the blue region of the ferrous-4CNPy adduct is a metal-to-ligand charge transfer (MLCT) absorption, the energy of which varies linearly with respect to the P450 heme-reduction potential. By studying the energy of this MLCT for a series of P450s with differing reduction potential (E_o), the relationship $E_{\text{MLCT}} = (3.86 \times E_o) + 17122 \text{ cm}^{-1}$ was deduced. This relation holds for both wild-type P450 BM3 and P450cam – the two most intensively characterised P450s, and for the F393X series of mutants of P450 BM3. This molecule provides a quick and accurate spectrophotometric method of predicting the heme-reduction potentials for cytochromes P450, without the requirement for redox potentiometry.

List of abbreviations

Amino acids

Alanine	Ala	A	Leucine	Leu	L
Arginine	Arg	R	Lysine	Lys	K
Asparagine	Asn	N	Methionine	Met	M
Aspartic acid	Asp	D	Phenylalanine	Phe	F
Cysteine	Cys	C	Proline	Pro	P
Glutamic acid	Glu	E	Serine	Ser	S
Glutamine	Gln	Q	Threonine	Thr	T
Glycine	Gly	G	Tryptophan	Trp	W
Histidine	His	H	Tyrosine	Tyr	Y
Isoleucine	Ile	I	Valine	Val	V

Mutations

Amino acid mutations are represented as a code number → code, where the first code and number represents the original residue and its position on the polypeptide chain, and the second code represents the corresponding residue in the mutant enzyme. For example, the mutation of a phenylalanine, residue number 393, to an alanine is represented by Phe393→Ala, thus generating the mutant F393A.

Textual abbreviations

Abs	Absorbance
<i>B. megaterium</i>	<i>Bacillus megaterium</i>
4CNPy	4-cyanopyridine
CYP	Cytochrome P450
Δ_o	Octahedral crystal-field splitting parameter
Da	Daltons
DNA	Deoxyribonucleic acid
DPNH	diphosphopyridinenucleotide
E_o	Reduction potential
<i>E. coli</i>	<i>Escherichia coli</i>
EDTA	Ethylenediaminetetraacetic acid
EPR	Electron paramagnetic resonance (spectroscopy)
FAD	Flavin adenine dinucleotide
FMN	Flavin mononucleotide
ΔG	Free energy change
GC/MS	Gas chromatography/mass spectrometry
HD	Heme domain
Heme	Protoporphyrin IX
KPi	K_2HPO_4/KH_2PO_4 buffer
Mb	Myoglobin
MCD	Magnetic circular dichroism
MLCT	Metal-to-ligand charge transfer
MOPS	3-(morpholino)-propanesulfonic acid
M_r	Molecular mass

NMR	Nuclear magnetic resonance (spectroscopy)
NADH	β -Nicotinamide adenine dinucleotide
NADPH	β -Nicotinamide adenine dinucleotide phosphate
ODRC	<i>o</i> -dianisidine radical cation
NOS	Nitric oxide synthase
P450	Cytochrome P450 monooxygenase
PAGE	Polyacrylamide gel electrophoresis
PMSF	Phenylmethylsulfonylfluoride
<i>P. putida</i>	<i>Pseudomonas putida</i>
SHE	Standard hydrogen electrode
SDS	Sodium dodecylsulfate
TEMED	N,N,N',N'-tetraethylethylene diamine
Tris	Tris(hydroxy)aminomethane
UV	Ultraviolet
Vis	Visible

Kinetic Parameters

K_M	Michaelis constant
K_i	Inhibition constant
K_d	Dissociation constant
k_{cat}	Rate constant at substrate saturation
k_{lim}	Limiting rate constant
k_{obs}	Observed rate constant
k_{off}	Rate constant for oxy-ferrous decay

K_d^{app} Apparent K_d

Standard Units

m metre

g gram

s second

l litre

°C degree Celcius

M molar

V volt

Å Angstrom

CONTENTS

Chapter 1	INTRODUCTION	Page 1
1.1	Cytochromes P450	2
1.1.1	Discovery	2
1.1.2	General Background	3
1.1.3	Classification	4
1.1.4	Structure	5
1.1.5	The Catalytic Cycle	8
1.1.6	Reaction Types and Substrates of Cytochromes P450	19
1.1.7	Flavocytochrome P450 BM3	23
1.2	Biological Electron Transfer	30
1.2.1	Marcus Theory	32
1.2.2	Conclusions	37

Chapter 2	METHODS AND MATERIALS	Page 41
2.1	Site-Directed Mutagenesis	42
2.2	Transformation of <i>E. coli</i>	43
2.3	Growth of <i>E. coli</i>	43
2.4	Purification of Flavocytochrome P450 BM3	44
2.5	SDS PAGE	48
2.6	Substrate and Ligand Binding	52
2.7	Steady-State Kinetics	55

2.8	Stopped-Flow Spectrophotometry	55
2.9	Redox Potentiometry	59
2.10	Coupling Efficiency	61
2.11	Heme Content Determination	63
2.12	Protein Crystallography	64
2.13	Product Characterisation	65
2.14	Electron Paramagnetic Resonance	65
2.15	Cytochrome P450cam	66

Chapter 3	THE ROLE OF PHENYLALANINE 393	Page 67
3.1	Introduction	68
3.2	Results	71
3.2.1	Overexpression and Purification of Mutant Enzymes	71
3.2.2	Spectrophotometric Analysis of Carbon Monoxide Binding	71
3.2.3	Fatty-Acid Binding	73
3.2.4	Kinetics of Fatty-Acid Oxidation	74
3.2.5	Product Characterisation	76
3.2.6	Kinetics of Heme Reduction	77
3.2.7	Generation of the Oxy-Ferrous Complex	79
3.2.8	Kinetics of Oxy-Ferrous Decay	79
3.2.9	Heme-Domain Potentiometric Titrations	81
3.2.10	Electron Paramagnetic Resonance Spectroscopy	85
3.2.11	Crystallography	85
3.3	Discussion	88

3.3.1	The Consequence of Mutating Phe393	88
3.3.2	The Cause of the Thermodynamic Control	92
3.3.3	Re-evaluation of the Mechanistic Control Exerted by Substrate-Binding	98
3.4	Conclusion	100

Chapter 4	4-CYANOPYRIDINE	Page 102
4.1	Introduction	103
4.2	Results	105
4.2.1	Purification of 4-Cyanopyridine	105
4.2.2	The Mode of 4-Cyanopyridine Binding to P450 Heme	105
4.2.3	4-Cyanopyridine Binding to Cytochromes P450	105
4.2.4	Competitive Inhibition of 4-Cyanopyridine Binding by Substrate	108
4.2.5	Prediction of P450 Heme Reduction Potentials	112
4.3	Discussion	114
4.4	Conclusion	119

APPENDICIES

I	References	120
II	Derivation of Kinetic Equations	134
III	Peptide Sequence of Flavocytochrome P450 BM3	139
IV	Publications and Conferences Attended	142

LIST OF FIGURES

1.1	The Reaction Catalysed by Cytochromes P450	3
1.2	P450 Classification	5
1.3	The Heme Binding Region of Cytochromes P450	6
1.4	The Tertiary Structure of Cytochromes P450	7
1.5	The P450 Catalytic Cycle	9
1.6	The Electronic Configuration of a P450 Heme	10
1.7	Heterolytic <i>versus</i> Homolytic O-O Bond Cleavage	13
1.8	The “Push-Pull” Model for Dioxygen Bond Cleavage in Cytochromes P450 and Peroxidases	14
1.9	The Distal Charge Relay in P450cam	16
1.10	Substrate-Assisted Catalysis in P450 EryF and NOS	17
1.11	The Oxygen Rebound Mechanism: Fenton Reagent	18
1.12	The Oxygen Rebound Mechanism: Cytochromes P450	19
1.13	Carbon Hydroxylation	20
1.14	Aromatic Hydroxylation. The NIH Shift	21
1.15	N-Oxidation and N-Dealkylation	21
1.16	C-C Bond Cleavage	22
1.17	A Selection of P450 Substrates	23
1.18	Key Active-Site Residues in Flavocytochrome P450 BM3	25
1.19	Electron Transfer in Flavocytochrome P450 BM3	27
1.20	Crystal Structure of Mammalian NADPH-Dependent Cytochrome P450 Reductase	28
1.21	The Proposed FMN/Heme Electron Transfer Pathway in Flavocytochrome P450 BM3	30

LIST OF FIGURES cont'

1.22	Re-modelled FMN/Heme Electron Transfer Pathway in Flavocytochrome P450 BM3	31
1.23	The Energetics of Non-Adiabatic Electron Transfer	33
1.24	The Energetics of 'Activationless' Electron Transfer and the Marcus 'Inverted' Region	34
1.25	Plot of $\ln k_{ET}$ vs $-\Delta G$	35
1.26	The Photosynthetic Reaction centre from <i>Rb. sphaeroides</i>	36
1.27	The Various Types of Electron Transfer Pathways	37
1.28	The Cytochrome <i>c</i> : Cytochrome <i>c</i> Peroxidase Electron Transfer Complex	39
2.1	Example SDS PAGE Gel	49
2.2	The Absorption Shifts Observed Upon Substrate and CO Binding to P450 BM3	53
2.3	Example Substrate-Binding Titration	54
2.4	Example Michaleis Plots	56
2.5	Redox Induced Shifts in the P450 BM3 Absorbance Spectrum	60
2.6	Calibration of the Calomel Electrode	61
3.1	Space-Filled Representation of the Heme-Domain of P450 Bm3 and P450cam	69
3.2	The Shift in the P450 Absorption	72
3.3	The Bonding Interactions of CO with Ferrous Iron	72
3.4	The Extent of Substrate-Induced Spin-State-Shift with Substrates of Different Chain Length	74
3.5	Example Data for the Heme-Reduction Kinetics	78

LIST OF FIGURES cont'

3.6	Absorption Spectra of the Oxy-Ferrous Complex of P450 BM3	80
3.7	The Decay of the Oxy-Ferrous Complex	82
3.8	Comparison of the Thermodynamic and Kinetic Factors affecting the Stability of the Oxy-Ferrous Complex	83
3.9	Nernst Curves for the Heme-Domian Reduction Potentiometry	84
3.10	EPR Spectrum of P450 BM3 F393H-HD	86
3.11	Comparison of the Heme Binding Region of the F393X Mutants with Wild-Type P450 BM3	87
3.12	Superposition of X393	89
3.13	Electronic Perturbation Caused by Substitution of Phe393	93
3.14	Stereoview of the Heme-Binding Region of P450 BM3 F393H-HD	94
3.15	The Heme-Binding Region of iNOS	97
3.16	Redox-Induced Conformational Reorganisation	99
4.1	Comparison of Pyridine, Cyanide and 4-Cyanopyridine Binding to P450 BM3	106
4.2	The Binding of 4-Cyanopyridine to Ferric and Ferrous P450	107
4.3	Lineweaver-Burk Plots Showing the Competitive Inhibition of 4-Cyanopyridine Binding by Substrate	110
4.4	Variation of K_d^{app} with Substrate Concentration	111
4.5	Variation in the P450-4CNPY Metal-to-Ligand Charge Transfer Absorbance	113
4.6	Variation of E_{MLCT} with Heme Reduction Potential	114

LIST OF FIGURES cont'

4.7	Dissection of the Gibbs' Free Energy for Substrate-Binding and Reduction of Cytochromes P450	116
------------	---	------------

LIST OF TABLES

1.1	Examples of Cytochromes P450 from Every Domain of Life	3
1.2	Midpoint Reduction Potentials for the Flavin Cofactors of P450 BM3	27
2.1	Oligonucleotide Primers Used	42
2.2	Growth Media and Agar	44
2.3	Buffer A	45
2.4	Phosphate Storage Buffer	48
2.5	SDS PAGE Gel Preparation	50
2.6	SDS PAGE Electrophoresis Conditions	51
2.7	Assay Buffer	55
2.8	Stopped-Flow Assay: Heme Reduction Kinetics	57
2.9	Stopped Flow Assay: Oxygen Binding Kinetics	58
2.10	Redox Potentiometry Conditions	59
2.11	Pyridine Hemochromagen Assay	63
2.12	Crystallisation Conditions	64
3.1	Substrate Dissociation Constants and percentage spin conversions	73
3.2	Steady-State NADPH Oxidation Kinetics	75
3.3	Coupling Efficiencies	75
3.4	Product Characterisation	76
3.5	Pre-Steady State Kinetics of Heme Reduction	77

LIST OF TABLES cont'

3.6	Pre-Steady State Kinetics of Oxy-Ferrous Decay	81
3.7	Heme Reduction Potentials	83
3.8	Key Structural Parameters	88
4.1	4-Cyanopyridine Dissociation Constants	108
4.2	Competitive Inhibition of 4-Cyanopyridine Binding by Substrate	109
4.3	Position and Energy of the Ferrous P450/4-Cyanopyridine Metal-to Ligand Charge Transfer Absorption	112
4.4	Thermodynamic Parameters for Substrate Binding	117

*The great tragedy of science – the slaying
of a beautiful hypothesis by an ugly fact*

T.E. Huxley 1825 - 1895

Chapter 1:

Introduction

1 INTRODUCTION

1.1 Cytochromes P450

1.1.1 Discovery

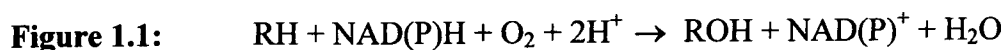
The serendipitous discovery of cytochromes P450 is attributed to the work of Klingenberg [1] in 1958, as a result of a discrepancy in the quantification of cytochrome b_5 from rat liver microsomes. Only half of the calculated protoheme concentration was accounted for by cytochrome b_5 , the remainder of which was observed to generate a CO-protoheme complex upon treatment of the microsomal suspension by cholate, in the presence of carbon monoxide. This complex had an unusual absorbance band at 450 nm.

However, the true identification of this “red pigment from liver microsomes” as a cytochrome was made by Omura and Sato [2-4] in the early 1960s. They demonstrated that CO had affinity only for the ferrous-form, and that treatment with ethylisocyanide gave difference spectra characteristic of hemoglobin and its derivatives. By comparison of aerobically and anaerobically DPNH (diphosphopyridinenucleotide)-reduced microsomes, spectral interference from cytochrome b_5 was removed, allowing the observation of the spectrum of the native pigment. This was shown to be that of a b -type cytochrome, different from cytochrome b_5 . It is from these unusual yet characteristic absorbance properties that the present terminology of cytochromes P450 (‘pigment-450’) originates.

The proposal that cytochromes P450 (P450s) were components of mixed function oxidase systems, catalysing many important reactions *in vivo* such as steroid hydroxylation and the oxidative demethylation and hydroxylation of drugs [5,6] implied a fundamental, physiological role for the enzymes, other than CO-binding. This impetus, along with the subsequent solubilisation, purification and reconstitution of active P450-containing complexes [7,8] has permitted a thorough and systematic understanding of the general P450 mechanism and their involvement in many biosynthetic and metabolic processes.

1.1.2 General Background

Cytochromes P450 are NAD(P)H-dependent *b*-type heme containing monooxygenases which can catalyse stereo- and regio-specific insertion of an atom of oxygen (derived from molecular oxygen) into a diverse range of organic compounds, with the concomitant production of water (Figure 1.1). Electrons are



derived from NAD(P)H, and are shuttled to the heme *via* one or two redox proteins, depending on the class of P450, at strategic points in the catalytic cycle.

P450s are found within organisms from every domain of life (Bacteria, Archaea and Eukarya (Table 1.1). By 1993, the number of partial or total nucleotide sequences

Table 1.1: Examples of cytochromes P450 from every domain of life

Domain	Example	Species	Ref.
Bacteria	CYP 101	<i>Pseudomonas putida</i>	[9]
	CYP102	<i>Bacillus megaterium</i>	[10]
	CYP 51	<i>Mycobacterium tuberculosis</i>	[11]
Eukarya	CYP 11A1	Human, rat, rabbit, bovine, pig	[12-16]
	CYP 2	<i>Caenorhabditis elegans</i>	[17]
	CYP 6A2	<i>Drosophila melanogaster</i>	[18]
	CYP 55	<i>Fusarium oysporum</i>	[19]
	CYP 51	<i>Saccharomyces cerevisiae</i>	[20]
	CYP 73A	<i>Arabidopsis thaliana</i>	[21]
Archaea	CYP 119	<i>Sulfolobus sulfotaricus</i>	[22]

identified as P450s exceeded 300 forms [23]. The solutions to the genomes of various species identify numerous additional isoforms [24] (53 from human [25], 20 from *Mycobacterium tuberculosis* [26], 80 from *Caenorhabditis elegans* [27], 83

from *Drosophila melanogaster* [28], 286 from *Arabidopsis thaliana* [29]), increasing the number of members constituting the P450 superfamily to over 500. An up to date compilation can be found at <http://drnelson.utmem.edu/CytochromeP450.html>.

Cytochromes P450 are implicated in a multitude of biosynthetic, metabolic and detoxification processes *in vivo*, for example: CYP11A1 converts cholesterol to pregnenolone in mammals; CYP101 metabolises camphor as an unusual energy source for its bacterial host *Pseudomonas putida*; CYP107A1 is required to hydroxylate an important precursor in erythromycin biosynthesis in fungi; CYP1A2 detoxifies caffeine in the liver and CYP107H1 is involved in biotin biosynthesis.

In most situations, oxygenation of substrates acts either to increase the polarity of the product with respect to the substrate to facilitate water solubility and hence excretion, or activates the substrate toward further reactions. Whilst this activity is, in the main, beneficial to the host, under certain conditions P450s can act as a double-edged sword – transforming inert, unreactive species into highly reactive and potentially mutagenic/carcinogenic derivatives. Illustrative of this are the epoxidation products of vinyl chloride and benzo(a)pyrene [30].

1.1.3 Classification

P450s are classed into three main groups according to their redox cofactor arrangement and are depicted in Figure 1.2.

Class 1: Class 1 P450s are three component systems, typified by the bacterial (Figure 1.2a) and mitochondrial P450s (Figure 1.2b). Here, electrons are derived from NADH and are passed sequentially onto a FAD-containing ferredoxin reductase, to a small iron-sulfur cluster (ferredoxin) and finally onto the P450. Bacterial Class 1 P450s are soluble (e.g. putidaredoxin reductase/putidaredoxin/P450cam) [31], whereas mitochondrial Class 1 P450s tend to be associated to the inner mitochondrial membrane by hydrophobic contacts (e.g. adrenodoxin reductase/adrenodoxin/ P450_{scc}) [32].

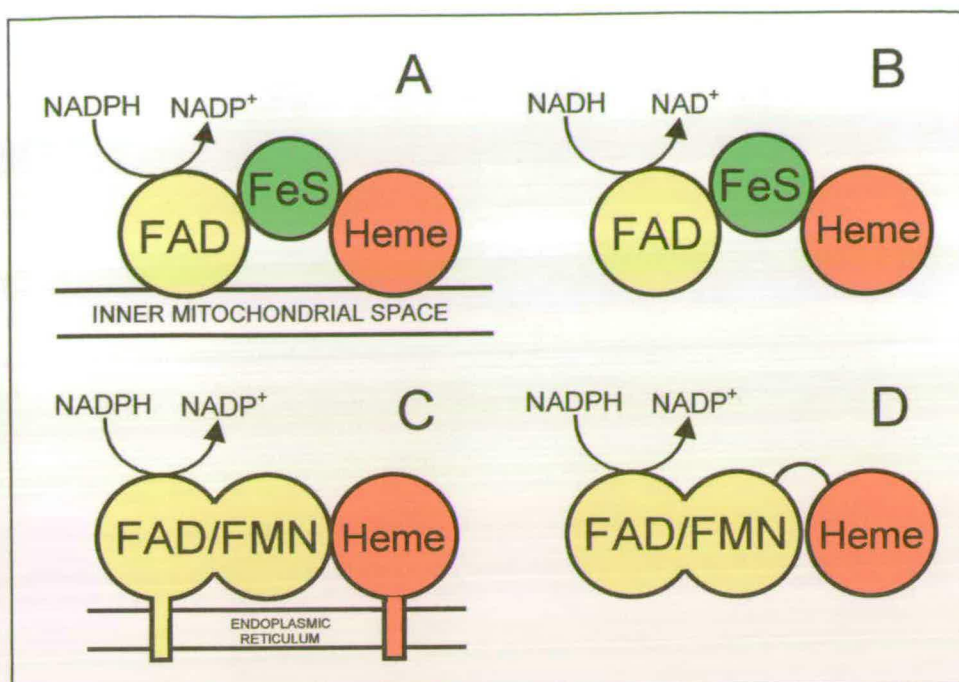


Figure 1.2: Diagrammatic representation of the three different classes of cytochrome P450 systems. A and B: Class 1 systems (microsomal and bacterial respectively) are composed of an FAD containing flavodoxin reductase, and iron-sulfur cluster containing ferredoxin and the P450. C: Class 2 P450 systems (e.g. mitochondrial P450) are membrane-bound and partnered by a diflavin reductase, whereas in D: the Class 3 P450s, the reductase and P450 are fused in one continuous polypeptide (e.g. P450 BM3).

Class 2: Class 2 P450s are two component systems, typified by the microsomal P450s whereby electrons are shuttled through a FAD/FMN-containing NADPH-dependent diflavin P450-reductase onto the P450. These P450s tend to be bound to the cytoplasmic side of the endoplasmic reticulum, through N-terminal membrane spanning anchors (Figure 1.2c).

Class 3: Class 3 P450s are one component systems, comprising a FAD/FMN containing diflavin NADPH-dependent P450-reductase domain, covalently attached to the P450 domain in one continuous polypeptide by a short hydrophilliic polypeptide linker. Class 3 P450s are typified by the bacterial P450 BM3 (Figure 1.2d).

1.1.4 Structure

Primary structure: In general, P450s comprise of 450 ± 100 amino acids with a C-terminal protoporphyrin IX binding motif (FXXGXXXCXG, Figure 1.3). The

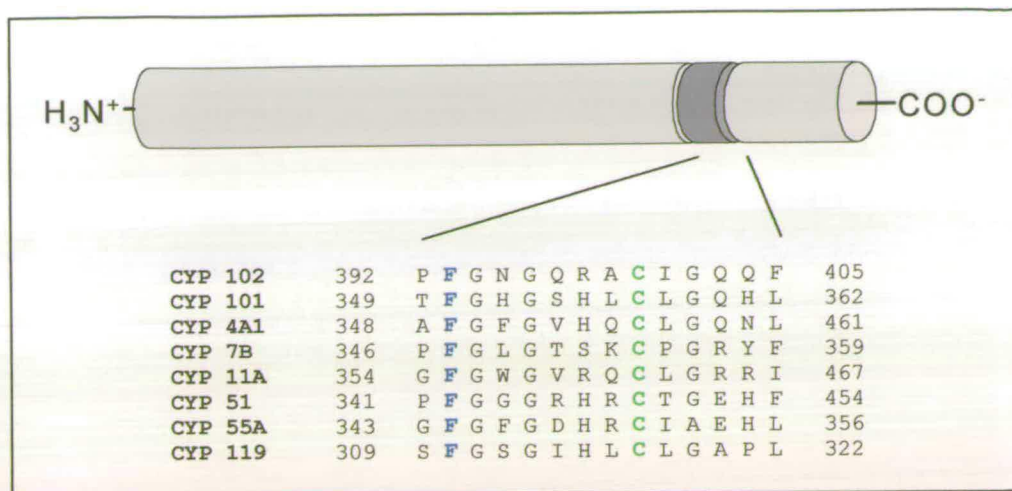


Figure 1.3: The heme-binding region of cytochrome P450 is located toward the C-terminal end of the P450, as indicated by the dark grey shaded region on the cartoon polypeptide. A sequence alignment for a selection of P450s shows the high degree of sequence homology in this region. The implicitly conserved cysteine residue (which provides the heme ligand, green) and the highly conserved phenylalanine (corresponding to Phe393 of P450 BM3, blue) are highlighted.

structural feature common to all P450s is the presence of a phylogenetically conserved cysteine residue which provides a thiolate as the fifth ligand to the heme iron [33] (Figure 1.3). The presence of this thiolate has been proposed to be the key to the unique reactivity displayed by P450s [34-37]. This cysteine is the only implicitly conserved residue throughout the P450 superfamily, although a small number (ca. 10) residues are very highly conserved (> 95 %), these include a threonine residue distal to the heme ligand (Thr268 in P450 BM3 [38]), a tryptophan π -stacking with the heme (Trp96 in P450 BM3) [39] and a proximal phenylalanine (Phe393 in P450 BM3) [40], all of which are believed to play critical roles in P450 mechanism.

Secondary and tertiary structure: Comparison of the available P450 crystal structures shows that despite the relatively low degree of sequence homology between these P450s (< 20 % on average), they all have secondary and tertiary structural elements in common. The P450 tertiary structure has an approximate trigonal prism arrangement, containing both α -helical and β -sheet regions (Figure 1.4). Helices dominate the structure, with the majority of these lying parallel to the heme plane. The heme is wedged in a relatively hydrophobic cleft between two

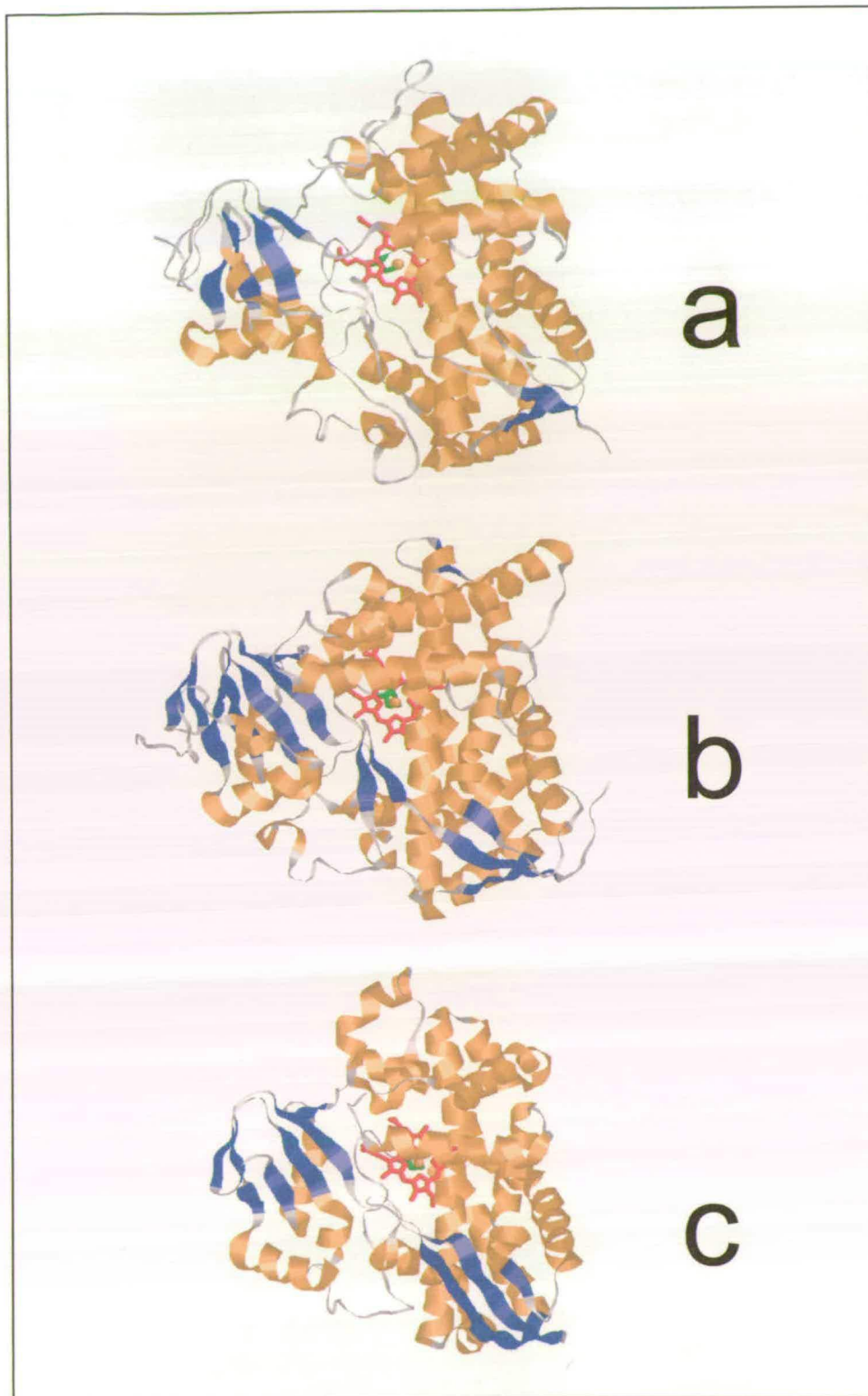


Figure 1.4: Schematic representation of the tertiary structure, common to all P450s. Shown are the structures of P450s from a eukaryote (a, CYP 2C5 from Rabbit), a prokaryote (b, CYP 102 from *Bacillus megaterium*) and from an archaeon (c, CYP 119 from *Sulfolobus sulfotarius*). The α -helical and β -sheet regions are shown in orange and blue respectively, the heme is shown in red

protein spanning α -helices (the I- and L-helices) with the cysteine thiolate located at the N-terminal end of the L-helix. Being at the positive dipole end of the L-helix allows stabilisation of the thiolate anion, a feature key to characteristic P450 activity which helps to stabilise the anionic thiolate, thereby influencing P450 reactivity (in contrast, the histidine heme-ligand of peroxidases is located at the C-terminus of a helix, which stabilises the positive imidazolate ligation observed in this class of hemoprotein). The heme is buried within the core of the protein, with the substrate binding site on the distal face of the heme, *trans* to the thiolate ligand.

1.1.5 The Catalytic Cycle

The majority of P450 mechanistic information has been determined for the soluble, camphor hydroxylase, P450cam, from *P. putida*. The mechanism shown in Figure 1.5 is the product of almost 30 years research into the catalytic mechanism of P450. Although P450cam is a bacterial P450, the nature of the reactive species and intermediates are believed to be applicable to all members of the P450 family by analogy.

In its resting state, the P450 heme is ferric low-spin, with essentially octahedral geometry [41]. The mixed ligand set is comprised of four nitrogenous ligands (provided by the porphyrin macrocycle), a thiolate (provided by cysteine) [42] and a weakly bound water molecule in the sixth coordination site.

Step 1: Substrate Binding

Step 1 of the catalytic cycle shown in Figure 1.5 is substrate binding to the active site of the P450. There are a number of structural features which contribute to the overall substrate binding energy such as hydrophobicity, electrostatic interactions and hydrogen bonding networks. The level of contribution of each of these factors is determined by the identity of the substrate and the nature of the substrate-binding cavity, and hence are details specific to a particular P450. Yet despite the high degree of variability of potential substrates, one generic feature is that substrate binding causes a perturbation in the low- to high-spin state equilibrium of the heme iron.

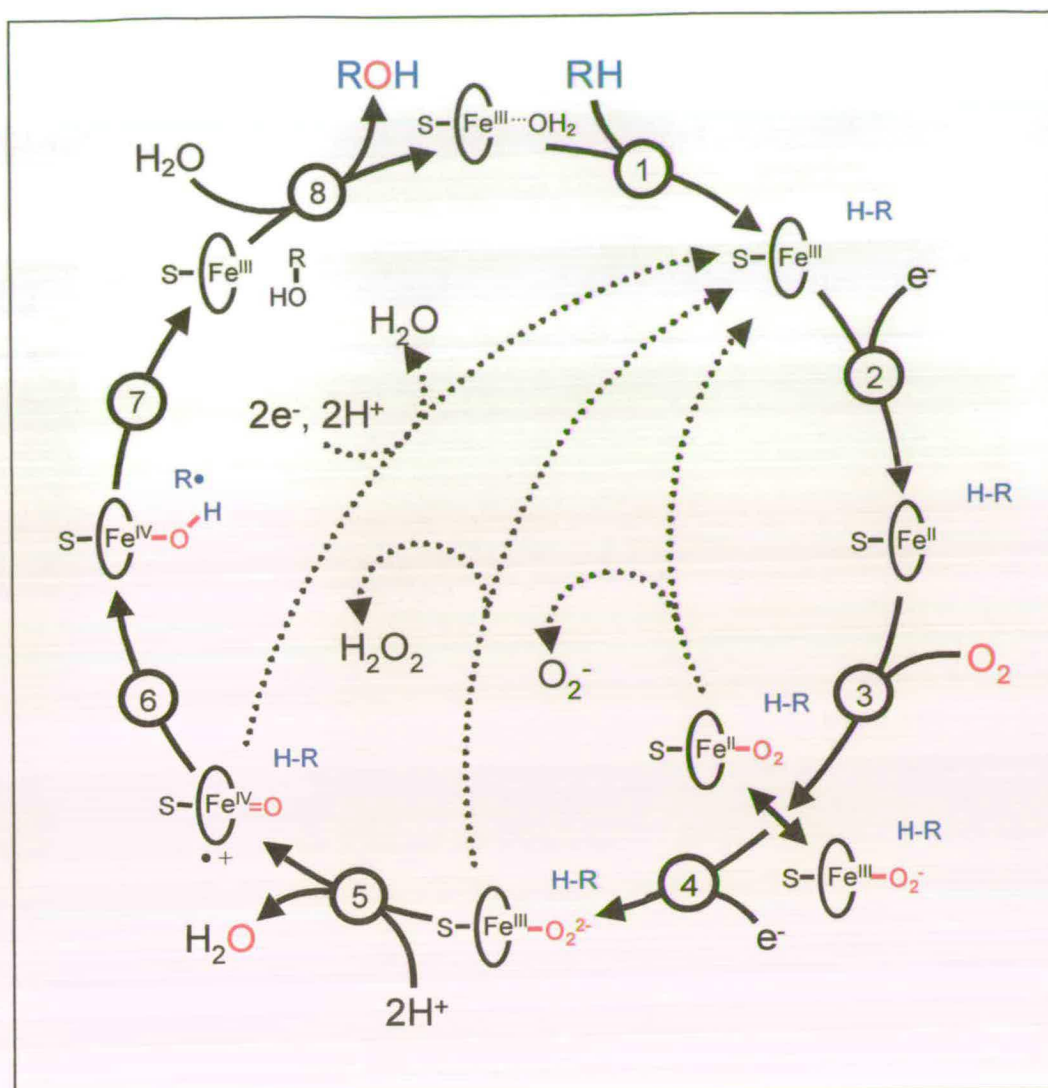


Figure 1.5: The P450 catalytic cycle. The individual steps are discussed in detail in the text (Section 1.1.5). The dashed lines indicate the three major uncoupling pathways observed in P450s, leading to the 1-, 2- and 4-electron reduced forms of molecular oxygen. Substrate is shown in blue, oxygen (from molecular oxygen) is shown in red where appropriate.

Dehydration of the heme by substrate causes the iron to move out of the plane of the porphyrin (toward the thiolate) and invokes a change in the iron coordination geometry from octahedral to square based pyramidal. This change in geometry is accompanied by a modification in the energetic ordering of the d-orbitals (Figure 1.6) and a rearrangement of the d-electrons from low-spin ($S = 1/2$) to high-spin ($S = 5/2$). Perturbations in this low- to high-spin equilibrium are solely attributable to the binding equilibrium of the sixth ligand and not as a result of a

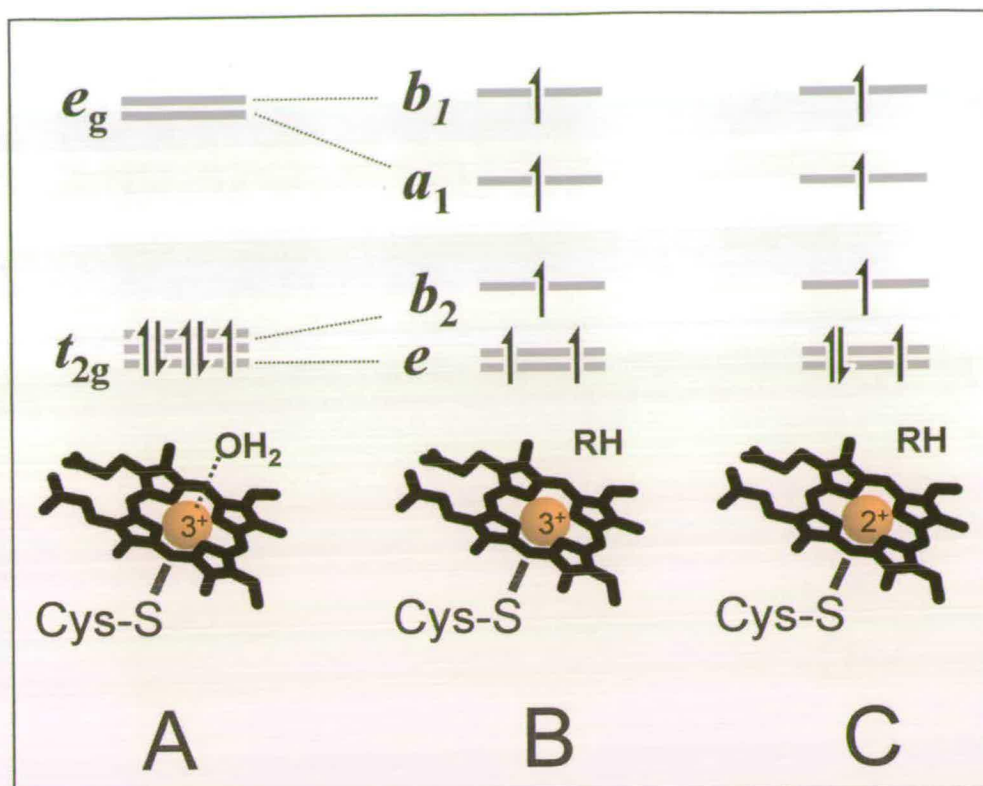


Figure 1.6: Diagram illustrating the changes in d-orbital arrangement and d-electron configuration of A: low spin ferric P450 heme iron, B: upon substrate binding and C: reduction.

purely electronic spin equilibrium (implying iron being hexacoordinate in both spin states). All high-spin P450 complexes are pentacoordinate.

The degree to which the spin state equilibrium is perturbed is dependent on the substrate binding affinity. Substrates with low dissociation constants are better substrates (by definition) and induce a greater shift to the high-spin form. This is clearly illustrated in the case of P450cam and P450 BM3, where the best substrates (camphor and arachidonate respectively) induce almost complete spin conversion to the high spin form (> 90 %), whereas poorer substrates (norcamphor and laurate respectively) only induce a partial (< 40 %) shift. This spin state shift is fundamental to the P450 catalytic cycle, as substrate binding is accompanied by a large, positive increase (~ +100 mV) in the heme reduction potential. In this way, substrate binding acts as a thermodynamic switch. In the absence of substrate, the heme reduction potential is too negative to permit electron transfer from the reductase, preventing the futile oxidation of valuable NAD(P)H equivalents and the production of undesirable,

uncoupled reduced oxygen species. Instead, P450s have a built in mechanism which only allows heme reduction when in the catalytically-prepared, substrate-bound form. It also holds true that poorer substrates have a similarly less pronounced effect on increasing the reduction potential and are consequently poorer 'switches'.

Step 2: First Electron Transfer

The second step in the P450 catalytic cycle is the one-electron reduction of the substrate-bound P450. This is essential as molecular oxygen has strict selectivity for ferrous-heme, dioxygen does not bind to ferric heme

The pentacoordinate ferrous-iron is exclusively high-spin (Figure 1.6) as determined initially by $^1\text{H-NMR}$ [43] and magnetic susceptibility of camphor-bound P450cam [44].

Reducing equivalents are ultimately derived from pyridine nucleotides (NAD(P)H) in the form of a hydride, with subsequent steps involving the transfer of individual electrons through a relay of electron transfer proteins (as described in Section 1.1.3) to the P450. The P450 redox partners constitute a 'potential gradient' to mediate electron transfer from NAD(P)H to the P450 heme. Heme reduction causes a conformational change in the active site, which is believed (at least for P450 BM3) to move substrate closer to the heme, and increase the affinity for substrate [45].

Step 3: Dioxygen Binding to Ferrous Heme

Under normal circumstances, the reaction between organic substrates and molecular oxygen is spin forbidden, hence in order for reaction to occur, the oxygen must be activated. This is the primary role of cytochromes P450. Oxygen binding is the first step in the process of oxygen activation.

Reduction of ferric P450 allows the ligation of molecular oxygen, to the coordination site vacated by the water molecule, *trans* to the thiolate ligand. The oxy-P450 complex of P450cam was first reported by Peterson *et al* in 1971, and has been observed since for other P450s. The complex has a red-shifted visible absorbance relative to the ferrous P450, indicative of the formation of a hexacoordinate, low-spin

P450 [46-48]. Whilst this adduct is readily formed under controlled conditions (stoichiometrically reduced P450 in the presence of excess oxygen), it is likely that the formal nature of the complex is superoxy-ferric, as opposed to oxy-ferrous. Whilst experiments have been conducted to determine features such as the O-O stretching frequency [49], these values correspond to the superoxy-ferric form as opposed to the oxy-ferrous form, as demonstrated by Collman *et al* [50]. Electronic rearrangement is likely to be rapid and although dioxygen initially binds to the ferrous form, the superoxy-ferric adduct is likely to be the favoured (stabilised) canonical form. This can be further justified on thermodynamic grounds, as the heme reduction potential is more negative than the one electron reduction potential of oxygen to superoxide (-160 mV), this reductive driving force would favour the formation of the superoxy-ferric form.

Steps 4 - 8: Second Electron Transfer to Product Dissociation

The oxy-P450 complex is the last observable intermediate in the P450 catalytic cycle. Although the rate of second electron transfer to P450cam has been measured and has been reported to be the rate limiting step in P450 catalysis [51-53], the identity of the intermediates after this point remain unresolved and their identity only speculated upon. It seems likely that reduction leads to the formation of a peroxy-ferric complex, the subsequent protonation of which would result in the liberation of a water molecule, and the generation of the reactive intermediate. It has been proposed that the reactive moiety is an oxy-ferryl radical cation ($[\text{Fe}^{\text{IV}}=\text{O}]^{\bullet+}$).

Cleavage of the O-O bond of heme-bound peroxide: Central to the proposed mechanism is the manner in which the peroxide O-O bond is cleaved to allow generation of the oxy-ferryl intermediate. This oxygen splitting reaction must occur after the introduction of the second electron, as the oxy-P450 species itself is catalytically incompetent at oxygenating substrates [54]. The peroxy-ferric complex can be envisioned to decay to the oxy-ferryl species by one of two mechanisms, either the homolytic or heterolytic cleavage of the O-O bond.

Model porphyrins have been used to probe this feature with the nature of the product being illustrative of the pathway of oxygen scission. The validity of this biomimetic approach is questionable, since both homolytic and heterolytic O-O cleavage can be demonstrated, depending on the nature of the oxidant, solvent and coordinating ligands. For example, Hirobe *et al* [55,56] demonstrated that simple porphyrins such as Fe^{3+}TPP catalysed the exclusive conversion of phenylperoxyacetic acid to phenylacetic acid (evidence of heterolytic cleavage) in favour of the formation of various benzyl-radical derived products (evidence of homolytic cleavage) (Figure 1.7), whereas Labeque and Marnett [57] have shown that Fe^{3+}TPP reduces fatty acid hydroperoxides homolytically in the absence of a strongly electron donating proximal ligand, but heterolytically in the presence of excess imidazole. These types of study do demonstrate that either mechanism is chemically feasible for P450s, yet are fundamentally flawed by virtue of the fact that they do not completely mimic the

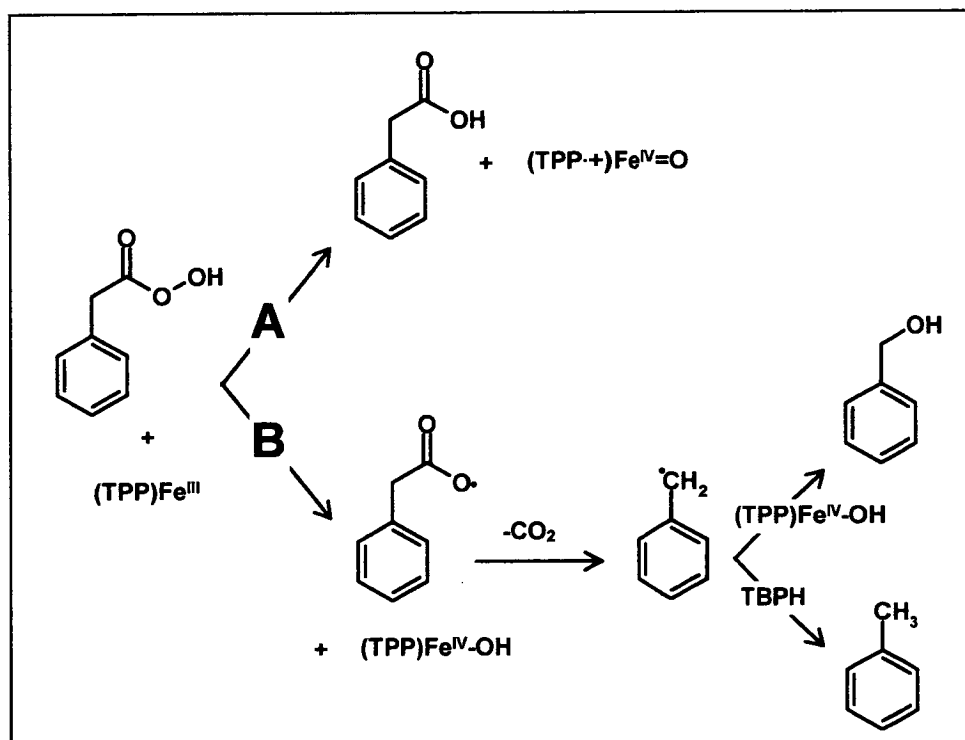


Figure 1.7: The mode of O-O bond cleavage mediated by phenylperoxyacetic acid (PPAA) in the presence of tetraphenylporphyrin ($\text{Fe}(\text{TPP})$) can be used as a convenient mechanistic probe. The oxidation of 2,4,6-tri-tert-butylphenol (TBPH) by PPAA affords only phenylacetic acid if the O-O bond of PPAA breaks heterolytically (Pathway A), or benzyl radical-derived products if the O-O bond is broken homolytically (Pathway B). Reactions using a sulfur ligated $\text{Fe}(\text{TPP})$ -derivative catalysed only heterolytic cleavage of the O-O bond, suggesting this to be analogous to the mechanism operative in the thiolate-ligated cytochromes P450.

environment of the active site. This is an important point, as recent studies suggest that the features of the protein superstructure are essential for oxygen activation and O-O bond scission.

In peroxidases, oxygen activation is achieved by what is termed the “push-pull” mechanism (Figure 1.8a), first proposed by Poulos [58]. The peroxy-ferric complex is activated by a ‘push’ from the proximal histidine ligand, and a ‘pull’ from interactions with two distal residues, a histidine and an arginine. The imidazolate character of the proximal histidine is enhanced by hydrogen bonding interactions with neighbouring aspartate, increasing the electron density of the heme iron. In association with this, the distal histidine hydrogen-bonds with the bound peroxide (providing the outer oxygen atom with the proton required for the formation of water) and the cationic guanidino group of the arginine, serves to stabilise the negative charge which develops during O-O scission.

Unlike peroxidases, P450s do not have residues in the distal cavity able to provide the analogous acid/base interactions required to assist the O-O bond cleavage.

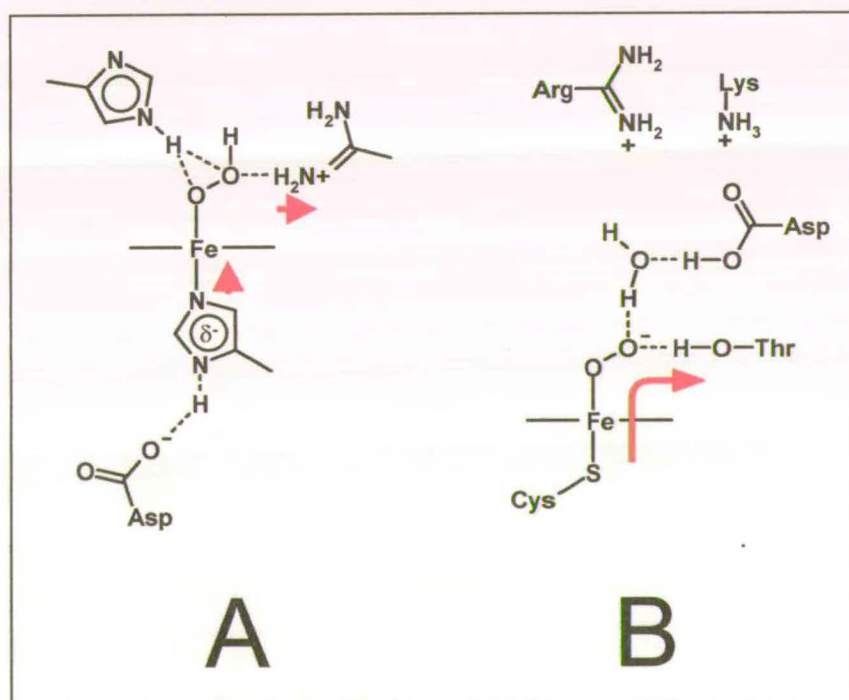


Figure 1.8: Schematic representation of the “push-pull” model for O-O bond cleavage of heme-bound peroxide in histidine (A, e.g. peroxidases) and thiolate (B, e.g. P450s) ligated systems

Consequently, it has been proposed that the strong electron donating character of the thiolate ligand from the proximal cysteine residue is the primary factor responsible for the activation of oxygen in P450, by providing a 'big push' (Figure 1.8b). Evidence for the strong electron releasing character of cysteinate has been provided by comparisons with myoglobin, where thiolate ligands *trans* to the endogenous cysteinate display enhanced basicity [59,60], whilst small anionic ligands have a much lower affinity for ferric P450 than ferric myoglobin. Also, substitution of the endogenous histidine ligand of myoglobin (Mb) by cysteine generates a myoglobin variant which enhances the heterolytic cleavage of cumene hydroperoxide, as observed by a change in the heterolytic/homolytic product ratio [61] from 3.2 (WTMb) to 7.2 (H93C Mb).

Recent studies on P450cam by Sligar *et al*, have demonstrated that although there are no residues in the P450 distal cavity able to perform acid/base catalysis, two residues (T252 and D251) were of critical importance for the enzyme to catalyse the hydroxylation of camphor. These residues cause a kink in the I-helix, generating a putative oxygen binding cleft. The mutation T252A resulted in extensive uncoupling, i.e. only ~ 5 % of the reducing equivalents from NADH supported the hydroxylation of camphor, with the remaining electrons consumed in the 2- or 4-electron reduction of oxygen to peroxide or water (respectively). The D251N mutant of P450cam decreased the overall rate of reaction by an order of magnitude. Both of these residues participate in a distal charge relay [62] (Figure 1.9), creating a hydrogen-bonding network for the transfer of protons from the bulk solvent to the active site.

This motif is highly conserved throughout the P450 superfamily, with only a few exceptions, suggestive of the fact that it plays an important role in the reaction of heme with oxygen. P450EryF is an example of one such P450 lacking the charge relay machinery, having an alanine (A245) in place of the threonine [63]. A similar kink in the I-helix of P450EryF is observed to that in P450cam, yet is stabilised (in the absence of the threonine side-chain) by a hydrogen-bonding network involving substrate and water molecules. The C5 hydroxyl group of the substrate 6-DEB (6-deoxyerythronolide B) hydrogen bonds to a water molecule, which in turn hydrogen bonds to the heme-bound oxygen (Figure 1.10a). In the absence of the threonine,

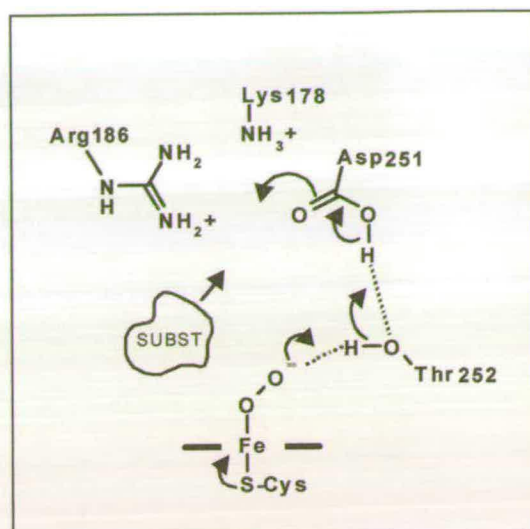


Figure 1.9: The proposed distal charge relay operational in P450cam, involved in the stabilisation and activation of heme-oxygen complexes. It also serves to conduit for proton transfer from the aqueous solvent, to the buried heme.

substrate appears to be aiding catalysis [64]. A similar observation has been made for nitric oxide synthases (closely related, heme-thiolate monooxygenases) where the substrate (L-arginine) forms a hydrogen bond with heme-bound oxygen to activate it (Figure 1.10b), due to the absence of distal cavity residues with the required functionality [65].

In the case of P450s, the requirement for distal residues to perform acid/base catalysis in parallel with a weakly electron donating proximal ligand (histidine) as seen for peroxidases, has been replaced by a strongly electron donating proximal ligand (cysteine) acting in concert with hydrogen bonding interactions from hydrophilic residues and water molecules in the distal cavity, to achieve efficient oxygen activation.

Mechanism of oxygen insertion: As mentioned previously, the identity of the reactive oxygen species responsible for the oxygenation reaction is a reactive iron-oxo species, the putative oxy-ferryl radical cation ($[\text{Fe}^{\text{IV}}=\text{O}]^{*\dagger}$). Hydroxylation is believed to occur via a hydrogen-abstraction/oxygen insertion reaction, termed the oxygen rebound mechanism [66,67] first described by Groves and McClusky in 1976. They utilised a modified Fenton reagent ($\text{Fe}^{2+}/\text{H}_2\text{O}_2/\text{CH}_3\text{CN}$) to show that aliphatic hydroxylation occurred via an iron-bound oxidant, rather than by a free hydroxyl

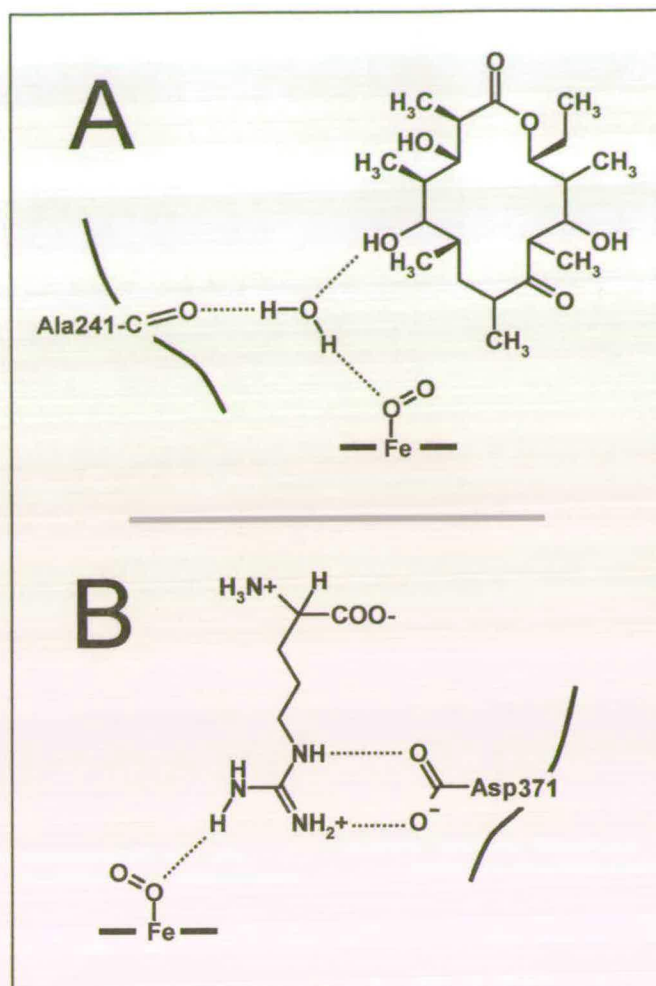


Figure 1.10: Schematic representation of the substrate-assisted oxygen stabilisation proposed for P450 EryF (A) and nitric oxide synthase (B, iNOS numbering). Hydrogen bonds are shown by dotted lines.

radical. The Fe²⁺-catalysed hydroxylation of cyclohexanol by *meta*-chloroperbenzoic acid (MCPBA) liberated all possible diol products, of which the *cis*- and *trans*-1,2-diols constituted 75 % of the total product profile (Figure 1.11). The presence of ¹⁸O-enriched water did not lead to the incorporation of labelled oxygen into the diol, providing evidence that the source of the oxygen atom was the peroxyacid, and that the mechanism of hydroxylation occurred without equilibration with water.

Whilst this mechanism appeared to be non-selective (~1:1 *cis:trans* diol products), examination of the products of the hydroxylation of *trans*-2-deuteriocyclohexanol showed that *cis* hydrogen abstraction led preferentially to the formation of the *cis* diol, whilst *trans* hydrogen abstraction afforded the *trans* diol. The specific

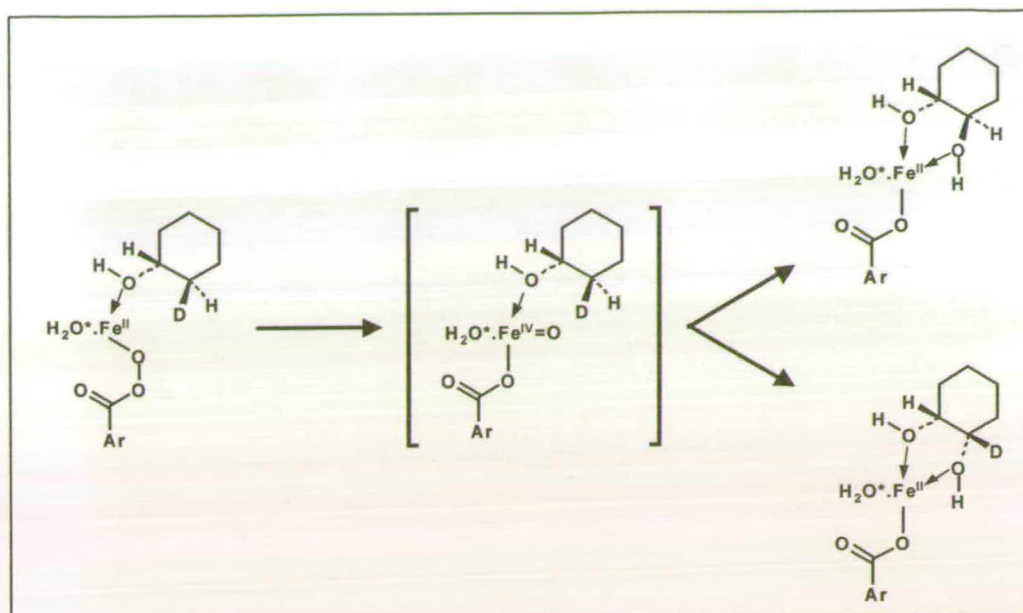


Figure 1.11: The mechanism of oxygen insertion into 2-cis/trans-deuterocyclohexanol by the oxygen rebound mechanism. The stabilised ferrous/peracid/substrate complex readily rearranges to liberate the highly reactive iron-oxo ($Fe^{IV}=O$) moiety responsible for hydroxylation. The intimate association of the $Fe^{IV}=O$ species and substrate is justified by the observation that the cis-cyclohexanol affords the cis-diol and vice-versa.

incorporation of the peroxy oxygen and the retention of C-2 H-abstraction/oxygen rebound led to the proposal that an iron-oxo intermediate (formally a ferryl ion) was responsible for hydroxylation.

Although the equivalent species has not been formally identified as the active moiety in the P450 catalytic mechanism, the oxygen rebound mechanism reported above can be successfully applied to the heme iron of P450s as shown in Figure 1.12. Whilst it is incorrect to refer to the oxy-ferryl intermediate formally as $[Fe^{IV}=O]^{*+}$ (because of its various possible canonical forms), it has become the convention to do so, with the radical cation located on either the porphyrin macrocycle, or a neighbouring aromatic residue. It is more appropriate to consider the species as a high-valent iron-oxo complex, and refer to it as $[FeO]^{3+}$ whilst the formal identity of the intermediate remains unknown.

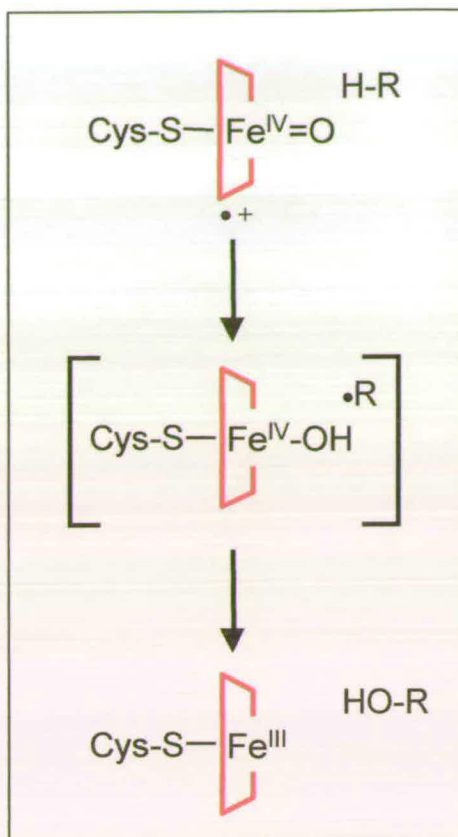


Figure 1.12: The oxygen rebound mechanism applied to cytochromes P450. The porphyrin macrocycle is represented by the red box.

1.1.6 Reaction Types and Substrates of Cytochromes P450

Reaction types:

Despite the conformity of cytochromes P450 to the same catalytic cycle, the variety of reactions catalysed by these versatile enzymes is quite extraordinary. Their ability to catalyse reactions unachievable by conventional synthetic chemical routes under mild conditions, is remarkable. Various explanations have been proposed to explain P450 catalysis, including the generation of mobile oxidants such as superoxide, but the mechanism outlined in Section 1.1.5 (in particular the generation of the $[\text{FeO}]^{3+}$ species and its participation in the oxygen rebound mechanism) have become adopted as the most likely sequence of events leading to reaction.

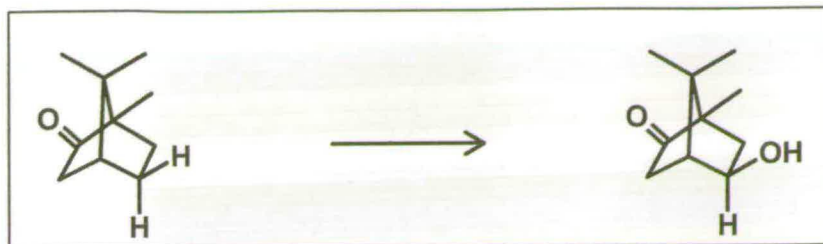


Figure 1.13: Example of carbon hydroxylation performed by cytochrome P450. The 5-*exo* hydroxylation of camphor by P450cam

The compilation of a detailed inventory, listing every reaction type or substrate specificity displayed by the members of the P450 superfamily, would constitute a significant body of work in itself, and hence, is beyond the scope of this thesis. However, it is important to demonstrate these diversities in order to establish a context within which the catalytic importance of these enzymes can be evaluated. The subsequent section is intended to illustrate this point, by considering a few pertinent examples of common, yet diverse, reaction types exhibited by P450s.

Carbon Hydroxylation: This is possibly the most common reaction type displayed by P450s (Figure 1.13). There are many examples of this type of reaction, for example, the hydroxylation of fatty acids (CYP 4A, CYP 102 [68,69]), the 7 α - and 11 β -hydroxylation of steroids (CYP 7, CYP11B1 [70,71]), the 5-*exo* hydroxylation of D-camphor by CYP 101 [72] and the hydroxylation of precursors in the erythromycin biosynthetic pathway (CYP 107) [73].

Aromatic hydroxylation: Aromatic hydrocarbons are notoriously unreactive, the derivatisation of which (by conventional chemical synthetic routes) often requires the use of forcing conditions. The electron-rich nature of these compounds make hydroxylation a particularly difficult reaction to achieve *in vitro*. P450s can catalyse aromatic hydroxylation under mild conditions. The most common mechanism involves initial arene epoxidation, followed by epoxide ring opening, hydride migration to the generated carbocation, and the subsequent tautomerisation of the ketone to give the hydroxylated product [74] (Figure 1.14). This mechanism has been termed the NIH shift. Aromatic hydroxylation has been observed for P450s from hepatic microsomes.

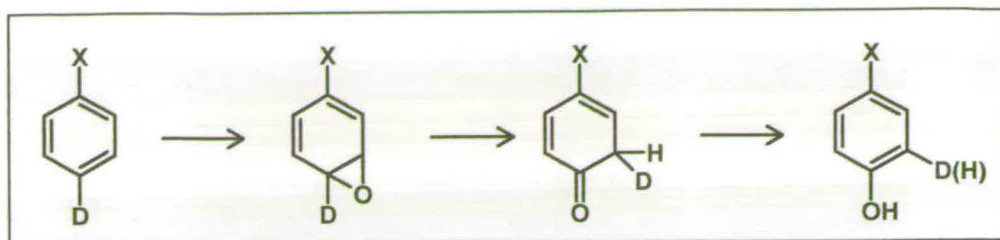


Figure 1.14: The mechanism of the NIH shift for the aromatic hydroxylation by cytochrome P450

Heteroatom Dealkylation and oxygenation: P450s have been shown to add oxygen to, and remove alkyl groups from, heteroatoms within organic substrates. The reactions are limited to compounds containing N, S, P and halogens as heteroatoms. The mechanisms for N-dealkylation and N-oxidation are shown in Figure 1.15, reactions with sulfur and phosphorus are presumed to follow an analogous mechanism, although evidence is limited. As shown in Figure 1.15, oxidation of alkylamines can result in either N-dealkylation or N-oxidation [75,76]. N-oxides are uncommon products, but tend to be favoured over N-dealkylation reactions when the nitrogen atom is locked in a ring system.

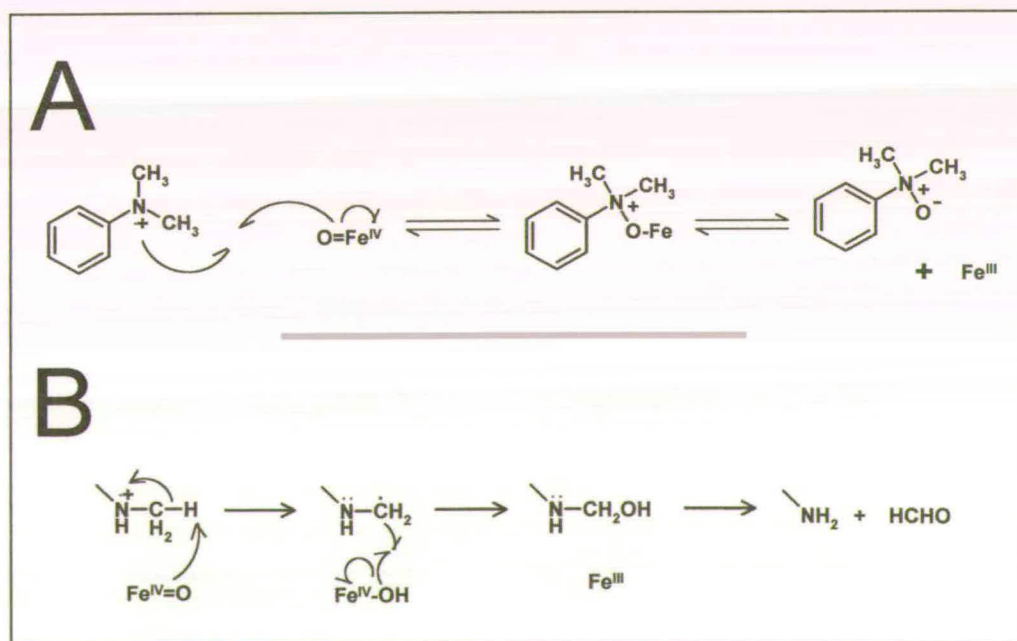


Figure 1.15: The mechanisms of A: N-oxidation and B: N-dealkylation by cytochromes P450

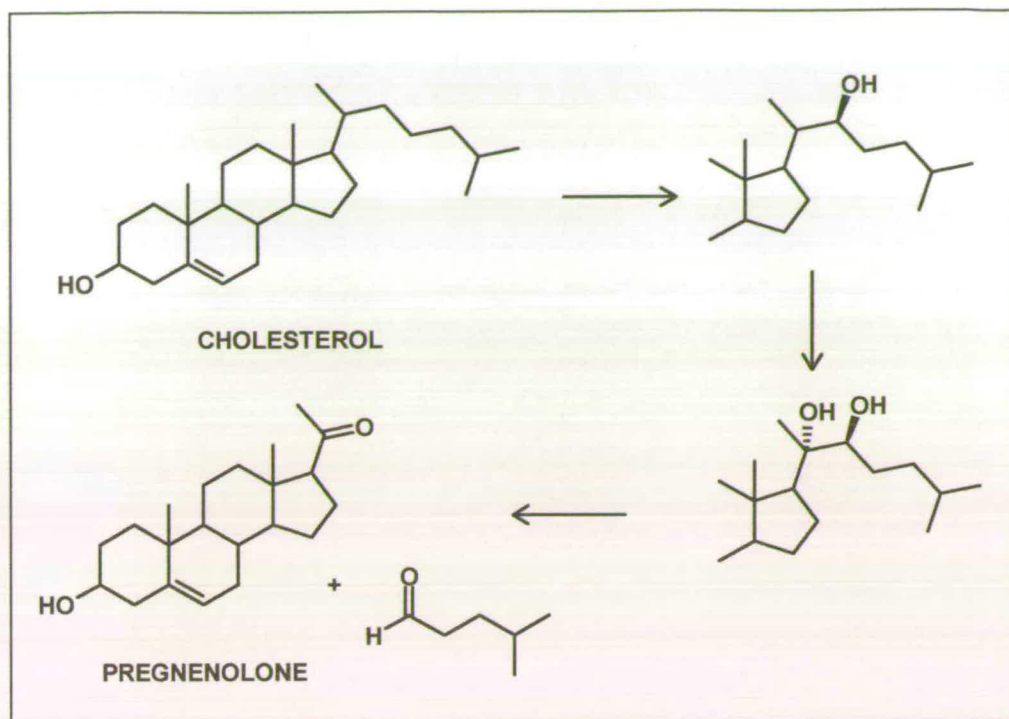


Figure 1.16: An example of the unusual C-C bond cleavage reaction of cytochromes P450. The conversion of cholesterol to pregnenolone catalysed by P450 scc.

Oxidative bond cleavage: The oxidative cleavage of a C-C bond is an example of an unusual, yet vitally important, reaction catalysed by P450s. Illustrative of this is P450scc which is involved in the metabolism of cholesterol to pregnenolone [77]. The oxidative cleavage is the last of three sequential oxygenation steps catalysed by the mitochondrial enzyme (Figure 1.16), each involving the consumption of 1 mole of NADPH and oxygen. The first two steps involves straightforward carbon hydroxylation to generate the 20(S),22(R)-dihydroxy cholesterol [78]. Whilst the first two steps are typical reactions, the mechanism of the third C-C cleavage step is of mechanistic interest. This step can be considered to occur *via* one of two possible mechanisms, involving either an alkoxy radical or the formation of an iron-hydroperoxide intermediate with either the 20(S)-, or 22(R)-hydroxyl group. Members of the CYP11A1 (14 α -demethylation of lanosterol) and CYP 17A (progesterone 17 α -hydroxylase/17,20-lyase) families are also implicated in oxidative bond cleavage reactions [79,80].

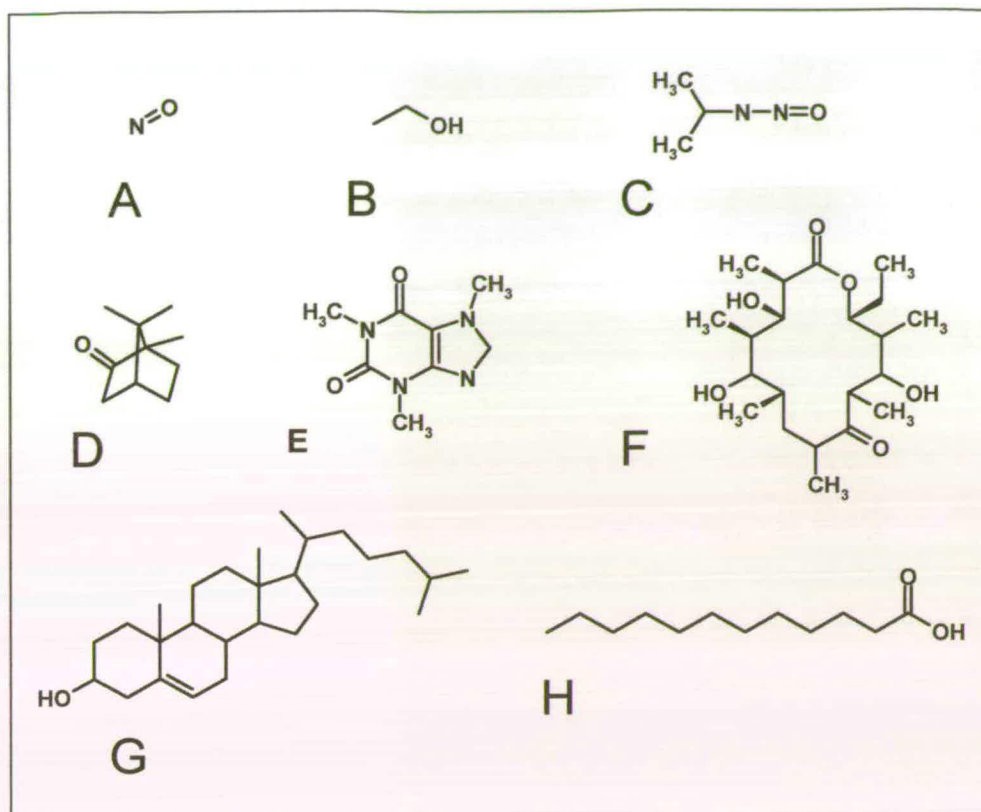


Figure 1.17: A selection of substrates illustrating the wide variety of molecules which act as substrates for cytochromes P450. Shown are the A: nitric oxide (P450 nor), B: ethanol (P450 2E1), C: N-nitrosodimethylene (P450 2E1), D: camphor (P450cam), E: caffeine (P450 1A2), F: 6-deoxyerythronilide B (P450 EryF), G: cholesterol (P450scc) and H: fatty acids (P450 4A and P450 BM3).

Substrate types:

A selection of P450 substrates is shown in Figure 1.17, as an illustration of the diversity of specificities displayed by members of the P450 superfamily. These range in size and reactivity from small diatomic molecules such as nitric oxide (substrate for P450 nor) to large polycyclic compounds such as steroids (eg. substrate for P450 scc). For a more comprehensive compilation of the variety of P450 substrates, the reader is directed to <http://www.icgeb.trieste.it/~p450srv>.

1.1.7 Flavocytochrome P450 BM3

In 1986, Nahri and Fulco reported the barbiturate-induced expression of an immunologically cross-reacting, 119 kDa P450-containing fatty acid hydroxylase

from a number of strains of *Bacillus megaterium* [81]. The soluble P450-containing protein from strain ATCC 14581 is known as flavocytochrome P450 BM3 (P450 BM3) [82]. It is an example of a Class 3 P450, binding all of the necessary redox cofactors in one continuous polypeptide. P450 BM3 is comprised of a 55 kDa N-terminal *b*-type heme-binding cytochrome domain, linked *via* a short, trypsin cleavable, hydrophilic linker to the 66 kDa C-terminal FAD/FMN containing reductase [83]. P450 BM3 is a catalytically self-sufficient fatty-acid hydroxylase, activity is observed in the presence of substrate, oxygen and NADPH without the requirement for additional redox cofactors. The sequence of the intact flavocytochrome [84] was established in 1989 and provided evidence for its synthesis as a single continuous polypeptide (Appendix III) - the DNA encoded both domains within the same continuous reading frame. It has the highest activity of any isolated P450 to date, probably as a result of the close association of the redox cofactors, and the requirement for intramolecular as opposed to intermolecular electron transfer.

Substrate specificity of P450 BM3

P450 BM3 catalyses the subterminal (ω - n , where $n = 1-3$) hydroxylation of saturated and non-saturated long chain fatty acids, modest activity toward long chain alcohols and amides [69], as well as the mid-chain epoxidation of monounsaturated fatty acids [85] has also been reported. The crystal structure of the substrate-free [86] and palmitoleate-bound [87] forms of the heme domain of P450 BM3 have been solved, and enable an insight to be gained as to the reasons for, and determinants of, the observed substrate specificity. In contrast to the compact active site of P450cam [88], the active site of P450 BM3 consists of a long, hydrophobic channel, extending from the distal face of the heme to the protein surface, ideal for the binding of long-chain fatty acids. The hydrophobicity of the active site is a major factor in substrate binding, facilitating the partitioning of these lipophilic substrates from the aqueous bulk solvent, e.g. it has been shown that linear hydrocarbons (e.g. dodecane) can act as substrates. In addition to these hydrophobic effects, a number of residues located within the active site provide important interactions, these are discussed in detail.

Y51/R47 binding motif: At the mouth of the active site are located the residues Y51 and R47. Fatty-acid substrate binds to P450 BM3 and forms two important interactions with the carboxylate head, namely a hydrogen bond from Y51 and a salt bridge to R47 (Figure 1.18). Site-directed mutagenesis studies have shown that the formation of the salt bridge to be the most important of the two interactions, whilst Y51 may play a more important role in transition state stabilisation.

F42: One further notable residue at the mouth of the active site is F42, which appears to cover the mouth of the active site, providing what might be termed a hydrophobic lid. Presumably the presence of such a lid would help to maintain the hydrophobicity of the active site, as well preventing water from disrupting the favourable R47 ion pair interaction.

F87: Phenylalanine 87 is located at the base of the active site, whose conformation changes when substrate binds. In the substrate-free structure, the phenyl sidechain of F87 is at an angle, perpendicular to the heme plane, yet when substrate-binds, the

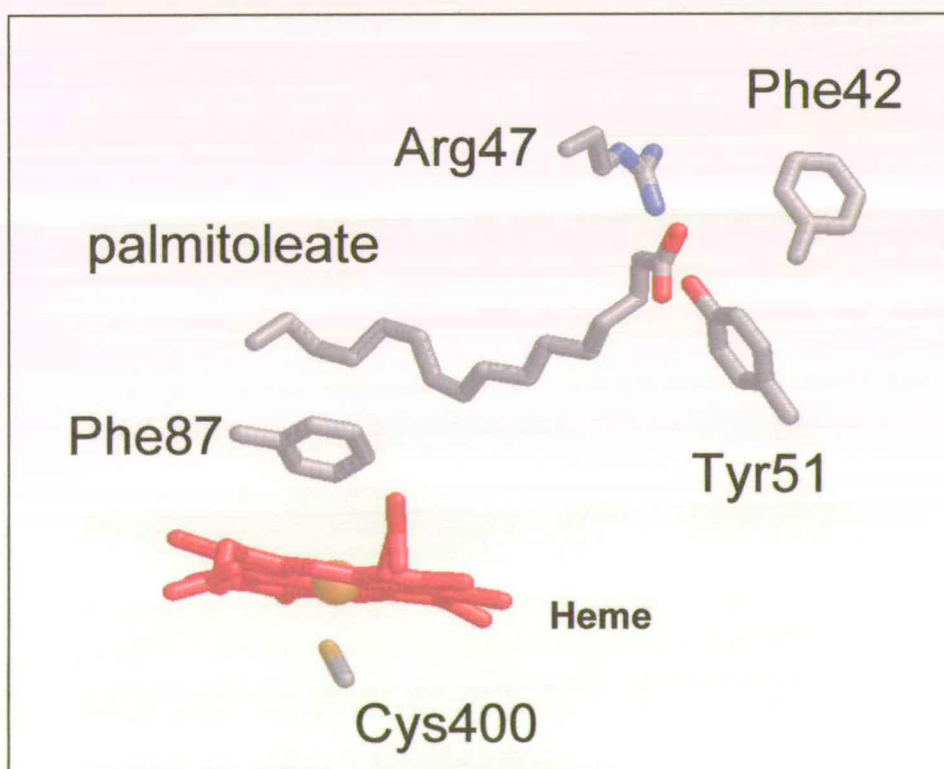


Figure 1.18: Key active site residues in P450 BM3, implicated in substrate binding (Arg47/Y51), the control of regiospecificity of hydroxylation (Phe87) and prevention of water entry into the active site during turnover (Phe42). Also shown are the substrate (palmitoleate), the heme, and the cysteine heme ligand (Cys400).

ring adopts a more parallel alignment relative to the heme. This feature has control over the regiospecificity of P450 BM3, as it prevents the ω -terminus of the fatty acid from becoming hydroxylated. Consistent with this, substitution of F87 by alanine converts P450 BM3 from a fatty acid hydroxylase that hydroxylates at the ω -1 to ω -3 positions, to one that performs terminal ω -hydroxylation [89], a reaction not observed for wild-type P450 BM3 (yet one which is common to many mammalian P450s such as the members of the 4A1 family). This change in regiospecificity was also accompanied by a decrease in the K_d for laurate binding, suggestive of an increase in the affinity of the enzyme toward medium chain length fatty-acids (e.g. C₁₂).

Modelling studies have shown that the absence of the phenyl sidechain enables the ω -terminus of laurate to approach closer to the heme in the F87A mutant than in wild-type (ω -CH₃...Fe = 5.1 and 3.1 Å respectively) [45]. This may provide evidence for the mixed product distribution observed for wild-type P450 BM3, and the almost exclusive (> 90 %) ω -terminal hydroxylation demonstrated by the F87A variant.

Electron transfer in P450 BM3:

As mentioned earlier, flavocytochrome P450 BM3 is a catalytically self-sufficient fatty acid hydroxylase. As a result, it provides a unique system, ideal for studying the intimate steps which comprise the total electron transfer reaction from NADPH to product, without the complications that arise from protein-protein recognition and interaction steps required for other bacterial or eukaryotic systems. The driving force for the reaction is the large, positive difference between the midpoint potential of NADPH reduction ($E_o = -320$ mV vs SHE) and that of the highly oxidising oxy-ferryl species ($E_o \sim +1.8$ V vs SHE) [90]. The electron-transfer steps are outlined in Figure 1.19 and are discussed below. Hydride transfer from NADPH is the first step in the electron-transfer pathway in P450 BM3, and results in the transient formation of the two electron reduced hydroquinone form of FAD. The fully reduced FAD is thermodynamically less stable relative to either its semiquinone-form or the less negative potential FMN of the same domain, hence spontaneous, thermodynamically

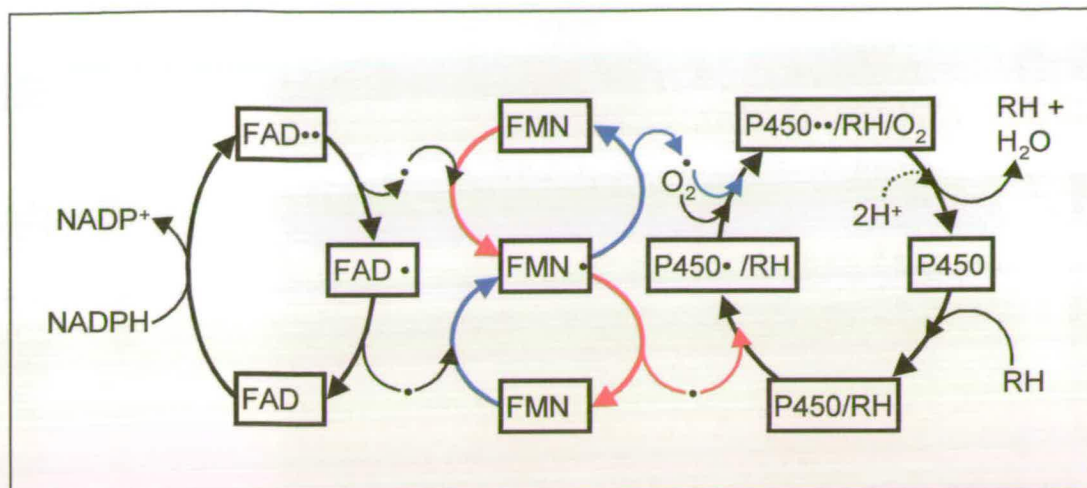


Figure 1.19: Electron transfer steps in flavocytochrome P450 BM. Electrons are transferred to the FAD from NADPH by hydride transfer. Electrons are shuttled through the FAD and FMN and onto the heme at strategic points in the catalytic cycle. The red and blue arrows relate to the transfer of the first and second electrons through the FMN to the heme respectively (as the FMN only cycles through its FMN_{ox}/FMN_{sq} states).

favourable, electron transfer occurs from the $FADH_2$ to generate the $FMNH_2$ (reduction potentials for all of the species have been determined [40,91], and are shown in Table 1.2). In the case of the FMN, the two electron reduced hydroquinone form is more stable than its one electron reduced

Table 1.2: Midpoint reduction potentials for the flavin cofactors in P450 BM3

	$F_{ox} + 2e^- \leftrightarrow F_{red}$ (mV)	$F_{ox} + e^- \leftrightarrow F_{sq}$ (mV)	$F_{sq} + e^- \leftrightarrow F_{red}$ (mV)
diflavin FAD	-332	-292	-372
diflavin FMN	-203	-213	-193
holoenzyme FAD	-	-289	-
holoenzyme FMN	-196	-216	-177
FAD domain	-303	-269	-337
FMN domain	-192	-206	-177

semiquinone form. This stability is so pronounced that formation of the FMN hydroquinone allows the formation of a three-electron reduced reductase, a dead-end complex from which heme reduction cannot occur. It has been proposed that the FMN cycles only through its oxidised and semiquinone states and that second

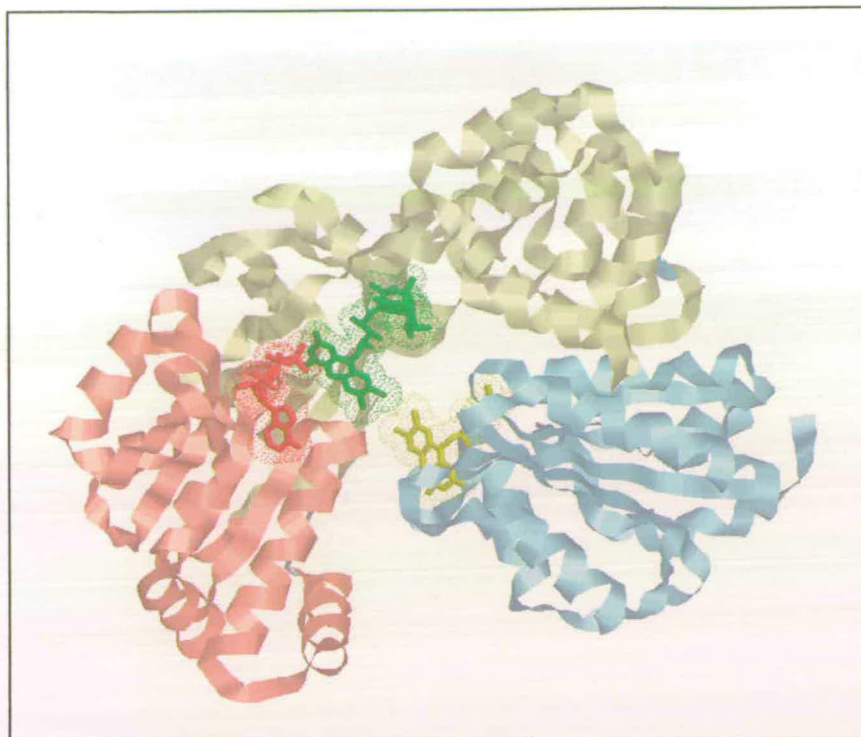


Figure 1.20: The crystal structure of the mammalian NADPH-dependent cytochrome P450 reductase. The NADPH (red), FAD (green) and FMN (yellow) cofactors are clearly visible and in close proximity to each other.

electron transfer occurs *via* a thermodynamically unstable red anionic semiquinone [92]. The lifetime of this species is short and hence its reduction potential remains unknown so experimental confirmation of this scenario is still required.

The most probable route of interflavin electron transfer is through-space (see Section 1.2.1) involving no intervening species, as the recently solved crystal structure of the mammalian P450 reductase [93] shows the FAD and FMN to be exposed and within van der Waals contact (Figure 1.20). Although the structure of P450 BM3 reductase has not been solved, sequence alignments show a high degree of identity between the two proteins, so the arrangement of FAD and FMN in P450 BM3 is likely to be the same. Electron transfer from the FMN to the heme occurs by 2 sequential, one electron transfers at appropriate points in the catalytic cycle, the first of which cannot occur until the long-chain fatty acid has bound (and induced the increase in reduction potential discussed in Section 1.1.5). Once substrate has bound, the first electron transfer to heme becomes more thermodynamically favourable. The sequence of events after first flavin to heme electron transfer (oxidising the FMN_{sq} to the FMN)

must be rapid, i.e. ferrous-oxy formation, else the transient FMN_{sq} semiquinone would decay prior to supplying the second reducing equivalent to the heme. Once oxygen has bound, the final electron transfer can take place (from FMN_{sq} to the FMN), committing P450 BM3 to the unavoidable sequence of events that lead to hydroxylation. Under low physiological concentrations of NADPH, P450 BM3 reductase never becomes more than two-electron reduced. This is believed to be due to the tight binding of NADP⁺ which prevents recombination with another molecule of NADPH prior to the completion of the electron-transfer event [94]. At high concentrations of NADPH, the reductase can adopt an inactive three-electron reduced form, caused by the competitive displacement of NADP⁺ by NADPH. The formal route of FMN to heme electron transfer has not been established, although it has been discussed in a recent publication reporting the solution to the crystal structure of a complex between the FMN- and heme-domains to 2 Å resolution [95]. The authors propose a convoluted route for protein mediated flavin-to-heme electron transfer which is consistent with their structure (Figure 1.21), but which is unlikely for a number of reasons. These include non-stoichiometric equivalents of FMN and heme in the asymmetric unit, the excessively long edge-to-edge distance from FMN to heme and that a direct, through space route would be more appropriate than the doubtful proteinaceous pathway proposed. It is likely that the reported structure is an artefact of crystallisation and not a true representation of the catalytically competent electron transfer complex. Also, the linker region between the FMN and the heme is missing in the structure, suggesting the structure is that of two proteolysed fragments.

The FMN in the mammalian P450 reductase structure is partially exposed to the solvent, a feature which supports the idea that FMN to heme electron transfer is more likely to occur directly, through space, rather than through bond. In fact, a modelled complex [96] of the two fragments gave a single, energy minimised solution, with a more satisfactory distance of closest contact of 9 Å, within which a through space model of electron transfer could be envisaged (Figure 1.22). This would also be more consistent with the high rates of heme reduction (wild-type, $k_{\text{lim}} = 360 \text{ s}^{-1}$ in the presence of arachidonate) that have been reported.

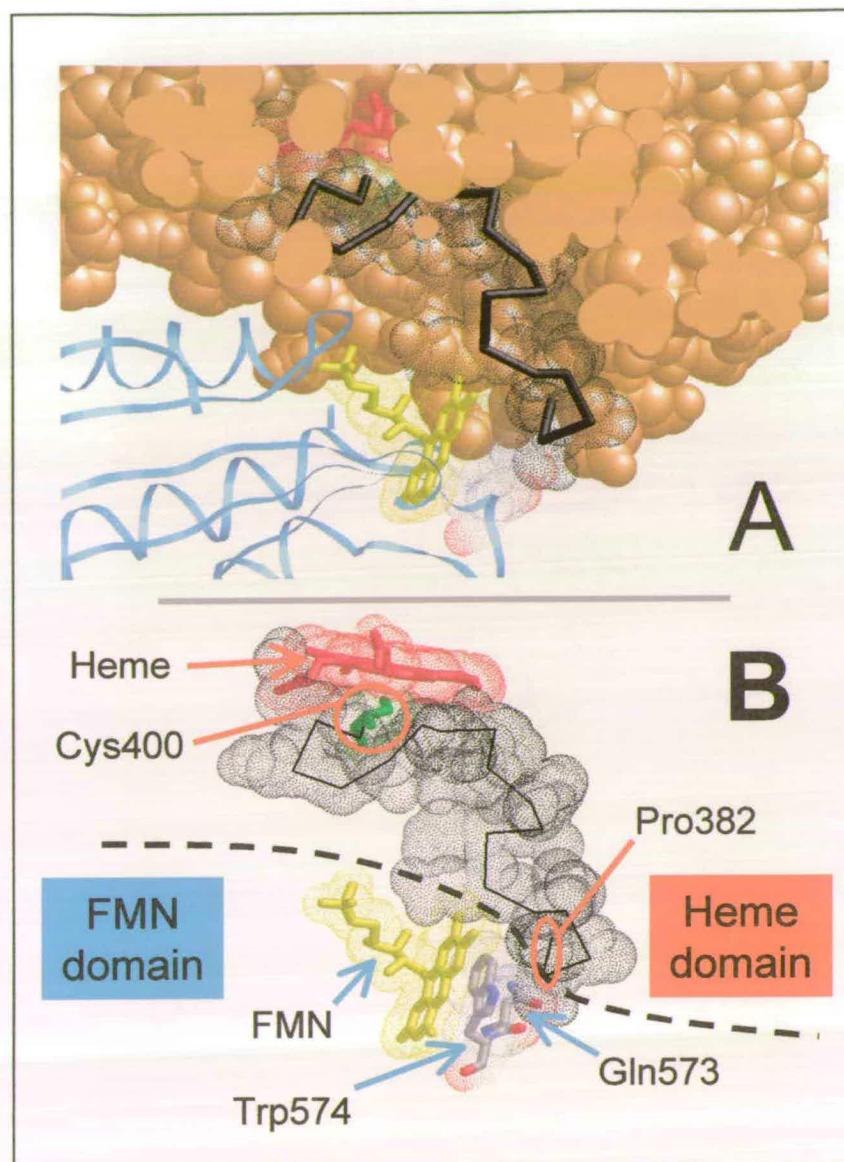


Figure 1.21: The proposed FMN/P450 BM3 electron transfer complex. Panel A shows the relative orientation of the FMN domain (blue) with respect to the heme domain (orange). Panel B shows more clearly the orientation of the FMN relative to the heme, and the proposed through bond electron transfer pathway (black).

1.2 Biological Electron Transfer

The general principles by which cells obtain energy from their environment are central to cell biology. All animal and plant cells are powered by chemical energy stored in the chemical bonds of organic molecules. This stored energy is inaccessible to the cell directly, and hence must be 'extracted' in a usable form, this is achieved by a process of gradual oxidation, often catalysed by proteins. This oxidation is not

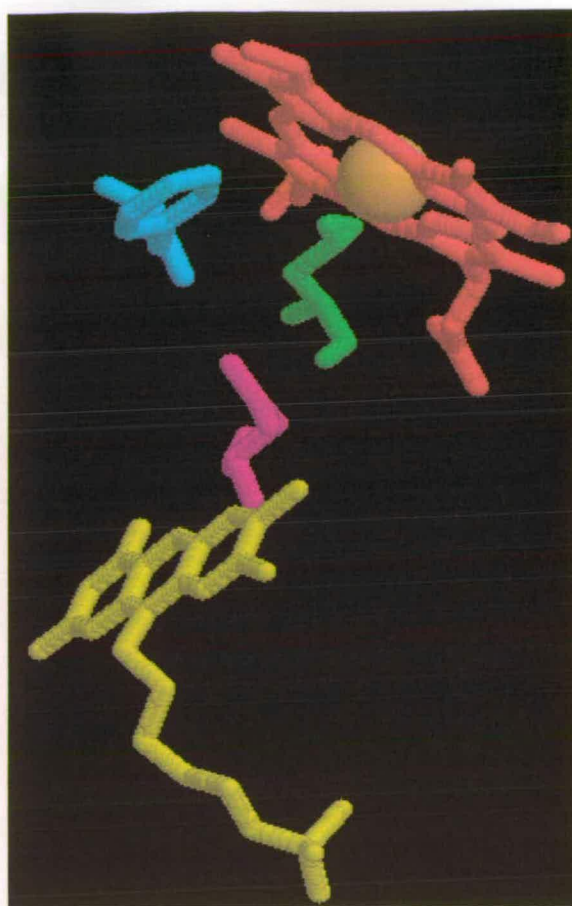


Figure 1.22: An energy minimised model of the interaction of the FMN domain with the heme domain of P450 BM3. Here, the FMN (yellow) adopts a more likely orientation with respect to the heme ligand (Cys400, green), allowing a direct through space electron transfer (9 Å) from the N5 nitrogen of FMN to the heme to be envisioned. Also shown are Phe393 (cyan) and an intervening residue Asn537 (magenta).

necessarily due to the direct reaction with oxygen, but due to the transfer (loss) of electrons. Often these molecules are substrates for oxidoreductases, which catalyse substrate oxidation, coupled to the reduction of a cosubstrate or cofactor. In oxidoreductases, there are three different classes of electron-transfer reaction [97]:

Electron pair exchange: The cooperative removal or insertion of a pair of electrons (e.g. NADPH hydride transfer). Typical transfer distances 3- 6 Å.

Transduction: Involving a redox centre which can accumulate multiple electrons, yet which can transfer them in multiple, single electron transfer events (e.g. FMN of

P450 BM3 can accumulate two electrons from the FAD, yet transfers single electrons to the heme at strategic points in the catalytic cycle).

Non-adiabatic electron transfer: The transfer of electrons between two weakly coupled intra- or inter-molecular redox centres e.g. in the capture of light energy during photosynthesis (driving the reduction of CO₂ and H₂O to generate O₂ and carbohydrates), or in mitochondrial respiration (the four electron reduction of oxygen to water which drives ATP synthesis).

1.2.1 Marcus Theory

Traditionally, the enzymatic view of the chemical potential energy surface of an adiabatic reaction involves the energy minima of reactant and product separated by an activation barrier. The activation energy (i.e. the height of the barrier) can be empirically evaluated by measuring the temperature dependence of the reaction. However, it is difficult to estimate the height of this energy barrier based on the relative energies of the reactants and products alone.

This problem is circumvented in non-adiabatic long range electron transfer, as the reactant and product energy surfaces are not strongly coupled. Marcus theory [98] describes a basic treatment for non-adiabatic, long range electron transfer, which considers the reactants and products as simple harmonic oscillators, lying in separate parabolic potential energy wells. In order for reaction to occur, the energy and nuclear configuration (according to the Franck-Condon principle) of the reactants and products must be identical: the point which corresponds to the intersection of the two parabolas (Figure 1.23).

The activation energy, ΔG^* , is related to the overall driving force, ΔG , and the reorganisation energy, λ (the energy required to change the nuclear configuration of the product to that of the reactant without undergoing electron transfer), by the following equation:

$$\Delta G^* = (\Delta G + \lambda)^2 / 4\lambda$$

and hence to the rate of electron transfer according to the gaussian function:

$$k_{ET} = k_{max} e^{-(\Delta G + \lambda)^2 / 4\lambda k_B T}$$

where k_{ET} is the observed electron transfer rate, k_{max} is the electron transfer rate when ΔG^* is zero and k_B is the Boltzmann constant.

According to Marcus theory, for a given system, variation of ΔG (with constant λ) causes the parabolas to shift relative to each other, which has a direct effect on the rate of electron transfer. Three distinct cases can be observed and are depicted in Figure 1.24 and are termed the *normal* ($\lambda > -\Delta G$); *activationless* ($\lambda = -\Delta G$); and

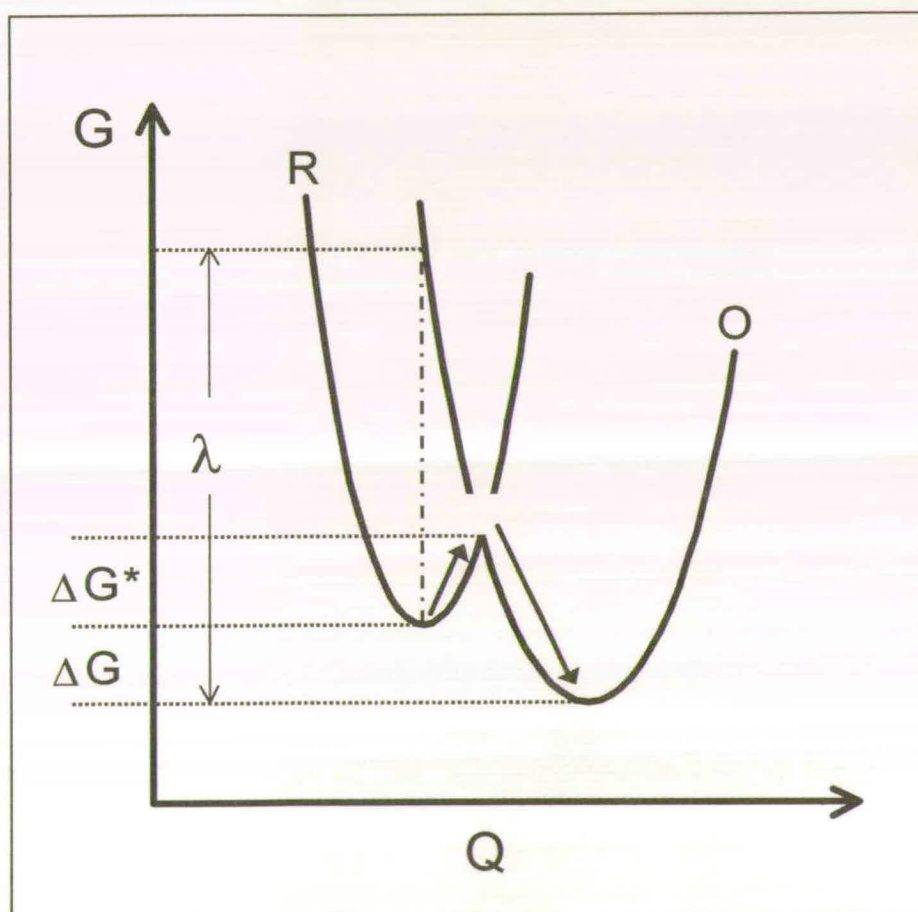


Figure 1.23: A schematic diagram describing the relationship between free energy (G) and nuclear displacement (Q) for a typical electron transfer reaction between reduced (R) and oxidised (O) species. Electron transfer occurs at the intersection of the two parabolas. ΔG is the free energy change of reaction, ΔG^* is the activation energy and λ is the reorganisation energy

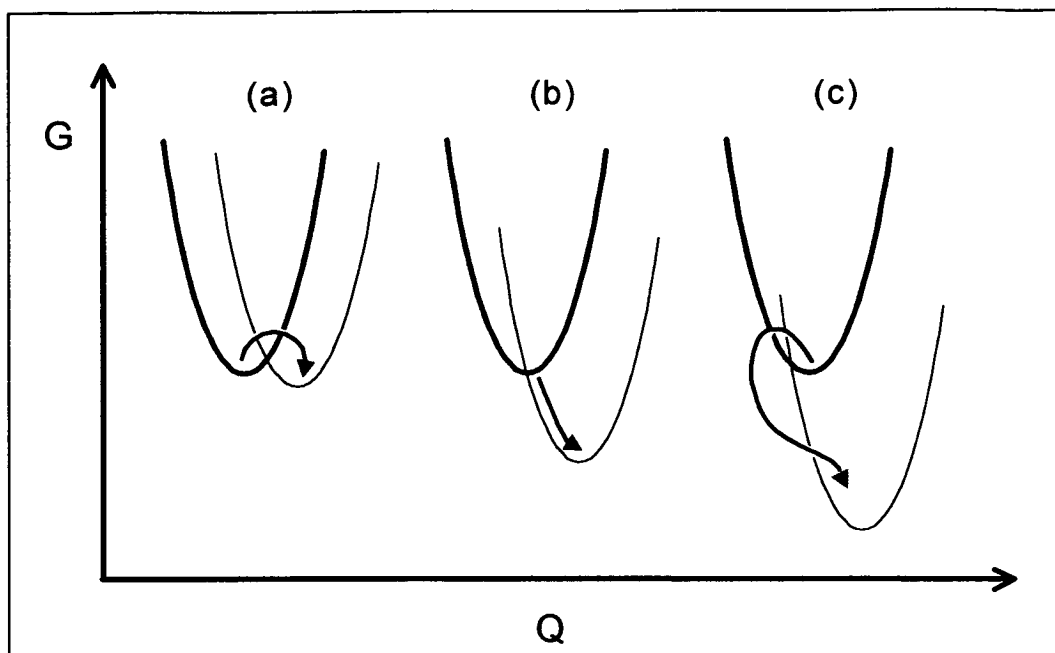


Figure 1.24: Potential energy diagrams showing the conditions required for (a) 'normal' electron transfer, (b) 'activationless' electron transfer and (c) electron transfer in the Marcus' inverted' region. Axes are labeled as in Figure 1.23.

inverted ($\lambda < -\Delta G$) regions. In the activationless region, there is no activation energy barrier to surmount, at this point, $k_{ET} = k_{max}$. The inverted region is counter-intuitive, as the activation energy for electron transfer increases as the driving force increases, slowing electron transfer. The variation of k_{ET} with ΔG is shown in Figure 1.25.

The electron transfer rate is proportional to the overlap of the donor and acceptor electronic wavefunctions across the space separating the electron donor and acceptor molecules, the greater the degree of overlap, the faster the rate. This overlap deteriorates exponentially with edge-to-edge distance (d) and is modified by a coefficient (β) which describes the contribution made by the intervening medium in propagating the wavefunction. The rate of decay is given the value β such that:

$$k_{max} \propto e^{-\frac{1}{2}\beta(d-d_0)}$$

This relationship yields a maximal electron transfer rate at van der Waals contact range for two redox cofactors (3.6 Å) of 10^{13} s^{-1} which is consistent with the characteristic frequency of the nuclei considered in the Franck-Condon term, and the transient lifetime of the encounter complex. According to Marcus theory, the

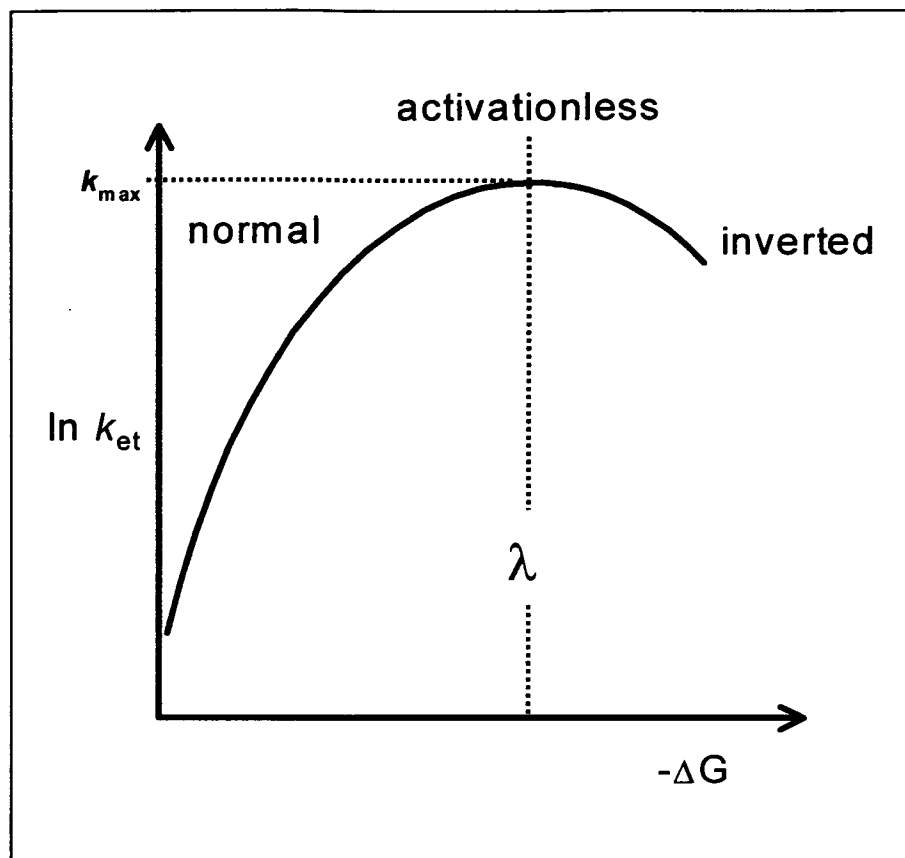


Figure 1.25: The variation of the logarithm of the electron transfer rate constant (k_{ET}) with free energy between reactants and products (ΔG).

proportionality constant for the equation above is $(4\pi^3/h^2\lambda k_B T)^{1/2} \cdot H_0^2$, where H_0 is the coupling matrix element at distance d_0 .

Values of β vary, depending on the nature of the intervening medium, *in vacuo* $\beta = 2.8 - 3.5 \text{ \AA}^{-1}$ [99,100] and 0.9 \AA^{-1} for covalently bridged redox centres in synthetic systems [101] and 0.7 \AA^{-1} for a peptide bond. Dispute remains over the nature of β for a protein matrix, the two major schools of thought are discussed below.

The *through space* model for electron transfer necessitates only a single value for β (1.4 \AA^{-1}), with electron transfer occurring directly from donor to acceptor, regarding the intervening protein as a homogenous matrix akin to an organic glass [99,102,103]. The photosynthetic reaction centre from *Rhodobacter sphaeroides* has provided the majority of the experimental evidence for this hypothesis. The

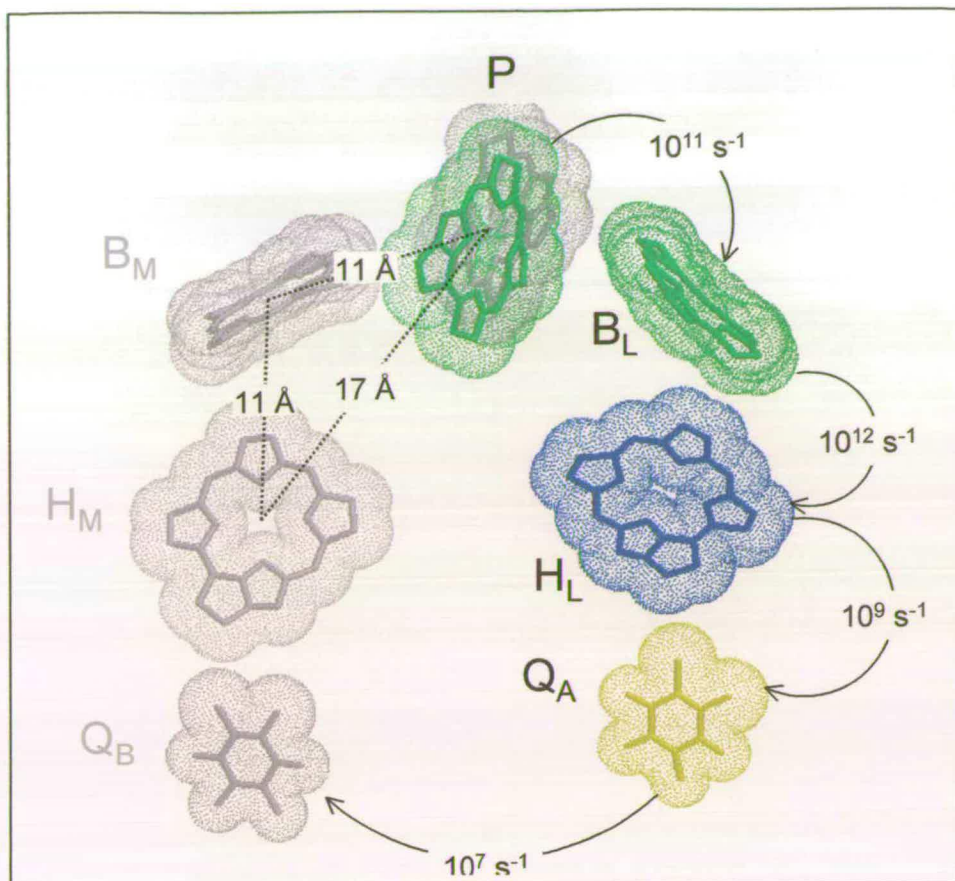


Figure 1.26: A simplified representation of the photosynthetic reaction centre from the bacterium *Rhodobacter sphaeroides*, clearly showing the close proximity of the redox cofactors. Site P is a bacteriochlorophyll dimer (BChl₂), B are bacteriochlorophyll monomers (BChl), H are bacteriopheophytins (Bph) and Q are quinones. The approximate rate constants are given for the electron transfer steps indicated by the arrows.

efficiency of the photosynthetic reaction centre is due to the well organised array of redox cofactors (Figure 1.26 Dutton 1992) which has evolved to optimise the harvesting of energy directly from the sun. The through space model provides a good description for these types of system, where the cofactors are sufficiently well arranged to maximise orbital overlap and facilitate electron transfer. Such specialised systems are the exception rather than the rule, and may not provide a suitable basis for a universally rigorous model for electron transfer.

In such redox systems where the cofactors are less well organised, or the intervening matrix is more heterogeneous [104], the *through bond* model may be more applicable. This alternative description considers the route long range electron transfer to occur *via* a series of combinations of discrete tunnelling pathways through

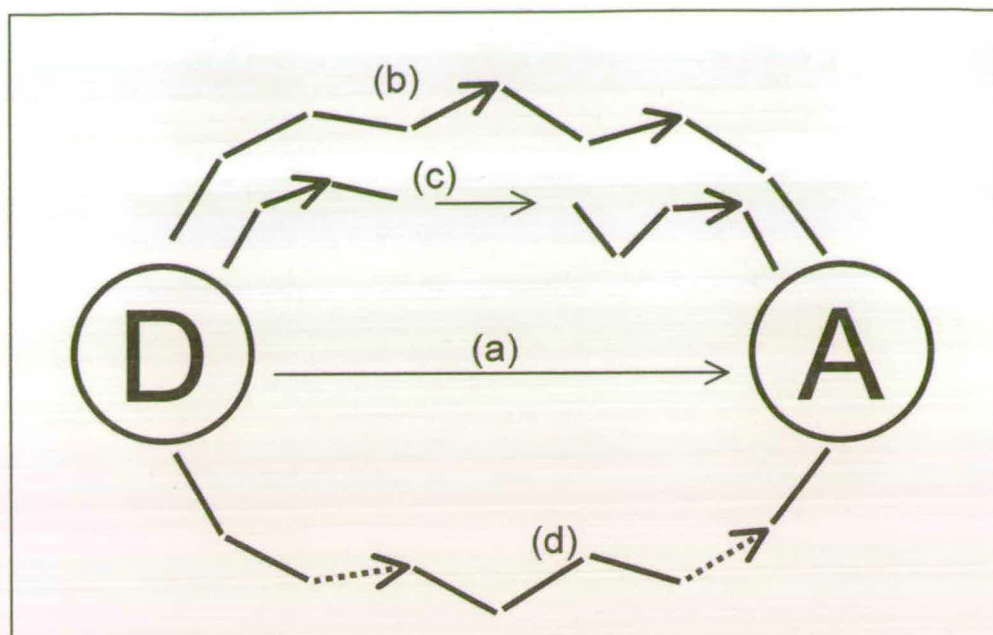


Figure 1.27: Schematic diagram illustrating the various types of pathways for electron transfer from donor (D) to acceptor (A): (a) direct through-space (thin continuous arrow); (b) through-covalent bond (thick line); (c) through-bond and a hop through-space; (d) through covalent and hydrogen-bond (dotted line) pathways.

covalent σ -bonds, hydrogen-bonds, or short through-space hops which comprise a distinct pathway through the intervening medium [100,105,106]. A simplifying approximation can be made that the coupling through all covalent bonds is the same, and the coupling through a hydrogen bond is comparable to that across two covalent bonds, and that a through space hop is distance dependent (Figure 1.27). Evidence to support this model comes from the study of ruthenated derivatives of cytochrome *c* [107]. The variation in electron-transfer rates from ruthenated histidines at differing distance from the heme correlate better with the through bond model, rather than a single exponential dependence on distance. The azurin from *Pseudomonas aeruginosa* displays an anomalous rate of decay (1.1 \AA^{-1}) as a result of a heterogeneous matrix arising from preferential electron transfer through its β -sheet domain as opposed to its α -helical domain [108].

1.2.2 Conclusions

Whilst dispute remains over whether or not specific pathways are involved to mediate biological electron transfer, it is clear that rates are fundamentally dependent

on the distance of separation between the redox centres, the reorganisation energy for the process and the overall driving force of reaction. Obviously, the intervening protein serves a role in the mediation of electrons but can equally be thought of as an insulator or a conductor. The amalgamation of conducting and insulating regions could be considered as a homogenous glass, or the separation of conducting regions by insulating regions considered as a pathway. Interestingly, in the physiological cytochrome *c*:cytochrome *c* peroxidase complex, regarded as the quintessential example of an optimised through-bond electron transfer pathway (Figure 1.28), the route also constitutes the shortest through-space distance.

Ultimately, the choice of through-bond vs through-space is likely to reduce to one of semantics, as there is evidence in support of both, but proponents of both models agree that the participation of the protein matrix is essential to propagate electron transfer (the rate of electron transfer through a protein is attenuated an order of magnitude slower than through a vacuum for each 1.7 Å of separation between redox centres). In the absence of a universally consistent theory, it may be more acceptable to regard electron transfer from a dual perspective, combining features from both models where appropriate. In situations where a high density of redox centres are present (cell membranes, photosynthetic reaction centre etc.), a through space model would be more suitable, whereas if the redox centres were remotely spaced, a through bond, tunnelling approach could conceivably provide a selection of the minimally attenuated, favoured pathways. In many situations, the decision can be made intuitively, for example, if the edge-to-edge distance between donor and acceptor is a few angstroms, then electron transfer is more likely to proceed directly through space, as opposed to negotiating a convoluted through-bond tunnelling pathway. Conversely, if both donor and acceptor are buried within the protein, then a conduit for electron transfer may be expected and satisfied by a tunnelling pathway. Defined pathways such as these may act as control mechanisms, serving to promote the coupling of electron transfer solely between physiological redox partners, preventing the possibility of unfavourable transfers to other non-physiological redox cofactors in the cellular environment.



Figure 1.28: Illustration of the electron transfer complex between cytochrome c (orange) and its physiological redox partner yeast cytochrome c peroxidase (blue). The heme cofactors of each protein are shown in red. The proposed through bond electron transfer pathway is composed solely of residues from cytochrome c peroxidase (residues 191-194, black). Trp194 can act as a redox mediator itself by converting to/from its free radical form.

Statistically less probable events such as molecular collision, interprotein recognition and the dynamics of protein association (e.g. the intramolecular interaction of reductase and heme in P450 BM3, or the intermolecular association of putidaredoxin reductase/putidaredoxin/P450cam) are more likely to have a governing influence over the absolute rate of electron transfer, than the precise route of electron transfer between cofactors. Once all of the relevant components of a redox system are assembled, and so long as the overall driving force of the reaction is large, the flow of electrons will occur regardless of either the nature of, or the route to, intermediates along the pathway. A metaphor for this would be the course of a river. Irrespective of the number of twists, turns, pools or waterfalls which obstruct the flow of water, the driving force (i.e. the height of the spring above sea level) is always sufficient to

convey the water downhill to the sea. The importance of distance can also be appreciated in this analogy, as although the river may meander its way to the sea, a shorter, hence faster path (i.e. a straight pipeline) can be envisioned.

Chapter 2:

Methods and Materials

2 METHODS AND MATERIALS

2.1 Site-Directed Mutagenesis (with Dr. C.S.Miles)

Site-directed mutagenesis was performed by the Kunkel method of non-phenotypical selection [109], to generate the F393A, F393H and F393Y mutations. *E. coli* strain TG1 [*supE*, *hsdΔ5*, *thi*, $\Delta(lac-proAB)$, F' [*traΔ36*, *proAB*⁺, *lacI*^q, *lacZΔM15*]] was used for all cloning work and for overexpression of intact P450 BM3 and its component cytochrome domain. The preparation of plasmids for the overexpression of intact P450 BM3 (pBM23) and heme domain (P450, residues 1-472; pBM20) has been described in previous publications [110,111]. Mutants F393A, F393H and F393Y (intact) and F393A HD, F393H HD and F393Y HD (HD denotes Heme Domain) were constructed by oligonucleotide-directed mutagenesis of pBM23 and pBM20 respectively. Single-stranded DNA was prepared using the helper phage M13KO7. Oligonucleotide primers used in the mutagenesis procedures are shown in Table 2.1 (mismatches are indicated by the underlined bases and the names of the resulting expression plasmids are in parentheses).

Table 2.1: Oligonucleotide primers used in the mutagenesis procedures

Mutant enzyme	Plasmid code	Oligonucleotide primer
F393A	pCM36	5' CTGACCGTTTCCAG <u>CC</u> GGTTTAAACGC 3'
F393A HD	pCM80	
F393H	pCM37	5' CTGACCGTTTCCAT <u>G</u> CGGTTTAAACGC 3'
F393H HD	pCM81	
F393Y	pCM109	5' CCGTTTCCATA <u>C</u> GGTTTAAAC 3'
F393Y HD	pCM125	

To ensure that no secondary mutations had occurred, pCM 36, pCM37, pCM109 and pCM125 were sequenced by the dideoxy chain termination method. These plasmids were digested with restriction enzymes *Sna*BI and *Spe*I, generating a 3 kbp fragment containing the required mutation. The *Sna*BI/*Spe*I fragment was then ligated with the

4 kbp band liberated from a similar digestion of pBM23 (containing the WT P450 BM3 coding sequence under the control of the native CYP102 promoter) generating pJM1, pJM2 and pJM3 respectively.

Mutants were overexpressed in *E. coli* strain TG1 in an identical fashion to the wild-type clone.

2.2 Transformation of *E. coli*

5 to 10 ng of supercoiled plasmid DNA were added to 100 μ l of competent *E. coli* cells (pre-treated with 50 mM CaCl_2) in a 1.5 ml eppendorf tube and left on ice for 30 minutes. The cells were then heat shocked at 42 °C for 90 seconds and returned to ice for 5 minutes. 1 ml of LB broth was added to the cells, and were subsequently incubated at 37 °C for 1 hour. The cells were then pelleted in a microfuge (1 min, 12,000 g) and resuspended in 100 μ l LB broth. Aliquots (25 μ l and 75 μ l) were spread onto LB-agar plates supplemented with 100 μgml^{-1} ampicillin. The plates were incubated overnight at 37 °C.

2.3 Growth of *E. coli*

20 ml starter cultures of *E. coli* were grown in LB broth (Table 2.2) supplemented with 25 μgml^{-1} final concentration of carbenicillin (1 μml^{-1} , 25 mgml^{-1} stock in ultrapure water), at 37 °C inoculated from single colonies on LB-agar plates using a sterile wire loop. Cultures were grown overnight in a shaker-incubator. A 1 ml aliquot from each starter culture was pelleted by centrifugation to check for overexpression (pale pink colouration).

Different strategies were employed for the large-scale growth of the intact flavocytochromes and the isolated heme domain proteins. *Inact flavocytochromes*: 1 ml of overnight starter culture was used to inoculate by sterile transfer, litre flasks (unbaffled) containing 400 ml of LB broth supplemented with 25 μgml^{-1} final concentration of carbenicillin. Flasks were grown for 24 hours at 37 °C, 200 r.p.m. without induction (proteins constructed from clone pBM23 retained the native

CYP102 promoter sequence, which allowed constitutive expression in the stationary growth phase) in a shaker-incubator. *Heme domains*: 1 ml of overnight starter culture was used to inoculate by sterile transfer, litre flasks (baffled) containing 200 ml of terrific broth supplemented with 25 μgml^{-1} final concentration of carbenicillin. Flasks were grown for 6 hours at 37 °C followed by a further 42 hours at 30 °C, at 100 r.p.m. without induction (under these conditions, the heme domain proteins were found to overexpress to high levels without the requirement for IPTG) in a shaker incubator.

Cells were harvested by centrifugation (15 minutes at 6000 g) in a Sorvall RC-5B centrifuge, using a SLA 3000 head, and stored at -20 C as frozen cell paste prior to protein purification. Typical cell yields, harvested from 5 l of either LB or TB culture were 20 g and 50 g respectively (wet weight).

Table 2.2: Growth media and agar

Luria Bertani broth (LB)	per litre: 10 g Tryptone; 5 g Yeast extract; 5 g NaCl.
Terrific broth (TB)	per litre: 20 g Tryptone; 10 g Yeast extract; 4 ml glycerol (800 ml), KH_2PO_4 2.6 g; Na_2HPO_4 4.3 g (200 ml). Broth and buffer solutions were autoclaved separately to avoid precipitation. Once cooled, broth and buffer were combined by sterile transfer (to 1 litre total) and sub-divided into 200 ml growth volumes.
All broths were prepared with Millipore Q ultrapure water and autoclave sterilised at 121 °C and allowed to cool to room temperature prior to addition of carbenicillin.	
LB-agar plates	Agar 15 g l^{-1} dissolved in LB (Table 2.1) Sterilised LB-agar solution was allowed to cool to the touch prior to addition of ampicillin (50 $\mu\text{g l}^{-1}$). Cooled agar was poured into sterile petri dishes before solidification. Once poured, plates were kept refrigerated at 4 °C and used within 1 week of manufacture.

2.4 Purification of Flavocytochrome P450 BM3

The purification of both intact flavocytochromes and heme domain proteins of P450 BM3 outlined here follow a well established protocol [112]. The procedure for the

purification of each type of protein is essentially identical and are treated as such in this section. Specific differences will be remarked upon where appropriate.

Cell lysis

Frozen cell paste was defrosted at room temperature prior to resuspension in approximately 50 ml of ice cold Buffer A (Table 2.3) to which was added 1 ml of 60 mgml⁻¹ PMSF (EtOH) to prevent proteolysis. Lysis was effectively achieved by the disruption of the *E. coli* membranes *via* ultrasonication. Care was taken to prevent overheating of the sample during this procedure and so was performed on ice. Sonication (Soniprep 150, amplitude 15 microns) for 20 second bursts, interrupted by 1 minute periods of stirring in the absence of the ultrasonic probe was found to be adequate to maximise yield without denaturing protein. After lysis, cell debris was removed by centrifugation at 18 000 g for 1 hour (SS 34 head). The resultant supernatants, containing the desired protein, were pooled and kept on ice prior to further purification.

Table 2.3: Buffer A

50 mM Tris.HCl + 1 mM EDTA, pH 7.40

Buffer A was prepared in MilliQ ultrapure water, with the pH corrected by small aliquots of conc. HCl.

Ammonium sulfate fractionation

The lysis supernatant was fractionated by the selective precipitation of unwanted protein by addition of ammonium sulfate. Solid ammonium sulfate was slowly added to the stirring supernatant to 30 % saturation (176 g l⁻¹) over a 30 minute period. Unwanted proteins from this 30 % 'cut' were discarded as the 18 000 g centrifuged pellet. Further slow addition of ammonium sulfate from 30 - 60 % saturation (198 g l⁻¹) caused precipitation of both intact, and the heme domain of flavocytochrome P450 BM3. Continual stirring of the suspension at 4 °C for an hour ensured maximum yield. This 60 % cut was collected as the centrifuged precipitate, and the supernatant discarded.

Dialysis

Prior to column chromatography purification, the 60 % ammonium sulfate pellets had to be equilibrated into Buffer A, this was achieved by dialysis. The salt pellets were reconstituted in approximately 20 ml Buffer A, and the resultant suspension poured into dialysis tubing (12 kDA exclusion limit). Dialysis was performed overnight at 4 °C against 5 l buffer A to ensure the diffusion of ammonim sulfate and other small contaminants. The dialysate was centrifuged at 18 000 g to remove any aggregated protein.

Column chromatography

Extracted P450s were further purified by column chromatography. All steps were conducted at 4 °C.

DEAE Sephacel anion exchange column: Sigma DEAE Sephacel anion exchange resin consists of diethyl-aminoethyl groups, covalently crosslinked to a cellulose matrix. When equilibrated to pH 7.4, the immobilised phase is positively charged and hence provides a favourable interaction with negatively charged regions of proteins. Typically, 50 ml of DEAE Sephacel was poured into a 30 x 2 cm glass column (Biorad) and equilibrated by elution of approximately 20 column volumes of buffer A through the resin. This ensured thorough pH equilibration and removed traces of storage solvent (ethanol). Protein was loaded directly to the top of the equilibrated column. When properly equilibrated, P450 BM3 adheres to the column, and forms a tight red band at the top with minimal migration. Once loaded, the bound P450 was washed with 10 column volumes of buffer A to remove any non-bound species. Elution of this semi-purified band was achieved by running a linear KCl gradient (0 – 500 mM buffer A), fractions were collected in a Pharmacia fraction collector, the 5 most intensely coloured fractions pooled and carried forward for further purification. Under this gradient, intact flavocytochrome P450 BM3 elutes at 250 mM KCl, whereas the heme domain elutes slightly earlier at 200 mM KCl. Column regeneration was achieved by elution of 10 column volumes of 1 M KCl in buffer A and subsequent re-equilibration by buffer A.

At this stage, the purity of the proteins was typically 25 % based on the UV/visible peak height ratio A_{419}/A_{280} . Pure intact, and heme domain P450 BM3 have $A_{419}/A_{280} = 0.5$ and 2 respectively. This method uses the Soret peak height to quantitate the amount of P450 and the UV peak height as a crude measure of total protein concentration [113].

Hydroxyapatite column: Hydroxyapatite (Biorad) is a calcium phosphate resin, although its interaction with proteins is not fully understood, the affinity is most likely to occur between the phosphate anions and positively charged regions of proteins, hence providing an opposite interaction to that observed for DEAE sephacel. Hydroxyapatite was suspended in 50 ml buffer 25 mM KPi (Table 2.4) and washed to remove finings (hydroxyapatite dust). This process was repeated until no finings were observed, at which point, the column was poured and the resin equilibrated further by elution with 10 column volumes of 25mM KPi. The pooled eluate from the DEAE sephacel column was dialysed against 5 l of 25mM KPi and then loaded onto the hydroxyapatite column, forming a tight red band. After washing with 10 column volumes of 25mM KPi, the P450s were eluted with a linear gradient of 25 - 500 mM KPi. Fractions were collected in a Pharmacia fraction collector, the 5 most intensely coloured fractions pooled. Under this gradient, intact flavocytochrome P450 BM3 elutes at 200 mM KPi, whereas the heme domain elutes slightly earlier at 180 mM KPi. For the majority of experiments, the purity after this stage was sufficient to preclude further purification steps. However, for crystallography trials, additional steps were introduced to maximise purity.

ADP agarose affinity chromatography: An additional chromatography step was introduced to maximise the purity of intact flavocytochrome P450 BM3. The NADPH-binding region of the reductase portion of intact P450 BM3 interacts with immobilised N⁶-(6-aminoethyl) adenosine 2'5' bisphosphate molecules, covalently bound to the agarose resin. This provides a highly specific interaction allowing ultimate discrimination between P450 BM3 and other contaminants. ADP agarose was equilibrated by washing with 10 volumes of buffer A, and poured to form a 10 x 1 cm column. Intact P450 was loaded onto the gel with the formation of a tight red

band which was washed with 10 column volumes of buffer A. The band was eluted with 10 mM NADP⁺ in buffer A. Excess NADP⁺ was removed by exhaustive dialysis.

Strong anion exchange chromatography: The use of a Q-Sepharose (quaternary ammonium bound to agarose) strong anion exchange column was employed to further purify the heme domain proteins of P450 BM3. This step was essentially the same as outline for the DEAE Sephacel chromatography, except that the purification was conducted on a pre-packed HiLoad Q-Sepharose column (Pharmacia) attached to a Pharmacia FPLC. Bound protein was washed with buffer A, and was eluted by the linear gradient 0 – 500 mM KCl in buffer A. Under these conditions, the heme domain of P450 BM3 eluted at 230 mM KCl.

P450 concentration and storage

Purified P450s were dialysed against buffer A and concentrated to ~200 μM by ultracentrifugation (using Amicon Centripreps, 30 kDa cut-off), followed by dialysis into the storage buffer (Table 2.4) and were frozen at –20 °C until required. Proteins were used with 1 month of manufacture.

Table 2.4: Phosphate and Storage buffer

Buffer 25 mM KPi	25 mM K ₂ HPO ₄ / 25 mM KH ₂ PO ₄ . pH 6.5
	Buffer made up in MilliQ ultrapure water. pH adjustment achieved by titration of 25mM KH ₂ PO ₄ into 25 mM K ₂ HPO ₄
Storage Buffer	30 % glycerol in Buffer A

2.5 SDS PAGE

SDS PAGE (sodium dodecyl sulfate polyacrylamide gel electrophoresis) was used to verify the purity of purified P450 BM3 and also to check that intact P450 M3 had not become cleaved during purification. Protein separation by molecular weight [114] on a denaturing gel should lead to a single band of 119 kDa for the intact P450 BM3,

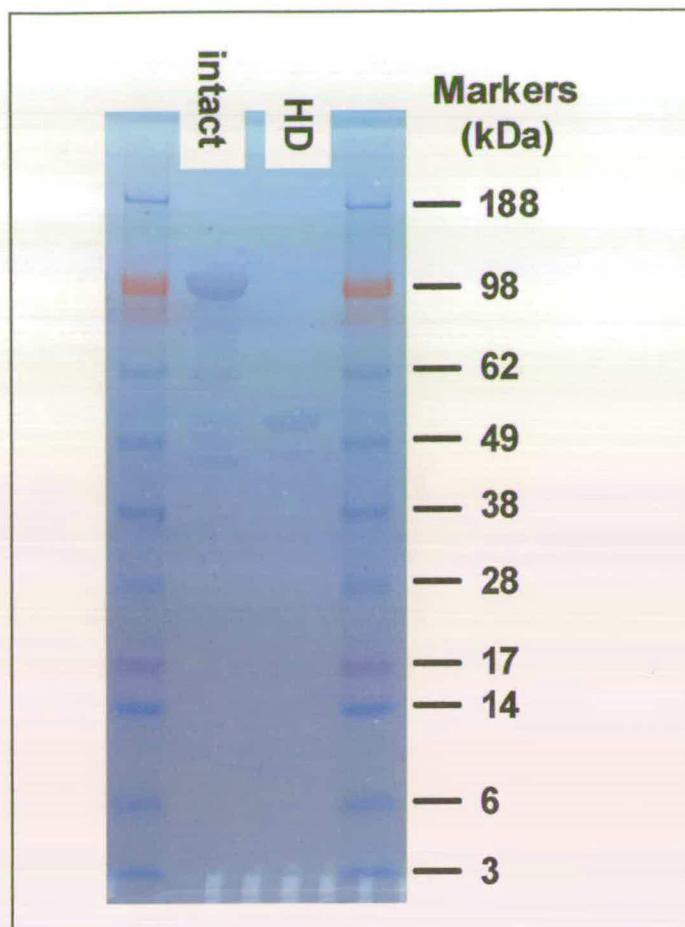


Figure 2.1: Example SDS PAGE gel showing the relative molecular weights of intact (119 kDa) and the heme domain (55 kDa) of wild-type flavocytochrome P450 BM3.

and a single band of 55 kDa for the heme domain. Figure 2.1 shows an example gel for wild-type P450 BM3 in both its intact and heme domain preparations.

Gel preparation

A typical SDS gel is comprised of two regions of different composition. The first region constitutes 4/5 of the total gel and is termed the resolving gel – the portion of the gel within which the proteins are separated. The second region constitutes 1/5 of the total gel, and is termed the stacking gel – this helps to concentrate the loaded proteins prior to them being drawn through the resolving gel. The composition of the two gels, and their associated buffers are shown in Table 2.5. The components of the resolving gel were mixed (addition of TEMED as the final ingredient initiated

polymerisation) and the polymerising gel poured between two glass plates. Water-saturated butanol was added to the top of the resolving gel in order to form a clean

Table 2.5: SDS PAGE gel preparation

Resolving gel (10 %; 30 ml)	Protogel (30 % acrylamide, 0.8 % bis acrylamide); 4 x resolving buffer (below)	10 ml
	H ₂ O	7.5 ml
	10 % ammonium persulfate	12.3 ml
	TEMED	190 µl
		50 µl
Resolving buffer (4 x)	H ₂ O	750 ml
	Trizma base	181.6 g
	SDS	4.0 g
	c.HCl (added to adjust to pH 8.8)	10 ml
	H ₂ O (added to take to final vol 1L)	~ 250 ml
Stacking gel (5 %; 10 ml)	Protogel (30 % acrylamide, 0.8 % bis acrylamide); 4 x stacking buffer (below)	1.6 ml
	H ₂ O	2.5 ml
	10 % ammonium persulfate	5.9 ml
	TEMED	30 µl
		50 µl
Stacking buffer (4 x)	H ₂ O	400 ml
	Trizma base	30.3 g
	SDS	2.0 g
	c.HCl (added to adjust to pH 6.8)	15 ml
	H ₂ O (added to take to final vol 0.5 L)	~ 100 ml

interface between the resolving and stacking gels. The gel was left to set (1 hour) and the butanol layer poured off. The stacking gel was mixed in an analogous fashion, and poured on top of the resolving gel, a comb was inserted into the unset stacking gel to create sample wells.

Electrophoresis

The set gel was clamped into a vertical electrophoresis tank which was filled with running buffer (Table 2.6). The comb was removed and protein samples (prepared in sample buffer and boiled for 60 seconds) injected into the vacated wells.

Table 2.6: SDS PAGE electrophoresis conditions

Sample buffer (2x)	H ₂ O	80 ml
	Tris.HCl pH 6.8 (1M)	3.3 ml
	SDS	2 g
	Glycerol	9 ml
	2-mercaptoethanol	5 ml
	Bromophenol blue (1 %)	1 ml
Running buffer (5x)	H ₂ O	500 ml
	Trizma base	15.1 g
	Glycine	94 g
	SDS	2g
	HCl (1M)	added to adjust to pH 8.8
Gel stain	H ₂ O	375 ml
	Isopropanol	125 ml
	Acetic acid	50 ml
	Coomassie brilliant blue	0.5 ml
Destain	H ₂ O	50 ml
	Methanol	40 ml
	Acetic acid	10 ml

The gel was connected to the power supply (200 V) and electrophoresed until the dye front reached the foot of the gel. After the removal of the gel from the electrophoresis tank, the gel was stained overnight and then destained to reveal the position of the migrated proteins.

2.6 Substrate and Ligand Binding

Substrate and ligand binding to P450s are often accompanied by quantifiable changes in their absorption spectra. Perturbations causing a blue-shift in the ferric P450 spectrum are typified by substrate binding and reduction, whereas perturbations causing a red-shift in the ferric P450 spectrum are typified by the ligation of exogenous ligands such as CO, CN⁻ and imidazole. UV/visible spectroscopy provides a convenient route to measure the binding characteristics of such compounds (Figure 2.2).

UV/visible absorption spectra were recorded over the 300-800 nm range using a Shimadzu 2101 spectrophotometer and quartz cuvettes of 1 cm pathlength. Typically, the concentration of wild-type or mutant P450 BM3 used was 1-5 μM in 1 ml of assay buffer (Table 2.7) at 30 °C. The total concentration of substrates or ligands added never exceeded 1 mM. Binding characteristics of certain ligands were investigated in both the ferric and ferrous forms of P450 BM3, addition of a 10 μl aliquot of a 5 mgml^{-1} solution of sodium dithionite was sufficient to achieve reduction anaerobically.

Fatty acid binding titrations

For enzyme titrations with arachidonic acid, aliquots (0.1-0.5 μl ; not exceeding 5 μl total addition) of a 33 mM solution (EtOH) were added to the enzyme solution. For enzyme titrations with sodium laurate, 10 μl aliquots of P450 BM3 were withdrawn and replaced with aliquots of a solution of enzyme at identical concentration in the same buffer, but containing in addition 1 mM sodium laurate. Spectra were recorded after each addition of substrate (Figure 2.3). Difference spectra were generated by subtraction of each spectrum recorded from the substrate-free spectrum. Substrate dissociation constants (K_d) were determined by plotting the maximal absorbance changes calculated from each difference spectrum against the concentration of substrate, and fitting the data to a rectangular hyperbola using Origin software (Microcal).

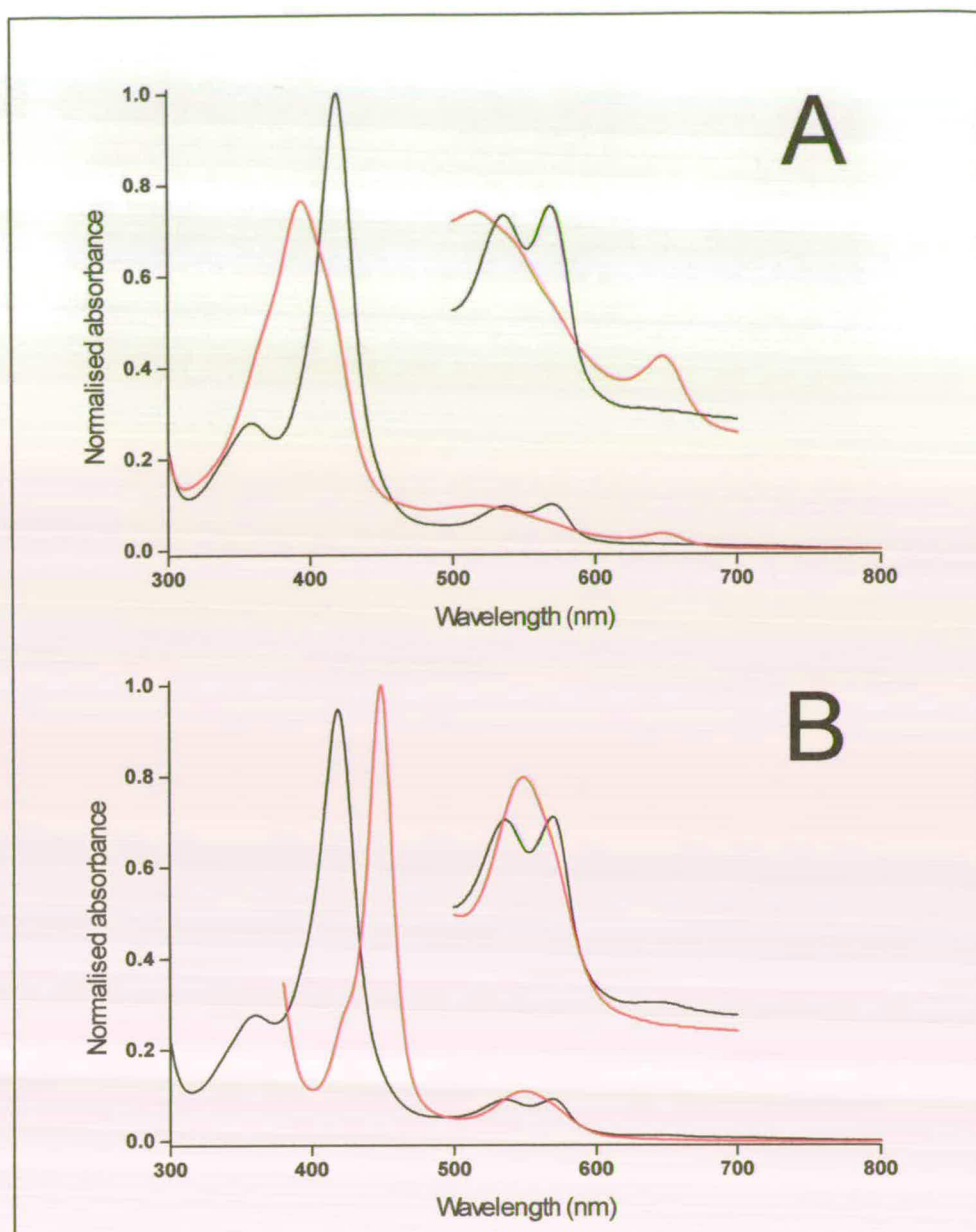


Figure 2.2: Absorbance spectra of wild-type P450 BM3 heme domain. Absolute ferric (black), ferric-substrate bound (Panel A, red line) and ferrous-CO bound (Panel B, red line). A $5 \times$ magnification of the α/β region is shown inset for clarity.

Carbon monoxide binding

Ferrous-CO complexes of wild-type and the mutant enzymes were prepared in the same fashion. P450 solutions were reduced by the addition $10 \mu\text{l}$ of 5 mgml^{-1} sodium dithionite solution and were converted to the P450-complexes by slow bubbling of the solutions with carbon monoxide gas (Sigma) for one minute.

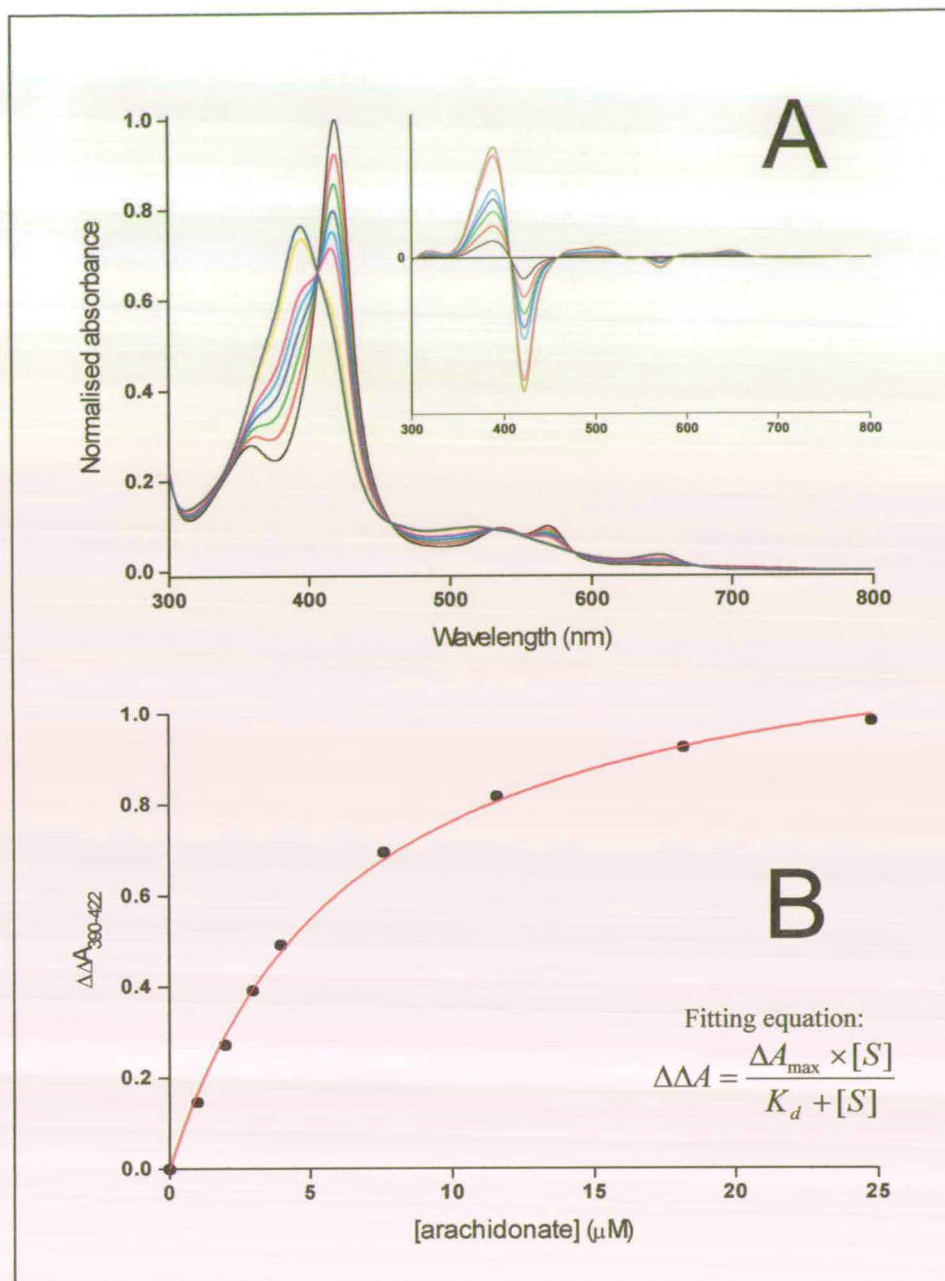


Figure 2.3: Typical spectral perturbations induced upon substrate binding to wild-type P450 BM3 (Panel A). Substrate binding dehydrates the heme iron, and causes a low-spin ($\lambda = 419$ nm) to high-spin ($\lambda = 392$ nm) transition. Inset is a series of difference spectra, generated by subtraction of substrate-free spectrum from each substrate-bound spectrum. Panel B describes the relationship between maximal absorbance change ($\Delta\Delta A_{390-422}$, difference spectra) versus substrate concentration. The data is fitted to the Michaelis-Menten equation, from which substrate dissociation constants can be evaluated. The equation used to fit the data shown in Panel B is shown inset.

Table 2.7: Assay buffer

20 mM MOPS + 100 mM KCl, pH 7.4

Assay buffer was prepared in MilliQ ultrapur water, with the pH corrected by small aliquots of 5 M NaOH

2.7 Steady-State Kinetics

All steady-state kinetic measurements were performed at 30° C in assay buffer using 1 cm pathlength quartz cuvettes. Initial rates of fatty acid (arachidonate and laurate) oxidation were measured as described previously [115], by monitoring the oxidation of NADPH at 340 nm (ϵ_{340} 6.21 mM⁻¹ cm⁻¹) with 10-100 nM enzyme and NADPH at saturating concentration (200 μ M). The initial arachidonate concentration was varied by addition of small volumes (<2.0 μ l) from a 33 mM or 3.3 mM ethanolic stock using a 10 μ l Hamilton gas-tight syringe (Hamilton, Reno, NV, USA), and the initial laurate concentration was varied by dilution of a 1 mM aqueous stock. Rate measurements were converted into activity units, s⁻¹ (mol of NADPH oxidised/sec per mol of P450) and plotted against fatty acid concentration (Figure 2.4). Data were fitted to the Michaelis-Menten equation (Appendix I) using Origin software.

2.8 Stopped-Flow Spectrophotometry

Stopped-flow spectrophotometry involves the rapid mixing of two equal volumes of two solutions within a spectrophotometric cell of fixed path length. On mixing, the instrument is immediately triggered to record the absorbance of the reacting solution and to generate a 'trace' with a specified time-base. The resolution of the instrument is limited by its dead-time, a value which is derived by calculating the time difference between the point at which the reaction can be traced back to ($t = 0$) and the point at which the absorbance is actually recorded ($t = dt$). The dead-time can be measured by recording any single exponential reaction over which the total absorbance change is known. The dead-time for the Applied Photophysics instrument is estimated to be between 0.9 – 1.1 ms. However, resolution is also impaired by the

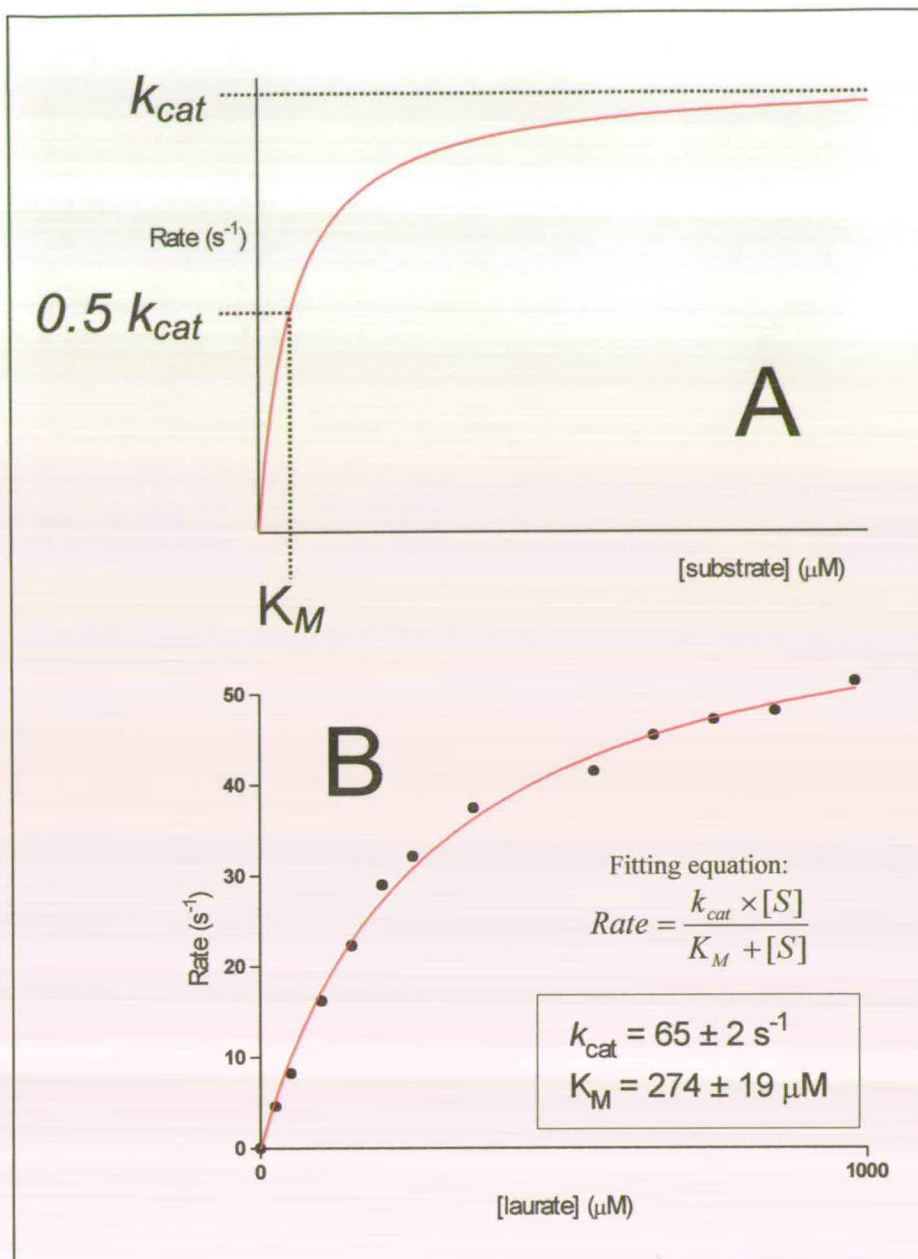


Figure 2.4: The rectangular hyperbola in Panel A describes the relationship between reaction rate and substrate concentration for a typical enzymatic reaction, from which the turnover number (k_{cat}) and the Michaelis constant (K_M) can be evaluated. K_M is defined as the concentration of substrate, which gives an initial rate of $0.5k_{cat}$. The equation used to fit the data shown in Panel B is shown inset.

mixing time, a value which is more difficult to quantify. Once the two solutions are in the reaction chamber observation will begin, but until mixing is complete the reaction will not be up to maximum velocity and a lag will be observed. This phenomenon, as well as the dead-time itself, will depend upon the physical attributes of the reacting solutions, including temperature and viscosity. Generally, reactions

occurring faster than 1000 s^{-1} are impossible to resolve and, depending on the dead-time, a significant percentage of the absorbance change is lost. All stopped-flow experiments were conducted in an Applied Photophysics SF.17 Micro Volume stopped-flow spectrophotometer path length 1 cm, at a single wavelength specified for each experiment.

Kinetics of heme reduction

Measurement of the rate of the first flavin-to-heme electron transfer step was performed at $30 \text{ }^\circ\text{C}$ as described previously [111] using CO-saturated assay buffer ($\sim 1 \text{ mM}$) [116] and monitoring the formation of the ferrous-CO adduct at 450nm using intact wild-type or mutant P450 BM3. Assay conditions are outlined in Table 2.8. Both syringes contained assay buffer of identical substrate concentration (arachidonate or laurate), previously deoxygenated (by bubbling extensively with oxygen-free nitrogen) and saturated with CO by bubbling for 5 minutes.

Table 2.8: Stopped-flow assay – heme reduction kinetics

Syringe A	CO saturated assay buffer ($[\text{CO}] \sim 1 \text{ mM}$) 200 μM NADPH Substrate ($[\text{arachidonate}] = 0 - 80\mu\text{M}$) ($[\text{laurate}] = 0 - 1 \text{ mM}$)
Syringe B	CO saturated assay buffer ($[\text{CO}] \sim 1 \text{ mM}$) 1 - 5 μM Enzyme Substrate ($[\text{arachidonate}] = 0 - 80 \mu\text{M}$) ($[\text{laurate}] = 0 - 1 \text{ mM}$)

Rates for each substrate concentration (k_{obs}) were obtained by fitting the progress curves obtained to a double exponential function using the Applied Photophysics. The k_{lim} values were calculated by plotting the observed rates, k_{obs} , versus fatty acid concentration, and fitting the data to the Michaelis-Menten equation using Origin

software (in an analogous fashion to the evaluation of the steady-state kinetic measurements, see Section 2.7).

Kinetics of oxyferrous formation and decay

The rate of formation and decay of the oxy-ferrous complex of the heme domain of wild-type and mutant P450 BM3 were measured by anaerobic stopped-flow spectrophotometry. Measurements were conducted within a Belle Technology anaerobic glovebox with the oxygen concentration maintained at less than 5 ppm. Measurements were conducted at 15 °C in both the absence and presence of arachidonate (66 μM). Assay conditions are shown in Table 2.9. Wild-type and mutant P450 heme domain (20 – 40 μM) were pre-reduced by addition of 10 μl of a 5 mgml⁻¹ sodium dithionite solution. Excess dithionite was removed prior to experimentation by elution of the reduced P450s through a pre-equilibrated Biorad DS-10 desalting gel-filtration column. Reduction was confirmed by UV/visible spectrometry on a Varian Carey 50 Bio spectrophotometer, also contained within the glovebox. The decay of the oxy-ferrous P450 complex ($\text{Fe}^{2+}\text{-O}_2 \rightarrow \text{Fe}^{3+} + \text{O}_2$) was monitored at 424 nm (substrate saturated) and at 380 nm (substrate-free), wavelengths at which the decay was monophasic and fitted well to a single exponential.

Table 2.9: Stopped-flow assay - oxygen binding kinetics

Syringe A	Anaerobic buffer (100 mM MOPS, pH 7.0) 20 -40 μM reduced P450 Substrate ([arachidonate] = 66 μM)
Syringe B	Air saturated buffer (100 mM MOPS, pH 7.0)

2.9 Redox Potentiometry

Redox potentiometry was employed in the determination of the midpoint potentials of the $\text{Fe}^{3+}/\text{Fe}^{2+}$ redox couple of the heme domain of wild-type and mutant P450 BM3. All redox titrations were conducted within a Belle Technology glove box under a nitrogen atmosphere, with the oxygen concentration maintained at less than 5 ppm. Degassed, concentrated P450s (3 ml, 20 μM) were eluted through an anaerobic Biorad Econo-pac 10DG gel filtration column, pre-equilibrated with 100 ml degassed buffer (100 mM KPi, pH 7.0) immediately upon admission of the sample to the glove box. This ensured removal of all traces of oxygen.

Enzyme solutions were titrated electrochemically according to the method of Dutton [117] using sodium dithionite as reductant and potassium ferricyanide as oxidant. Electrochemical mediators were added (Table 2.10) to facilitate electrical communication between enzyme and electrode, prior to titration. After a sufficient equilibration period (typically 10-15 minutes) following each reductive/oxidative addition, visible spectra were recorded over a 300-800 nm range using a Shimadzu 2101 UV-visible spectrophotometer contained within the anaerobic environment.

Table 2.10: Redox potentiometry conditions

Protein solution	3 ml, 20 mM P450 heme domain in 100 mM Kpi pH 7		
Electrochemical mediators	1.0 μM phenazine methosulfate	E_o	+ 30 mV
	5.0 μM 2-hydroxy-1,4-napthoquinone		-145 mV
	2.0 μM FMN		-200 mV
	1.0 μM benzyl viologen		-310 mV
	0.3 μM methyl viologen		-430 mV
Reductant	30 mM $\text{Na}_2\text{S}_2\text{O}_4$		- 450 mV
Oxidant	20 mM $\text{K}_3\text{Fe}(\text{CN})_6$		+ 440 mV

The electrochemical potentials of the equilibrated sample solutions were monitored using a CD740 meter (WPA) coupled to a Pt/calomel combination electrode (Russell

pH Ltd.) at 25 ± 2 °C. Both the substrate-free and substrate-saturated heme midpoint potentials were determined (Figure 2.5). For substrate-bound redox titrations, arachidonate was added to the sample prior to the titration. Conversion to the high-spin form was observed spectrophotometrically as a shift from 418 to 390 nm. The K_M values for arachidonate for all the enzymes studied were much lower than 10 μM . Therefore, 33 μM arachidonate was sufficient in all cases to saturate the P450 (no further spin-state shift was observed upon further additions of substrate).

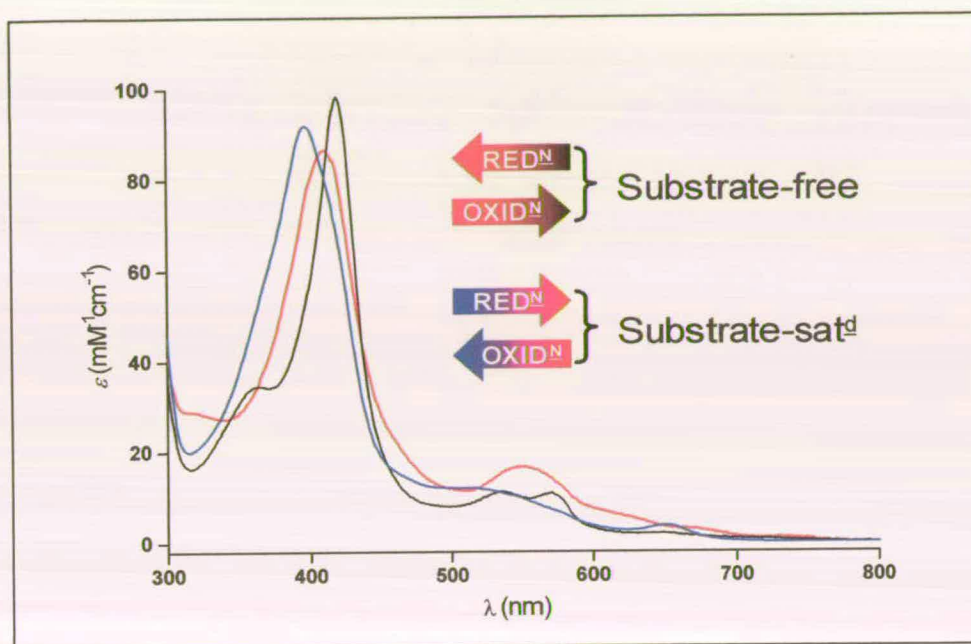


Figure 2.5: Visible absorbance spectra showing the spectral shifts associated with reduction and re-oxidation of substrate-free and substrate-saturated (33 μM arachidonate) P450 BM3 heme domain. Inset is a key showing the absorbance shifts with the appropriate redox states. The reduction/re-oxidation of all heme domains was freely reversible with minimal observed hysteresis. Complete reoxidation of the ferrous forms results in the regeneration of the initial ferric starting spectra (low- or high-spin).

Calibration of the calomel electrode

The calomel electrode used for the potentiometric measurements was calibrated prior to each titration to ensure accuracy. The electrode was calibrated using the $\text{Fe}^{3+}/\text{Fe}^{2+}$ EDTA couple as a standard (+108 mV vs SHE). A factor of +242 mV was employed to correct relative to the standard hydrogen electrode. The potential of 40 μl of an Fe^{3+} solution (720 μM FeCl_3) was recorded initially, and after each successive addition of 3 x 10 μl aliquots of an Fe^{2+} solution (71 mM

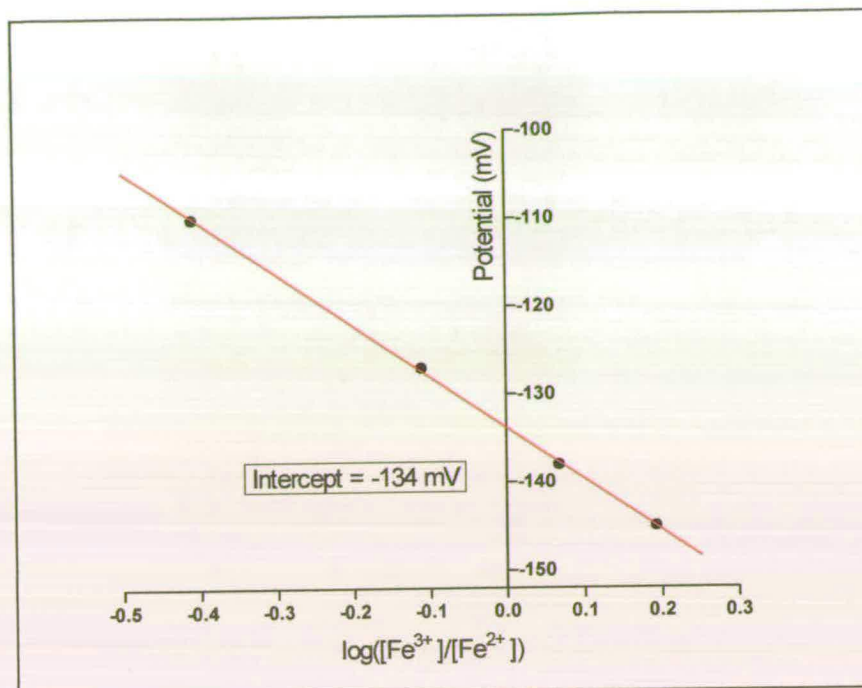


Figure 2.6: Calibration of the calomel electrode using the Fe^{3+}/Fe^{2+} EDTA couple as standard. The above plot should be linear, with an intercept $y = -134$ mV. This couple has a midpoint of + 108 mV vs SHE, so a factor of + 242 mV is employed to correct to the standard hydrogen electrode.

$Fe(NH_4)_2(SO_4)_2$). A plot (Figure 2.6) of recorded potential vs $\log([Fe^{3+}]/[Fe^{2+}])$ (i.e. proportion reduced) was linear (intercept = -134 mV) and confirmed the integrity of the electrode.

2.10 Coupling Efficiency

The coupling of NADPH consumption to product turnover is an important concept as it is a measure of the suitability of a substrate for a particular P450, of enzymatic efficiency, and as a probe of how specific mutations effect catalysis. Two methods were employed to determine the degree of coupling for wild-type and mutant P450 BM3 with arachidonate.

Horseradish peroxidase/*o*-dianisidine assay

This simple spectrophotometric assay was used to determine the degree of uncoupling to peroxide [118] (the 2 electron reduction of oxygen). The consumption of NADPH was monitored in the presence of saturating concentrations of substrate

(33 μM arachidonate) and catalytic concentration of enzyme (ca. 0.2 μM). The initial concentration of NADPH was calculated from its absorbance spectrum ($\epsilon_{340} = 6.21 \text{ mM}^{-1}\text{cm}^{-1}$). After complete depletion of NADPH, 40 μl of 8mM *o*-dianisidine and 10 μl of 5 mgml^{-1} horseradish peroxidase were added to the cuvette. The peroxide generated from the P450 uncoupling pathway reacts stoichiometrically with the *o*-dianisidine to form a blue radical cation with an extinction coefficient of $\epsilon_{440} = 11.6 \text{ mM}^{-1}\text{cm}^{-1}$. The degree of uncoupling to peroxide can be calculating by comparing the concentration of NADPH consumed to ODRC produced.

Negative-ion Electrospray Mass Spectrometry

The overall coupling P450 efficiency (to account for all uncoupled species, e.g. superoxide, peroxide and water) for wild-type and the mutant holoenzymes was determined by negative-ion electrospray mass spectrometry.

Turnover assays were performed on each P450 under limiting concentrations of NADPH and excess arachidonate and oxygen (980 μl 20mM MOPS pH 7.4, 4 μl 33mM arachidonate, 5 μl 19.7 mM NADPH and 10 μl 4 μM P450). Reactions were initiated by addition of P450. The air-saturated concentration of oxygen in aqueous solution [119] was $\sim 260 \mu\text{M}$. Under these conditions, NADPH consumption can only be coupled to product formation or oxygen reduction (due to the absence of other electron acceptors in the assay and with both [substrate] and [oxygen] in excess of [NADPH]). Samples of each reaction mixture were injected into the mass spectrometer (Micromass Platform electrospray mass spectrometer) and analysed under the following conditions: ESI-ve, cone voltage = 35 V, acquired range 150 – 500 Da. The concentration of unreacted substrate ($m/z = 303$) and hydroxylated substrate ($m/z = 319$) in each reaction mixture was evaluated from the total ion current for each peak (MassLynx software). The concentration of NADPH was calculated from its absorption spectrum ($\epsilon_{340} = 6.21 \text{ mM}^{-1}\text{cm}^{-1}$). All appropriate controls were run, and under these conditions no interfering signals from NADPH, buffer or enzyme were observed, with monohydroxylated arachidonate being the

only observable product. The reactions were performed at 30 °C and conditions were optimised so that each reaction proceeded to completeness (total consumption of NADPH) within 30 seconds of initiation by addition of the catalytic concentration of enzyme.

Percentage coupling was calculated from the relative stoichiometries of NADPH consumed to product formed, and is an average of 4 separate experiments.

2.11 Heme Content Determination

In certain cases, mutagenesis of residues in, or close to, the heme binding site of hemoproteins can lead to the dissociation or poor incorporation of heme. This problem is more acute for P450s, whose *b*-type heme is non-covalently bound to the protein. It is important to quantify heme content as heme loss could be a result of an introduced mutation, or could explain changes in measured activity.

The concentration of P450 was based on the total heme content, determined by the pyridine hemochromagen assay [120]. A solution of P450 (5 μ M) was thoroughly mixed with an equal volume of reagent A (Table 2.11), followed by the immediate addition of 10 μ l of 5 mgml^{-1} $\text{Na}_2\text{S}_2\text{O}_4$ solution. Spectra of the reduced pyridine

Table 2.11: Pyridine hemochromagen assay

Reagent A	200 μ l of 5 M NaOH 2.5 ml pyridine 2.3 ml H_2O
Reductant	10 μ l $\text{Na}_2\text{S}_2\text{O}_4$ in H_2O
Pyridine hemochromagen characteristics	$\Delta\epsilon_{556-540} = 22.1 \text{ mM}^{-1}\text{cm}^{-1}$ α -band = 556 nm β -band = 524 nm γ -band = 420 nm

hemochromagen were recorded in 1 ml quartz cuvettes. Heme concentrations were calculated using the difference extinction coefficient $\Delta\epsilon_{556-540} = 22.1 \text{ mM}^{-1}\text{cm}^{-1}$ [121]. The appearance of the reduced pyridine hemochromagen was time-dependent and so sufficient equilibration was allowed following the addition of dithionite. Each determination was performed in triplicate to ensure accuracy.

2.12 Protein Crystallography (with Dr. C.G. Mowat)

Crystallization of the heme domains of the F393A, F393H and F393Y mutants of P450 BM3 was carried out by hanging drop vapour diffusion at 4 °C in Linbro plates. Crystals were obtained from wells whose composition are shown in Table 2.15. Plates of up to 1 × 0.3 × 0.3 mm were formed after about 1 week. Crystallisation conditions were the same for all mutants (Table 2.12).

Crystals were immersed in well solution containing 22 % glycerol as a cryoprotectant, before being mounted in nylon loops and flash-cooled in liquid nitrogen. Data sets were collected at Daresbury and Hamburg synchrotron sources using a MAR CCD detector. All crystals were isomorphous with those of the hemoprotein domain of wild-type flavocytochrome P450 BM3 (unit cell dimensions of $a = 59.4 \text{ \AA}$, $b = 154.0 \text{ \AA}$, $c = 62.2 \text{ \AA}$, and $\beta = 94.7^\circ$) [86] and had two molecules in the asymmetric unit. Data processing was carried out using the HKL package [122]. The wild-type P450 BM3 heme domain structure (PDB: 2HPD), stripped of water, was used as the initial model. Electron density fitting was carried out using the program O [123]. Restraints for the heme group were calculated from the CNS parameter file. Structure refinement was carried out using SHELX-97 [124].

Table 2.12: Crystallisation conditions

Well solution	Hanging drop
40 mM MgSO ₄ ,	2 μ l, 41.7 mgml ⁻¹ protein
100 mM Na PIPES, pH 6.5,	2 μ l well solution
18-21 % PEG 8000	

2.13 Product Characterisation (with Dr. A.J. Fulco)

The products of the catalytic turnover of myristic acid (tetradecanoic acid) by wild-type P450 BM3 and F393H mutant were determined using gas chromatography/mass spectrometry according to the following methodology. A Hewlett Packard 5971A GC/MS utilizing electron impact ionisation (70 eV) instrument was used to determine structural information on the monohydroxylated metabolites of myristic acid. Metabolites were generated by incubation of 120 μ M myristate in the presence of 5 mM NADPH and a catalytic amount of P450 (ca. 1 nM) in 2 ml samples of 100mM K_2HPO_4/KH_2PO_4 pH 8.

The metabolites were extracted into diethylether and converted to their methyl ester derivatives using diazomethane, before analysis by GC/MS. Chromatography of the samples was performed on a HP-35 capillary column (30 m x 0.25 mm id x 0.25 μ M film thickness) with a thermal gradient beginning at 100 °C for 0.5 mins and increasing to 200 °C at a rate of 5 °C/min for 5 min and then to a final temperature of 250 °C at a rate of 10 °C/min. Injector temperature was set to 250 °C and the GC/MS transfer line was set at 280 °C. Column flow rate was set at 0.76 ml/min.

The mass spectra of the products from the control run (wild-type P450 BM3) were used to identify each GC peak. Monohydroxylated products were identified by their characteristic fragmentation pattern [125]. The distribution of products was based on the relative peak area of the gas chromatogram, in which the total ion current was used to assess quantity.

2.14 Electron Paramagnetic Resonance (with Dr. M.R. Cheesman)

EPR spectra were recorded on an EPR spectrometer comprising an ER-200D electromagnet and microwave bridge interfaced to an EMX control system (Brüker Spectrospin) and fitted with a liquid helium flow cryostat (ESR-9, Oxford Instruments) and a dual-mode X-band cavity (Brüker, type ER4116DM).

2.15 Cytochrome P450cam

Purified samples of cytochrome P450cam were a generous gift from Dr. Luet Wong, Oxford University, and were used in the experiments outlined in Chapter 4.

Chapter 3:

The role of phenylalanine 393

3 THE ROLE OF PHENYLALANINE 393

3.1 Introduction

Whilst the path of electron transfer through the NADPH-dependent P450-reductase can be rationalised by considering the close proximity of the NADPH, FAD and FMN cofactors (from examination of the crystal structure [93]), the formal route from the FMN to the heme in flavocytochrome P450 BM3 has not been established. This is due in part to the absence of a crystal structure for the intact holoenzyme, and also due to controversy over the relevance of the recently reported Heme:FMN crystal structure complex [95].

Studies with the putidaredoxin reductase/putidaredoxin/P450cam ternary complex have demonstrated that the most likely interaction of putidaredoxin with P450cam to be electrostatic in nature [126,127], occurring at the proximal face of the heme [128]. Whilst the heme is buried within the hydrophobic core of P450cam, one of the heme propionates and the cysteine ligand are partially exposed (Figure 3.1), allowing a plausible route for direct electron transfer between the ferredoxin and the heme. Modelling of P450cam with cytochrome *b*₅ showed that the electrostatic association of a cluster of basic residues on the surface of P450cam with conserved acidic carboxylates of cyt *b*₅, formed a convenient complex where the iron-to-iron distance was 18 Å. The highly conserved phenylalanine residue Phe350 of P450cam was found to be located directly between the *b*₅ (9 Å) and P450cam hemes (4 Å), implicating it in the mediation of electron transfer. Putidaredoxin contains a similar acidic binding surface and it is believed that the physiological association between P450cam and putidaredoxin occurs in the same fashion as that for the P450cam/cyt *b*₅ modelled complex.

Although a number of basic residues are located in the vicinity of the proximal surface of P450 BM3, these do not appear to constitute a discernible patch, whereby an analogous (to P450cam) electrostatic interaction between the FMN- and heme-domains could be formed. However, this type of interaction is likely to be less

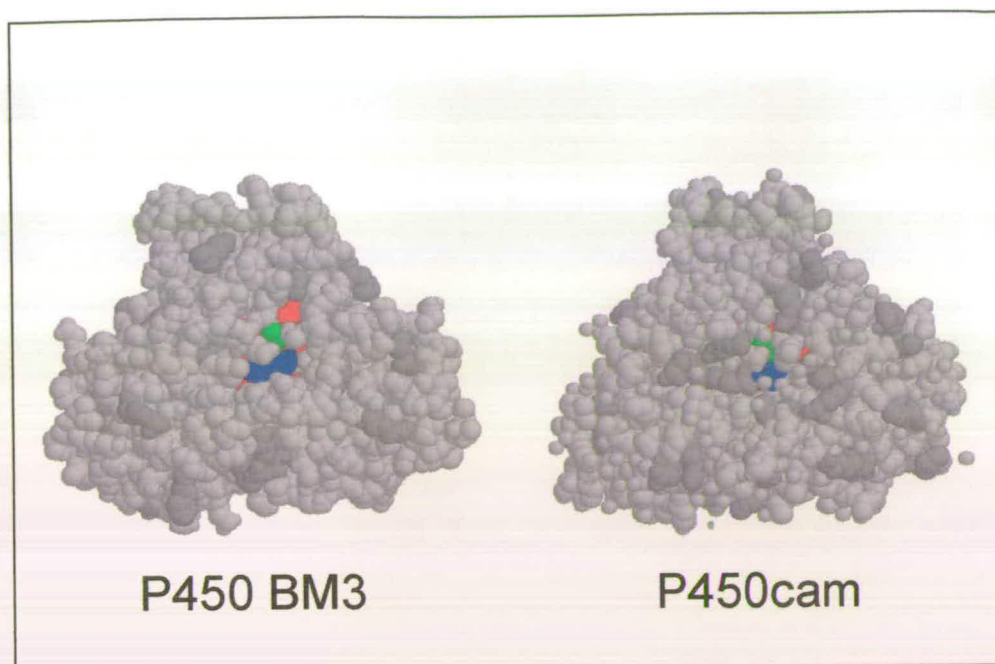


Figure 3.1: Space-filled representation of the heme domain of P450 BM3 and of P450cam, showing the proximal surface of the enzymes. The heme (red) lies buried within the core of the P450s, and is only slightly solvent exposed. Also shown are the cysteine heme-liagand (green) and phenylalanine 393 (Phe350 in P450cam, blue). These residues are slightly more exposed in P450 BM3 than in P450cam. Darker grey regions highlight basic residues. These collectively form a patch in the vicinity of the heme in P450cam - the likely docking site for putidaredoxin. No analogous region is observed for the heme-domain of P450 BM3. This reflects the fact that electrostatic interactions between the reductase and the heme of flavocytochrome P450 BM3 are less important (due to the arrangement of the redox cofactors in one continuous polypeptide) than for the formation of the ternary P450cam complex.

important in forming the electron transfer complex in flavocytochrome P450 BM3, as the cofactors are pre-organised in a single protein. Despite these differences, the heme-propionate and cysteine ligand of P450 BM3 are similarly exposed (Figure 3.1) as those of P450cam, allowing a comparable path of direct electron transfer to be envisioned.

Phenylalanine 393 of P450 BM3 is analogous to Phe350 of P450cam, and is one of the 4 highly conserved residues within what is termed the P450 heme-binding motif [129]. The high level of conservation of this residue implies its importance in the catalytic competence of P450s, mediation of electron transfer from the reductase to the heme is a likely candidate for its role. The results from mutagenesis studies designed to probe the role of this conserved phenylalanine in P450cam (F350), in rat P450 1A2 (F449) and rabbit P450 2E1 (F429) were inconclusive. In P450 1A2, F449

mutants showed diminished catalytic capacity and were affected in heme binding [130, 130a], whilst in P450 2E1, only an effect on heme binding was observed in F429 mutants [131]. None of these studies provided a satisfactorily comprehensive understanding of the role this phenylalanine plays in the P450 mechanism.

Interestingly, the P450s in which this phenylalanine is not conserved (CYP 74: allene oxide synthase [132]; CYP 74: divinyl ether synthase [133]; CYP 8: prostacyclin synthase [134] and CYP 3: thromboxane synthase [135]) fall into a group which do not have to activate molecular oxygen. In all cases, the phenylalanine is substituted by either proline or tryptophan. Unlike typical P450s, these enzymes do not function as monooxygenases and do not require molecular oxygen or NAD(P)H dependent P450 reductase for activity. These examples catalyse rearrangement or isomerisation reactions, for which the activation of molecular oxygen is non-essential. This more subtle observation could be key to why a phenylalanine in close proximity to the heme ligand is necessary for conventional P450 monooxygenation.

The aim of the research was to elucidate the role of phenylalanine 393 of flavocytochrome P450 BM3 by characterising both the kinetic and thermodynamic properties of a series of site directed mutants (F393A, F393H and F393Y). These were designed to probe how removal of steric bulk, aromaticity, hydrophobicity, introduction of charged residues and potential hydrogen-bonding interactions affect catalysis.

3.2 Results

3.2.1 Overexpression and purification of mutant enzymes

The successful overexpression and subsequent purification of the holoenzymes F393A, F393H and F393Y, along with the heme domains (HD) F393A HD and F393H HD and F393Y HD, immediately negated the previous assumption that phenylalanine 393 (Phe393) was essential for heme incorporation and stability. All mutant enzymes expressed to high levels, similar to wild-type, and remained stable when stored at -20°C . All of the enzymes generated a native-like P450 absorbance spectrum, with no P420 contribution. An absorption peak at 420 nm would indicate the presence of enzyme with non-cysteine heme ligation.

3.2.2 Spectrophotometric analysis of carbon monoxide binding

Typically, treatment of a sample of reduced P450 with carbon monoxide will generate the characteristic P450-CO Soret absorption at 450 nm. This was the case for both wild-type P450 BM3 ($A_{\text{max}} = 449 \text{ nm}$) and the most conservative mutant F393Y. However, a $\sim 5 \text{ nm}$ blue-shift in the P450-CO Soret absorption for mutants F393A ($A_{\text{max}} = 444 \text{ nm}$) and F393H ($A_{\text{max}} = 445 \text{ nm}$) was observed (Figure 3.2).

This shift in the Soret position of the F393A and F393H mutants relative to wild-type most likely reflects changes in the relative energies of the π and π^* porphyrin molecular orbitals, caused by the mutations. This is likely to be due to change in the degree of iron π bonding to the porphyrin ligand. A blue shifted Soret absorption peak indicates stronger π bonding to the porphyrin ligand and weaker backbonding to π^* molecular orbitals. Consequently the π^* backbonding to the CO (Figure 3.3) molecule weakens in conjunction with the blue shift. Substitution of phenylalanine by either histidine or alanine appears to decrease the energy of the iron t_{2g} orbitals, a suggestion which is supported by evidence that the ferrous-forms of mutants F393A and F393H are stabilised more so than in wild-type (ability to generate reduced spectra under aerobic conditions). The nature of the residue at position 393 appears to have an influence over this fundamental property of the

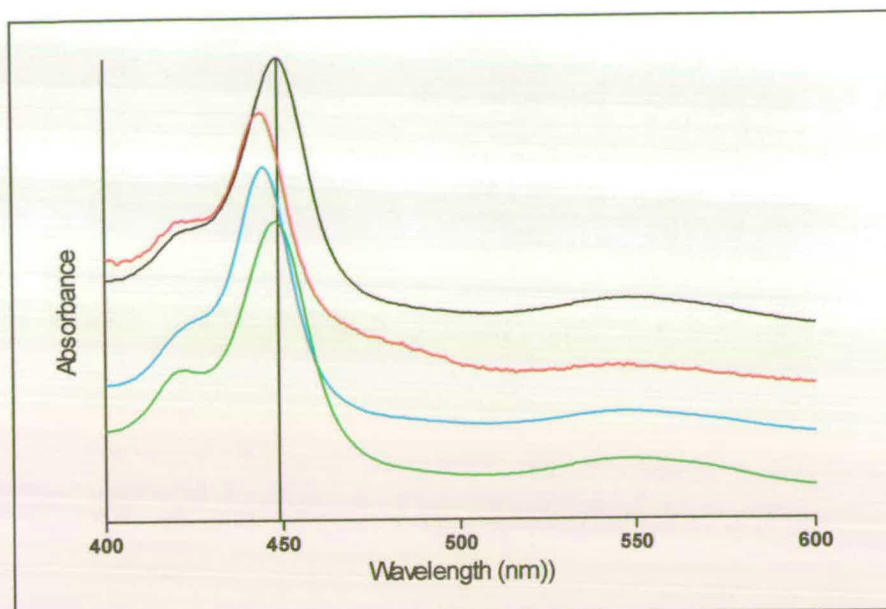


Figure 3.2: Comparison of the visible absorption spectra of the ferrous-CO complexes of wild-type (black), F393A (red), F393H (blue) and F393Y (green) P450 BM3. The spectra have been offset along the absorbance axis in the order indicated, for clarity. The Soret peak positions are blue-shifted by 4 nm (F393H), 5 nm (F393A) and 0 nm (F393Y) relative to that of wild-type ($A_{max} = 449$ nm, vertical line).

heme. The most conservative substitution of phenylalanine (by tyrosine) does not appear to affect significantly the heme environment as its spectral properties are identical to wild-type.

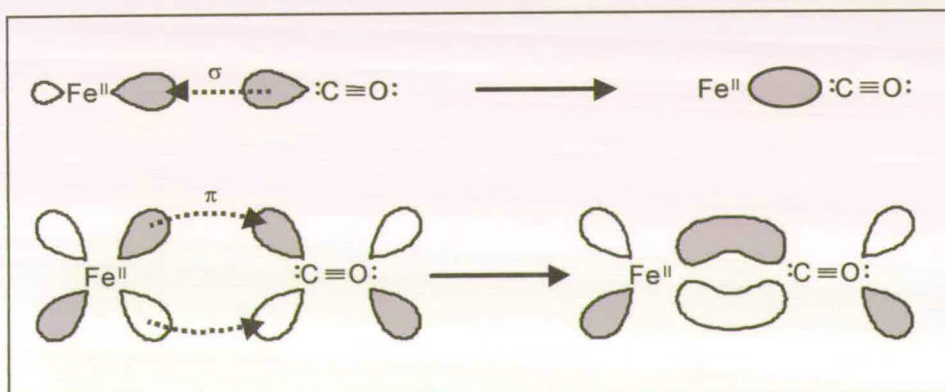


Figure 3.3: Schematic representation of the σ -acid/ π -base character of carbon monoxide when ligated to ferrous iron. Back-donation (π) from the iron into the π^* anti-bonding CO orbital destabilises the CO bond. A blue shift in the Soret absorption, as observed for the F393A and F393H mutants, is indicative of a strengthening of the CO bond. This is a consequence of a decrease in the degree of π -back donation from a less electronegative heme than wild-type.

3.2.3 Fatty acid binding

The values for the dissociation constants for arachidonate and laurate binding to wild-type P450 BM3 and the mutant enzymes F393A, F393H and F393Y are shown in Table 3.1. The major observation is that changing the nature of the side chain of residue 393 does not significantly alter the fatty acid-binding properties of the enzyme.

Table 3.1: Substrate Dissociation Constants (percentage spin conversion in parentheses)

	K_d (μM)			
	wild-type	F393A	F393H	F393Y
Arachidonate	3.6 ± 0.3 (100)	2.6 ± 0.3 (97)	7.6 ± 0.5 (96)	4.2 ± 0.3 (100)
Laurate	241 ± 9 (48)	230 ± 11 (60)	525 ± 10 (47)	520 ± 9 (54)

This is intuitive considering the fact that the mutation is on the opposite side of the heme to the substrate-binding channel. Although mutations of Phe393 appeared to have little effect on substrate binding, differences in the degree of spin state shift (low- to high-spin) associated with the dehydration of the ferric iron centre are apparent. For wild-type P450 BM3, there is a correlation between the degree of spin-state conversion and both the K_d and chain length of saturated fatty acid substrates (Figure 3.4).

Fatty acids of chain length C_{15} and C_{16} (pentadecanoic and palmitic acids) have the lowest K_d values, and induce the largest degree of spin-state change. However, these substrates are highly insoluble in water. Lauric acid has better solubility in aqueous media (to approximately 1.2 mM) and has a K_d of $\sim 250 \mu\text{M}$. A much better substrate for P450 BM3 than any of the saturated fatty acids is the C_{20} , tetra-unsaturated arachidonic acid ($K_d \sim 4 \mu\text{M}$), which also has acceptable water solubility. Arachidonate induces a much greater spin-state shift than laurate (>95% and <60% respectively). Comparisons between the mutants and wild-type P450 BM3 show differences in the degree of spin-state conversion with lauric acid. The arachidonate-induced (33 μM) spin-state shift for wild-type and all mutants was >95%, whereas

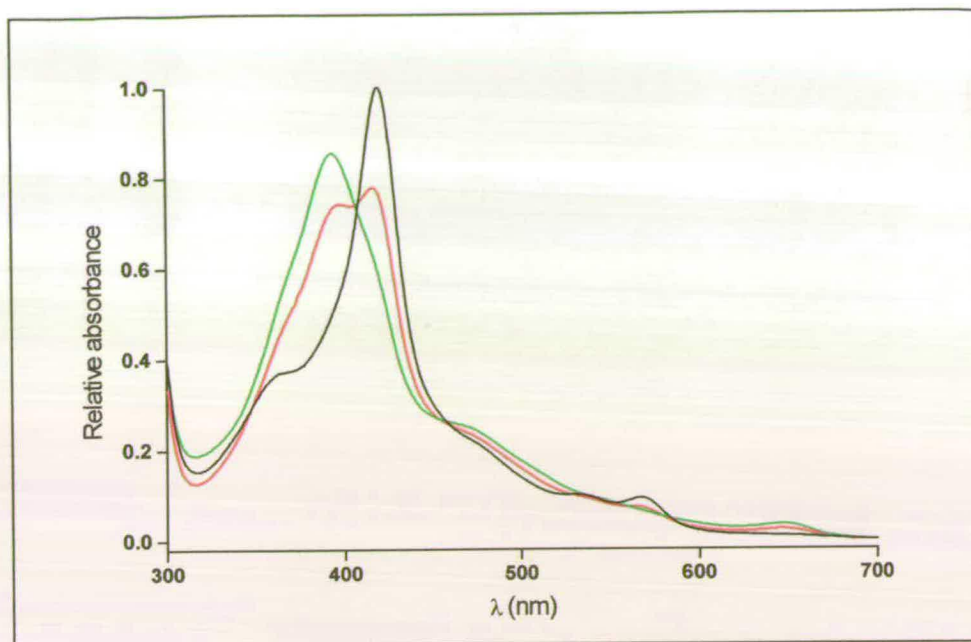


Figure 3.4: Comparison of the effect of binding substrates of different chain length has on the heme iron spin-state equilibrium. Substrate binding causes a low- to high-spin shift in the electronic configuration of the iron. In P450 BM3, the extent of the perturbation is directly related to substrate chain length. The binding of laurate (C_{12} saturated fatty acid, red line) induces only partial (< 60 %) conversion to the high-spin form, whereas the binding of arachidonate (C_{20} tetra-unsaturated fatty acid, green line) induces almost complete conversion (> 90 %) to its high-spin form, under saturating conditions.

the laurate-induced (1.0 mM) spin-state shift varies across the series F393A>F393Y>WT>F393H, with F393A giving ~12 % higher proportion of the high-spin form than wild-type P450 BM3 (see Table 3.1).

3.2.4 Kinetics of fatty acid oxidation

Although binding of the fatty acids was essentially unaffected by the nature of the residue at position 393, steady-state kinetic analysis (as outlined in Section 2.7) shows significant differences in the rates of turnover of the mutant flavocytochromes compared to wild-type (Table 3.2). The background rate of NADPH oxidation in the absence of substrate was less than 0.3 mol NADPH/sec/mol P450, for all enzymes studied. For both arachidonate and laurate oxidation, the observed trend in k_{cat} was WT>F393Y>>F393H>F393A. The differences in turnover are most obvious when arachidonate is the substrate, with 14-, 8- and 2-fold decreases in k_{cat} for F393A, F393H, F393Y, respectively, compared to wild-type P450 BM3. Although the magnitude of the difference between wild-type P450 BM3 and the mutants is smaller

when laurate is the substrate, the trend is the same. Clearly some step in the catalytic cycle, other than substrate binding, has been perturbed and has become rate-limiting in the mutant enzymes.

Table 3.2: Steady-State NADPH Oxidation Kinetics

	Arachidonate		Laurate	
	k_{cat} (s^{-1})	K_M (μM)	k_{cat} (s^{-1})	K_M (μM)
wild-type	285 ± 3	4.7 ± 0.3	86 ± 2	288 ± 15
F393A	21 ± 1	2.7 ± 0.3	29 ± 1	19 ± 3
F393H	33 ± 1	3.8 ± 0.5	37 ± 1	60 ± 5
F393Y	143 ± 8	9.5 ± 1.1	65 ± 2	274 ± 20

The coupling efficiencies for wild-type, F393Y and F393H (~90 %) for arachidonate hydroxylation are all within experimental error of each other (Table 3.3) and suggest near exclusive coupling of NADPH oxidation to product formation. Whilst the coupling of the F393A mutant is lower than the other P450s studied, this decrease cannot fully account for the order of magnitude difference observed between the steady-state parameters for the F393A mutant with respect to wild-type.

Table 3.3: Coupling efficiencies

	[Unreacted substrate] (μM)	[Product] (μM)	% coupling
Wild-type	43 ± 3	89 ± 7	91 ± 11
F393A	77 ± 6	55 ± 5	56 ± 8
F393H	53 ± 4	79 ± 6	81 ± 10
F393Y	39 ± 3	93 ± 7	95 ± 11

This indicates that all enzymes are catalytically functional, and that the lowered catalytic activity observed for all the F393 mutants is due to decreased rate(s) of steps in the catalytic cycle subsequent to substrate-binding and not as a result of the uncoupled reduction of oxygen.

3.2.5 Product characterisation (with Dr. A.J. Fulco)

It is well established that wild-type P450 BM3 displays strict substrate-specificity for long-chain fatty acids, performing hydroxylation in a highly regio-specific manner. For wild-type enzyme, the sole hydroxylation products of palmitic acid are the ω -1, ω -2 and ω -3 hydroxy derivatives [136,137]. The same trend has been demonstrated here for the hydroxylation of myristate (Table 3.4) by wild-type and the F393H mutant P450 BM3.

The F393H mutant shows comparable affinity toward laurate and arachidonate as wild-type ($K_d = \sim 250 \mu\text{M}$ and $\sim 4 \mu\text{M}$ respectively). Characterisation of the F393H-mediated turnover of myristate reveals an identical product profile to wild-type,

Table 3.4: Product Characterisation

	Product Distribution (%)			
	ω -1	ω -2	ω -3	unreacted
Wild-type	53.6	24.5	20.0	1.9
F393H	57.7	22.5	15.0	4.8

indicating that both the substrate specificity and the regiospecificity of hydroxylation is unaffected by the F393H substitution. There is a virtually identical product profile to wild-type, although there appears to be a slightly higher proportion of the ω -1 metabolite with respect to the ω -3 product for F393H compared to wild-type. Notwithstanding this, the trend in regiospecificity between wild-type and the F393H mutant is the same (ω -1: ω -2: ω -3:unreacted = 28:13:11:1 (12:5:3:1) respectively). There is a slightly higher proportion of unreacted myristate in the case of F393H turnover, resulting from the lower overall catalytic activity in this mutant, i.e. the F393H mutant turns over less myristate in the same time period as wild-type.

The important result is that the substitution of phenylalanine 393 by histidine results in a mutant-form that retains the same selectivity for long-chain fatty acids and displays the same regiospecificity of hydroxylation as wild-type P450 BM3.

Similar product analyses were not conducted for the F393A or F393Y mutants, in light of the results from the F393H mutant and their similarity with the product profile of wild-type.

3.2.6 Kinetics of heme reduction

Stopped-flow experiments were undertaken to investigate whether the kinetics of flavin-to-heme electron transfer in the F393 mutants was affected. The rate of the first electron transfer step from the reductase FMN to the substrate-bound P450 BM3 heme can be conveniently measured using CO-saturated buffer and monitoring the formation of the ferrous iron-CO adduct at 450 nm (as described in the Section 2.8). The observed initial fast-phase rate constants (k_{obs}) for heme reduction were plotted against substrate concentration and fitted to a rectangular hyperbola (Figure 3.5). From these data, maximal apparent rates of first electron transfer to the heme iron (k_{lim}) and apparent dissociation constants for the substrates (K_d) were obtained, and are shown in Table 3.5. The observed trend in k_{lim} F393A>F393H>>F393Y~WT was the reverse of that obtained from the steady-state turnover of both laurate and arachidonate. Thus, although steady-state experiments suggest an overall decrease in

Table 3.5: Pre-Steady State Kinetics of Heme Reduction

	Arachidonate		Laurate	
	k_{lim} (s ⁻¹)	K_d (μM)	k_{lim} (s ⁻¹)	K_d (μM)
Wild-type	348 ± 17	13.8 ± 2.0	172 ± 14	300 ± 65
F393A	1176 ± 78	19.3 ± 3.5	468 ± 11	124 ± 13
F393H	832 ± 53	13.3 ± 2.9	439 ± 20	291 ± 37
F393Y	366 ± 11	6.4 ± 0.8	215 ± 10	400 ± 42

the turnover rates of these F393 mutant enzymes, the first flavin-to-heme electron transfer reaction is actually faster in all the mutant enzymes than in wild type. In the wild-type P450 BM3, the apparent rate of flavin-to-heme electron transfer (as measured by the formation rate of the ferrous-CO adduct) is 348 s⁻¹, where the overall turnover rate of the enzyme is 285 s⁻¹ (in the presence of arachidonate).

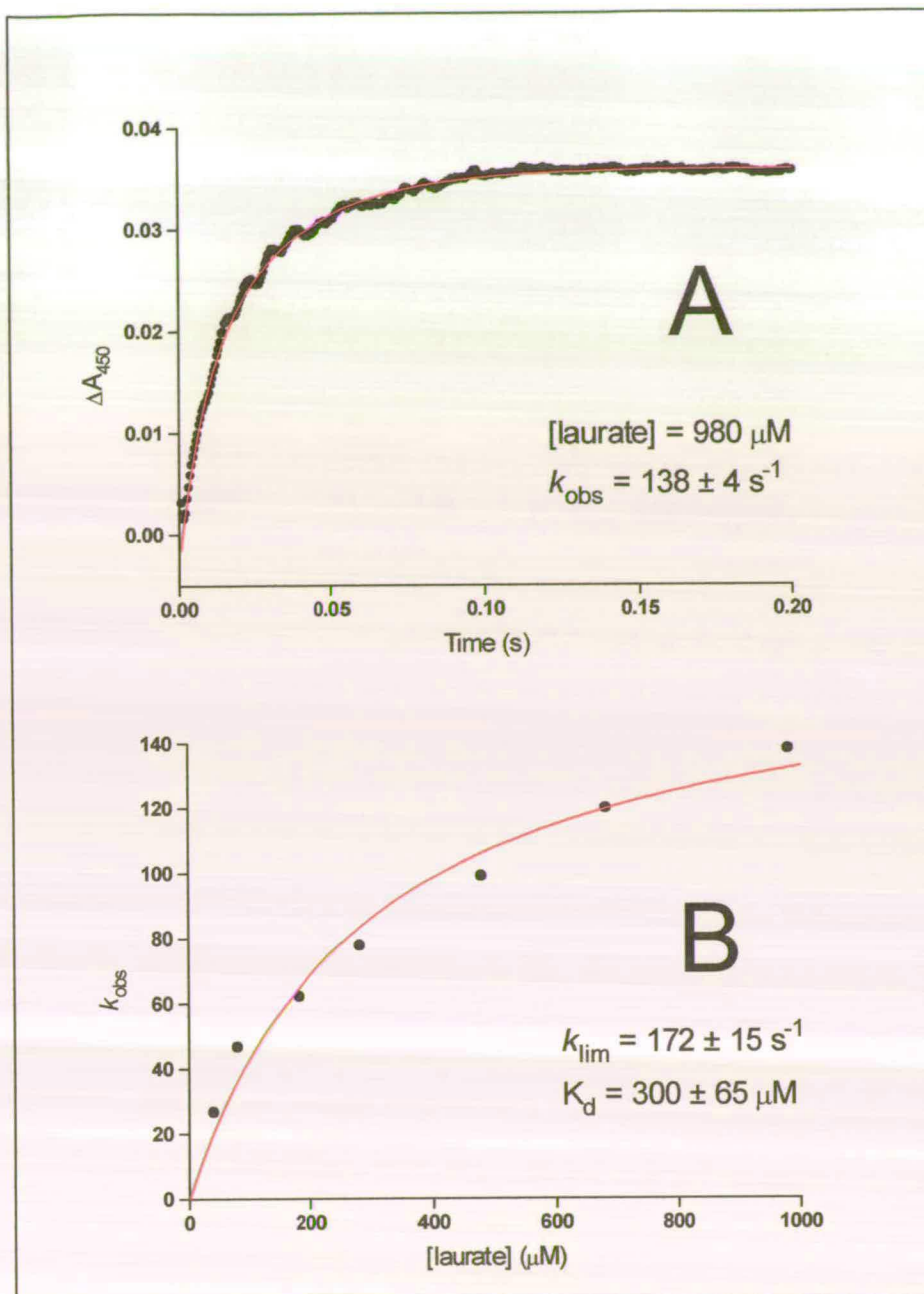


Figure 3.5: Example stopped-flow traces for the pre-steady-state heme reduction kinetics. Panel A shows an example stopped-flow trace for wild-type P450 BM3 in the presence of 980 μM laurate, from which values of k_{obs} were obtained. A plot of k_{obs} at different substrate concentration is shown in Panel B, from which k_{lim} (the rate of heme reduction), was evaluated. See Section 2.8 for details.

Clearly this microscopic rate is the major determinant of catalytic turnover rate, as observed previously [112]. However, with the F393A and F393H mutants, the situation is markedly different. For instance, in F393A, the flavin-to-heme rate is

1176 s^{-1} but the steady-state rate is only 21 s^{-1} . Evidently, a step subsequent to the first electron transfer to the heme iron has become rate-limiting in these mutants.

3.2.7 Generation of the oxy-ferrous complex

Binding of oxygen to the ferrous wild-type heme domain and F393Y-HD was too transient to be monitored on a macroscopic time-scale, no absorbance spectrum for an oxy-ferrous species could be obtained for either of these enzymes. Addition of oxygenated buffer to the pre-reduced protein led to immediate oxidation to the ferric resting state, without noticeable formation of any oxy-ferrous intermediate. This was unsurprising considering that the oxy-ferrous intermediate has only been transiently observed for wild-type P450 BM3 at cryogenic temperatures [138]. However, the formation of the oxy-ferrous complex for the F393A-HD and F393H-HD were observed (Figure 3.6), in both the substrate-free and arachidonate-saturated ($66 \mu\text{M}$) forms. This result provides evidence of an increase in the stability of the ferrous-form of the F393A and F393H mutants with respect to wild-type, i.e. the stable binding of oxygen to the heme for a appreciable period prior to eventual reoxidation of the heme. This supports the idea that the substitution of phenylalanine 393 alters considerably the reactivity of the P450 heme with molecular oxygen.

3.2.8 Kinetics of oxy-ferrous decay

Although the lifetime of the oxy-ferrous complex of wild-type and F393Y enzymes was too transient to record an absorbance spectrum, the pre-steady-state kinetics of the decay of the complexes (as well as those for F393A and F393H) could be comfortably measured using stopped flow spectrophotometry (as outlined in Section 2.8). At the chosen wavelengths, the rate of decay (k_{off}) was exponential with time indicative of the first-order dissociation of superoxide from ferric heme (Table 3.6). Example traces for the decay of the oxy-ferrous complex of wild-type P450 BM3 are shown in Figure 3.7. The rate of formation of the oxy-ferrous complex was too fast for accurate evaluation, occurring within the dead-time of the stopped-flow. The results show that the stability of the oxy-ferrous complex of the F393Y mutant in both the substrate-free and substrate-saturated forms is essentially the same as

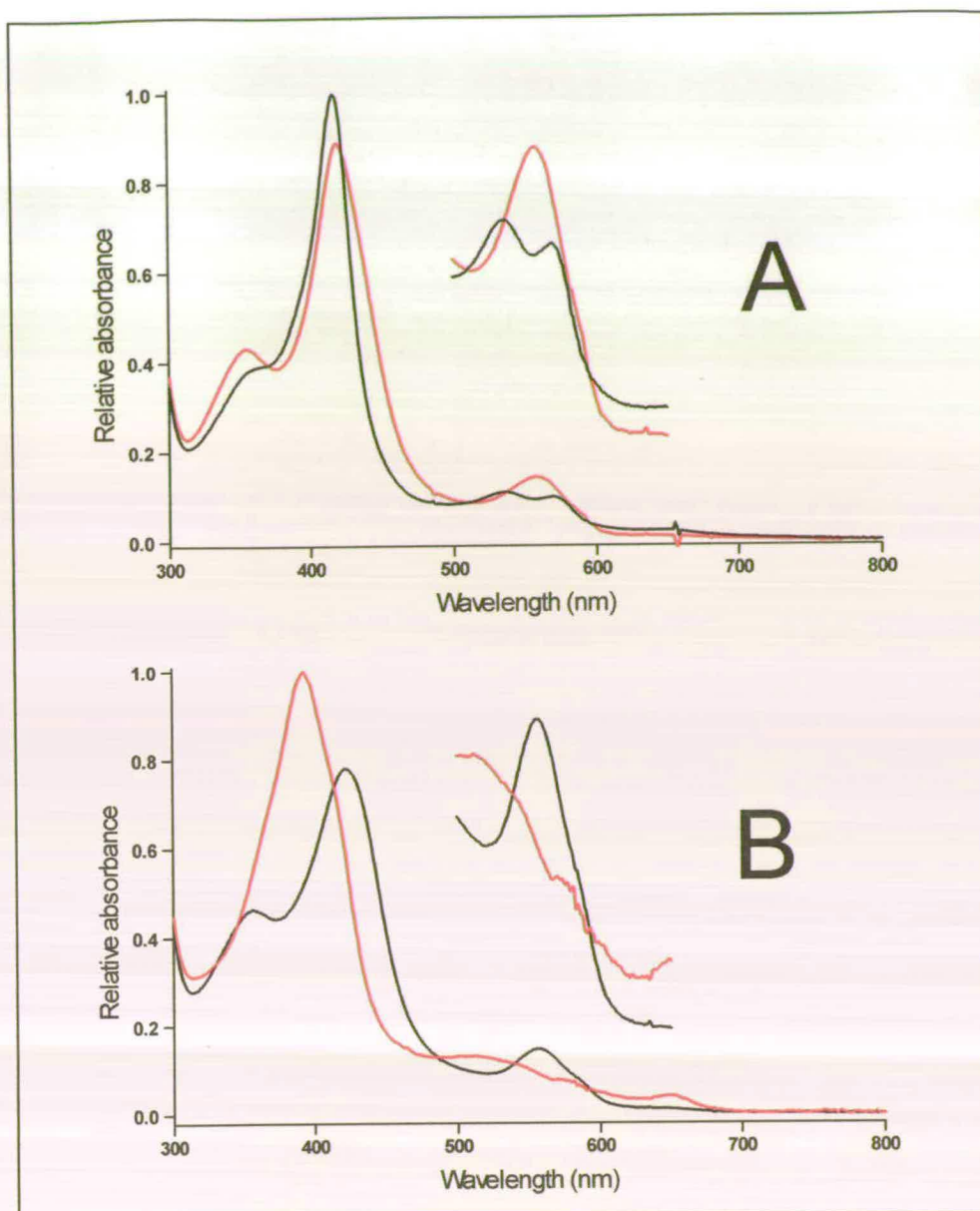


Figure 3.6: Visible absorbance spectra for the oxy-ferrous complex (black line) for substrate-free (Panel A, $A_{\max} = 420$ nm) and substrate-saturated (Panel B, $A_{\max} = 424$ nm) forms of the F393A mutant of P450 BM3. Inset is a 5x magnification of the α/β region for clarity. .

wild-type. Yet F393A and F393H display considerably more stable oxy-ferrous complexes (between 18 to 40-fold) than wild-type. The complexes are also more stable in the presence, than in the absence, of substrate. Both of these observations correlate with the changes in reduction potential observed as a consequence of mutating F393 or the binding of substrate. The magnitude of the difference in k_{off}

Table 3.6: Pre-steady state kinetics of oxy-ferrous decay

	Substrate-free (A_{380})	Substrate-saturated (A_{424})
	k_{off} (s^{-1})	k_{off} (s^{-1})
Wild-type	$0.17 \pm 5.9 \times 10^{-4}$	$0.12 \pm 4.5 \times 10^{-4}$
F393A	$6.4 \times 10^{-3} \pm 1.9 \times 10^{-5}$	$3.0 \times 10^{-3} \pm 2.6 \times 10^{-5}$
F393H	$9.4 \times 10^{-3} \pm 7.7 \times 10^{-5}$	$2.6 \times 10^{-3} \pm 1.3 \times 10^{-5}$
F393Y	$0.12 \pm 4.2 \times 10^{-4}$	$0.10 \pm 1.2 \times 10^{-4}$

between wild-type and the F393A or F393H mutants in the presence of substrate is twice that in the absence of substrate, whilst the difference between their reduction potentials (hence driving force) is essentially constant (Figure 3.8). This suggests that the stability of the oxy-ferrous complex is not dictated solely by thermodynamic factors and that the physical presence of substrate plays an important role in the stability of this complex. This could be due to differences in the hydrophobicity or conformation of the active site induced upon substrate binding.

3.2.9 Heme domain potentiometric titrations

The substrate-free and arachidonate-saturated (33 μM) reduction potentials of WT-HD, F393A-HD, F393H-HD and F393Y-HD were measured in an attempt to establish effects of the mutations on the thermodynamic properties of these variants. Figure 2.5 shows the spectral shifts observed during the course of these potentiometric titrations. At the high P450 concentration ($\sim 20 \mu\text{M}$) required for efficient communication between the P450/mediators/electrode, the absorption at the Soret maximum is much too high for accurate spectrophotometric measurement. A convenient part of the spectrum that reflects accurately the change in reduction state of the heme iron at this P450 concentration is the region between 460 nm and 470 nm. Therefore, data for the substrate-free titrations at 465 nm were plotted against measured potential (mV vs SHE). Due to the spectral differences generated upon addition of substrate to the enzymes, substrate-saturated titrations were evaluated differently, plotting the difference in absorbance $A_{484} - A_{730}$ against measured

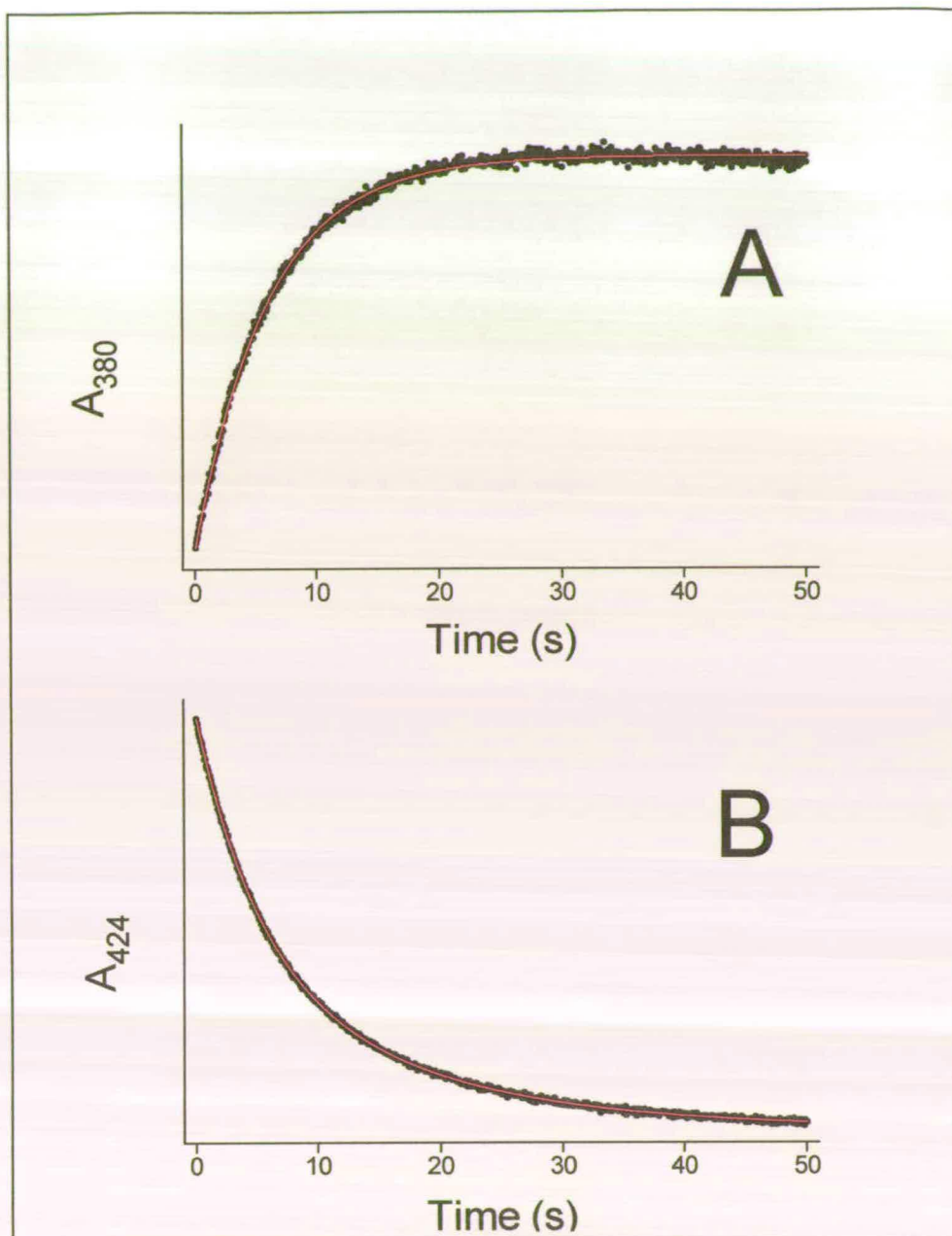


Figure 3.7: Example stopped-flow traces for the time-dependent decay of the oxy-ferrous complex of wild-type P450 BM3 in the absence (Panel A) and presence (Panel B) of substrate. At the wavelengths monitored, the data fits well to a single exponential (red line).

potential (Figure 3.9). Data were fitted to a one-electron Nernst function, and values obtained are presented in Table 3.7.

The first observation is that the reduction potential of the wild-type P450 BM3 heme iron has been more accurately re-determined in light of improved experimental techniques. The more negative reduction potential determined fits better to the

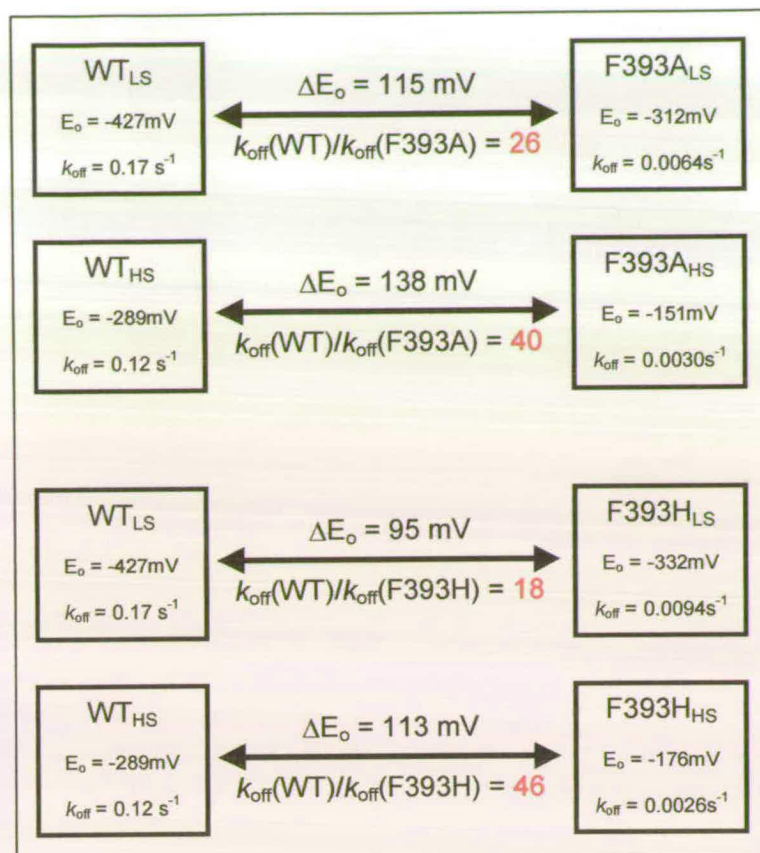


Figure 3.8: Comparison of the thermodynamic and kinetic factors effecting the stability of the oxy-ferrous complexes of the F393A and F393H mutants, and their comparison with wild-type P450 BM3.

proposed redox organisation within P450 BM3. At this potential, the substrate-induced redox switch [139] can still operate, since binding of substrate increases the reduction potential by 138 mV (to -289 mV) allowing electron transfer from NADPH, through the reductase and ultimately to the heme.

Table 3.7: Heme Reduction Potentials

	E_o (mV vs SHE)			
	Wild-type HD	F393A HD	F393H HD	F393Y HD
Substrate-free	-427 ± 4	-312 ± 4	-332 ± 6	-418 ± 6
Arachidonate-sat ^d (33 μ M)	-289 ± 5	-151 ± 4	-176 ± 4	-295 ± 6

However, there is tighter control than previously imagined over uncoupling by virtue of the fact that the substrate-free heme potential is considerably more negative than

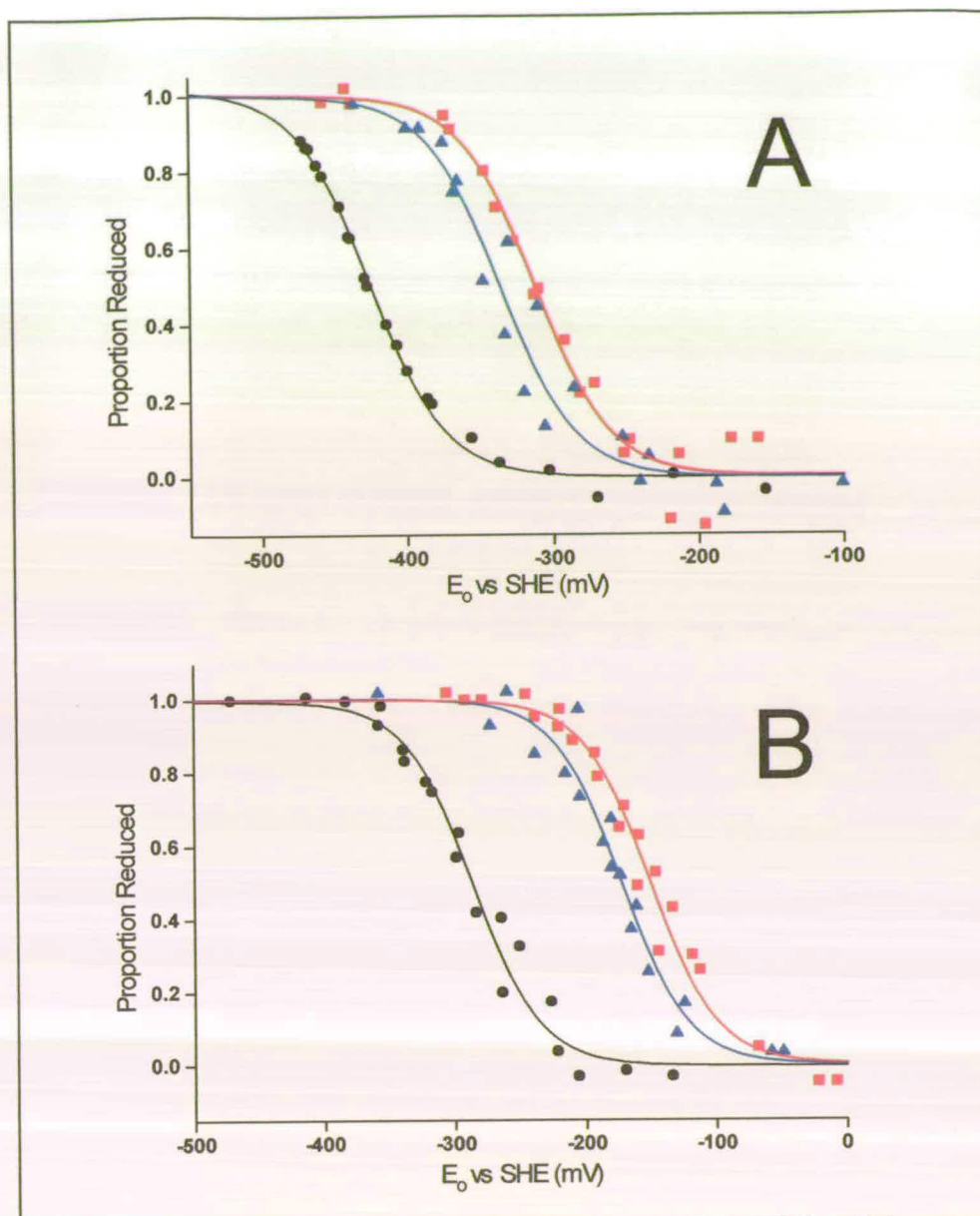


Figure 3.9: Heme-domain reduction potentials of wild-type and mutant P450s BM3. Overlaid, normalised one-electron Nernst curves showing the changes in the proportion of reduced species with reduction potential (vs. standard hydrogen electrode) are presented. The data for F393Y-HD is essentially identical to WT-HD, and has been omitted for clarity. From these, the mid-point potentials of the substrate-free (Panel A) and arachidonate-saturated (Panel B) wild-type heme domain (black), F393A-HD (red) and F393H-HD (blue) were determined (see Table 3.7). The measured heme reduction potentials of both the F393A-HD and F393H-HD (substrate-free and substrate-saturated) mutants are considerably more positive than wild-type heme domain (between 95 and 138 mV) suggesting stabilization of their ferrous forms. The substrate-induced redox shift, observed for wild-type, still operates in the F393A, F393H mutants as observed in wild-type. The nature of the residue at position 393 appears to control the thermodynamic properties of the heme.

that of the physiological electron donor NADPH ($E_0 = -320$ mV) in the low-spin ferric form of wild-type P450 BM3. The midpoint potentials of the two mutants

F393A and F393H are considerably more positive than wild-type ($E_0 = -312$ and -332 mV respectively) and both display similar magnitudes of reduction potential shift upon substrate binding to wild-type ($\sim 140 - 160$ mV shift). The more positive heme reduction potentials of these two mutants are also consistent with the higher rates of flavin-to-heme electron transfer observed. A thermodynamic consequence of the more positive reduction potentials of the heme iron is an increase in the stabilization of the ferrous form.

This is borne out by the ability to generate the ferrous form ($A_{\max} = 410$ nm) for the F393H and F393A mutant P450s aerobically, whereas this is achievable only under strictly anaerobic conditions for the wild-type P450 BM3. It is notable that the increase in reduction potential correlates to the relative size of the sidechain at position 393. As the steric bulk is decreased (Phe/Tyr \rightarrow His \rightarrow Ala), the reduction potential increases accordingly ($E_0 = -427/-418 \rightarrow -332 \rightarrow -312$ mV).

3.2.10 Electron Paramagnetic Resonance

Figure 3.10 shows the perpendicular-mode X-band EPR spectrum of F393H, recorded at 10 K using 2.01 mW microwave power. The g-values of features discussed are indicated on the figure. Minor signals at $g \sim 5.8$ and 4.3 are due to trace amounts of high-spin ferric heme and adventitious Fe^{III} ion respectively. The three major features at $g = 2.43, 2.25, 1.92$ are characteristic of a low-spin ferric heme and are virtually identical to those for the F393A and F393Y mutants and previously reported for the wild-type protein [140,141]. These g-values are typical of native low-spin ferric P450s and nitric oxide synthases (NOS) in which the heme is bound axially by cysteinate and water and also match those of adducts in which the water is displaced by a range of oxygen-donor ligands [42,142-144]. The position of these bands was the same for all of the mutants.

3.2.11 Crystallography (with Dr. C.G. Mowat)

The crystallographic results will not be discussed in detail, as the solution to the substrate-free F393 mutant structures was the work of Dr. C.G. Mowat, however the

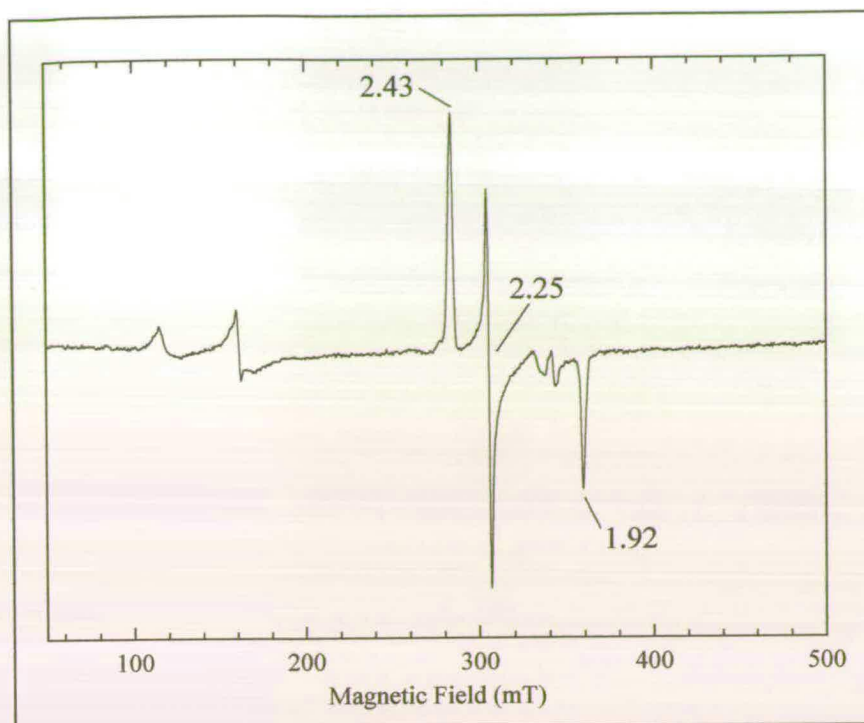


Figure 3.10: EPR spectrum of ferric P450 BM3 F393H heme domain. The spectrum was recorded at 10 K, using a 1 mT modulation and 2.01 mW microwave power. Sample concentration was 218 μM . The g -values of 2.43, 2.25 and 1.92 are typical of low spin, ferric heme. Signals at $g \sim 5.8$ and 4.3 are due to small amounts of high spin ferric heme and adventitious iron.

pertinent features of the structures are referred to. Detailed results for the solution of the F393H HD are reported in Ost *et al* 2001 (PDB: 1JME) [125], the structures of F393A and F393Y are as yet unpublished.

The substrate-free crystal structures of the F393 mutants (all solved to ~ 2.0 Å) clearly shows the substitution of the six membered phenyl sidechain of phenylalanine by either methyl (F393A-HD), imidazole (F393H-HD) or phenol (F393Y-HD), Figure 3.11. In the case of the F393H-HD and F393Y-HD mutants, the side-chain of residue 393 adopts a very similar position to the phenylalanine of wild-type, sandwiched between the side-chains of Pro392 and Gln403, with no major conformational changes of surrounding residues as a result of the mutation. In the F393H-HD structure, a solvent water molecule positioned on the opposite side of His393 to the heme, is hydrogen-bonded to N δ 1 of the histidine side-chain (N...O = 2.77 Å). The apparent protonation state of this histidine and the presence of an intermolecular hydrogen-bond to water, appears to preclude the formation of an intramolecular His393...Cys400 hydrogen-bond. In the F393A-HD structure, the

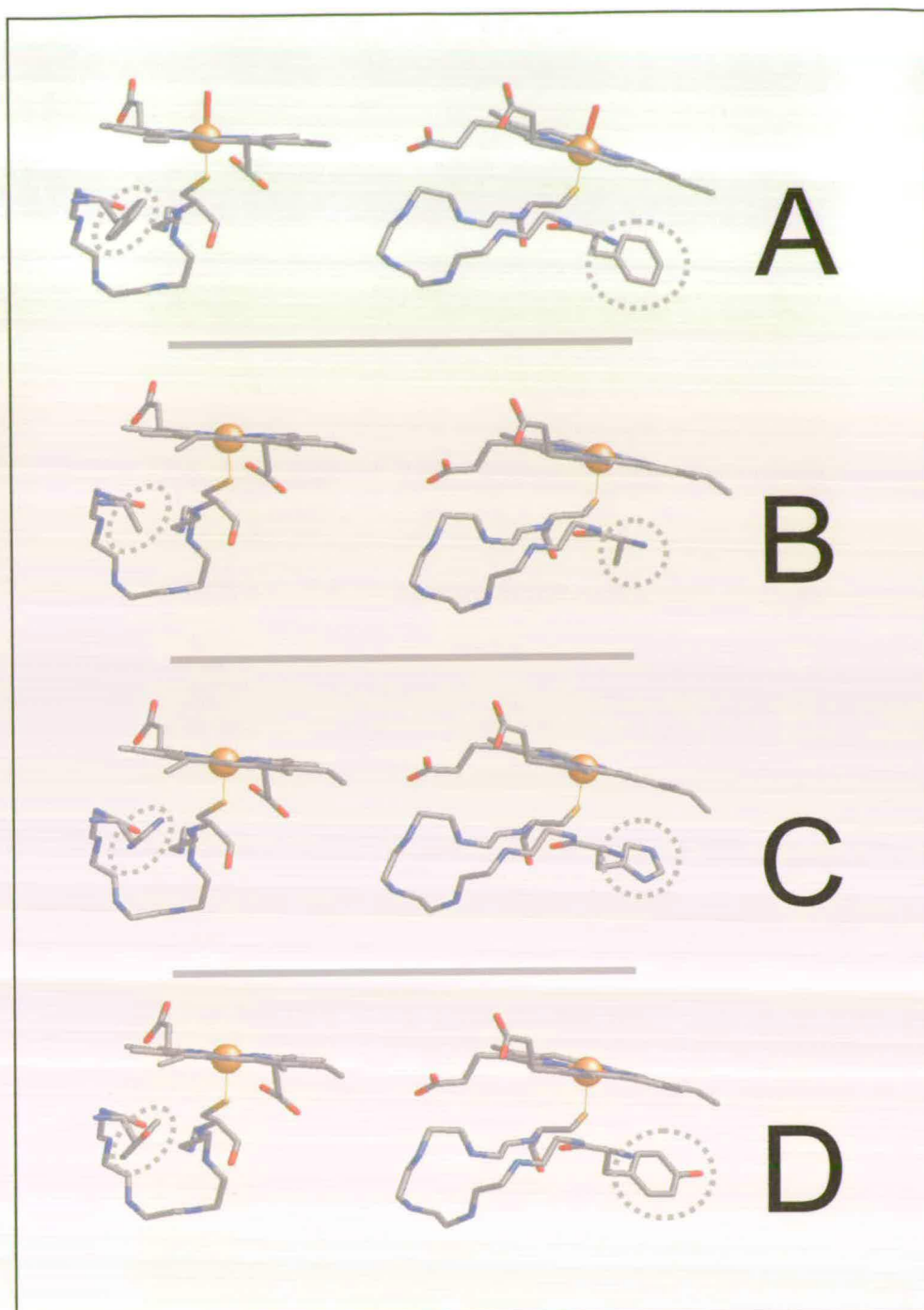


Figure 3.11: Panels A-D show the crystal structure of the heme and the backbone chain of the heme-binding loop (residues 393-400) of (a) P450 BM3 wild-type, (b) F393A, (c) F393H, (d) F393Y mutants. The dotted circle highlights residue 393. The two different views indicate the position and orientation of the sidechain of residue 393 relative to the heme and the cysteine ligand.

electron density for the Gln403 residue suggests that it is conformationally flexible, capable of adopting one of two possible orientations with the amide group pointing toward or away from the heme. Refinement of the structure favoured adoption of the former conformation, with an estimated occupancy of ca. 85 %, whereby the amide head of Gln403 moves to accommodate the space created by the substitution of phenylalanine393 by alanine (Figure 3.12).

Table 3.8 lists key structural parameters of the substrate-free wild-type HD and F393X HD (X = A, H or Y) mutant crystal structures.

Table 3.8: Key Structural Parameters

	Structural Feature			
	Fe...S (Å)	F393X...Cys400 (Å)	F393X...heme (Å)	∠ Fe-S-Cys (°)
Wild-type HD	2.05	3.67	3.57	111.70
F393A HD	2.22	3.94	5.29	104.34
F393H HD	2.13	3.50	3.45	109.17
F393Y HD	2.26	3.69	3.57	107.08

3.3 Discussion

3.3.1 The consequence of mutating Phe393

Certain parallels can be drawn between these data and those reported previously for mutants of P450 1A2 (e.g. similar blue-shifts in the ferrous-CO spectra) [130] and P450 2E1 (slower turnover kinetics) [131]. However, in the light of this study, it is clear that previous assumptions made as to the role of the phenylalanine (decreased enzyme stability and alteration of electron flow) are unlikely to fully account for the observed decreases in catalytic activity.

The successful overexpression of F393A, F393H and F393Y mutants demonstrates the lack of a requirement for a phenyl ring to stabilise heme binding. Also, the

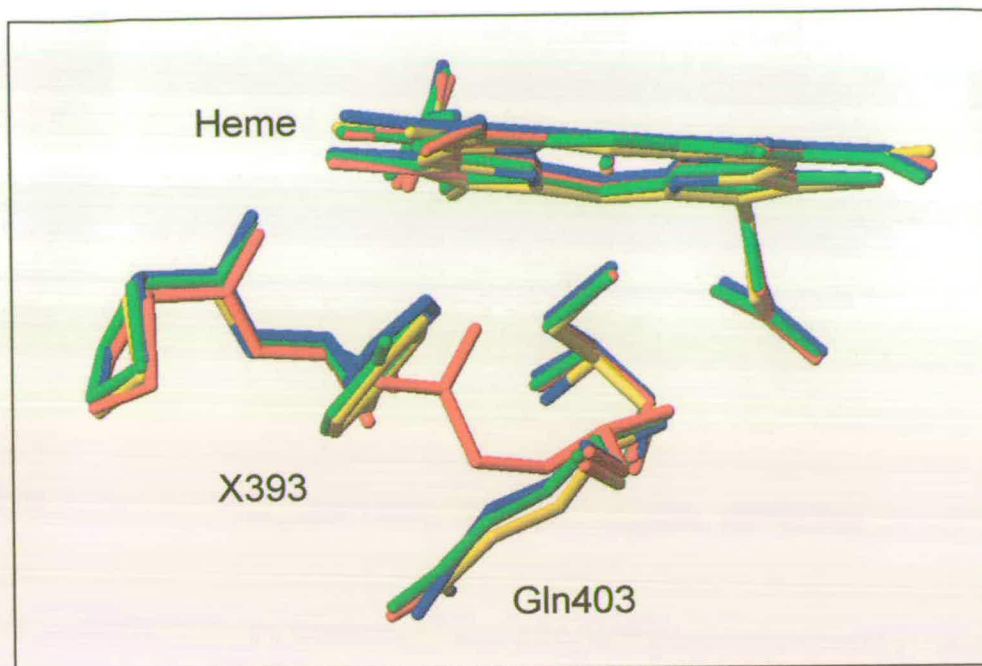


Figure 3.12: Superposition of the heme and residues Phe393 and Gln403 of P450 BM3 wild-type (yellow), F393A (red), F393H (blue) and F393Y (green) mutants. The sidechain of residue Gln403 is in the same orientation in the F393H and F393Y mutants as in wild-type, but moves to accommodate the space created by the F393A substitution. In the F393A mutant, it is proposed that an intramolecular hydrogen bond is formed between the cysteine ligand and the amide nitrogen of Gln403 in this new conformation.

kinetic profiles of these mutant enzymes dismisses the argument that this residue is essential in facilitating electron transfer to the heme. It has been demonstrated that whilst the F393A and F393H enzymes are less catalytically competent (lower turnover rate), the study of individual steps in the catalytic cycle reveals that the rate of heme reduction is actually faster for these mutants than for wild-type. Thus, replacement of the phenylalanine can actually elevate the rate of heme reduction. Contrary to previous suggestions, the residue is non-essential for mediation of electron transfer, either directly or indirectly, to the heme. It is not required absolutely for electron transfer, but instead plays a vital role in the control of the process. The question is then one of how this control is achieved. The most convenient starting point for discussion is with the thermodynamic data obtained from the potentiometric titrations. All other results are consistent with, and can be explained in light of, data from these experiments.

Substitution of phenylalanine 393 by either histidine or alanine results in an increase of the heme iron reduction potential with respect to wild type P450 BM3, whereas the reduction potential is unchanged upon substitution by tyrosine. This explains the apparent contradiction in effects on steady-state (decreased) and heme-reduction (increased) kinetic rates observed for the mutants relative to wild-type P450 BM3. Creating a large positive gap in reduction potential between the electron donor (NADPH at $E_o = -320$ mV ultimately providing the electron(s) to the FMN semiquinone at $E_o = -213 \pm 5$ mV) and the substrate-bound heme (e.g. $E_o = -151 \pm 4$ mV for F393A) increases the driving force (ΔG) for heme reduction in this system (Figure 3.13). The observed increase in pre-steady state flavin-to-heme electron transfer kinetics ($k_{lim} = 1180$ s⁻¹ (F393A) cf. 348 s⁻¹ (WT)) is totally consistent with the more positive reduction potentials of heme iron (suggesting stabilization of the ferrous form) in the F393A and F393H mutants. However, the fact that F393A and F393H mutants give much lower steady-state rates of fatty acid-dependent NADPH oxidation suggests that some step, other than substrate-binding or first electron transfer, has become rate limiting in these mutants. The increased stability of the oxy-ferrous intermediate of these mutants with respect to wild-type infers that a step subsequent to oxygen binding is likely to be responsible for the steady-state discrepancy.

Product analysis of the F393H mutant-catalysed myristate-turnover was essentially identical to wild-type, with ω -1 hydroxylation predominating [125]. No unusual oxidation products, suggestive of a change in the specificity of the mutant, were observed. From this we can conclude that F393 does not significantly influence either the regio- or substrate-specificity of the enzyme. This is an important observation, confirming that F393H is able to act as a P450, yet is catalytically impaired relative to wild-type.

For wild-type P450 BM3, the rate of first electron transfer to the ferric heme (348 s⁻¹ with arachidonate) is similar to the steady-state k_{cat} for turnover of this substrate (285 s⁻¹), indicating that the sequence of events leading to the first electron transfer to the heme plays a major role in the rate limitation of turnover. By contrast, in the

F393A and F393H mutants, not only are the rates of heme reduction elevated (1176 s^{-1} and 832 s^{-1} , respectively, with arachidonate), but the steady-state turnover rates are diminished (21 s^{-1} and 33 s^{-1} , respectively). Obviously, there is a new major factor in overall rate limitation that occurs subsequent to the first heme reduction and, presumably, does not involve substrate binding (as the binding characteristics of the mutants are essentially identical to wild-type). This factor almost certainly reflects the increased stability of the oxy-ferrous form in the mutants. The elevated reduction potential of their hemes results in the stabilisation of the oxy-ferrous form to a greater extent than that observed for wild-type. The change in the reduction potential does not significantly alter the rate of oxygen association to ferrous heme (presumably due to the high affinity of ferrous heme for oxygen), but does effect the rate of decomposition of the oxy-ferrous complex. The dissociation of the oxy-ferrous complex in wild-type is 27- and 18-fold faster than either F393A or F393H respectively, providing conclusive evidence for the increased stability of the ferrous-forms of the F393A and F393H mutant enzymes. A more pronounced difference in the stability of the oxy-ferrous complex is observed when substrate is bound, as oxy-ferrous dissociation is 40- and 46-fold slower for F393A and F393H mutants than wild-type. Substrate participates in the stabilisation of the oxy-ferrous complex in a manner which is currently unresolved, but which is likely to be the result of an increase in the hydrophobicity or a conformational change in the active site.

The consequence of the elevated heme reduction potential in F393A and F393H is that oxygen activation is disfavoured, and that the stabilized oxy-ferrous intermediate becomes a thermodynamic trap, which decreases the rate of overall catalysis. Speculation as to the actual step perturbed can be made based on the evidence compiled. Of the remaining steps in the catalytic cycle, changes in i) the rate of second electron transfer, ii) O-O bond scission and iii) the reactivity of the oxy-ferryl moiety could all be responsible for rate limitation. Any significant alteration to steps involving dioxygen cleavage or oxygen atom insertion would be expected to change the extent of uncoupling *via* either the peroxide or oxidase pathways respectively. A change in the specificity of reaction may also have been expected if a modification of oxy-ferryl reactivity had occurred. The results do not support these possibilities as

neither mutant is extensively uncoupled and the product profile for the F393H mutant was essentially identical to wild-type. Although experimental verification is still required, it appears likely that in these mutants, the rate of second electron transfer replaces the rate of heme reduction as the overall rate limiting step.

3.3.2 The cause of the thermodynamic control

The two dominant factors which influence reduction potentials in proteins are a) the dielectric environment, and b) bonding interactions at, and to, the redox centre [146]. Whilst the effects on the kinetic and thermodynamic properties have been experimentally substantiated, the results from the spectroscopic and structural analysis of wild-type P450 BM3 and the F393 mutants allow a qualitative discussion regarding the physical process (i.e. the precise *cause*) by which these differences have occurred. The F393Y mutation is so conservative, that only minor deviations from the characteristics of wild-type P450 BM3 were observed. Consequently, the discussion will concentrate on the factors responsible for the dramatic differences between the F393A and F393H mutants with respect to wild-type. For the purpose of the discussion, the F393Y mutant is regarded the same as wild-type, unless otherwise stated.

The EPR spectrum of each of the F393 mutants is identical to that of the wild-type enzyme. This infers that the iron in the ferric form is in a similar environment (no change in *g* values) in both enzymes, and that they share a common ferric resting state. The form of the EPR spectrum is determined mainly by the relative splitting of the ferric *d*-orbitals, if all five are moved in energy together by a process that does not substantially alter the iron geometry, then the spectrum would remain the same. It is surprising, therefore, that the elevation in the reduction potential of the heme does not induce a significant change in the EPR spectrum. This observation implies that the positive shifts in reduction potential of the F393A or F393H mutants relative to wild-type (reported previously [125]) are due to differences in the energy of their ferrous-forms, relative to the observed, common ferric ground state (Figure 3.13). Electrons are more easily introduced to the iron frontier orbitals of the F393A and F393H mutants as a consequence of the difference in the energy (ΔE) between the

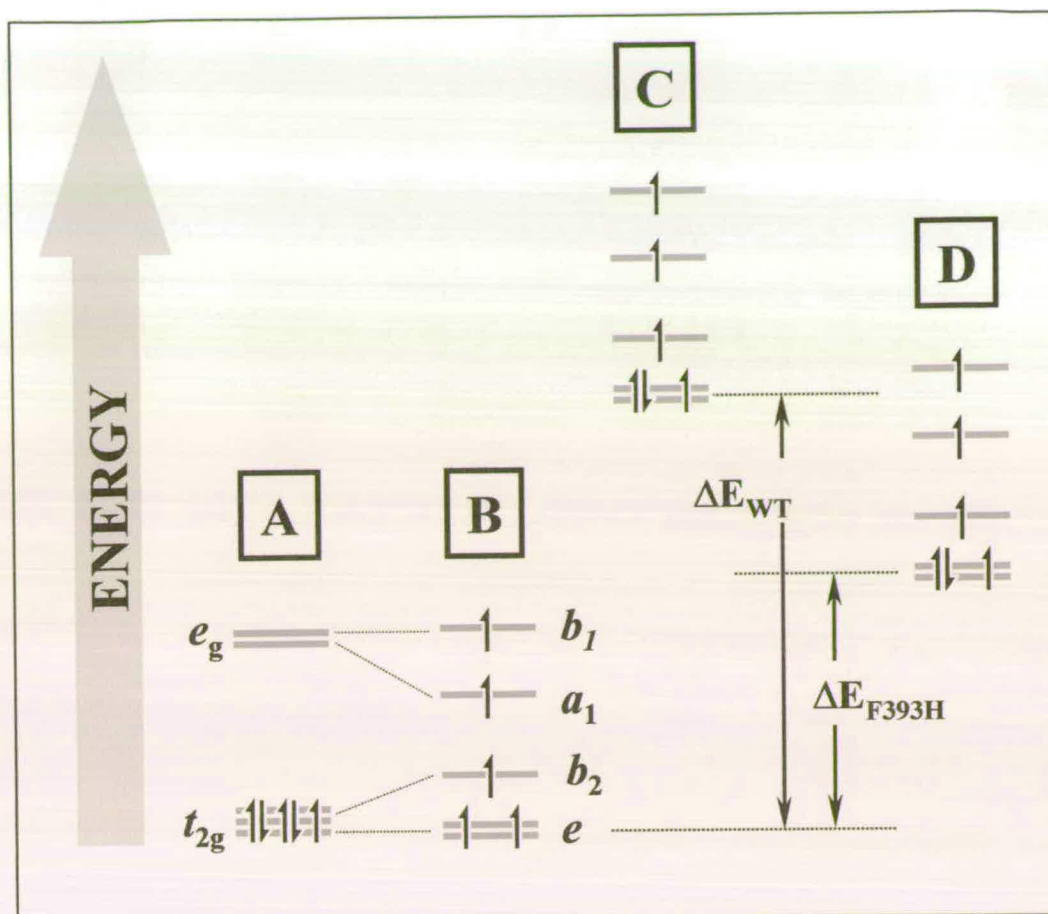


Figure 3.13: Diagrammatic representation of the proposed perturbation in the iron d-orbital energies between the ferric-resting state (A), the substrate-bound state (B) and the one-electron reduced forms of wild-type (C) and F393H mutant (D), caused by the substitution of phenylalanine 393 by histidine. The energy difference (ΔE) between the ferric- and ferrous-d-orbitals (related to the $\text{Fe}^{\text{III}}/\text{Fe}^{\text{II}}$ reduction potential by the Nernst equation, $\Delta G = -nF\Delta E$) is smaller for the F393H mutant (ΔE_{F393H}) than wild-type (ΔE_{WT}). This is consistent with the elevated reduction potential of the F393H mutant compared to the wild-type enzyme. The similarity of the ferric-EPR spectra for the F393H and wild-type enzymes suggest that the magnitude of the crystal field splitting parameter (Δ_o) is unchanged by the mutation.

ferric- and ferrous-forms being smaller than for wild-type. This is reflected in the $\text{Fe}^{\text{III}}/\text{Fe}^{\text{II}}$ couple for the F393A and F393H mutants being more positive than wild-type (reduction requires less energy). Whilst this is an unusual observation, it is not unique. It has been demonstrated that loading the core of the bacterioferritin from *Azotobacter vinelandii* drops the reduction potential of its heme group by ~ 250 mV, without changes being observed in the EPR spectra of the loaded and unloaded forms [147].

Changes in the dielectric environment of the heme

The study of the F393X mutant structures allows us to qualitatively evaluate how, or even if, changes in size, hydrophobicity and electrostatics affect the heme reduction potential and provides a useful context for discussion.

Neither the F393A, F393H nor F393Y substitutions grossly increase the exposure of the heme to solvent, or dramatically change the hydrophobicity of the heme binding pocket relative to wild type. Whilst the N δ 1 of the His393 is solvent exposed (formation of a His...H₂O H-bond (Figure 3.14)), the steric bulk of the histidine residue is sufficient to prevent the penetration of water which would alter the dielectric environment at the iron, and hence the redox properties, of the heme. The movement of Gln403 toward the heme in the F393A structure also serves to minimise heme exposure, which may have been predicted by the significant steric effect of replacing a phenyl ring by a methyl group.

The crystal structure of the F393H HD was determined at pH 6.5, a pH at which His

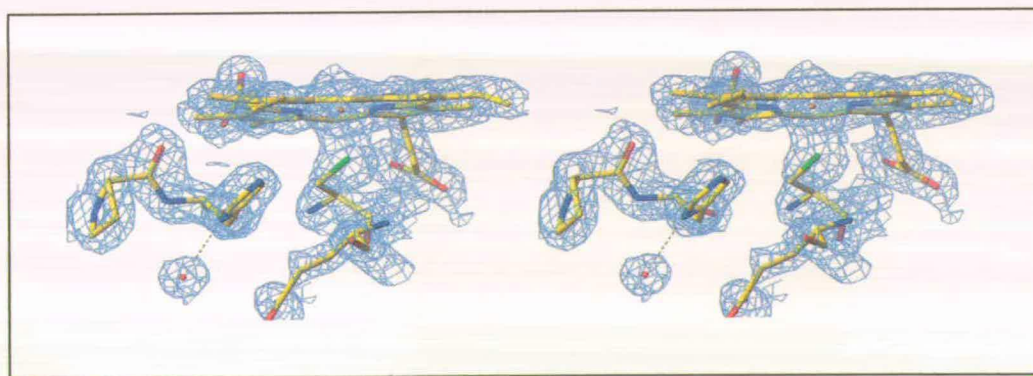


Figure 3.14: A stereo view of the heme binding region of the F393H mutant. Electron density is shown in cyan, whilst the heme macrocycle and peptide are shown in atom-type colours (red = oxygen, blue = nitrogen and green = sulfur), the heme iron is depicted in orange. This figure clearly shows electron density for water molecule X and the likelihood of an intermolecular hydrogen-bond to histidine 393. The electron density map was calculated using Fourier coefficients ($2F_o - F_c$), where F_o and F_c are the observed and calculated structure factors respectively. The contour level is 1.5σ , where σ is the rms electron density. This diagram was generated using TURBO-FRODO.

may be expected to be partially protonated, with the resulting imidazolium interacting with Cys400. Redox titrations of both wild-type and the F393H mutant have been performed over a pH range 6 - 8 (data not shown) and neither show a significant (< 15 mV) deviation from the value of the reduction potential determined at pH 7.0. Since the redox potential of the F393H mutant is not pH dependent, one must conclude that His393 remains in the same protonation state through the pH range 6-8. How the His-water hydrogen-bond affects the pKa of this residue is unquantifiable, but if, for example, it is dramatically increased (i.e. toward the pKa of free imidazole, pKa = 9), it is plausible that the residue would have mainly imidazolium character within the range pH 6 - 8. The presence of a positive charge so close to the heme-ligand would introduce a significant electrostatic interaction between His393 and Cys400. This increase in Lewis acidity would destabilize the Fe-S bond, by drawing electron density away from the iron and toward His393, with a possible concomitant effect of lengthening, hence weakening, the Fe-S bond.

It seems unlikely that any of the single point mutations discussed would cause a large enough change in the hydrophobicity or dielectric environment of the heme to account for the dramatic differences observed in the reduction potentials. The comparison of cytochrome *c* with the octapeptide (methionine) complex (formed by the hydrolysis of cytochrome *c*) is the classic study of how heme solvation and the change in the dielectric environment of the heme affects redox properties [148]. Here a heme reduction potential shift of 300 mV is observed between the semi-exposed, partially solvated heme of cytochrome *c*, with the fully exposed and solvated heme of the octapeptide (hence, the difference in solvation being substantial and influential). It is also interesting to note that the reduction potential in a series of F82 mutants of cytochrome *c* (a highly conserved phenylalanine in cytochrome *c*, in a similar environment to F393 in P450 BM3) shift only slightly (by 43 mV) upon substitution of phenylalanine by glycine [149]. Previously, the minor redox potential changes of these cytochrome *c* Phe82 mutants had been rationalized by assuming the removal of the steric bulk of phenylalanine was compensated for by a refolding of the peptide. Whilst this resulted in a change in the dielectric environment of the heme (increased the number of polar amide backbone groups in the hydrophobic heme

pocket, due to the refolding) no overall increase in the degree of heme solvation was observed compared to wild-type cytochrome *c* [150,151]. The fact the F393 mutations involve such a slight steric substitution suggests that the changes in hydrophobicity and heme-exposure, would be minimal.

Distortions to the heme-plane would cause perturbations in the energy levels of the porphyrin macrocycle, leading to modifications of the thermodynamic properties of heme. Residue 393 is within van der Waals contact of the heme plane, so any increase or decrease in steric bulk at this position would have an impact on the degree of this interaction. Direct structural comparison of heme planes is difficult, as the degree of distortion depends highly upon the constraints placed on the heme during refinement of the X-ray structure. However, none of the hemes look particularly distorted with no significant difference in the B-factor of the hemes between the structures.

Bonding interactions to the redox centre

More plausible reasons for the modification of the redox properties observed, are the factors affecting the bonding interactions of the redox centre. The iron-cysteine bond is central to the reactivity of P450s. It has been suggested that the cysteinate ligand provides a 'push' effect, whereby the strong electron donating nature of the thiolate pushes electron density toward the heme iron. This increases the electron-rich nature of the heme [65,152], facilitating the stabilisation of high iron oxidation states, and also helping the heterolytic cleavage of the O₂ bond. Therefore, it is likely that factors affecting the nature of the Fe-S bond are likely to have significant implications on the P450 catalytic cycle. In nitric oxide synthases (NOSs), there is a highly conserved tryptophan residue six residues downstream of the cysteine ligand, which forms an intramolecular hydrogen-bond with the heme ligand [153] (Figure 3.15). Mutation of Trp409 of nNOS to either phenylalanine or tyrosine, results in mutant forms in which heme reduction is slowed relative to wild-type [154]. This decrease in rate was attributed to the removal of the hydrogen-bond, resulting in a decrease in the heme reduction potential. By analogy, the formation of a hydrogen bond with the cysteine ligand of P450 BM3 could cause an increase in the heme

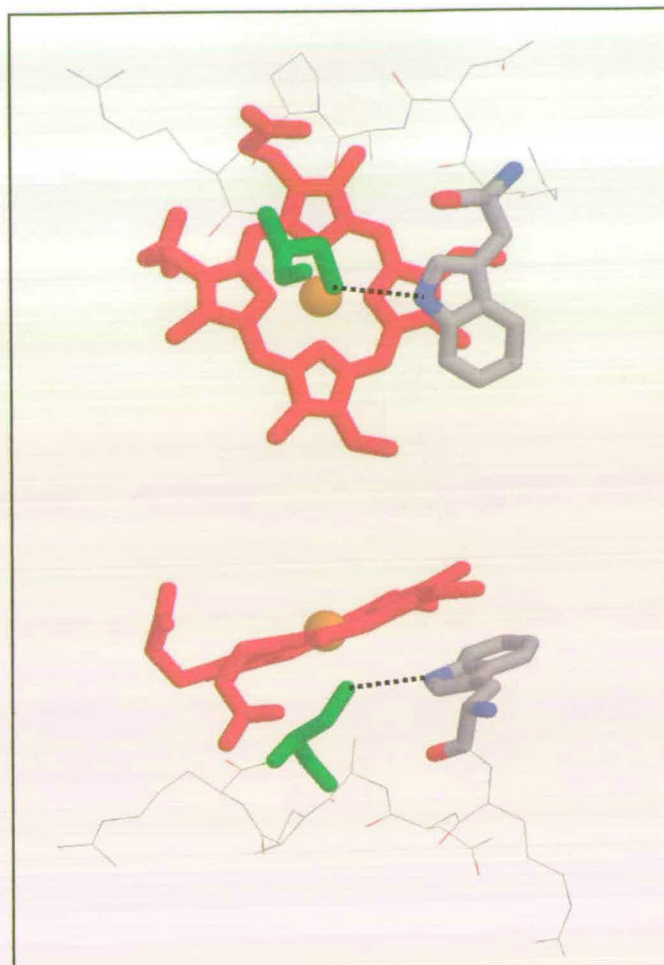


Figure 3.15: Illustration of the heme binding region of inducible nitric oxide synthase (iNOS). Shown are the heme (red) and residues the residues which constitute an analogous cysteine ligand loop to that observed in P450s (from Trp188-Cys194). Tryptophan 188 (atom type colours) forms an intramolecular hydrogen bond (dotted line, 3.74 Å) to the heme ligand Cys194 (green). The presence of this hydrogen bond serves to modulate the heme electronegativity, and acts as a feedback control mechanism in the reaction of NOS with oxygen and nitric oxide.

reduction potential, which would account for the effects observed for the F393A and F393H mutants. The formation of an intramolecular hydrogen-bond would remove electron density from the Fe-S bond, reducing the ability of the thiolate to stabilize high oxidation states. Alternatively, this thiolate can be considered as being more highly tuned to stabilising low oxidation states (e.g. nNOS, $E_{1/2} = -239$ mV [155]).

From inspection of the F393H mutant alone, it is impossible to decide categorically whether or not H393 hydrogen bonds to the cysteine for several reasons: i) His393 forms an intermolecular hydrogen bond with a solvent water molecule; ii) the

relative orientations of H393 and Cys400 are incorrect; and iii) the F393A mutant (without the functionality to form a hydrogen bond) displays a similar pronounced effect on the heme reduction potential.

In the structures of wild-type, F393H and F393Y, the residue sidechain is sandwiched between Gln403 and Pro392, with the amide group of Gln403 pointing toward the solvent. In the structure of the F393A HD, Gln403 moves ca 180° to accommodate the space created by substitution of phenylalanine393 by alanine (Figure 3.12). The new conformation adopted by Gln403 brings the amide nitrogen within hydrogen bonding distance of Cys400. This hydrogen-bond rationalises the observed increase in the heme reduction potential of the F393A mutant according to the reasoning discussed above.

A similar argument can be made for the F393H mutant. Interpretation of crystal structures can often be misleading as they are static representations of dynamic molecules. Consequently, it is conceivable that the intermolecular His393...water hydrogen bond observed in the F393H crystal structure is an artefact of crystallisation, with the orientation of the His393 not being a true reflection of its solution conformation. If rotated, the imidazole head of histidine can adopt an orientation allowing the formation of the desired intramolecular His393...Cys400 hydrogen bond, analogous to that observed for the tryptophan residue of NOS. In fact, the proposed hydrogen bonding distance (3.7 Å) in F393H is identical (within crystallographic error) to that determined for NOS.

3.3.3 Re-evaluation of the mechanistic control exerted by substrate-binding

Substrate binding to P450s is believed to act as a thermodynamic switch, a control mechanism which prevents the futile uncoupled oxidation of NADPH. Displacement of the weakly ligated water molecule from the heme iron induces a change in the iron coordination geometry which is accompanied by an increase in the heme reduction potential. This redox shift is generally accepted to be the factor that prevents heme reduction in the absence of substrate. Little or no consideration is given to the physical significance of the change in coordination geometry of the iron. The

behavior of the F393A mutant appears contradictory, and challenges these ideas. The substrate-free heme reduction potential of the F393A mutant ($E_0 = -312$ mV) is comparable to the reduction potential of substrate-saturated wild-type ($E_0 = -289$ mV). The thermodynamic driving force for the reduction of substrate-free F393A mutant is roughly equivalent to that of substrate-bound wild-type. If substrate-binding exerted only thermodynamic control, then electron transfer to the heme of the F393A mutant would be expected in the absence of substrate, at an appreciably higher rate than substrate-free wild-type (resulting in the uncoupled reduction of oxygen). This is not the case, as the background (substrate-free) rate of NADPH oxidation is the same for the F393A mutant as for wild-type.

This shows that the spin-state change is more important in activating electron transfer in the wild-type enzyme, and that the change in the driving force associated with substrate binding is much less important. Conversely, electron transfer in the F393A mutant is therefore limited by the requirement for a simultaneous change in the ligand coordination sphere (Figure 3.16), so to achieve heme reduction either the water molecule must be lost first or the hexacoordinate iron must first be reduced. This

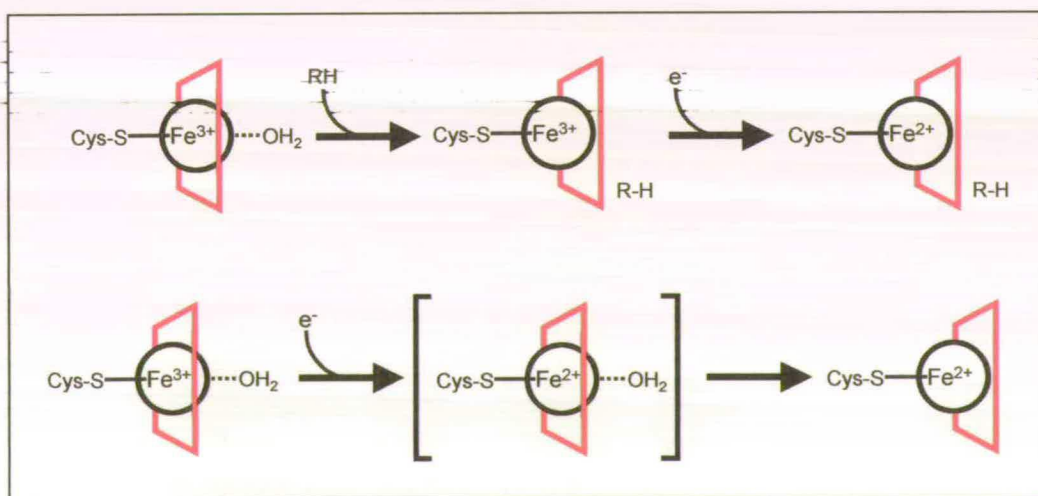


Figure 3.16: Schematic describing the sequence of events leading to P450 heme reduction in the presence and absence of substrate. The porphyrin macrocycle is denoted by the red box. In the absence of substrate, the heme must undergo a redox-induced geometry reorganisation before iron reduction can take place. This reorganisation energy is a kinetic barrier for heme reduction, a scenario that is avoided when substrate is present. The act of substrate binding induces an analogous geometry change, avoiding the requirement for a redox-induced geometry reorganisation.

additional step acts as a kinetic barrier. In P450s, substrate binding exerts kinetic control by preorganising the iron geometry prior to reduction. The shift in heme reduction potential is therefore less important than the change in spin-state induced by substrate binding. This provides the first piece of experimental evidence to support previous assumptions [155b] that the change in driving force for heme reduction is not the primary control mechanism in operation induced by substrate binding.

The previous conclusion that substrate-binding exerted purely thermodynamic control was a logical conclusion, with no requirement to invoke a kinetic argument, as the reduction potential of substrate-free P450 BM3 was considerably more negative than that of NADPH. In light of the observations for the F393A mutant, it is more applicable to consider substrate binding as exerting kinetic control over heme reduction.

3.4 Conclusion

It has been established for flavocytochrome P450 BM3 that the highly conserved phenylalanine residue F393 has an fundamental role in the P450 catalytic mechanism – it exerts thermodynamic control over the heme. The use of site directed mutagenesis has shown that the nature of the residue at position 393 is critical for competent monooxygenase activity. The bulky, aromatic, hydrophobic, chemically neutral character of phenylalanine are features which are required to maintain the hydrophobic environment of the heme and to prevent any intermolecular (solvation) or intramolecular (hydrogen-bond) interactions with the heme ligand. It is by virtue of these influences that phenylalanine exerts its thermodynamic control. The nature of the heme environment imposed by the presence of phenylalanine poises the heme reduction potential such that a likely trade-off is established between NADPH oxidation and oxygen activation. Although this remains speculative and does not rule out possible changes to subsequent steps, e.g. second electron transfer, perturbation of such a balance could result in a considerable loss of enzymatic efficiency.

Furthermore, this study highlights the electronic influence the cysteine ligand has in dictating the characteristic reactivity of P450s, and its sensitivity to its chemical environment. Modulating the electron density of the Fe-S bond (introduction of intramolecular hydrogen bonds) has a direct effect on the ability of P450s to bind and activate molecular oxygen. This point is key to the high degree of conservation of this residue throughout the P450 superfamily – monooxygenation requires oxygen activation. This phenylalanine is conserved in every member which needs to perform this activation, for the small number that do not, the nature of this residue varies.

Chapter 4:

4-cyanopyridine

4 4-CYANOPYRIDINE

4.1 Introduction

One contentious and unresolved issue regarding the general P450 mechanism is the effect heme-reduction has on the affinity of substrate binding.

Although the effect of heme-reduction on substrate binding can be tentatively evaluated by considering the difference between the substrate-free and substrate-bound heme reduction potentials ($-RT\ln K_d = -nF\Delta E_o$), substrate dissociation constants have not been formally quantified for the ferrous-form of the enzymes. It is, however, believed that the affinity of the enzyme for substrate increases dramatically upon reduction (possibly by an order of magnitude) in preparation for reactions between the heme and the substrate in subsequent steps of the catalytic cycle [156,45].

The method by which ferric dissociation constants are determined relies on the visible spectral shifts associated with the low-spin (419 nm) to high-spin (390 nm) conversion of the heme-iron induced upon addition of substrate [157-159]. Binding of substrate to P450s displaces a weakly ligated water ligand that occupies the sixth coordination site of the heme-iron, hence the iron geometry changes from octahedral (low-spin) to square-based pyramidal (high-spin)[160]. Although substrate must bind to the ferric P450 before reduction (hence $Fe^{3+} K_d \sim K_M$), quantitation of the substrate dissociation constant for the reduced, catalytically relevant form of the enzyme is of particular interest. Unfortunately, this value cannot be determined in an analogous manner to the oxidised enzyme, as the substrate-free- and substrate-bound-ferrous absorption spectra are identical ($A_{max} = 410$ nm).

It is generally accepted that P450s are mechanistically regulated at the level of substrate binding. A redox switch operates whereby the iron spin state conversion induced upon substrate binding is accompanied by a positive shift in the heme reduction potential [41,91]. This redox shift gates the flow of electrons from the reductase to the heme, only allowing transfer of the first electron to the heme when

substrate is bound. This regulatory mechanism discourages uncoupling (the unfavourable reduction of oxygen to superoxide or peroxide) and conserves precious reducing equivalents (NAD(P)H). Quantification of P450 heme reduction potentials is therefore a highly desirable outcome, yet is experimentally complicated for several reasons. The inherent reactivity of P450-heme with molecular oxygen means that potentiometry has to be performed in strictly anaerobic conditions, often requiring the use of sophisticated cells or glove boxes [91,155]. The logistics of performing such experiments makes the technique inherently awkward and prone to systematic errors. The technique also requires soluble protein of high concentration (to achieve efficient electrical communication with the electrode) and long equilibration periods which is why such data has been almost exclusively restricted to P450s from bacterial sources. The majority of physiologically relevant (i.e. mammalian P450s) P450s are membrane-bound and the problems of insolubility, protein precipitation and insufficient protein concentration make them inaccessible to be studied by this technique. Direct electrochemical methods are also inappropriate due to poor electrical communication between P450s and electrodes, mainly as a consequence of the well insulated, buried heme (in the case of P450 BM3 heme domain, although a monolayer film could be generated on the surface of a PGE electrode, direct electrical reduction was not observed, K.L. Turner, personal communication). A spectroscopic method for predicting the midpoint potential of such hemoproteins “on the bench” would be of considerable usefulness, and would circumvent many of these disadvantages.

This chapter describes the development of such a method using the novel heme ligand 4-cyanopyridine as an extremely useful spectroscopic tool.

4.2 Results

4.2.1 Purification of 4-cyanopyridine

Crude 4-cyanopyridine (4CNPy) was purchased from Sigma (~80 % purity) and was purified by vacuum sublimation. Purified 4CNPy was stored in a desiccator at room temperature, and used within 1 month of manufacture. The use of crude 4CNPy was avoided as it contains a significant amount of free cyanide, the ligation of which (submicromolar K_d) to P450 is irreversible, and preferential to the binding of 4CNPy. Vacuum sublimation liberates sufficiently pure 4CNPy (spectrum of ferrous P450-4CNPy has no trace of ferrous P450-CN) for the purpose of these experiments. The aqueous 4CNPy stocks were prepared using assay buffer (100 mM MOPS, pH 7.0). Fresh stocks ($[4CNPy] = 180 \text{ mM}$) were used for each experiment.

4.2.2 The mode of 4-cyanopyridine binding to P450 heme.

The mode of binding of 4CNPy to P450 heme was determined to be through the pyridine ring nitrogen, as opposed to the cyano-nitrogen. This was deduced by comparing the 4CNPy-bound spectrum to the CN-bound and pyridine-bound spectra (Figure 4.1). These two adducts have characteristically different absorption spectra. The absorption spectra of the ferrous-4CNPy complex and ferrous-pyridine complex are essentially identical. Subtle differences are observed in the spectra and will be discussed in detail later, but the major observation is that the ferrous-4CNPy spectra is more ferrous-pyridine-like than ferrous-cyanide-like. The ferrous-pyridine spectra of P450 BM3 are comparable to those shown previously for pyridine-binding to P450cam by Griffin *et al* [161].

4.2.3 4-cyanopyridine binding to cytochromes P450.

Visible absorption spectra showing the typical shifts associated with the binding of 4CNPy to the oxidised and reduced forms of P450 are shown in Figure 4.2, exemplified by the binding to P450cam (the same observation was made for P450 BM3 and the F393 mutants). The visible spectra of the ferric P450-4CNPy

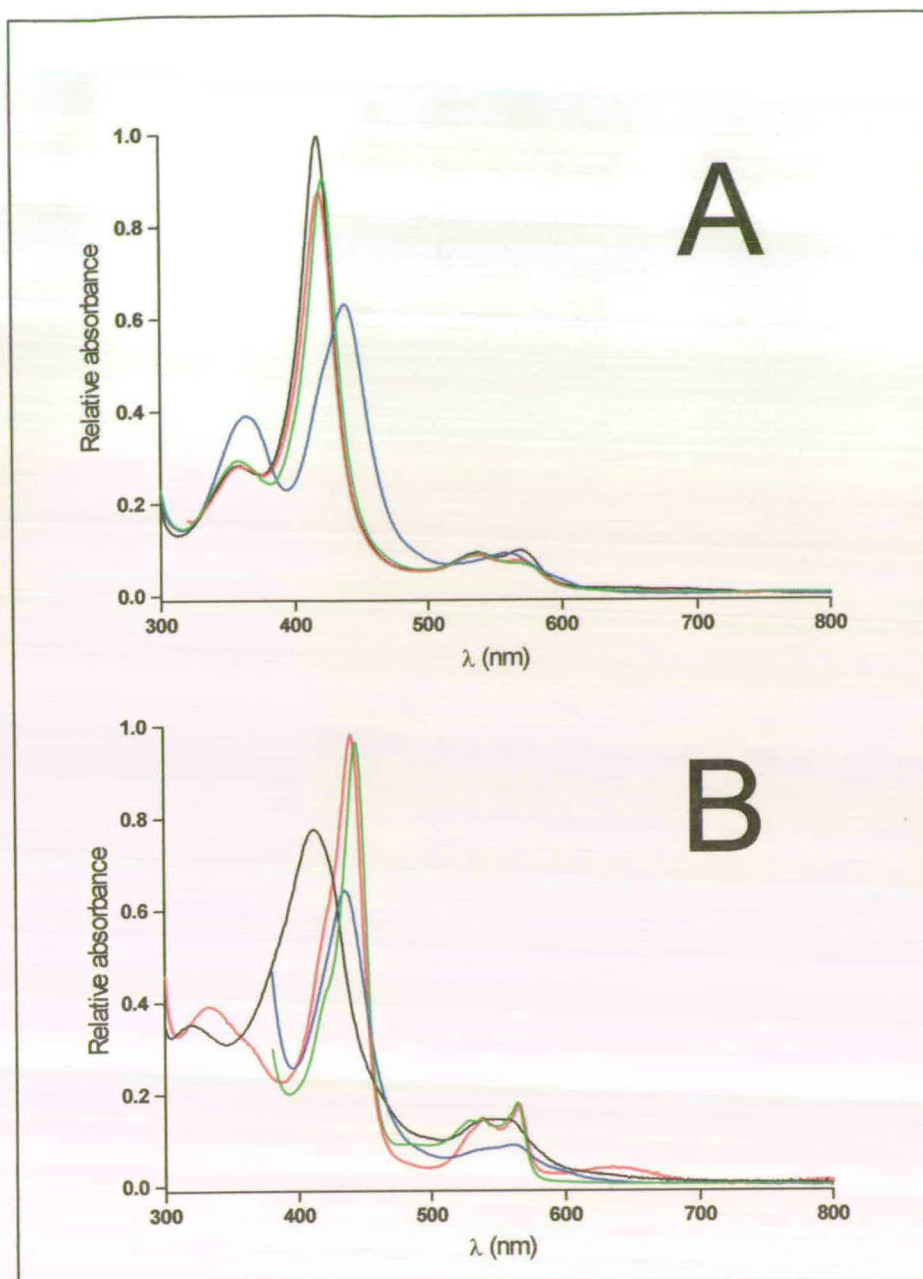


Figure 4.1: Comparison of the binding of pyridine (green), cyanide (blue), and 4CNPy (red) to A: ferric and B: ferrous P450. Absolute spectra of ferric and ferrous forms are shown as solid black lines in both panels.

complexes are essentially the same as their respective ligand-free, ferric forms. Reduction of ferric P450-4CNPy complexes yielded the ferrous P450-4CNPy complexes, which was accompanied by a dramatic change in the absorption spectra (shift in the Soret absorption from 419 nm (ferric) \rightarrow 440 nm (ferrous-4CNPy)). Similar shifts were observed for all proteins studied.

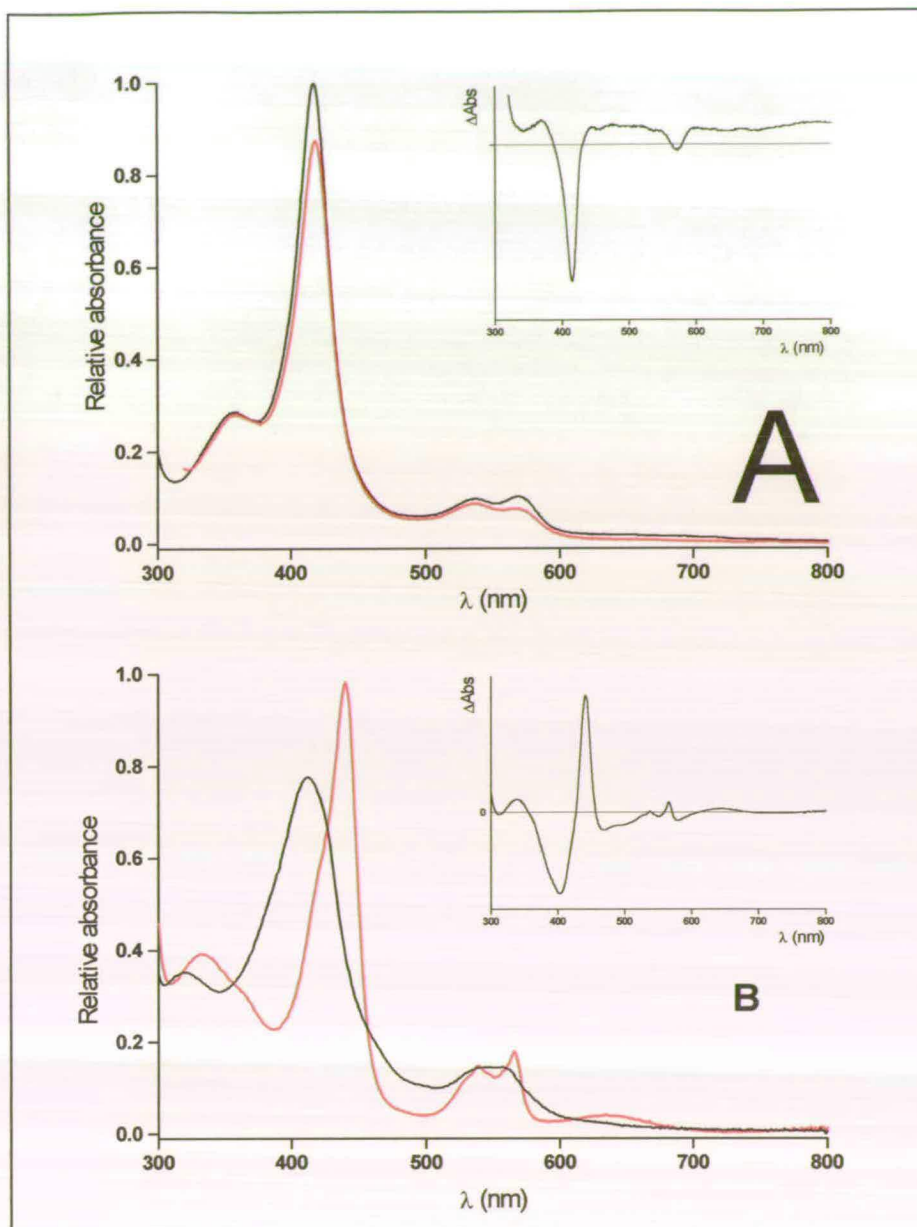


Figure 4.2: Absorbance spectra showing the ligation of 4CNPy to A: ferric and B: ferrous P450cam. Difference spectra are shown inset.

The dissociation constants for 4CNPy with wild-type P450 BM3 and P450cam were determined by titrating small aliquots of aqueous 4CNPy (180 mM stock) into samples of either oxidised or reduced protein (ca. 5 μ M) and recording the resultant visible absorption spectrum after each addition. Difference spectra were generated by subtraction of the absolute oxidised (or reduced) protein spectrum from each 4CNPy-bound spectra. Dissociation constants were calculated by plotting the maximum

absorbance change in the difference spectra versus [4CNPy], and evaluated as outlined in Section 2.6.

Two noteworthy observations are: the formation of a new metal-to-ligand charge transfer (MLCT) absorption band (assigned MLCT due to 4CNPy being a good π -acceptor (π -acid) with low lying π^* anti-bonding orbitals [162,163]) in the blue-region of the spectrum ($A_{\max} = 620 - 650 \text{ nm}$); and the increase in affinity for 4CNPy for ferrous-heme (Table 4.1).

Table 4.1: 4CNPy dissociation constants for ferric and ferrous P450

	4CNPy K_d (μM)	
	P450 _{ox}	P450 _{red}
Wild-type P450 BM3	1130 \pm 45	11.3 \pm 0.7
Wild-type P450cam	845 \pm 70	0.9 \pm 0.1

The affinity of 4CNPy for reduced heme is ~ 2 -3 orders of magnitude greater than for oxidised heme, this has implications for the competitive binding studies which will be discussed in detail later.

4.2.4 Competitive inhibition of 4-cyanopyridine binding by substrate.

The ferrous-form of both wild-type P450 BM3 or P450cam displayed competitive ligation between 4CNPy and substrate, enabling the K_d of the substrate for the ferrous-form ($K_{d(\text{red})}$) to be calculated. The apparent dissociation constants for the competitive binding of 4CNPy to reduced P450 (K_d^{app}) were determined essentially as described above (Section 4.2.3), but in the presence of varying concentration of substrate. For P450 BM3, the substrate was laurate ($K_{d(\text{ox})} = 241 \mu\text{M}$; [laurate] used = 25, 50, 100 and 200 μM), for P450cam, the substrate was fenchone ($K_{d(\text{ox})} = 52 \mu\text{M}$; [fenchone] used = 4, 21, 42 and 84 μM). Titration of 4CNPy into substrate-bound, ferrous P450 competitively displaces substrate as it ligates the heme. Sub-optimal substrates were chosen for the two P450s as their K_d values for the oxidised protein were in the range 50 – 250 μM , which was found to be sufficient to be displaced by a

modest concentration of 4CNPy. Optimal substrates bound too tightly and thus did not display competitive binding with 4CNPy.

In the case of both wild-type P450 BM3 and P450cam, the apparent 4CNPy K_d (K_d^{app}) increased with increasing substrate concentration. In this respect, substrate can be considered as acting as an inhibitor of 4CNPy ligation (in this context, substrate will be referred to as the ‘inhibitor’ of 4CNPy binding). K_d^{app} was evaluated by plotting the maximum absorbance change induced upon 4CNPy ligation to the ferrous heme, versus [4CNPy] at each inhibitor concentration (Table 4.2).

Table 4.2: Competitive inhibition of 4CNPy binding by substrate

	[substrate] (μM)	K_d^{app}	Gradient (units)	Intercept (μM)	K_I (μM)
P450 BM3 (substrate = laurate)	25 ± 2	27 ± 2	21.7 ± 5.5	0.46 ± 0.1	47 ± 6
	50 ± 3	49 ± 4			
	100 ± 4	72 ± 8			
	200 ± 6	111 ± 5			
P450cam (substrate = fenchone)	4 ± 0.4	32 ± 2	11.3 ± 7	7.2 ± 0.1	1.5 ± 1
	21 ± 1	169 ± 3			
	42 ± 3	317 ± 10			
	84 ± 4	610 ± 28			

The double reciprocal plots ($1/\Delta A_{max}$ vs $1/[4\text{CNPy}]$ at each [inhibitor]) for P450 BM3 (laurate) and P450cam (fenchone) are shown in Figure 4.3 and confirm the nature of the inhibition to be purely competitive [164]. By plotting K_d^{app} versus inhibitor concentration, a linear relationship was observed (Figure 4.4), from which the inhibitor constant ($K_I = \text{intercept}/\text{gradient}$) was determined (Table 4.2) by applying a variation of the Michaelis Menten equation in the presence of inhibitor (Appendix II) as shown in Equation 4.1.

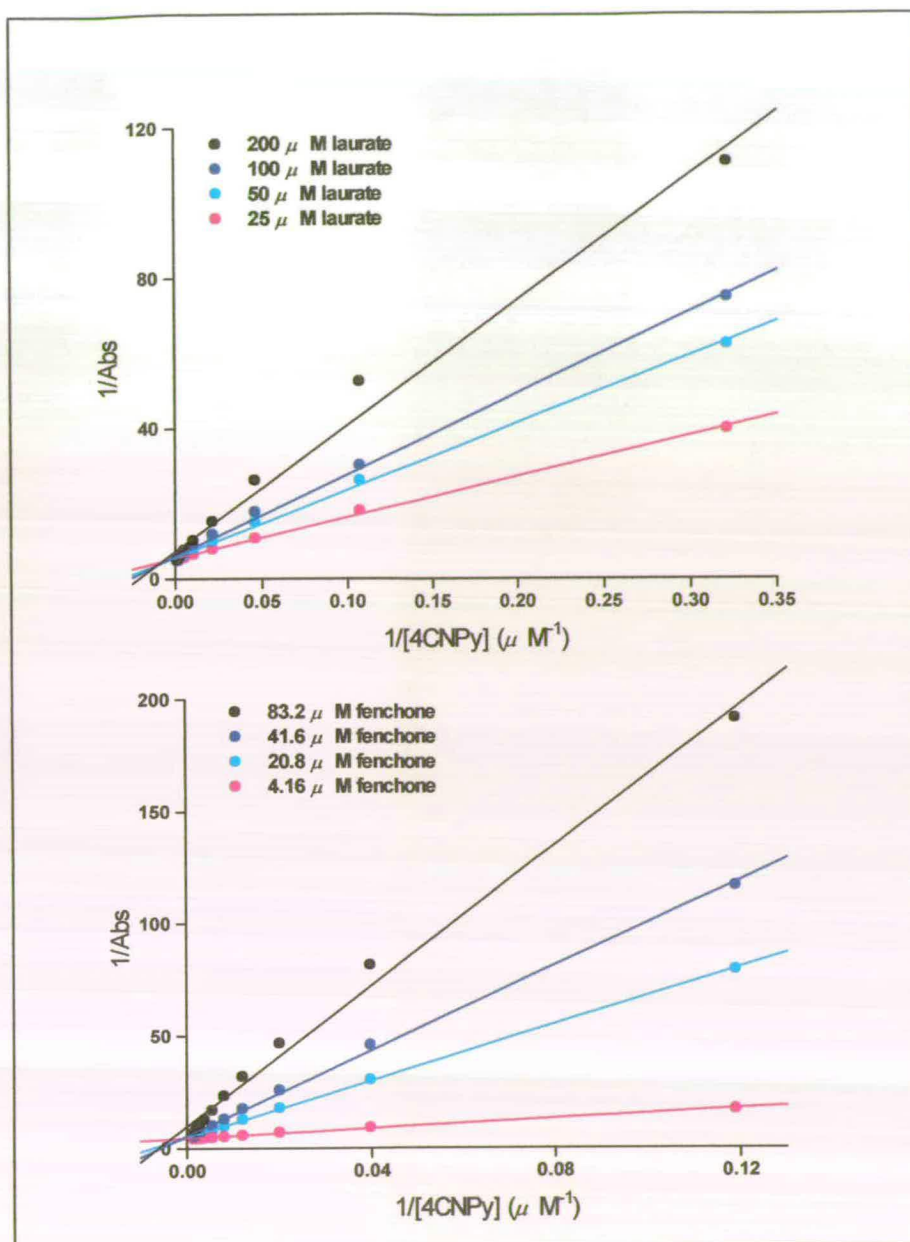


Figure 4.3: Double reciprocal plots, demonstrating the competitive inhibition of 4CNPY binding to A: P450 BM3 in the presence of laurate and B: to P450cam in the presence of fenchone.

As the substrate is acting as the inhibitor in this situation, $K_d(\text{red})$ can be simply evaluated (since under these circumstances $K_I = K_d(\text{red})$). For P450 BM3, $K_d(\text{red})$ (laurate) = $47 \pm 6 \mu\text{M}$, for P450cam, $K_d(\text{red})$ (fenchone) = $1.5 \pm 6 \mu\text{M}$ (this in comparison to the oxidised dissociation constants P450 BM3, $K_d(\text{ox})$ (laurate) = $241 \mu\text{M}$, for P450cam, $K_d(\text{ox})$ (fenchone) = $52 \mu\text{M}$, data not shown). Although the errors

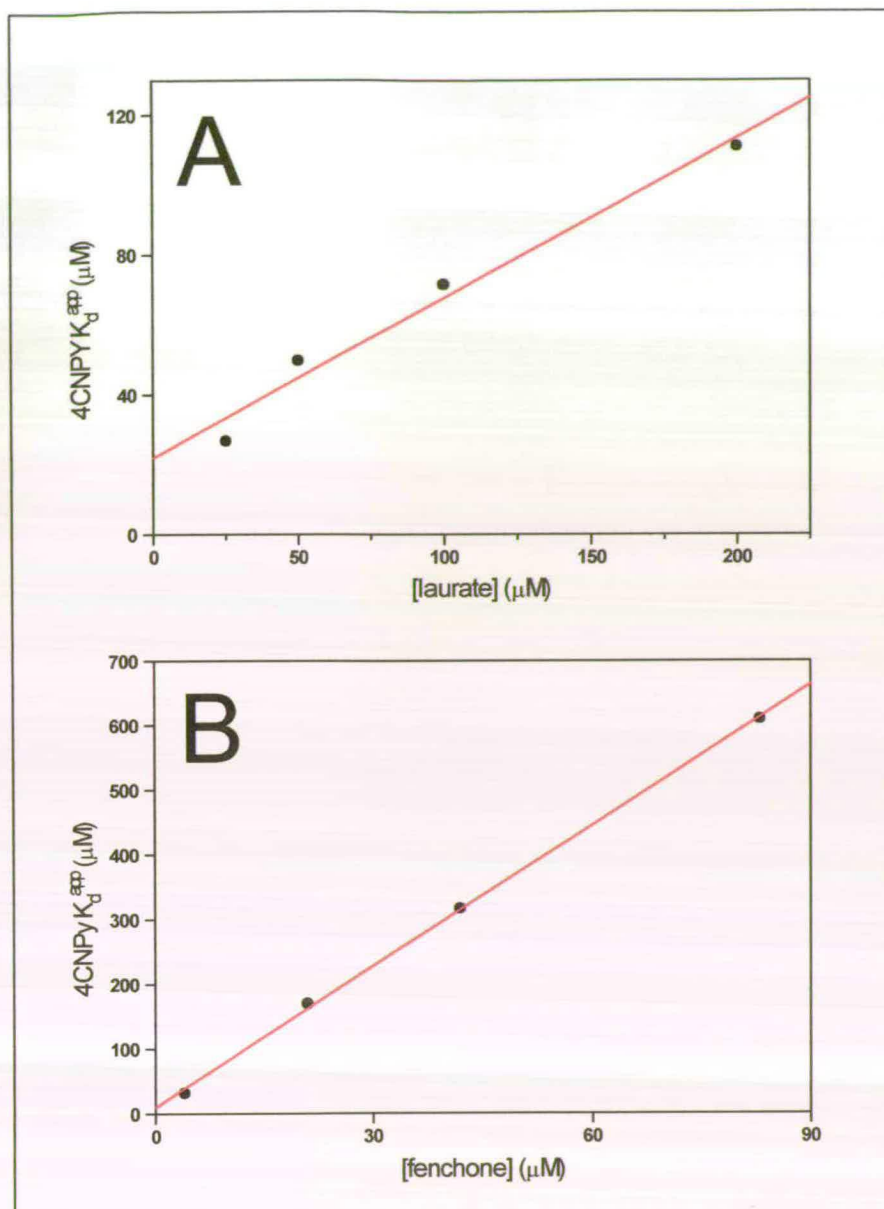


Figure 4.4: The linear variation of K_d^{app} (4CNPy) with increasing substrate concentration (Panel A, P450 BM3/laurate, Panel B, P450cam/fenchone). From this, K_I can be evaluated.

in K_I (hence $K_d(\text{red})$) are large, this is to be expected due to the large variation in the affinity of 4CNPy in the presence of modest concentrations of substrate, this is especially true for P450cam/fenchone. Substrate binding affinity to the ferrous form of both P450 BM3 and P450cam is 5- and 35-fold increased (respectively) with respect to their ferric forms. Here, the effect is more pronounced for P450cam/fenchone than P450 BM3/laurate, as fenchone is not as poor a substrate

analogue for P450cam, as laurate is for P450 BM3. Reduction is therefore accompanied by a substantial increase in the affinity of the enzyme for the substrate.

Equation 4.1: Variation of the Michaelis-Menten equation to calculate K_I for 4CNPy in the presence of substrate

$$A = \frac{\Delta A_{\max} [E_T][S]}{[S] + K_d + \left(\frac{K_d[I]}{K_I} \right)} \text{ which approximates to } A = \frac{\Delta A_{\max} [E_T][S]}{K_d^{\text{app}} + [S]} \text{ when } [I] = 0$$

$$\text{therefore, } K_d^{\text{app}} = K_d + \left(\frac{K_d[I]}{K_I} \right)$$

where $K_d = K_d(4\text{CNPy})$ when $[I] = 0$, $K_d^{\text{app}} = K_d(4\text{CNPy})$ when $[I] > 0$; $S = 4\text{CNPy}$;
 $I = \text{laurate/fenchone}$

4.2.5 Prediction of P450 heme reduction potentials

The position of the new MLCT absorption (λ_{MLCT}) generated upon ligation of 4CNPy to ferrous heme was seen to vary with the proteins studied (Figure 4.5). The wavelength of this absorption band for the P450s studied is shown in Table 4.3 alongside their respective substrate-free reduction potentials. The F393 mutants of P450 BM3 provided a convenient set of proteins to study, as the mutation causes the redox potential to shift without a change in the affinity for substrates or ligands [40].

Table 4.3: Position and energy of the ferrous P450-4CNPy MLCT

	Parameter		
	λ_{MLCT} (nm)	E_{MLCT} (cm ⁻¹)	E_o (mV vs SHE)
P450 BM3 WT	647 ± 1	15456	-427
P450 BM3 F393A	628 ± 1	15924	-312
P450 BM3 F393H	632 ± 1	15823	-332
P450 BM3 F393Y	644 ± 1	15528	-420
P450cam WT	626 ± 1	15974	-300

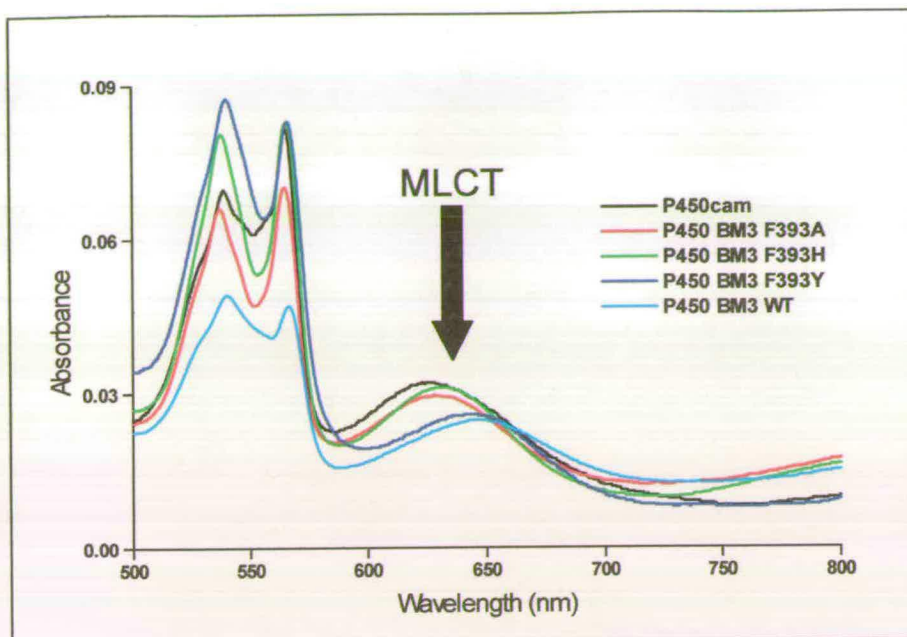


Figure 4.5: Expansion of the α/β region (500–800 nm) of the ferrous-4CNPy adducts of P450cam (black), P450 BM3 F393A (red), F393H (green), F393Y (blue) and wild-type (cyan), showing the shift in the newly formed MLCT between proteins.

When the energy of the absorption band ($E_{\text{MLCT}, \text{cm}^{-1}}$) is plotted versus substrate-free reduction potential (E_0 , mV) a linear relationship is observed (Figure 4.6),

$$\text{where, } E_{\text{MLCT}} = (3.86 \times E_0) + 17122 \text{ cm}^{-1}$$

The standard deviation of the line (0.9966, $n=5$) confirms the accuracy of the linear relationship. This suggests that the origin of the absorption is sensitive to the redox nature of the heme iron, and hence can be used as a method for accurately estimating substrate-free P450 reduction potentials. The correlation between charge transfer bands and reduction potentials is a well recognised practise for inorganic coordination complexes [165–169], and seems equally applicable in this circumstance.

Interestingly, this phenomena was not restricted solely to P450s, as treatment of ferrous iNOS $\Delta 65$ (P450 domain of iNOS, data not shown) liberated an analogous

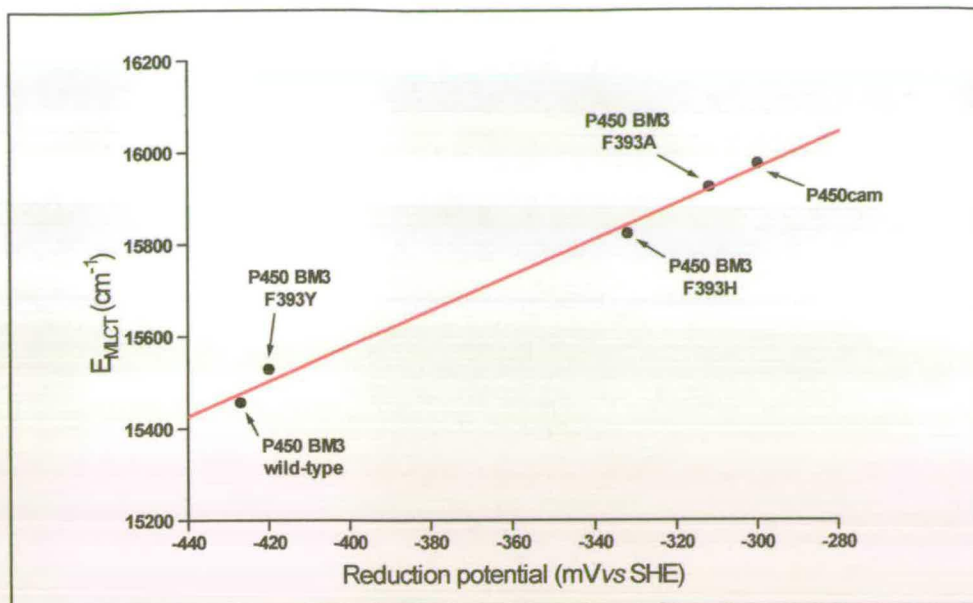


Figure 4.6: The linear variation in E_{MLCT} with P450 reduction potential.

MLCT, whose absorption maxima fits the same linear relationship observed for the P450s. It seems as though this relationship could hold for all P450-like, thiolate ligated hemoproteins.

4.3 Discussion

The two features of 4-cyanopyridine which make it an ideal ligand for the type of studies outlined previously are, firstly, its essentially exclusive, tight reversible binding to ferrous heme (with little affinity for ferric heme) and secondly, the unusual spectral properties of the 4CNPy-ferrous heme adduct. Therefore, we have: a ligand with strict selectivity for ferrous heme; a convenient spectroscopic handle; and completely reversible ligand binding. The methodology outlined to calculate the substrate dissociation constants for reduced P450 exploits these observations.

The specificity of 4CNPy for reduced P450 allows the evaluation of substrate dissociation constants for purely the reduced enzyme and eliminates interference from binding of 4CNPy/substrate to ferric heme. Previously, pyridine had been used in an analogous manner to estimate $K_d(\text{red})$ [161,170], the magnitude of which (4.5 nM) is likely to be inaccurate for a number of reasons. Pyridine has a high affinity for both oxidised and reduced P450 (so interference from binding to the ferric form

cannot be discounted), the quoted value was an average of only 5 single absorption measurements in the presence of camphor (as opposed to full titrations at each camphor concentration), and thirdly, high concentrations of pyridine were used (≤ 19 mM) which could have a detrimental effect on the integrity of the P450. The highest concentration of 4CNPy added to a P450 sample in any given experiment was 1.5 mM, the integrity of the protein was checked by bubbling CO through the samples subsequent to titration. In every case, full conversion to the characteristic P450 complex was observed, synonymous with intact non-denatured P450. For these reasons, 4CNPy is a much more applicable ligand for these types of study than pyridine, combined with its additionally useful absorption properties when bound to ferrous heme.

An increase in substrate binding affinity upon heme reduction, is key to the mechanism of action in the P450s. This is inferred by the difference between the substrate-free and substrate-bound heme reduction potentials. Introduction of substrate into the active site increases the heme-reduction potential and thus thermodynamically controls electron transfer from the reductase. Consideration of the Gibbs' Free Energy equation ($\Delta G = -RT\ln K$) suggests that this increase in reduction potential must be due to a decrease in the magnitude of the equilibrium constant, K - in this situation, K can be considered as the substrate dissociation constant (K_d). Theoretically, K_d should decrease upon protein reduction. It is widely accepted that there is considerable peptide motion upon substrate binding associated with dehydration of the active site [171,88] of P450 BM3. A similar conformational contraction may be expected upon reduction, to bring the substrate closer to the heme to facilitate oxygenation. This is substantiated by NMR relaxation experiments on P450 BM3, which show a dramatic 6 Å movement of the substrate toward the heme upon reduction [45]. The active site contraction probably serves two purposes, to ensure dehydration of the active site and also to stabilise the Michaelis-complex. This movement can be interpreted as an increase in affinity of the reduced heme for the substrate, hence one would expect a concomitant decrease in the substrate dissociation constant for this form of the enzyme. Inspection of the crystal structure of the palmitoleate-bound, ferric P450 BM3 heme domain [87] (PDB:1FAG), shows

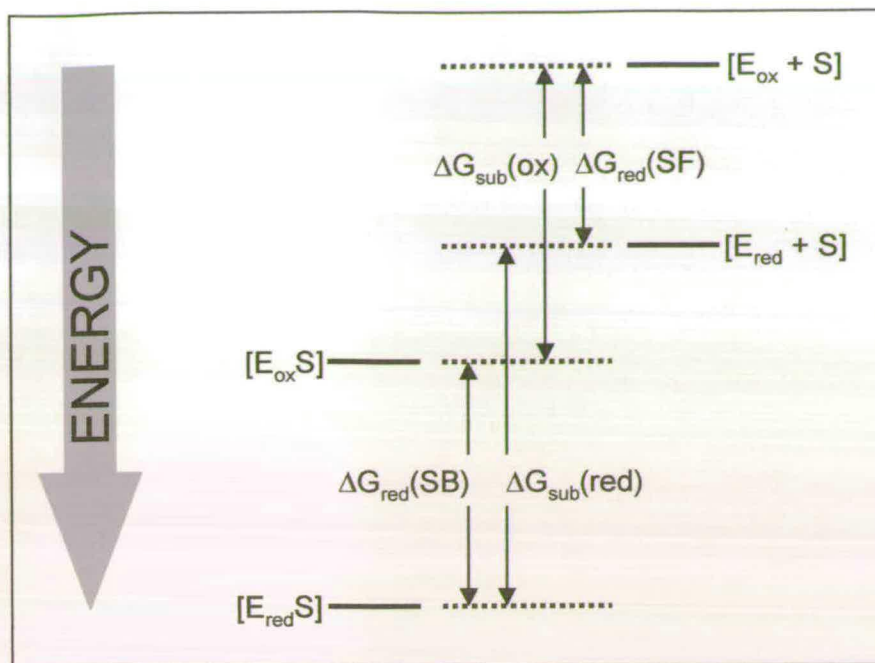


Figure 4.7: A schematic showing the dissection of the total Gibbs' free energy for substrate-binding and reduction to a P450, into its components. E_{ox} = oxidised P450, E_{red} = reduced P450, $E_{ox}S$ = oxidised P450/substrate complex, $E_{red}S$ = reduced P450/substrate complex, $\Delta G_{red}SF$ and $\Delta G_{red}SB$ are the free energies of reduction for the substrate-free and substrate-bound P450 (respectively), $\Delta G_{sub}(ox)$ and $\Delta G_{sub}(red)$ are the free energies of substrate binding to oxidised and reduced P450 respectively.

that the substrate terminus is $\sim 8 \text{ \AA}$ away from the heme, too far for hydroxylation, suggesting that a movement of the substrate must occur in order for reaction to take place. For the first time, we report the determination of substrate dissociation constants for ferrous P450 BM3 and P450cam. These concentrations are considerably lower than those determined for the ferric enzymes (~ 5 -35-fold) and quantify the degree to which substrate is bound tighter to the active site in the enzymes catalytically relevant, ferrous-form. Whilst the effect of reduction seems to only have a modest effect on substrate binding, it has to be reiterated that the values were determined for sub-optimal substrates for the particular P450s (laurate and fenchone for P450 BM3 and P450cam respectively). It can be expected that the increase in affinity for physiological substrates for the ferrous form to be more pronounced.

The importance of determining $K_d(red)$ cannot be understated. Once determined for a particular substrate, a wealth of (otherwise unquantifiable) mechanistic data can be

calculated, enabling the deconvolution of important steps in the P450 catalytic cycle. Figure 4.7 illustrates the dissection of the substrate binding equilibrium into its constitutive components and the Gibbs free energy (ΔG) terms associated with each transition (the terms $\Delta G_{\text{sub(ox)}}$, $\Delta G_{\text{sub(red)}}$, ΔG_{SF} and ΔG_{SB} are defined in the figure legend), the magnitude of which are given in Table 4.4. The most important parameter is $\Delta\Delta G$ – this is a measure of the relative stability of the ferric-substrate-bound P450 compared to the ferrous-substrate-bound P450, determined by the 4CNPy competitive inhibition titration (determination of $K_d(\text{red})$).

The sign of $\Delta\Delta G$ demonstrates that the ferrous-substrate complex is more stable (lower in energy) than the ferric-substrate complex. Interestingly, although the $\Delta\Delta G$ values for arachidonate- and camphor-bound P450 BM3 and P450cam respectively were not measured directly (rather, calculated from the known, measured reduction potentials [40,172] by assuming $-nF\Delta E = -RT\ln K_d(\text{red})$), they are of greater magnitude than for the sub-optimal substrates - an intuitive interpretation. By definition, the best substrates bind tightest, hence forming the most stable Michaelis-complexes (largest $\Delta\Delta G$). The fact that $\Delta\Delta G = \Delta G_{\text{SB}}$ allows estimation of the substrate-bound heme reduction potential for a sub-optimal substrate (i.e. by calculating $K_d(\text{red})$) and affirms the accuracy of the estimation of $K_d(\text{red})$ for a physiological substrate from the energy difference (ΔE_0) between the substrate-free

Table 4.4: Thermodynamic parameters for substrate binding to ferric and ferrous P450

	Thermodynamic parameters (kJmol ⁻¹)			
	$\Delta G_{\text{sub(ox)}}$	$\Delta G_{\text{sub(red)}}$	$\Delta\Delta G$	ΔG_{SB}
P450 BM3 + laurate	20.5	24.7	-4.2	-
P450 BM3 + arachidonate	30.8	42.7*	-	-13.2
P450cam + fenchone	24.3	33.2	-8.9	-
P450cam + camphor	32.8	45.3*	-	-12.4

*Calculated from ΔE_0

and substrate-bound heme reduction potentials. Sub-optimal substrates tend to only induce a partial spin-state shift [125] (e.g. for P450 BM3, laurate induces ~60 % spin state shift, whereas arachidonate > 95 %) and this limits the range of substrates available to study by redox potentiometry. Substrate-bound heme reduction potentials can be significantly underestimated if the conversion from low-spin to high-spin is incomplete [91]. The determination of $K_d(\text{red})$ allows the prediction of these substrate-bound reduction potentials for these sub-optimal substrates. This can be illustrated in the case of either P450 BM3 with laurate (predicted $E_0 = -383$ mV), or P450cam with fenchone (predicted $E_0 = -208$ mV) – the substrate-bound potentials for either case have not previously been evaluated. Although the dissociation constants for sub-optimal substrates with ferrous P450 were only modestly decreased with respect to their ferric counterparts, calculation of $K_d(\text{red})$ for the physiological substrates suggests a significantly more pronounced increase in affinity, such that the $K_d(\text{red})$ for these substrates is in the nanomolar region (32 nM P450 BM3/arachidonate; 11 nM P450cam/camphor).

It has also been demonstrated that 4-cyanopyridine can be exploited to predict the substrate-free P450 heme reduction potentials. This feature makes 4-cyanopyridine a fundamentally important mechanistic probe. The energy of the MLCT absorption band (upon formation of the 4CNPy-ferrous adduct) varies linearly with heme reduction potential. This is an observation which has been used effectively in studying the correlation of absorption band energy of simple inorganic complexes with reduction potential [165-169]. This provides a convenient route by which heme reduction potentials can be accurately estimated for P450s for which such information has been previously unobtainable (due to either purification/extraction or stability problems). The versatility of such a ligand may even allow the evaluation of heme reduction potentials of P450 in crude microsomal fractions. The data presented here could act as a calibration chart, against which subsequent P450 reduction potentials can be estimated. The relationship shown in Figure 4.6 ($E_{\text{MLCT}} = (3.86 \times E_0) + 17122 \text{ cm}^{-1}$) allows the evaluation of a P450 heme reduction potential, simply by knowing the energy of the MLCT absorption of the ferrous-4CNPy adduct. The advantage of the 4CNPy MLCT is that the shift from P450 to P450 occurs over a

large wavelength range (~ 20 nm, WT \rightarrow F393A), allowing accurate estimation of reduction potential when E_{MLCT} is plotted against reduction potential.

Whilst the number of P450s tested in this study is relatively small, the inclusion of data for P450s with distinctly different catalytic sites (P450 BM3 versus P450cam), suggests that this trend could be applicable to all heme-thiolate proteins. However, a larger sample of proteins needs to be considered before such a hypothesis can be justified.

4.4 Conclusion

4-cyanopyridine has been demonstrated to be a ligand that can be exploited as an invaluable mechanistic tool for cytochromes P450, and even heme-thiolate proteins in general. Its strict selectivity for ferrous-heme and the unusual spectral properties of the ferrous-4CNPy adduct have enabled the quantification of previously unmeasurable properties. It provides a quick, convenient and accurate method of determining substrate dissociation constants for reduced P450s, for predicting heme reduction potentials of P450s bound with sub-optimal substrates, and can even be used to estimate the reduction potential of P450s for which conventional experimental techniques, such as redox potentiometry, are unsuitable.

APPENDIX I

REFERENCES

- 1 Klingenberg, M. 1958. *Arch. Biochem. Biophys.* **75**, 376-386
- 2 Omura, T., Sato, R. 1962. *J. Biol. Chem.* **237**, 1375-1376
- 3 Omura, T., Sato, R. 1964. *J. Biol. Chem.* **239**, 2370-2378
- 4 Omura, T., Sato, R. 1964. *J. Biol. Chem.* **239**, 2379-2385
- 5 Cooper, D.Y., Levin, S., Narasimhulu, S., Rosenthal, O., Estabrook, R.W. 1965. *Science* **147**, 400
- 6 Omura, T., Sato, R., Cooper, D.Y., Rosenthal, O., Estabrook, R.W. 1965. *Fed. Proc.* **24**, 1181
- 7 Lu, A.Y.H., Coon, M.J. 1968. *J. Biol. Chem.* **243**, 1331-1332
- 8 Strobel, H.W., Lu, A.Y.H., Heidema, J., Coon, M.J. 1970. *J. Biol. Chem.* **245**, 4851-4954
- 9 Katagiri, M., Ganguli, B.N., Gunsalus, I.C. 1968. *J. Biol. Chem.* **243**, 3543
- 10 Fulco, A.J., Kim, B.H., Matson, R.S., Narhi, L.O., Ruttinger, R.T. 1983. *Mol. Cell. Biochem.* **53057**, 155-161
- 11 Bellamine, A., Mangla, A.T., Nes, W.D., Waterman, M.R. 1999. *Proc. Natl. Acad. Sci. U.S.A.* **96**, 8937-8942
- 12 Chung, B-C., Matteson, K.J., Voutilainen, R., Mohandas, T.K., Miller, W.L. 1986. *Proc. Natl. Acad. Sci. U.S.A.* **83**, 8962-8966

- 13 Oonk, R.B., Parker, K.L., Gibson, J.L., Richards, J.S. 1990. *J. Biol. Chem.* **265**, 22392-22401
- 14 Yang, X., Iwamoto, K., Wang, M., Artwohl, J., Mason, J.I., Pang, S. 1993. *Endocrinology* **132**, 1977-1982
- 15 Morohashi, K., Fului-Kariyama, Y., Okada, Y., Sogawa, K., Hirose, T., Inayama, S., Omura, T. 1984. *Proc. Natl. Acad. Sci. U.S.A.* **81**, 4647-4651
- 16 Mulheron, G.W., Stone, R.T., Miller, W.L., Wise, T.H. 1989. *Nucleic Acids Res.* **17**, 1773-1773
- 17 Waterston, R., Martin, C., Craxton, M., Huyah, C., Cioulson, A., Hillier, L., Durbin, R.K., Green, P., Shorkeen, R., Halloran, N., Hawkins, T., Wilson, R., Berks, M., Du, Z., Thomas, K., Thierry-Mieg, J., Sulston, J. 1992. *Nat. Genetics* **1**, 114-123
- 18 Dunkov, B.C., Guzov, V.M., Mocelin, G., Shotkoski, F., Brun, A., Amichot, M., Ffrench-Constant, R.H., Feyereisen, R. 1997. *DNA Cell Biol.* **16**, 1345-1356
- 19 Kizawa, H., Tomura, D., Oda, M., Fukamizu, A., Hoshino, T., Gotoh, O., Yasui, T., Shoun, H. 1991. *J. Biol. Chem.* **266**, 10632-10637
- 20 Kalb, V.F., Woods, C.W., Turi, T.G., Dey, C.R., Sutter, T.R., Loper, J.C. 1987. *DNA* **6**, 529-537
- 21 Bell-Lelong, D.A., Cusumano, J.C., Meyer, K., Chapple, K. 1997. *Plant Physiol.* **113**, 729-738
- 22 Wright, R.L., Harris, K., Solow, R., White, R.H., Kennelley, R.H. 1996. *FEBS Lett.* **384**, 235-239
- 23 Nelson, D.R., Kamataki, T., Waxman, D.J., Guengerich, F.P., Estabrook, R.W., Feyereisen, R., Gonzalez, F.J., Coon, M.J., Gunsalus, I.C., Gotoh, O., Okuda, K., Nerbert, D.W. 1993. *DNA Cell Biol.* **12**, 1-50

- 24 Guengerich, F.P. 2001. *Chem. Res. Toxicol.* **14**, 611-650
- 25 The International Human Genome Sequencing Consortium, 2001. *Nature* **409**, 860-921
- 26 Cole, S.T., Brosch, R., Parkhill, J., Garnier, T., Churcher, C., Harris, D., Gordon, S.V., Eiglmeier, K., Gas, S., Barry III, C.E., Tekaiia, F., Basham, D., Brown, D., Chillingworth, T., Connor, R., Davies, R., Devlin, K., Feltwell, T., Gentles, S., Hamlin, N., Holroyd, S., Hornsby, T., Jagels, K., Krogh, A., McLean, J., Moule, S., Murphy, L., Oliver, K., Osborne, J., Quail, M.A., Rajandream, M-A., Rogers, J., Rutter, S., Seeger, K., Skelton, J., Squares, R., Squares, S., Sulston, J.E., Taylor, K., Whitehead, S., Barrell. 1998. *Nature* **393**, 537-544
- 27 The *C. elegans* sequencing Consortium. 1998. *Science* **282**, 2012-2018
- 28 The *D. melanogaster* Sequencing Consortium. 2000. *Science* **287**, 2185-2195
- 29 The *Arabidopsis* Genome Initiative. 2000. *Nature* **408**, 796-815
- 30 Gelboin, H.V., Huberman, E., Sachs, L. 1969. *Med. Sci.* **64**, 1188-1194
- 31 Gunsalas, I.C., Pederson, T.C., Sligar, S.G. 1975. *Annu. Rev. Biochem.* **44**, 377
- 32 Lambeth, J.D., Kamin, H. 1979. *J. Biol. Chem.* **254**, 2766-2774
- 33 Sono, M., Andersson, L.A., Dawson, J.H. 1982. *J. Biol. Chem.* **257**, 8308-8317
- 34 Dawson, J.H., Sono, M. 1987. *Chem. Rev.* **87**, 1255-1276
- 35 Liu, H.I., Sono, M., Kadkhodayan, S., Hager, L.P., Hedman, B., Hodgson, K.O., Dawson, J.H. 1995. *J. Biol. Chem.* **270**, 10544-10550
- 36 Poulos, T.L., 1996. *J. Biol. Inorg. Chem.* **1**, 356-359

- 37 Auclair, K., Moenne-Loccoz, P., Ortix de Montellano, P.R. 2001. *J. Am. Chem. Soc.* **123**, 4877-4885
- 38 Yeom, H., Sligar, S.G., Li, H., Poulos, T.L., Fulco, A.J. 1995. *Biochemistry* **34**, 14733-14740
- 39 Munro, A.W., Malarkey, K., McKnight, J., Thomson, A.J., Kelly, S.M., Price, N.C., Lindsay, J.G., Coggins, J.R., Miles, J.S. 1994. *Biochem. J.* **303**, 423-428
- 40 Ost, T.W.B., Miles, C.S., Munro, A.W., Murdoch, J., Reid, G.A., Chapman, S.K. 2001. *Biochemistry* **40**, 13421-13429
- 41 Sligar, S.G., Gunsalus, I.C. 1976. *Proc. Natl. Acad. Sci. U.S.A.* **73**, 1078-1082
- 42 Dawson, J.H., Andersson, L.A., Sono, M. 1982. *J. Biol. Chem.* **257**, 3606-3617
- 43 Keller, R.M., Wurthrich, K., Debrunner, P.G., 1972. *Proc. Natl. Acad. Sci. U.S.A.* **69**, 2073
- 44 Champion, P.M., Munck, E., Debrunner, P.G., Moss, T.H., Lipscombe, J.D., Gunsalus, I.C. 1975. *Biochim. Biophys. Acta.* **376**, 579
- 45 Modi, S., Sutcliffe, M.J., Primrose, W.U., Lian, L-Y., Roberts, G.C.K. 1996. *Nat. Struct. Biol.* **3**, 414-417
- 46 Ishimura, Y., Ullrich, V., Peterson, J.A. 1971. *Biochem. Biophys. Res. Commun.* **42**, 140
- 47 Dawson, J.H., Cramer, S.P. 1978. *FEBS Lett.* **88**, 127
- 48 Peterson, J.A., Ishimura, Y., Griffin, B.W. 1971. *Arch. Biochem. Biophys.* **149**, 197-208

- 49 Bangcharoenpaurpong, O., Apostolos, K.R., Champion, P.M., Jollie, D., Sligar, S.G., 1986, *J. Biol. Chem.* **261**, 8089-8092
- 50 Collman, J.P., Brauman, J.I., Halbert, T.R., Suslick, K.S. 1976. *Proc. Natl. Acad. Sci. U.S.A.* **73**, 3333-3337
- 51 Tyson, C.A., Lipscomb, J.D., Gunsalus, I.C. 1972. *J. Biol. Chem.* **247**, 5777-5784
- 52 Hui Bon Hoa, G., Begard, ., Debey, P., Gunsalus, I.C. 1978. *Biochemistry* **17**, 2835-2839
- 53 Brewer, C.B., Peterson, J.A. 1988. *J. Biol. Chem.* **263**, 791
- 54 Lipscombe, J.D., Sligar, S.G., Namtvedt, M.J., Gunsalus, I.C. 1976. *J. Biol. Chem.* **251**, 1116-1124
- 55 Higuchi, T., Uzu, S., Hirobe, M. 1990. *J. Am. Chem. Soc.* **112**, 7051-7053
- 56 Higuchi, T., Shimada, K., Maruyama, N, Hirobe, M. 1993. *J. Am. Chem. Soc.* **115**, 7551-7552
- 57 Labeque, R., Marnett, L.J. 1989. *J. Am. Chem. Soc.* **111**, 6621-6627
- 58 Poulos, T.L. 1988. *Adv. Inorg. Biochem.* **7**, 1
- 59 Sono, M., Andersson, L.A., Dawson, J.H. 1982. *J. Biol. Chem.* **257**, 8308-8320
- 60 Liu, H.I., Sono, M., Kadkhodayan, S., Hager, L.P., Hedman, B., Hodgson, K.O., Dawson, J.H. 1995. *J. Biol. Chem.* **270**, 10544-10550
- 61 Adachi, S-I., Nagano, S., Ishimori, K., Watanabe, Y., Morishima, I. 1993. *Biochemistry* **32**, 241-252
- 62 Gerber, N.C., Sligar, S.G. 1992. *J. Am. Chem. Soc.* **114**, 8742-8743

- 63 Cupp-Vickery, J.R., Poulos, T.L. 1994. *Nat. Struct. Biol.* **2**, 144-153
- 64 Cupp-Vickery, J.R., Poulos, T.L. 1997. *Steroids* **62**, 112-116
- 65 Crane, B.R., Arvai, A.S., Gachhui, R., Wu, C., Ghosh, D.K., Getzoff, E.D., Stuehr, D.J., Tainer, J.A. 1997. *Science* **278**, 425-431
- 66 Groves, J.T., McCluskey, G.A. 1976. *J. Am. Chem. Soc.* **98**, 859-861
- 67 Groves, J.T. 1985. *J. Chem. Edu.* **62**, 928-931
- 68 Gibson, G.G., Orton, T.C., Tamburini, P.P. 1982. *Biochem. J.* **203**, 161-168
- 69 Miura, Y., Fulco, A.J. 1974. *J. Biol. Chem.* **249**, 1880-1888
- 70 Stapleton, G., Steel, M., Richardson, M., Mason, J.O., Rose, K.A., Morris, R.G.M., Lathe, R. 1995. *J. Biol. Chem.* **270**, 29739-29745
- 71 Imai, Tadashi, Yamakazi, T., Kominami, S. 1998. *Biochemistry* **37**, 8097-8104
- 72 Gelb, M.H., Heimbrook, D.C., Malkonen, P., Sligar, S.G. 1982. *Biochemistry* **21**, 370-377
- 73 Andersen, J.K., Hutchinson, C.R. 1993. *Biochemistry* **32**, 1905-1913
- 74 Jerina, D.M., Daly, J.W. 1974. *Science* **185**, 573-582
- 75 Heimbrook, D.C., Murray, R.E., Egeberg, K.D., Sligar, S.G., Nee, M.W., Bruice, T.C. 1984. *J. Am. Chem. Soc.* **106**, 1514-1515
- 76 Seto, Y., Guenerich, F.P. 1993. *J. Biol. Chem.* **268**, 9986-9997
- 77 Simpson, E.R. 1979. *Mol. Cell. Endocrinol.* **13**, 312-227
- 78 Burstein, S., Middleditch, B.S., Gut, M. 1975. *J. Biol. Chem.* **250**, 9028-9037

- 79 Sonoda, Y., Endo, M., Ishida, K., Sato, Y., Fukusen, N., Fukuhara, M.
Biochem. Biophys. Acta. **1170**, 92-97
- 80 Barnes, H.J., Arlotto, M.P., Waterman, M.R. 1991. *Proc. Natl. Acad. Sci. U.S.A.* **88**, 5597-5601
- 81 Nahri, L.O., Fulco, A.J. 1986. *J. Biol. Chem.* **261**, 7160-7169
- 82 Fulco, A.J., Reuttinger, R.T. 1987. *Life. Sci.*, **40**, 1769-1775
- 83 Nahri, L.O., Fulco, A.J. 1987. *J. Biol. Chem.* **262**, 6683-6690
- 84 Ruettinger, R.T., Wen, L-P., Fulco, A.J. 1989. *J. Biol. Chem.* **264**, 10987-10995
- 85 Reuttinger, R.T., Fulco, A.J. 1981. *J. Biol. Chem.* **256**, 5728-5734
- 86 Ravichandran, K.G., Boddupalli, S.S., Hasemann, C.A., Peterson, J.A., Diesenhofer, J. 1993. *Science* **261**, 731-736
- 87 Li, H.Y., Poulos, T.L. 1997. *Nat. Struct. Biol.* **4**, 140-146
- 88 Poulos, T.L., Finzel, B.C., Howard, A.J. 1987. *J. Mol. Biol.* **195**, 687-700
- 89 Oliver, C.F., Modi, S., Sutcliffe, M.J., Primrose, W.U., Lian, L.Y., Roberts, G.C.K. 1997. *Biochemistry* **36**, 1567-1572
- 90 Macdonald, T.L, Gutheim, W.G., Martin, R.B., Guengerich, F.P. 1989. *Biochemistry* **28**, 2071-2077
- 91 Daff, S.N., Chapman, S.K., Turner, K.T., Holt, R.A., Govindaraj, S., Poulos, T.L., Munro, A.W. 1997. *Biochemistry* **36**, 13816-13823
- 92 Sevrioukova, I.F., Shaffer, C., Ballou, D.P., Peterson, J.A. 1996. *Biochemistry* **35**, 7058-7068

- 93 Wang, M., Roberts, D.L., Pashke, R., Shea, T.M., Masters, B.S.S., Kim, J.-J.P. 1997. *Proc. Natl. Acad. Sci. U.S.A.* **94**, 8411-8416
- 94 Murataliev, M. B., Klein, M., Fulco, A.J., Feyeresisen, R. 1997. *Biochemistry* **36**, 8401-8412
- 95 Sevriokova, I.F., Li, H., Peterson, J.A., Poulos, T.L. 1999. *Proc. Natl. Acad. Sci. U.S.A.* **96**, 1863-1868
- 96 Lysek, D.A. Unpublished results.
- 97 Moser, C.C., Page, C.C., Farid, R., Dutton, P.L. 1995. *J. Bioenergetics and Biomembranes* **27**, 263-274
- 98 Marcus, R.A., Sutin, N. 1985. *Biochim. Biophys. Acta.* **811**, 265-322
- 99 Moser, C.C., Keske, J.M., Warncke, K., Farid, R.S., Dutton, P.L. 1992. *Nature* **355**, 796-802
- 100 Beratan, D.N., Onuchic, J.N., Winkler, J.R., Gray, H.B., 1991. *Science* **258**, 1740-1741
- 101 Smalley, J.F. Feldberg, S.W., Chidsey, C.E.D., Linford, M.R., Newton, M.D., Liu, Y-P. 1995. *J. Phys. Chem.* **99**, 13141-13149
- 102 Miller, J.R., Beitz, J.V., Huddleston, R.K. 1984, *J. Am. Chem. Soc.* **106**, 5057-5068
- 103 Moser, C.C., Dutton, P.L. 1992. *Biochim. Biophys. Acta.* **1101**, 171
- 104 Winkler, J.R., Gray, H.B. 1992. *Chem. Rev.* **92**, 369
- 105 Betts, J.N., Beretan, D.N., Onuchic, J.N. 1992. *J. Am. Chem. Soc.* **114**, 4043-4046

- 106 Curry, W.B., Grabe, M.D., Kurnikov, I.V., Skourtis, S.S., Beratan, D.N., Regan, J.J., Aquino, A.J.A., Beroza, P., Onuchic, J.N. 1995. *J. Bioenergetics and Biomembranes* **27**, 285-293
- 107 Karpishin, T.B., Grinstaff, M.W., Komarpanicucci, S., McLendon, G., Gray, H.B. 1994. *Structure* **2**, 415-422
- 108 Langen, R., Chang, I-J., Germanas, J.P., Richards, J.H., Winkler, J.R., Gray, H.B. 1995. *Science* **268**, 1733-1735
- 109 Kunkel, W.H. 1985. *Proc. Natl. Acad. Sci. U.S.A.* **82**, 488-492
- 110 Miles, J.S., Munro, A.W., Rospendowski, B.N., Smith, W.E., McKnight, J. and Thomson, A.J. (1992). *Biochem. J.* **288**, 503-509.
- 111 Munro, A.W., Daff, S., Coggins, J.R., Lindsay, J.G. and Chapman, S.K. (1996). *Eur. J. Biochem.* **239**, 403-409.
- 112 Noble, M.A., Miles, C.S., Chapman, S.K., Lysek, D.A., Mackay, A.C., Reid, G.A., Hanzlik, R.P. and Munro, A.W. (1999). *Biochem. J.* **339**, 371-379.
- 113 Pajot, P., Groudinsky, O. 1970. *Eur. J. Biochem.* **12**, 158-164
- 114 Laemmi, U.K. 1970. *Nature* **227**, 680-685
- 115 Munro A.W., Noble M.A., Miles C.S., Daff S.N., Green A.J., Quaroni L., Rivers S., Ost T.W.B., Reid G.A., Chapman S.K. 1999. *Biochem. Soc. Trans.* **27**, 190-196.
- 116 Dawson, R.M.C., Elliott, D.C., Elliott, W.H., Jones, K.M. 1986. *Data for Biochemical Research*, 3rd Ed., Oxford Science Publications
- 117 Dutton, P.L. 1978. *Methods Enzymol.* **54**, 411-435
- 118 Macheroux, P., Massey, V., Thiel, D.J., Volokita, M. 1991. *Biochemistry* **30**, 4612-4619.

- 119 Abu-Soud, H.M., Ichimori, K., Presta, A., Stuehr, D.J. 2000. *J. Biol. Chem.* **275**, 17349-17357
- 120 Klatt, P., Schmidt, K., Werner, E.R., Mayer, B. 1996. *Meth. Enz.* **268**, 358-365
- 121 Berry, E.A., Trumpower, B.L. 1987. *Anal. Biochem.* **161**, 1
- 122 Otwinowski, Z., Minor, W. (1997) *Methods Enzymol.* **276**, 307-326
- 123 Jones, T.A., Zou, J.Y., Cowan, S.W., Kjeldgaard, M. (1991) *Acta. Cryst.* **A47**, 110-119
- 124 Sheldrick, G.M., Schneider, T.R. (1997) *Methods Enzymol.* **277**, 319-343
- 125 Ost, T.W.B., Munro, A.W., Mowat, C.G., Taylor, P.R., Pesseguiro, A., Fulco, A.J., Cho, A.K., Cheesman, M.R., Walkinshaw, M.D., Chapman, S.K. 2001. *Biochemistry* **40**, 13430-13438
- 126 Roome, P.W., Philley, J.C., Peterson, J.A. 1983. *J. Biol. Chem.* **258**, 2593-2598
- 127 Hintz, M.J., Peterson, J.A. 1981. *J. Biol. Chem.* **256**, 6721-6728
- 128 Stayton, P.S., Poulos, T.L., Sligar, S.G. 1989. *Biochemistry* **28**, 8201-8205
- 129 Nelson D.R., Koymans L., Kamataki T., Stegeman J.J., Feyereisen R., Waxman D.J., Waterman M.R., Gotoh O., Coon M.J., Estabrook R.W., Gunsalus I.C. and Nebert D.W. 1996. *Pharmacogenetics* **6**, 1-42.
- 130 Yasukochi, T., Okada, O., Hara, T., Sagara, Y., Sekimizu, K., Horiuchi, T. 1994. *Biochem. Biophys. Acta.* **1204**, 84 – 90.
- 130a Shimizu, T., Hirano, K., Takahashi, M., Hatano, M. and Fujii-Kuriyama, Y. 1988. *Biochemistry* **27**, 4138 – 4141.
- 131 Porter, T.D. 1994. *Biochemistry* **33**, 5942 – 5946.

- 132 Song, W-C., Funk, C.D., Brash, A.R. 1993 *Proc. Natl. Acad. Sci. U.S.A.* **90**, 8519-8523
- 133 Itoh, A., Howe, G.A. 2001 *J. Biol. Chem.* **276**, 3620-3627
- 134 Hara, S., Miyata, A., Yokoyama, C., Inoue, H., Brugger, R., Lottspiech, F., Ullrich, V., Tanabe, T. 1994 *J. Biol. Chem.* **269**, 19897-19903
- 135 Ohashi, K., Ruan, K-H., Kulmacz, R.J., Wu, K.K., Wang, L-H. 1992 *J. Biol. Chem.* **267**, 789-793
- 136 Ho, P.P., Fulco, A.J. 1976 *Biochim. Biophys. Acta.* **431**, 249-256
- 137 Boddupalli, S.S., Estabrook, R.W., Peterson, J.A. 1990 *J. Biol. Chem.* **265**, 4233-4239
- 138 Bec, N., Anzenbacher, P., Anzenbacherova, E., Gorren, A.C.F., Munro, A.W., Lange, R. 1999. *Biochem. Biophys. Res. Commun.* **266**, 187-189
- 139 Daff S.N., Chapman S.K., Turner K.L., Holt R.A., Govindaraj S., Poulos T.L. and Munro A.W. 1997. *Biochemistry* **36**, 13816-13823
- 140 Chevion, M., Peisach, J., Blumberg, W.E. 1977. *J. Biol. Chem.*, **252** 3637-3945
- 141 McKnight, J., Cheesman, M.R., Thomson, A.J., Miles, J.S., Munro, A.W. 1993. *Eur. J. Biochem.* **213**, 683-687
- 142 Berka, V., Palmer, G., Chen, P-F., Tsai, A.L. 1998. *Biochemistry* **37**, 6136-6144
- 143 Salerno, J.C., Frey, C., McMillan, K., Williams, R.F., Masters, B.S.S., Griffith, O.W. 1995. *J. Biol. Chem.* **270**, 27423-27428
- 144 Tsai, A-L., Berka, V., Chen, P-F., Plamer, G. 1996. *J. Biol. Chem.* **271**, 32563-32571

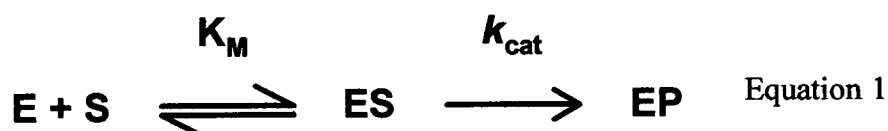
- 145 Ingram, L.L., Meyer, D.L. 1985. *Biochemistry of Dioxygen*, Plenum Press (New York)
- 146 Moore, G.R., Pettigrew, G.W., Rogers, N.K. 1986. *Proc. Natl. Acad. Sci. U.S.A.* **83**, 4998-4999
- 147 Watt, G.D., Frankel, F.H.A., Al-Basseet, J., Al-Massad, F., Farrar, J., Greenwood, C., Thomson, A.J., Moore, G.R. 1986. *Biochemistry* **85**, 4330-4336
- 148 Churg, A.K., Warshel, A. 1986. *Biochemistry* **25**, 1675-1681
- 149 Rafferty, S.P., Guillemette, J.G., Berghuis, A.M., Smith, M., Brayer, G.D., Mauk, A.G. 1996. *Biochemistry* **35**, 10784-10792
- 150 Louie, G.V., Brayer, G.D. 1989. *J. Mol. Biol.* **209**, 313-322
- 151 Rafferty, S.P., Pearce, L.L., Braker, P.D., Guillemette, J.G., Kay, C.M., Smith, M., Mauk, A.G. 1990. *Biochemistry* **29**, 9365-9369
- 152 Ghosh, D.K., Wu, C., Pitters, E., Moloney, M., Werner, E.R., Mayer, B., Stuehr, D.J. 1997. *Biochemistry* **36**, 10609-10619
- 153 Adak, S., Crooks, C., Wang, Q., Crane, B.R., Tainer, J.A., Getzoff, E.D., Stuehr, D.J. 1999. *J. Biol. Chem.* **274**, 26907-26911
- 154 Adak, S., Wang, Q., Stuehr, D.J. 2000. *J. Biol. Chem.*, **275**, 17434-17439
- 155 Presta, A., Weber-Main, A.M., Stankovich, M.T., Stuehr, D.J. 1998. *J. Am. Chem. Soc.* **120**, 9460-9465
- 155b Honeychurch, M.J., Hill, A.O., Wong, L-L. 1999. *FEBS Lett.* **451**, 351-353
- 156 Sligar, S.G. 1976. *Biochemistry* **15**, 5399-5406
- 157 Sharrock, M., Debrunner, P.G., Schultz, C., Lipscomb, J.D., Marshall, V., Gunsalus, I.C. 1973. *Biochemistry* **12**, 258

- 158 Tsai, R., Yu, C.A., Gunsalus, I.C., Peisach, J., Blumberg, W., Orme-Johnson, W.H., Beinert, H. 1970. *Proc. Natl. Acad. Sci. U.S.A.* **66**, 1157
- 159 Champion, P.M., Lipscomb, J.D., Munck, E., Debrunner, P.G., Gunsalus, I.C. 1975. *Biochemistry* **14**, 4151
- 160 Sono, M., Roach, M.P., Coulter, E.D., Dawson, J.H. 1996. *Chem. Rev.* **96**, 2841-2887
- 161 Griffin, B. W., Peterson, J. A. 1972. *Biochemistry* **11**, 4740 – 4746
- 162 Safo, M.K., Gupta, G.P., Watson, T.C., Simonis, U., Walfer, F.A., Scheidt, W.R. 1992. *J. Am. Chem. Soc.* **114**, 7066-7075
- 163 Safo, M.K., Walker, F.A., Raitsimring, A.M., Walters, W.P., Dolata, D.P., Debrunner, P.G., Scheidt, W.R. 1994. *J. Am. Chem. Soc.* **116**, 7760-7770
- 164 Palmer, T. 1991. Chapter 8. *Understanding Enzymes* 3rd Ed. Ellis Horwood Publishing
- 165 Ford, P., Rudd, D.F.P., Gaudner, R., Taube, H. 1968. *J. Am. Chem. Soc.* **90**, 1187-1194
- 166 Dodsworth, E. S., Lever, A.B.P. 1985. *Chem. Phys. Lett.* **119**, 61-66
- 167 Dodsworth, E. S., Lever, A.B.P. 1985. *Chem. Phys. Lett.* **124**, 152-158
- 168 Lever, A.P.B., Pickens, S.R., Minor, P.C., Licoccia, S., Ramaswamy, B.S., Magnell, K. 1981. *J. Am. Chem. Soc.* **103**, 6800-6806
- 169 Dei, A. 1993. *Inorg. Chem.* **32**, 5730-5733
- 170 Griffin, B.W., Peterson, J.A. 1972. *Biochemistry* **11**, 4740-4746
- 171 Poulos, T. L., Finzel, B. C., Howard, A. J. 1986. *Biochemistry* **25**, 5314 – 5322

- 172 Sligar, S.G. in *Cytochrome P450 Structure, Mechanism and Biochemistry*,
2nd Ed.

APPENDIX II**DERIVATION OF KINETIC EQUATIONS****1 The Michaelis-Menten equation**

The Michaelis-Menten equation applies for an enzyme catalysed reaction in which substrate binding is rapid and reversible and when product formation is rate



determining, e.g.

Where E, S, ES and P are, the enzyme, substrate, enzyme-substrate complex and product respectively. From this, the substrate-binding equilibrium constant (K_M) and initial rate (v) can be evaluated (Equation 2 and 3):

$$K_M = \frac{[E][S]}{[ES]} \quad \text{Equation 2}$$

$$v = k_{cat}[ES] \quad \text{Equation 3}$$

The total concentration of enzyme present, $[E_T]$, is equal to the sum of the free enzyme, $[E]$, and the bound enzyme, $[ES]$. The concentration of free enzyme, $[E]$, can therefore be represented as in Equation 4.

$$[E] = [E_T] - [ES] \quad \text{Equation 4}$$

Substitution of equation 4 into equation 2 gives:

$$K_M = \frac{([E_T] - [ES])[S]}{[ES]} \quad \text{Equation 5}$$

Which simplifies to Equation 6:

$$[ES] = \frac{[E_T][S]k_{cat}}{K_M + [S]} \quad \text{Equation 6}$$

Substitution of Equation 6 into Equation 3 gives the Michaelis-Menten equation (Equation 7).

$$v = \frac{[E_T][S]k_{cat}}{K_M + [S]} \quad \text{Equation 7}$$

2 The Lineweaver-Burk equation

To analyse data graphically, the Michaelis-Menten is often transformed into a linear form (Equation 8). The most common method is the double-reciprocal or Lineweaver-Burk plot (Figure A1.1). This is obtained by inverting both sides of Equation 7 and substituting v_{max} for $k_{cat}[E_0]$, where v_{max} is the limiting velocity.

$$\frac{1}{v} = \frac{K_M}{v_{max}[S]} + \frac{1}{v_{max}} \quad \text{Equation 8}$$

One disadvantage of this method is that data points at low concentrations are emphasised, whereas those at high concentrations are compressed. Departure from linearity for a particular enzyme catalysed reaction indicates that the assumptions inherent in the Michaelis-Menten equation are not valid in this instance.

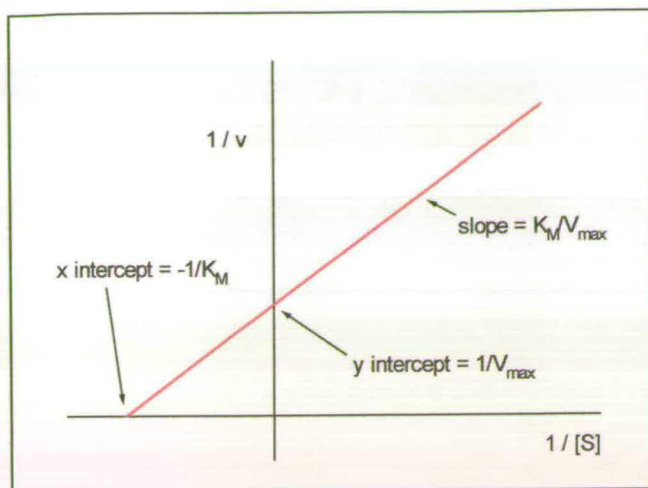
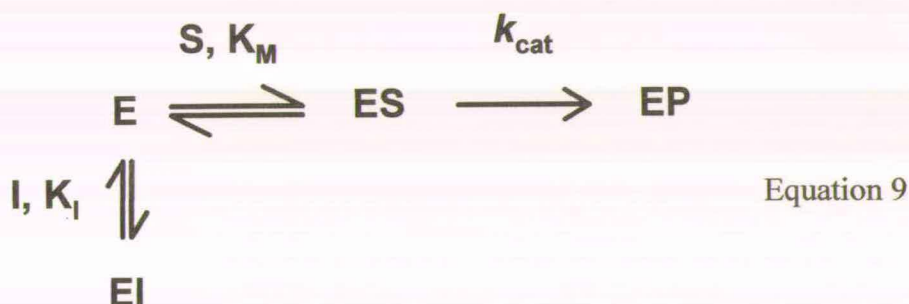


Figure A2.1

3 Competitive Inhibition

Competitive inhibitors often closely resemble in some respects, the substrates whose reactions they inhibit, and because of this structural similarity they may compete for the same binding site of the enzyme. In terms of the Michaelis-Menten mechanism, an additional equilibrium must be taken into consideration (Equation 9) and



described by Equations 10 to 16. Here, I is the inhibitor and EI is the enzyme-inhibitor complex, K_I is the inhibitor dissociation constant.

$$K_I = \frac{[\text{E}][\text{I}]}{[\text{EI}]}
 \quad \text{Equation 10}$$

and,

$$K_M = \frac{[E][S]}{[ES]} \quad \text{Equation 11}$$

In this case, the total concentration of enzyme must take into account the contribution from EI, hence equation 12:

$$[E_T] = [E] + [ES] + [EI] \quad \text{Equation 12}$$

Expressing Equation 12 in terms of [EI] and substituting into equation 4 gives:

$$[E_T] = [E] + [ES] + \frac{[E][I]}{K_I} \quad \text{Equation 13}$$

$$[E] = \frac{[E_T] - [ES]}{(1 + [I]/K_I)} \quad \text{Equation 14}$$

Expressing Equation 11 in terms of [E] and substituting into equation 15, gives:

$$K_M \left(1 + \frac{[I]}{K_I}\right) = \frac{([E_T] - [ES])[S]}{[ES]} \quad \text{Equation 15}$$

Finally, substituting $[ES] = v/k_{cat}$ into Equation 16 gives:

$$v = \frac{[E_T][S]k_{cat}}{[S] + K_M \left(1 + \frac{[I]}{K_I}\right)} \quad \text{Equation 16}$$

Equation 15 is expressed in the same form as the Michaelis-Menten equation and shows that for competitive inhibition, v is unchanged but K_M is apparently increased by $(1 + [I]/K_I)$. A typical series of inhibited Michaelis plots are shown in Figure A2.2, increasing inhibitor concentration increases the K_M without effecting the k_{cat} .

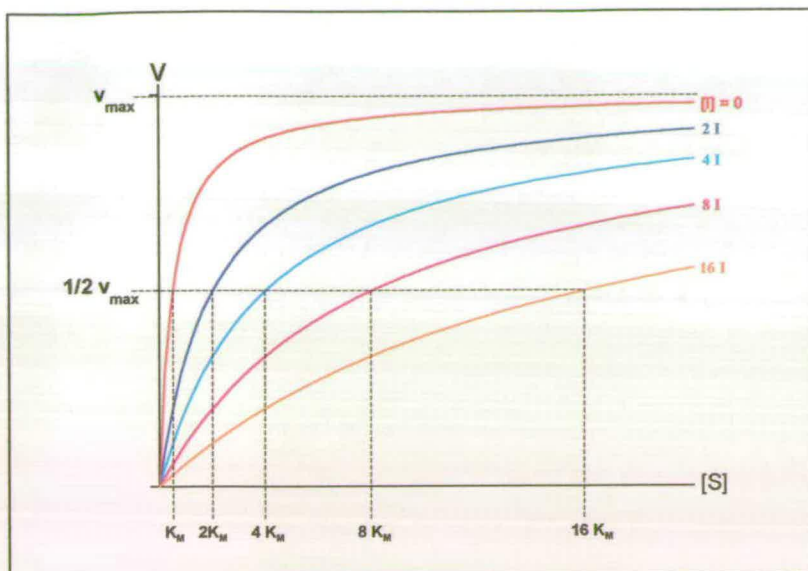


Figure A2.2

APPENDIX III

PEPTIDE SEQUENCE OF FLAVOCYTOCHROME P450 BM3

The heme binding residue, Cys400, is shown in green. Heme Domain: 1 – 472;
Reductase Domain: 473 – 1048.

1	10	20	30	40	50	60
TIKEMPQPKT	FGELKNLPLL	NTDKPVQALM	KIADELGEIF	KFEAPGRVTR	YLSSQRLIKE	
	70	80	90	100	110	120
ACDESRFDKN	LSQALKFVRD	FAGDGLFTSW	THEKNWKKAH	NILLPSFSQQ	AMKGYHAMMV	
	130	140	150	160	170	180
DIAVQLVQKW	ERLNADEHIE	VPEDMTRLTL	DTIGLCGFNY	RFNSFYRDQP	HPFITSMVRA	
	190	200	210	220	230	240
LDEAMNKLQR	ANPDDPAYDE	NKRQFQEDIK	VMNDLVDKII	ADRKASGEQS	DDLLTHMLNG	
	250	260	270	280	290	300
KDPETGEPLD	DENIRYQIIT	FLIAGHETTS	GLLSFALYFL	VKNPHVLQKA	AEEAARVLVD	

The Catalytic Control of Flavocytochrome P450 BM3

310	320	330	340	350	360
PVPSYKQVKQ	LKYVGMVLNE	ALRLWPTAPA	FSLYAKEDTV	LGGEYPLEKG	DELMVLIPQL
370	380	390	400	410	420
HRDKTIWGDD	VEEFRPERFE	NPSAIPQHAF	KPFGNGQRAC	IGQQFALHEA	TLVLGMMLKH
430	440	450	460	470	480
FDDEDHTNVE	LDIKETLTLK	PEGFVVKAKS	KKIPLGGIPS	PSTEQSAKKV	RKKAENAHNT
490	500	510	520	530	540
PLLVLYGSNM	GTAEGTARDL	ADIAMSKGFA	PQVATLDSHA	GNLREGAVL	IVTASYNGHP
550	560	570	580	590	600
PDNAKQFVDW	LDQASADEVK	GVRYSVFGCG	DKNWATTYQK	VPAFIDETLA	AKGAENIADR
610	620	630	640	650	660
GEADASDDFE	GTYEEWREHM	WSDVAAYFNL	DIENSEDNKS	TLSLQFVDSA	ADMPLAKMHG
670	680	690	700	710	720
AFSTNVVASK	ELQQPGSARS	TRHLEIELPK	EASYQEGDHL	GVIPRNYEGI	VNRVTARFGL

The Catalytic Control of Flavocytochrome P450 BM3

730	740	750	760	770	780
DASQQIRLEA	EEEKLAHLPL	AKTVSVEELL	QYVELQDPVT	RTQLRAMAAK	TVCPPHKVEL
790	800	810	820	830	840
EALLEKQAYK	EQVLAKRLTM	LELLEKYPAC	EMKFSEFIAL	LPSIRPRYYS	ISSSPRVDEK
850	860	870	880	890	900
QASITVSVVS	GEAWSGYGEY	KGIASNYLAE	LQEGDTITCF	ISTPQSEFTL	PKDPETPLIM
910	920	930	940	950	960
VGPGTGVAPF	RGFVQARKQL	KEQGQSLGEA	HLYFGCRSPH	EDYLYQEELE	NAQSEGIITL
970	980	990	1000	1010	1020
HTAFSRMPNQ	PKTYVQHVME	QDGKKLIELL	DQGAHFYICG	DGSQMAPAVE	ATLMKSYADV
1030	1040	1048			
HQVSEADARL	WLQQLEEKGR	YAKDVWAG			

APPENDIX IV

PUBLICATIONS AND MEETINGS ATTENDED

Publications:

Copies of the publications listed below are bound at the back of the thesis.

- **Flavocytochrome P450 BM3: A Paradigm for the Analysis of Electron Transfer and its Control in P450s**

Munro, A.W., Noble, M.A., Miles, C.S., Daff, S.N., Green, A.J., Quaroni, L., Rivers, S., Ost, T.W.B., Reid, G.A., Chapman, S.K., 1999. *Biochem. Soc. Trans.* **27**, 190 – 196

- **Key Binding Residues in Flavocytochrome P450 BM3**

Ost, T.W.B., Noble, M.A., Chapman, S.K., Miles, C.S., Murdoch, J., Reid, G.A., Munro, A.W. 1999. *Flavins and Flavoproteins 1999*, 147 – 150

- **Flavocytochrome P450 BM3 – Substrate Selectivity and Electron Transfer in a Model Cytochrome P450**

Munro, A.W., Noble, M.A., Ost, T.W.B., Green, A.J., McLean, K.J., Robledo, L., Miles, C.S., Murdoch, J., Chapman, S.K., Munro, A.W. 2000. *Subcellular Biochemistry* **35**, 297 – 316

- **Rational Re-design of the Substrate Binding Site of Flavocytochrome P450 BM3**

Ost, T.W.B., Miles, C.S., Murdoch, J., Cheung, Y-F., Reid, G.A., Chapman, S.K., Munro, A.W. 2000. *FEBS Lett.* **486**, 173 – 177

- **Protein Engineering in Cytochromes P450**

Miles, C.S., Ost, T.W.B., Noble, M.A., Munro, A.W., Chapman, S.K. 2000.
Biochem. Biophys. Acta., **1543**, 383 – 407

- **Phenylalanine 393 Exerts Thermodynamic Control Over the Heme of Flavocytochrome P450 BM3**

Ost, T.W.B., Miles, C.S., Munro, A.W., Murdoch, J., Reid, G.A., Chapman, S.K.
2001. *Biochemistry* **40**, 13421-13429

- **The Structural and Spectroscopic Characterisation of the F393H Mutant of Flavocytochrome P450 BM3**

Ost, T.W.B., Munro, A.W., Mowat, C.G., Pesseguiro, A., Fulco, A.J., Cho, A.K,
Cheesman, M.R., Walkinshaw, M.D., Chapman, S.K. 2001. *Biochemistry*.**40**,
13430-13438

Conferences Attended:

Biochemical Society:

The 668 th Biochemical Society Conference, University of Glasgow, March
1999 (speaker: **Key Active Site Residues of Flavocytochrome P450 BM3**).

The 672 nd Biochemical Society Conference, University of Sussex,
December 2000 (delegate).

Scottish Protein Structure Group:

St Andrews University, February 2000 (speaker: **Phenylalanine 393 of P450
BM3 – Modulates Rates and Redox States**).

Fifth International Symposium on P450 Biodiversity:

Elsinore, Denmark, July 2000 (delegate, abstract & poster presented).

2nd, 3rd, 4th and 5th Redox Enzymes Meeting:

Firbush Point Centre, Perthshire, Scotland, June 1998-2001 (as delegate and speaker).

Rational re-design of the substrate binding site of flavocytochrome P450 BM3

Tobias W.B. Ost^a, Caroline S. Miles^b, Jane Murdoch^b, York-Fong Cheung^c,
Graeme A. Reid^b, Stephen K. Chapman^a, Andrew W. Munro^{c,*}

^aDepartment of Chemistry, University of Edinburgh, West Mains Road, Edinburgh EH9 3JJ, UK

^bInstitute of Cell and Molecular Biology, University of Edinburgh, Mayfield Road, Edinburgh EH9 3JT, UK

^cDepartment of Pure and Applied Chemistry, University of Strathclyde, The Royal College, 204 George Street, Glasgow G1 1XL, UK

Received 19 October 2000; revised 3 November 2000; accepted 8 November 2000

First published online 23 November 2000

Edited by Vladimir Skulachev

Abstract *Bacillus megaterium* P450 BM3 is a fatty acid hydroxylase with selectivity for long chain substrates (C₁₂–C₂₀). Binding or activity with substrates of chain length < C₁₂ has not been reported. Rational mutagenesis was used to re-design the enzyme to encourage binding of short chain fatty acids (C₄–C₁₀). We show that wild-type P450 BM3 has activity and weak affinity for substrates as short as butyrate (C₄). However, turnover/binding of short chain substrates is dramatically increased by introducing a novel substrate carboxylate binding site close to the heme. Mutant L181K shows catalytic efficiency (k_{cat}/K_M) increased > 13-fold with butyrate, while the L75T/L181K double mutant has k_{cat}/K_M increased > 15-fold with hexanoate and binding (K_d) improved > 28-fold for butyrate. Removing the arginine 47/lysine 51 carboxylate binding motif at the mouth of the active site disfavours binding of all fatty acids, indicating its importance in the initial recognition of substrates. © 2000 Federation of European Biochemical Societies. Published by Elsevier Science B.V. All rights reserved.

Key words: Cytochrome P450; Substrate recognition; Rational mutagenesis

1. Introduction

Cytochromes P450 (P450s) are cysteine-ligated haem-containing monooxygenases widespread in nature [1]. They have important metabolic functions (including steroid syntheses and transformations), play roles in detoxification of drugs and xenobiotics, and catalyse breakdown of unusual compounds as carbon sources for growth [2,3]. Their predominant reaction is the mono-oxygenation of organic molecules by the activation and insertion of an atom from molecular O₂ (Scheme 1). However, other reactions (e.g. dealkylation) have also been reported [4].



Analysis of soluble bacterial P450s such as the camphor hydroxylase from *Pseudomonas putida* and the fatty acid hydroxylase from *Bacillus megaterium* have given insights into the structure and function of their membrane-bound eukaryotic counterparts [5]. The X-ray crystal structures of bacterial

P450s have allowed various aspects, key to their function, to be investigated by a rational approach. Bacterial structures also have important biotechnological roles as models for the eukaryotic P450s for e.g. design of new drugs, and have great potential to catalyse novel reactions inaccessible to conventional chemistry.

One of the most intensively studied of the bacterial P450s is the flavocytochrome P450 BM3, a high activity fatty acid hydroxylase from *B. megaterium* [6]. P450 BM3 is a natural fusion of a P450 to a mammalian-like diflavin NADPH-P450 reductase and is of great importance in understanding structure, function and electron transfer in this enzyme class.

In this study, we have altered substrate selectivity in P450 BM3. The substrate (palmitoleate)-bound P450 BM3 structure reveals several hydrophobic residues within van der Waals contact of the substrate [7]. Using rational site-directed mutagenesis, we have replaced selected neutral residues with positively charged or more hydrophilic residues in attempts to pinpoint substrate binding determinants. We have also attempted to copy the fatty acid carboxylate binding motif (R47/Y51, found at the mouth of the active site) at positions further down the substrate binding channel to encourage binding of shorter chain fatty acids. To date, no research has successfully addressed reasons for the observed substrate selectivity profile of this important flavocytochrome, which only has reported activity for fatty acids of chain length C₁₂–C₂₀. Here we provide evidence that rational mutagenesis can be used to convert P450 BM3 to favour binding of shorter chain (C₄–C₁₀) fatty acids.

2. Materials and methods

All P450 BM3 substrates (arachidonic acid and sodium laurate (C₁₂), decanoate (C₁₀), octanoate (C₈), hexanoate (C₆) and butyrate (C₄)) were from Sigma (St. Louis, MO, USA). Oligonucleotide primers were from PE Biosystems. Restriction and DNA modification enzymes were from New England Biolabs. All other reagents were from Sigma. The arachidonic acid stock solution was 33 mM (approximately 10 mg ml⁻¹) in ethanol. All other substrates were prepared as aqueous solutions in the assay buffer for P450 BM3 reactions (20 mM MOPS, pH 7.4, plus 100 mM KCl). NADPH was prepared as a 20 mM stock in ice-cold degassed assay buffer.

Cloning of P450 BM3 and generation of mutants R47A and Y51F has been described previously [8,9]. Site-directed mutagenesis of flavocytochrome P450 BM3 and its haem (P450) domain was according to Kunkel [10,11]. Oligonucleotides used to construct the indicated mutants were as follows (plasmid nomenclature in parentheses, underlined bases indicate mismatches): L181K (pCM21) – 5'-CATTGCTT-CATCCITGACGGACCATAC-3' L181R (pCM22) – 5'-GCTT-

*Corresponding author. Fax: (44)-141-5483727.
E-mail: andrew.munro@strath.ac.uk

CATCCCGTGCACGGAC-3' L437K (pCM23) – 5'-GGTTTAAAC-GTTTITAGTTTAAATATCC-3' L437R (pCM24) – 5'-GGTTTAAAC-GTTCCGAGTTTCTTTAAATATCC-3' I263K (pCM61) – 5'-GTTTC-GTGTCCCGCTTTTAAAGAATGTAAT-3' L75K (pCM59) – 5'-CG-TACAAATTTCTTCGCTTGACTTAAG-3' L181K/L75T (pCM60) – 5'-CGTACAAATTTAGTCGCTTGACTTAAG-3'

Double mutant R47A/Y51F was prepared by mutagenesis of existing clone pCM25 (R47A) [9] using primer 5'-GACTTGATAA-GAAGCGCGTTAC-3'. Triple mutant R47A/Y51F/L181K was generated by digestion of the existing plasmid clones pCM28 (R47A/Y51F) and pCM21 (L181K) with *SpeI* and *AflIII*, followed by purification of the smaller (1.5 kb) fragment from the pCM28 digest and the larger (~6.5 kb) fragment from the pCM21 digest by elution after agarose gel electrophoresis. These fragments were re-ligated to generate clone pCM29 (R47A/Y51F/L181K). All mutations were verified by sequencing the complete gene. Plasmid preparations, transformations and dideoxy DNA sequencing (to verify mutations) were performed by standard methods [12]. *Escherichia coli* strain TG1 was used for the expression of the enzymes [13].

Wild-type and mutant P450s BM3 were expressed under the control of the BM3 promoter system, which is highly active in stationary phase. Transformed *E. coli* cells were grown in Luria–Bertani medium supplemented with 25 $\mu\text{g ml}^{-1}$ carbenicillin. Enzymes were purified following the reported protocol [8]. Pure proteins were concentrated to ~200 μM by ultrafiltration, dialysed against 1 l of storage buffer (50 mM Tris–HCl, 1 mM EDTA, pH 7.4) containing 50% (v/v) glycerol, and stored frozen at -80°C .

Steady-state kinetic assays were performed at 30°C in assay buffer. Substrate oxidation assays were performed as described previously [9], monitoring coupled oxidation of NADPH at 340 nm ($\epsilon_{340} = 6210 \text{ M}^{-1} \text{ cm}^{-1}$). Enzyme concentration was $\leq 3 \mu\text{M}$ and substrate (carboxylic acids of differing chain length from butyric acid (C_4) up to arachidonic acid (C_{20})) was added over a range of different concentrations, according to the enzyme affinity. The reaction was initiated by addition of NADPH (200 μM). Initial rate of substrate oxidation was measured over the first minute. Specific enzyme rates were calculated and plotted against substrate concentration, and the data fitted to the Michaelis function to generate k_{cat} and K_{M} parameters.

Substrate dissociation constants (K_{d} values) were determined by following the low- to high-spin perturbations of the ferric absorption spectra (absorbance shift from 419 to 390 nm) upon substrate-induced removal of the sixth (water) ligand to the heme iron. Titrations were

performed either by addition of small (<0.5 μl) volumes of alcoholic arachidonic acid using a Hamilton syringe (<5 μl total), or by mixing aliquots of substrate-free enzyme solution with substrate-saturated aqueous solutions containing enzyme at the identical concentration. By mixing substrate-free and substrate-saturated enzyme solutions in different ratios, the desired substrate concentration is obtained. Spectra were recorded between 800 and 300 nm at each point in the titration. Difference spectra were generated and the maximum absorbance difference calculated. Differences were plotted against substrate concentration and fitted to a rectangular hyperbola to generate the K_{d} in each case. All data manipulations and non-linear least-squares curve-fitting were performed using Origin (Microcal).

Determinations of P450 integrity and concentration were achieved by generating the ferrous-CO adduct of each enzyme. Reduction was performed by addition of sodium dithionite to the enzyme (~5 μM) in assay buffer, and carbon monoxide gas was bubbled into the solution slowly for 60 s to generate the characteristic P450 complex. In all cases, there was near complete (>95%) conversion to the ferrous-CO adduct at 450 nm ('P450'), indicative of active protein. Negligible amounts of the inactive ('P420') species were observed. P450 concentration was determined from the reduced/CO-bound minus reduced difference spectrum, using $\epsilon_{450-490} = 91 \text{ mM}^{-1} \text{ cm}^{-1}$.

3. Results and discussion

Our mutagenesis strategy was based on examination of the active site of palmitoleate-bound P450. Residues in the central region of the long, hydrophobic channel in van der Waals contact with the substrate and less than 10 Å from the heme were selected as mutagenesis targets (Fig. 1). Since the Arg47, Tyr51 motif at the active site mouth is essential both for binding carboxylate groups of long chain substrates and transition state stabilisation [7,9], we constructed a series of mutants in which the selected hydrophobic amino acids (Leu75, Leu181, Ile263 and Leu437) were altered. These were changed to residues capable of forming hydrogen bonds or salt bridges to the carboxylate group of shorter substrates (C_4 – C_{10}). We also examined the effects of removing the R47/Y51 motif, to assess whether short-chain fatty acids were then

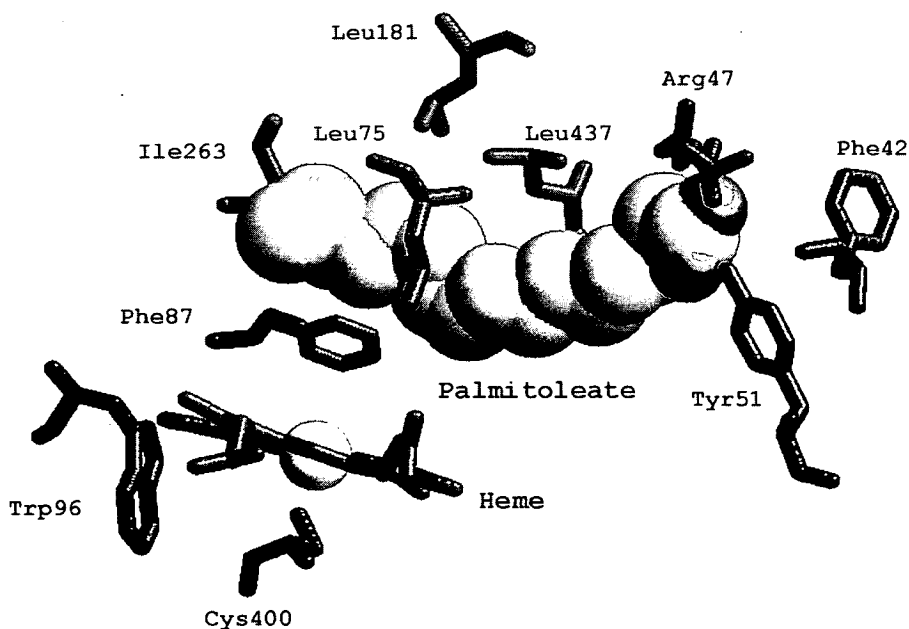


Fig. 1. Important amino acids in the X-ray atomic structure of palmitoleate-bound P450 BM3. Several amino acids have key roles in substrate association (R47, Y51, F42 [9]), regioselectivity of substrate oxidation (F87 [21]), haem incorporation and haem iron spin-state regulation (W96 [22]) and coordination of the haem iron (C400). Other residues within the substrate binding pocket are in van der Waals contact with substrate, and were targets for mutagenesis in this study.

Table 1
Catalytic parameters for wild-type and mutant P450s BM3

Enzyme		Substrate					
		C ₄	C ₆	C ₈	C ₁₀	C ₁₂	C ₂₀
Wild-type	k_{cat} (min ⁻¹)	88 ± 6	229 ± 26	1364 ± 153	6393 ± 486	5140 ± 90	17100 ± 190
	K_{M}	387 ± 66 mM	243 ± 49 mM	39 ± 9 mM	6 ± 1 mM	290 ± 20 μM	4.7 ± 0.3 μM
	$k_{\text{cat}}/K_{\text{M}}$ (mM min ⁻¹)	0.23 ± 0.065	0.94 ± 0.35	35 ± 15.5	1066 ± 310	17700 ± 1700	(3.64 ± 0.29) × 10 ⁶
R47A/Y51F	k_{cat} (min ⁻¹)	142 ± 16	156 ± 31	692 ± 61	1654 ± 88	2095 ± 88	3234 ± 199
	K_{M}	463 ± 123 mM	480 ± 134 mM	46 ± 10 mM	4.6 ± 0.6 mM	514 ± 48 μM	33 ± 4 μM
	$k_{\text{cat}}/K_{\text{M}}$ (mM min ⁻¹)	0.307 ± 0.154	0.325 ± 0.215	15.0 ± 5.9	360 ± 75	4080 ± 600	98000 ± 20400
L181K	k_{cat} (min ⁻¹)	353 ± 7	166 ± 10	747 ± 20	547 ± 35	693 ± 27	3073 ± 174
	K_{M}	116 ± 8 mM	121 ± 14 mM	4.0 ± 0.3 mM	3.8 ± 0.6 mM	134 ± 20 μM	6.3 ± 0.7 μM
	$k_{\text{cat}}/K_{\text{M}}$ (mM min ⁻¹)	3.04 ± 0.29	1.37 ± 0.27	187 ± 20	144 ± 38	51700 ± 11500	(4.88 ± 0.92) × 10 ⁵
L181K/L75T	k_{cat} (min ⁻¹)	205 ± 17	2590 ± 212	3256 ± 128	116 ± 7	269 ± 13	14006 ± 624
	K_{M}	602 ± 79.5 mM	177 ± 32.5 mM	19.7 ± 2.1 mM	2.67 ± 0.36 mM	316 ± 38 μM	9.3 ± 1.4 μM
	$k_{\text{cat}}/K_{\text{M}}$ (mM min ⁻¹)	0.34 ± 0.08	14.6 ± 4.8	165 ± 27	43 ± 10	850 ± 160	(1.51 ± 0.35) × 10 ⁶

The k_{cat} and K_{M} values were determined as described in Section 2. Catalytic efficiency of wild-type and mutant P450s was calculated as the $k_{\text{cat}}/K_{\text{M}}$ ratio. ND = 'not determinable', and indicates that catalytic rate was not significantly higher than background, preventing accurate determination of the k_{cat} and K_{M} values.

capable of diffusing further into the active site without becoming tethered in a position unfavourable for catalysis.

All mutant enzymes had a full complement of flavin and heme, indicating the mutations did not cause major disruption to the tertiary structure. Catalytic (k_{cat} and K_{M}) and substrate binding (K_{d}) studies of wild-type P450 BM3 showed there was modest binding (K_{M} , K_{d} in mM range) of substrates with chain length shorter than laurate (Tables 1 and 2). However, mutants L181R, L437K, L437R and R47A/Y51F/L181K showed weaker binding and lower catalytic activity than wild-type P450 BM3 with all substrates. The L437K and L437R mutant enzymes were particularly severely affected. L437R had rates of < 10 min⁻¹ with all substrates, and maximal activity obtained with L437K was only 120 ± 4 min⁻¹ with arachidonate, almost 150-fold lower than wild-type P450 BM3.

Mutants I263K and L75K retained considerable activity (k_{cat} , min⁻¹) with laurate (1014 ± 14 and 1090 ± 34, respectively cf 5140 ± 90 for wild-type P450 BM3) and arachidonate (1443 ± 73 and 1395 ± 54 cf 17100 ± 190 for wild-type P450 BM3), but showed no activity improvement (k_{cat}) with short chain substrates. However, K_{M} values (mM) for I263K and L75K were lower for hexanoate (49 ± 7.6 and 114 ± 18, respectively, cf 243 ± 49 for wild-type), octanoate (14.6 ± 1.1 and 9.8 ± 1.3 cf 39 ± 9.0) and decanoate (0.85 ± 0.06 and 2.5 ± 0.3 cf 6 ± 1). These K_{M} improvements lead to small increases in efficiency ($k_{\text{cat}}/K_{\text{M}}$) over wild-type for I263K with hexanoate (4.3-fold) and octanoate (1.9-fold), and for L75K with octanoate (2.7-fold). Spectral measurements also indicated improvements in hexanoate and decanoate binding for L75K (K_{d} values = 79 ± 19 mM and 0.63 ± 0.09 mM, respectively). A feature of mutant I263K was that, for all substrates, spin-

state perturbation on substrate binding was much less than for wild-type P450 BM3. This prevented accurate determination of K_{d} values for substrates other than laurate and arachidonate. Mutants I263K and L75K showed encouraging changes in substrate chain length specificity. However three other mutants (R47A/Y51F, L181K and L75T/L181K) showed more dramatic alterations in activity and selectivity, and are discussed in more detail below.

3.1. R47A/Y51F

In P450 BM3, both the arginine 47-to-carboxylate salt bridge and the tyrosine 51-to-carboxylate hydrogen bond are important for efficient catalysis [7]. The contribution of R47 is more important to fatty acid binding [9]. By creating the double mutant enzyme R47A/Y51F we sought to investigate two distinct problems: (1) whether total removal of this motif has severe effects on binding of long chain substrates, and (2) whether binding and catalysis of shorter chain substrates is favoured due to their ability to diffuse further into the active site, following removal of a motif that would otherwise 'trap' them distant from the heme iron. Significant decreases in k_{cat} and increases in K_{M} for both laurate and arachidonate were measured for R47A/Y51F (Table 1). These resulted in 4.3- and 37.1-fold decreases in efficiency ($k_{\text{cat}}/K_{\text{M}}$) for laurate and arachidonate, respectively, compared to wild-type. The cumulative effect of the two mutations is greater than the effect of either in isolation [9]. Thus, both residues are needed for efficient function of P450 BM3, supporting recent predictions [14].

Characterisation of the properties of the R47A/Y51F enzyme with fatty acids shorter than C₁₂ chain length showed that there was no improvement in binding (Table 2) and that

Table 2
Binding (dissociation) constants for wild-type and mutant P450s BM3

Enzyme	Substrate and K_{d} (mM)					
	C ₄	C ₆	C ₈	C ₁₀	C ₁₂	C ₂₀
Wild-type	261 ± 27	131 ± 10	12 ± 2	2.6 ± 0.4	(241 ± 7) × 10 ⁻³	(3.6 ± 0.3) × 10 ⁻³
R47A/Y51F	ND	ND	50 ± 14	ND	ND	(5.3 ± 0.2) × 10 ⁻³
L181K	91 ± 18	246 ± 32	4 ± 1	(312 ± 26) × 10 ⁻³	(255 ± 33) × 10 ⁻³	(2 ± 0.2) × 10 ⁻³
L181K/L75T	9.3 ± 1.9	18.5 ± 5.4	5.1 ± 0.9	0.99 ± 0.12	(297 ± 30) × 10 ⁻³	(14 ± 1.5) × 10 ⁻³

K_{d} values were determined by spectral titration as described in Section 2. ND = 'not determinable', and indicates that extent of spectral shift induced by the substrate was not great enough to enable the accurate determination of a K_{d} value.

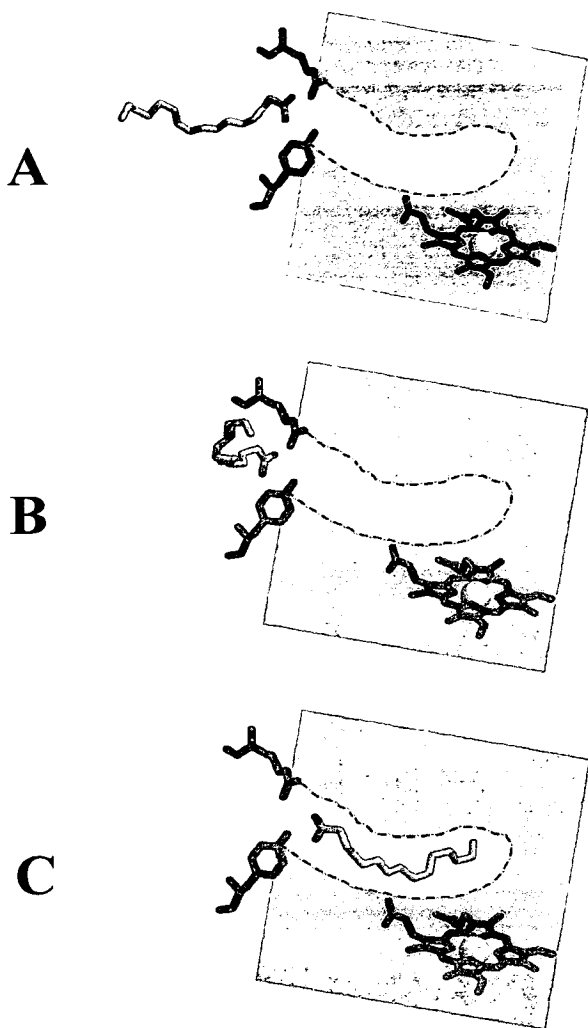


Fig. 2. Model for substrate interaction in P450 BM3. A hydrophobic patch adjacent to the active site entrance makes initial interactions with the alkyl chain of fatty acids. (A) Electrostatic forces orientate the substrate carboxylate group towards R47, and a hydrogen bond between the carboxylate and the hydroxyl group of Y51 further stabilises the binding. (B) The alkyl chain of the substrate is drawn into the active site channel, where favourable hydrophobic interactions ensure strong association. (C) The final catalytically competent orientation is achieved, in readiness for haem reduction and the initiation of the catalytic cycle.

catalytic efficiency was reduced >2 -fold for C_6 to C_{10} substrates. For butyrate, there was no significant difference in catalytic efficiency between R47A/Y51F and wild-type (Table 1). Clearly, removal of the motif does not improve the short chain selectivity by preventing molecules from binding at the mouth of the active site. In fact, it appears to be important for the binding of substrates of all chain length, probably by the recognition of substrates from the bulk solution (Fig. 2).

A hydrophobic patch at the surface of the haem domain, adjacent to the active site, is postulated to act as an initial surface for substrate interaction [7]. The palmitic acid binding properties of a P25Q mutant in this region (K_d increased ~ 100 -fold) are consistent with this postulate [15]. However, substrate cannot enter directly into the long hydrophobic active site channel, since mutual hydrophobic effects cannot be transmitted long-range in solution. Instead, we consider that

the fatty acid carboxylate is attracted by electrostatic (solution-transmissible) forces to the guanidinium group of R47 at the mouth of the active site. Once this occurs, a hydrogen bond to the hydroxyl group of Y51 can also form. At this point, there is a strong driving force for the movement of the long hydrophobic tail of the fatty acid from the polar solvent phase into the substrate binding channel. Once inside, interactions with several hydrophobic side-chains occur. Thus, the R47/Y51 motif is critical for guidance of fatty acids into the active site.

3.2. L181K

This was the most successful single mutant studied. L181K has decreased catalytic efficiency with long chain substrates, but markedly improved efficiency with shorter chain fatty acids, particularly butyrate (13-fold over wild-type) and octanoate (5-fold) (Table 1). Catalytic efficiency is not significantly different from wild-type for hexanoate, and is decreased 7-fold for decanoate. However, in both cases it is k_{cat} that is unfavourably affected. The K_M for hexanoate and decanoate is actually decreased compared to wild-type (Table 1). The L181K K_d is also decreased for butyrate, octanoate and decanoate. Mutant L181K shows large conversion in substrate selectivity, with the ratio of catalytic efficiency (k_{cat}/K_M) for short chain fatty acids to that for arachidonate increased 99-fold for butyrate and 40-fold for octanoate over wild-type.

Interestingly, L181R does not show similar characteristics and is severely affected in catalysis. The k_{cat} values for this mutant are $<40 \text{ min}^{-1}$ for all substrates $\leq C_{10}$, and only $584 \pm 14 \text{ min}^{-1}$ for arachidonate. Substrates of chain length $< C_{12}$ do not induce a significant spin-state shift in the L181R heme, preventing determination of K_d . Clearly, length and/or mobility of the lysine sidechain are critical factor(s) in promoting the observed substrate selectivity changes in L181K. Also notable is that triple mutant R47A/Y51F/L181K is severely impaired in binding and catalysis with all substrates. There is no measurable activity with substrates of chain length $< C_{10}$, and activity is only $1213 \pm 38 \text{ min}^{-1}$ with arachidonate. Clearly the L181K mutation cannot compensate for the absence of the R47/Y51 substrate binding motif.

3.3. L75T/L181K

In this double mutant, we combined the best single mutation (L181K) with a second mutation in which L75 was mutated to an amino acid (threonine) with a hydroxyl containing side-chain. Here, we attempted to recreate, close to the heme, a motif (lysine/threonine) with similar chemical character and bonding capability to the R47/Y51 motif at the active site mouth. The L75T/L181K double mutant also showed marked alterations in substrate selectivity (Tables 1 and 2). The most striking improvements in catalytic properties of L75T/L181K are the large increases in k_{cat} with hexanoate and octanoate. K_M values for these substrates are also lower than for wild-type, leading to 15.5-fold (hexanoate) and 4.7-fold (octanoate) increases in catalytic efficiency. K_d measurements also indicate considerable improvements in binding of butyrate and hexanoate, with the K_d for octanoate essentially unaltered from that for L181K. Catalytic efficiency with butyrate is also unaltered compared to L181K. The L75T/L181K double mutant has a binding and catalytic profile distinct from the L181K single mutant, with improved catalytic parameters for hexanoate.

Few amino acids are well conserved throughout the P450s, exceptions being those in the heme binding motif around the absolutely conserved cysteine that provides the sulfhydryl ligand to the heme iron (C400 in P450 BM3) [16]. However, the leucine corresponding to L181 in P450 BM3 is conserved in several P450s, particularly in members of the CYP 4 family – fatty acid hydroxylases. In many P450s, a hydrophobic residue is conserved at this position, usually a phenylalanine in P450s exhibiting specificity for aromatic substrates [17]. One of the most interesting of all P450 protein engineering results was obtained by mutation at the position corresponding to L181 in mouse P450s 2A4 and 2A5. These two enzymes differ by only 11 amino acids, but have marked differences in substrate specificity. P450 2A4 catalyses 15 α -hydroxylation of testosterone and has a leucine at position 209 (corresponding to L181 in P450 BM3). P450 2A5 catalyses coumarin 7-hydroxylation and possesses a phenylalanine here. Swapping these residues reverses substrate specificity, such that P450 2A4 L209F catalyses coumarin hydroxylation and vice versa for testosterone [18]. Thus it is possible that L181 of P450 BM3 is located at a position of importance in dictating P450 substrate selectivity. Leucine 181 is located in the centre of the F-helix, a motif postulated to be involved in substrate interactions as part of SRS2 (substrate recognition sequence 2) in Gotoh's model [19]. The leucine is also conserved as the conserved residue of the steroid recognition 'GERL' motif in P450s of subfamilies 11A and 11B [20].

Conclusions

In this study, we have demonstrated for the first time that P450 BM3 has measurable affinity for alkanolic acids shorter than C₁₂, and also that preference for fatty acids of this chain length can be selectively enhanced by rational mutagenesis. The single mutation L181K reduced the K_d for decanoate to micromolar levels ($312 \pm 26 \mu\text{M}$), and induced large increases in catalytic efficiency and affinity (K_d) for butyrate and octanoate. By introducing a second mutation (L75T), some further improvements were obtained. In particular, mutant L75T/L181K showed a huge kinetic improvement with hexanoate. Mutants L181K and L75T/L181K are considerably improved enzymes for the binding and catalysis of short-chain fatty acids, providing evidence for a key role for L181 in controlling P450 BM3 substrate selectivity.

Removal of the carboxylate binding R47/Y51 motif diminishes catalytic capacity with all substrate chain lengths, indicating its importance in preliminary substrate binding interactions (Fig. 2). Clearly, this motif should not be altered in future attempts to re-engineer P450 BM3 fatty acid chain length selectivity.

Acknowledgements: The authors wish to thank the BBSRC, Leverhulme Trust, Royal Society of Edinburgh and Caledonian Research Foundation, and Novo Nordisk for financial support for these studies.

References

- [1] Nelson, D.R., Koymans, L., Kamataki, T., Stegeman, J.J., Feyereisen, R., Waxman, D.J., Waterman, M.R., Gotoh, O., Coon, M.J., Estabrook, R.W., Gunsalus, I.C. and Nebert, D.W. (1996) *Pharmacogenetics* 6, 1–42.
- [2] Schuster, I. (1993) in: *Medicinal Implications in Cytochrome P-450 Catalyzed Biotransformations* (Ruckpaul, K. and Rein, H., Eds.), pp. 147–185, Akademie Verlag (VCH), Berlin.
- [3] Sligar, S.G. and Murray, R.I. (1986) in: *Cytochrome P450: Structure, Mechanism and Biochemistry* (Ortiz de Montellano, P.R.O., Ed.), pp. 429–503, Plenum, New York.
- [4] Porter, T.D. and Coon, M.J. (1991) *J. Biol. Chem.* 266, 13469–13472.
- [5] Munro, A.W. and Lindsay, J.G. (1996) *Mol. Microbiol.* 20, 1115–1125.
- [6] Narhi, L.O. and Fulco, A.J. (1986) *J. Biol. Chem.* 261, 7160–7169.
- [7] Li, H.-Y. and Poulos, T.L. (1997) *Nature Struct. Biol.* 4, 140–146.
- [8] Miles, J.S., Munro, A.W., Rospendowski, B.N., Smith, W.E., McKnight, J. and Thomson, A.J. (1992) *Biochem. J.* 288, 503–509.
- [9] Noble, M.A., Miles, C.S., Chapman, S.K., Lysek, D.A., Mackay, A.C., Reid, G.A., Hanzlik, R.P. and Munro, A.W. (1999) *Biochem. J.* 339, 371–379.
- [10] Zoller, M.J. and Smith, M. (1983) *Methods Enzymol.* 100, 468–500.
- [11] Kunkel, T.A. (1985) *Proc. Natl. Acad. Sci. USA* 82, 488–492.
- [12] Sambrook, J., Fritsch, E.F. and Maniatis, T. (1989) *Molecular Cloning, A Laboratory Manual*, Cold Spring Harbor Press, Cold Spring Harbor, NY.
- [13] Gibson, T.G. (1984) Ph.D. thesis, University of Cambridge, Cambridge.
- [14] Li, H.Y. and Poulos, T.L. (1999) *Biochim. Biophys. Acta* 1441, 141–149.
- [15] Maves, S.A., Yeom, H., McLean, M.A. and Sligar, S.G. (1997) *FEBS Lett.* 414, 213–218.
- [16] Poulos, T.L., Finzel, B.C. and Howard, A.J. (1987) *J. Mol. Biol.* 195, 687–700.
- [17] Lewis, D.F.V. (1996) in: *Cytochromes P450: Structure, Function and Mechanism* (Lewis, D.F.V., Ed.), pp. 209–291, Taylor and Francis, London.
- [18] Lindberg, R.L.P. and Negishi, M. (1989) *Nature Lond.* 339, 632–634.
- [19] Gotoh, O. (1992) *J. Biol. Chem.* 267, 83–90.
- [20] Gotoh, O., Tagashira, Y., Morahashi, K. and Fujii-Kuriyama, Y. (1985) *FEBS Lett.* 188, 8–10.
- [21] Oliver, C.F., Modi, S., Sutcliffe, M.J., Primrose, W.U., Lian, L.Y. and Roberts, G.C.K. (1997) *Biochemistry* 36, 1567–1572.
- [22] Munro, A.W., Malarkey, K., McKnight, J., Thomson, A.J., Kelly, S.M., Price, N.C., Lindsay, J.G., Coggins, J.R. and Miles, J.S. (1994) *Biochem. J.* 303, 423–428.

Review

Protein engineering of cytochromes P-450

Caroline S. Miles ^a, Tobias W.B. Ost ^b, Michael A. Noble ^b, Andrew W. Munro ^c,
Stephen K. Chapman ^{b,*}

^a Institute of Cell and Molecular Biology, University of Edinburgh, Mayfield Road, Edinburgh EH9 3JR, UK

^b Department of Chemistry, University of Edinburgh, West Mains Road, Edinburgh EH9 3JJ, UK

^c Department of Pure and Applied Chemistry, University of Strathclyde, 204 George Street, Glasgow G1 1XL, UK

Received 15 February 2000; received in revised form 18 September 2000; accepted 28 September 2000

Abstract

The cytochromes P-450 are an immensely important superfamily of heme-containing enzymes. They catalyze the monooxygenation of an enormous range of substrates. In bacteria, cytochromes P-450 are known to catalyze the hydroxylation of environmentally significant substrates such as camphor, phenolic compounds and many herbicides. In eukaryotes, these enzymes perform key roles in the synthesis and interconversion of steroids, while in mammals hepatic cytochromes P-450 are vital for the detoxification of many drugs. As such, the cytochromes P-450 are of considerable interest in medicine and biotechnology and are obvious targets for protein engineering. The purpose of this article is to illustrate the ways in which protein engineering has been used to investigate and modify the properties of cytochromes P-450. Illustrative examples include: the manipulation of substrate selectivity and regioselectivity, the alteration of membrane binding properties, and probing the route of electron transfer. © 2000 Elsevier Science B.V. All rights reserved.

Keywords: P-450; Protein engineering; Substrate specificity; Electron transfer; Chimeragenesis; Genetic fusion

1. Introduction

Protein engineering is generally understood to mean the use of site-directed or random mutagenesis to alter the properties of a protein or enzyme. This often involves the modulation of substrate specificity or selectivity of an enzyme. In this review we have extended the definition to encompass other important aspects of structure/function investigations, particularly the construction of chimeras and genetic fusions to investigate substrate specificity and electron transfer, and the modification of the N-terminal

membrane anchor of eukaryotic P-450s to facilitate overexpression and for the investigation of protein targeting. In the course of the review we will use specific examples to address these topics and highlight the most significant breakthroughs made in recent years. The variation of protein engineering experiments applied to the cytochromes P-450 is a reflection of the medical and technological importance of these enzymes. It is useful, therefore, to briefly consider the properties of the cytochromes P-450 and some of the major advances in our understanding of their biological roles and catalytic mechanisms.

The cytochromes P-450 are a family of b-type heme containing proteins found in virtually every organism [1]. They catalyze the monooxygenation

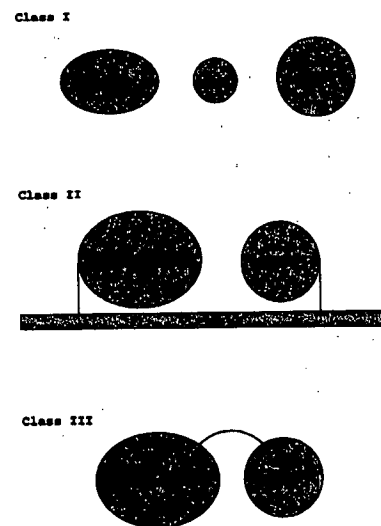
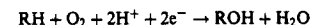


Fig. 1. Schematic representation of the different classes of cytochrome P-450 systems. Class I systems are composed of an FAD containing flavodoxin reductase, an iron-sulfur cluster containing flavodoxin and the P-450. The P-450 in a class II system is partnered by a diflavin reductase, and in a class III system, the diflavin reductase is fused to the P-450 in a single polypeptide.

of a diverse array of aromatic and aliphatic compounds in numerous biosynthetic and metabolic pathways. In mammals, they are central to the processes of drug metabolism and steroid hormone synthesis. In plants they play important roles in herbicide resistance and biosynthetic pathways (e.g. morphine biosynthesis), they are involved in antibiotic synthesis in fungi, plant toxin defence in insects, and in the metabolic and synthetic pathways of bacteria. The most common reaction catalyzed is hydroxylation (see below) but forms that catalyze epoxidation, dealkylation and sulfoxidation are known.



The P-450 reaction requires two electrons (provided by redox partner proteins), dioxygen and two pro-

tons. It proceeds via an activated oxygen species that effects controlled insertion of an oxygen atom into the substrate. Most bacterial and all of the eukaryotic mitochondrial P-450 systems are three component protein systems (class I): the redox partners consist of an NADH-dependent FAD containing ferredoxin reductase and a ferredoxin. Eukaryotic microsomal P-450 systems (those associated with the endoplasmic reticulum) are two component systems (class II): the redox partner is an NADPH-dependent diflavin (FAD and FMN containing) reductase. A third class (class III), of which the representative system is the bacterial P-450 BM3, is a one component system similar to class II but where the two components are fused in a single polypeptide. A schematic depiction of these system types [2] is illustrated in Fig. 1. In the P-450 itself, in all of these system classes, the heme iron is proximally ligated by a cysteine-thiolate, and in the resting state, the ferric iron is distally ligated by water. The reaction cycle is

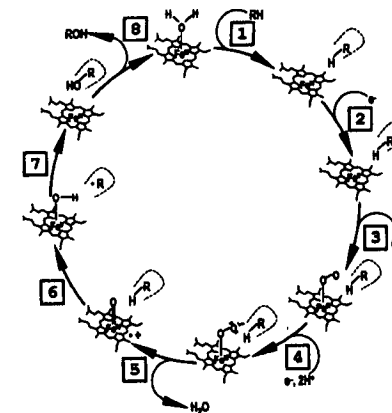


Fig. 2. The catalytic cycle of cytochrome P-450. The cycle is initiated by substrate (RH) binding to the ferric P-450 (1), permitting the first electron transfer (2) with consequent iron reduction and binding of oxygen (3). Second electron transfer (4) results in formation of the iron-peroxy species (4) and subsequently the oxyferryl intermediate (5). This reacts with bound substrate (6) and (7) to yield hydroxylated product that diffuses from the active site to complete the cycle (8).

* Corresponding author. Fax: +44 (131) 6504760/4743; E-mail: s.k.chapman@ed.ac.uk

represented in Fig. 2. Mechanistic information on this cycle has come largely from studies on the *P-450cam* system, and is generally assumed to hold for all *P-450s* [3]. The cycle is initiated by substrate binding close to the heme, which usually induces a change in the spin state of the iron from low to high spin. The iron is reduced to the ferrous form by the transfer of one electron from a redox partner and oxygen binds rapidly. The second electron transfer to the heme results in the cleavage of dioxygen and the formation of a transient oxy-ferryl intermediate (similar to compound I seen in peroxidases) and the release of water. Ultimately, the reactive oxyferryl species attacks the substrate, resulting in the mono-oxygenation of the compound.

The number of *P-450* genes now recognized is enormous and genome sequencing projects continue to add to this on a day-to-day basis. The sequences have been organized into what is now termed the *P-450* gene 'superfamily' [4] (see Kirill Degtyarenko's Directory of *P-450* systems at <http://www.icgeb.trieste.it/~p450srv/> and David Nelson's *P-450* home page at <http://drnelson.utmem.edu/CytochromeP450.html>), allowing a greater understanding of the evolution of the *P-450s* from primordial forms. The presence of a *P-450* in the archaeon *Sulfolobus solfataricus* indicates that they are ancient enzymes [5]. It is possible that they arose as a means for breaking down toxic oxygen when it first became abundant on earth, and an early physiological role may have been the modification of lipids for the cell membranes of microbes.

The presence of *P-450s* in organisms as diverse as bacteria and man is a reflection of the importance of the oxygen cleavage reaction that they catalyze. Through evolution, nature has adapted this reaction to suit the requirements of numerous different synthetic and degradative pathways. *P-450s* are adapted to act on molecules as small as nitric oxide (*P-450nor* from the fungus *Fusarium oxysporum*) [6] and as large as cholesterol and polycyclic aromatic hydrocarbons (e.g. mammalian *P-450scc* and *1A1*) [7,8]. This substrate diversity demonstrates the potential for strategic engineering to provide a route for the generation of *P-450* enzymes tailored to a chosen molecule, enabling the regio- and stereoselective oxygenation of new substrates. The reactivity of oxygen makes selective oxygenation difficult to achieve by

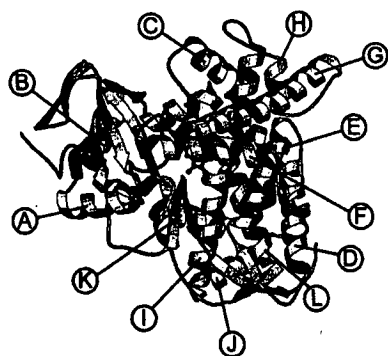


Fig. 3. Schematic representation of the heme domain of flavocytochrome *P-450* BM3, showing the characteristic *P-450* fold, produced using MOLSCRIPT [153]. The heme cofactor is visible as a ball-and-stick structure and helices A–L are labeled.

conventional chemical means. This is one area of great interest in the field of *P-450* engineering.

1.1. The structural basis for cytochrome *P-450* engineering

Rational re-design or re-engineering of an enzyme requires a firm structural basis. At present there are eight atomic structures for different cytochromes *P-450*. Only five of these are freely available at present, although two others (mammalian *P-450* 2C5 [9] and *S. solfataricus* CYP119 [10]) will be released in 2001. Four of those currently accessible are for soluble bacterial enzymes. These are cytochrome *P-450cam* (CYP101; camphor hydroxylase from *Pseudomonas putida*) [11]; the heme domain from cytochrome *P-450* BM3 (CYP102; a fatty acid hydroxylase from *Bacillus megaterium*) [12]; cytochrome *P-450terp* (CYP108; α -terpineol hydroxylase from a *Pseudomonas* species) [13]; and the substrate-bound form of *P-450eryF* (CYP107A1; 6-deoxyerythronolide B hydroxylase, involved in the synthesis of erythromycin biosynthesis in *Saccharopolyspora erythraea*) [14]. In addition, there are crystal structures of substrate-bound *P-450cam* and *P-450* BM3 heme domain [15,16], as well as other ligand-bound structures for these enzymes. The fifth struc-

ture currently accessible is also a soluble enzyme, cytochrome *P-450nor* (CYP55A1), a nitric oxide reductase from *F. oxysporum* [6]. The remaining *P-450* is *P-450 sca2* from *Streptomyces carbophilus*, an industrially important enzyme which catalyzes the final hydroxylation step in the synthesis of the cholesterol lowering drug pravastatin [17]. All these enzymes display close structural similarity, at least in terms of overall topology, in spite of very low sequence identity. Generally, sequence identities are no more than 20%. The *P-450* tertiary structure has an approximate trigonal prism arrangement containing both α -helical and β -sheet regions (Fig. 3). Helices dominate the structure, and many of these lie approximately parallel to the plane of the heme. The heme is bracketed by two helices: the I helix lies distal to the heme and spans the diameter of the protein structure, the shorter L helix lies proximal to the heme, and its N-terminus provides the cysteine-thiolate that proximally ligates the heme iron. The heme itself lies well buried within the structure, and the substrate binding site lies on its distal face. The substrate binding sites of the known *P-450* structures are considerably different in size and shape, reflecting the nature of their substrates (Fig. 4). These differences are due to both topological variation in the polypeptide backbone and the nature of the side chains lining the active sites. In *P-450* BM3, the long chain fatty acid substrate lies in an elongated hydrophobic channel that extends from the surface of the protein to the distal face of the heme [16]. By contrast, the substrate binding site of *P-450cam* is much deeper seated, and the substrate access channel is much less

apparent. Comparison of substrate-bound *P-450cam* and *P-450* BM3 structures with the respective substrate-free forms reveals conformational differences, demonstrating the importance of protein motion in allowing substrate access. The changes are particularly large for *P-450* BM3. Furthermore, a crystal structure of *P-450cam* complexed with an imidazole ligating inhibitor considerably larger than camphor reveals the range of protein conformational lability and highlights the access route to the binding site [18]. The substrate binding site of *P-450terp* more closely resembles that of *P-450eryF*, not unexpectedly given the similarity in substrate size, whilst that of *P-450eryF* is considerably larger. A further feature of *P-450eryF* is that in the substrate-bound form there is a network of hydrogen-bonded water molecules in the binding site. This is different from *P-450cam* and *P-450* BM3 where water molecules are excluded.

The crystal structures for seven of the eight *P-450s* described above are of soluble enzymes that are readily overexpressed, purified and crystallized. The eukaryotic *P-450s* are membrane-bound and present major problems for X-ray structural determination. Until recently, no such crystal structure had been determined. Rational engineering of these enzymes has relied on sequence comparisons with bacterial enzymes whose structures had been determined and also on the generation of homology models. For the *P-450* family 2, Gotoh [19] used sequence homology studies to identify six regions termed substrate recognition sites (SRS). These were based on the position of camphor in *P-450cam*, the only *P-450* whose structure had been solved at the time. Subsequent

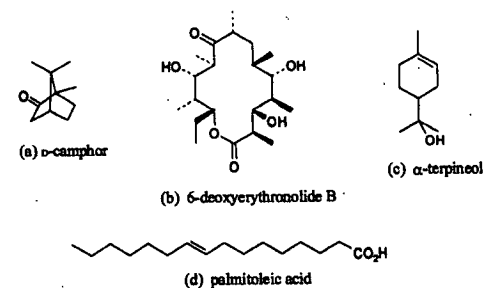


Fig. 4. Substrates for the cytochromes *P-450* cam (a), eryF (b), terp (c) and BM3 (d).

fatty acid) and Y51 (which can provide a hydrogen bond to the carboxylate). One further notable residue at the mouth of the active site, F42, appears to cover the opening to the active site channel, providing what might be termed a hydrophobic 'lid'. At the opposite end of the active site channel, close to the heme, lies the side chain of F87. The importance of this residue was highlighted by the large conformational difference adopted by the phenyl ring in the substrate-free and palmitoleate-bound crystal structures [12,16]. In the substrate-free form the side chain lies perpendicular to the heme plane but in the palmitoleate-bound form it has twisted to lie almost parallel to it. In this section we describe the site-directed mutagenesis studies that have defined roles for these residues in substrate binding and in the control of regioselectivity and altered substrate specificity.

The important contribution of the guanidinium group of R47 has been confirmed by mutagenesis experiments. In a study by Oliver et al. [40] the substrate binding characteristics of wild-type *P*-450 BM3 and the mutant R47E and their abilities to catalyze substrate oxidation were compared. The mutant enzyme retained activity towards C₁₂–C₁₆ fatty acids (but with k_{cat}/K_m values 14–21-fold lower than wild-type), as well as the regioselectivity of oxidation (ω -1 to ω -3). However, unlike the wild-type enzyme, the R47E mutant was able to efficiently hydroxylate C₁₂–C₁₆ alkylammonium compounds (also at the ω -1 to ω -3 positions), with k_{cat} values of up to 19 s⁻¹. Optical spectroscopy showed that fatty acid binding to the mutant is much weaker than to the wild-type enzyme, and paramagnetic relaxation experiments showed that the fatty acid adopted a different orientation in the active site channel. In a further study, Noble et al. [41] demonstrated the dominance of the side chain of R47 over that of Y51 in providing the major interaction with the fatty acid carboxylate. The same study highlighted the importance of the phenyl side chain of F42 in providing a hydrophobic 'lid' to the active site (K_m values were increased almost 10-fold for laurate and arachidonate turnover). This latter phenomenon was interpreted as the consequence of ingress of water molecules to the active site and the disruption of the strong ion pair interaction between the R47-guanidino group and the fatty acid carboxylate.

Phenylalanine 87 is located at the base of the ac-

tive site of *P*-450 BM3 and, from inspection of the palmitoleate-bound *P*-450 BM3 crystal structure, appears to protect the terminus of the fatty acid from ω -hydroxylation. Consistent with this, substitution of F87 by alanine converts *P*-450 BM3 from a fatty acid hydroxylase that oxidizes at the ω -1 to ω -3 positions to one that oxidizes at the ω position [42] (a reaction not observed for wild-type *P*-450 BM3 but common to many mammalian *P*-450s such as those belonging to the 4A1 family). In the F87A mutant enzyme a decrease in K_d for laurate of up to 6-fold was observed, showing that the removal of the bulky phenyl side chain facilitates tighter binding of medium chain (e.g. C₁₂) fatty acids. However, the K_m for laurate oxidation catalyzed by the F87A mutant was found to be identical to that seen for the wild-type enzyme. This was suggested to be due to a difference in the substrate binding to the ferrous and ferric forms. The implication is that the F87A mutation causes a change in the substrate binding, not in the initial Michaelis complex, but in a subsequent step in the catalytic cycle. Proton NMR experiments have shown that laurate and 12-bromolaurate bound in the active sites of wild-type and F87A *P*-450 BM3 move some 6 Å closer to the heme upon iron reduction [43]. Molecular modeling studies indicate that the absence of the phenyl ring enables the ω -terminus of laurate to approach closer to the heme in the F87A mutant than in the wild-type enzyme, and these data were supported by NMR studies (ω -CH₃–Fe = 5.1 Å in wild-type and 3.1 Å in the F87A mutant enzyme). This explains the mixed product distribution observed in wild-type for laurate hydroxylation and the almost exclusive (>90%) ω -terminal hydroxylation demonstrated by the F87A mutant.

2.3. Modification of the regioselectivity of cytochrome *P*-450 4A1

P-450s of the 4A family, found in the liver and kidneys of mammals, are long chain fatty acid monooxygenases that predominantly hydroxylate at the ω position. Of these, *P*-450 4A1 is the most extensively studied [44]. A possible explanation for the strict ω -terminal specificity is that the active site of *P*-450 4A1 is highly constrained, so that substrate binding orientation is precisely defined. The specific-

ity of this enzyme for a range of fatty acid chain lengths, such as laurate (C₁₂), palmitate (C₁₆) and arachidonate (C₂₀), suggests a possible structural similarity with *P*-450 BM3. Hence, by sequence alignment of *P*-450s 4A1 and BM3 (considered as the closest structurally defined model of the 4A family), two residues of 4A1, E320 and D323, were identified as structural equivalents of A264 and E267 in *P*-450 BM3. In the crystal structure of palmitoleate-bound *P*-450 BM3, these two residues lie close to the ω -terminus of the fatty acid tail. To establish the importance of these residues in *P*-450 4A1, the reciprocal mutants E320A, D323E and the double mutant E320A/D323E were constructed. For all three mutant *P*-450s, there was a relaxation of the regioselective hydroxylation of laurate: in wild-type *P*-450 4A1 the ω : ω -1 product ratio is 20:1. However, in the E320A/D323E double mutant enzyme this ratio drops to only 2:1. The NADPH consumption rate in the reconstituted *P*-450 mutant system did not vary from that observed for the wild-type (approx. 300 min⁻¹), but significantly lower laurate oxidation rates for the mutant-catalyzed reactions (<40 min⁻¹ for all three mutants, compared to 150 min⁻¹ for wild-type) were found, which indicates significant uncoupling. The conclusion is that the two residues, E320 and D323, are located in the active site and are involved in substrate binding. At present there is no experimental evidence for key roles for either A264 or E267 in *P*-450 BM3 substrate binding or catalysis. It would be interesting to see whether the reciprocal mutations in *P*-450 BM3 (A264E and E267D) would confer ω -hydroxylation activity.

2.4. Identification of key residues in *P*-450 3A4 involved in substrate and effector binding

Family 3 of the cytochromes *P*-450 consists of just one subfamily, *P*-450 3A [45], which plays a major role in hepatic biotransformation pathways. Human 3A4 is the most abundant *P*-450 in the liver (up to approx. 60% of total *P*-450 content in some cases) and metabolizes a wide range of clinically important drugs [46] in addition to steroids [47] and carcinogens [48]. Its importance is underlined by the fact that it is reported to be involved in the metabolism of around 50% of currently used drugs [46,49]. *P*-450 3A4 exhibits cooperativity towards some substrates;

for example, homotropic cooperativity with progesterone [50] and testosterone [51]. Activity can also be influenced heterotropically, as in the stimulation of progesterone and testosterone oxidation by the effector α -naphthoflavone (ANF) [50].

Rational protein engineering studies on *P*-450 3A4, to study, for example, the activation by ANF (several proposed mechanisms are outlined in [52]) or substrate specificity, are potentially obstructed by the absence of its crystal structure and the fact that there is little pronounced variation in substrate specificity for the 3A enzymes (in contrast to family 2, for example) [52]. However, the construction of homology models of 3A4 has greatly aided determination of candidates for mutagenesis. One structural model was based on amino acid sequence alignments with *P*-450 BM3 and a number of substrate and inhibitor interactions were investigated [53]. Another model was built using consensus modeling methods to base the structure on those of *P*-450s cam, BM3, terp and eryF [32]. Although this model bore most resemblance to BM3, the use of the eryF structure was reported to be important in defining the size of the active site through localization of the B' helix. Progesterone or erythromycin were docked at the active site and the potential contact residues noted.

The first site-directed mutagenesis study was carried out on *P*-450 3A4 using alanine scanning mutagenesis to probe the roles of residues 210–216 [52]. (It also indicated that Gotoh's substrate recognition site model was applicable to the *P*-450s 3A.) Mutant enzymes L210A and L211A led to a decrease in stimulation of testosterone and progesterone hydroxylation effected by ANF and changes in the regioselectivity of testosterone hydroxylation were also observed with L210A. This indicated that substrate and effector binding sites could be partially overlapping. To test this a double mutant was constructed in which L211 and D214 (the latter chosen after study of the Szklarz model [32]) were changed to phenylalanine and glutamic acid, respectively [54]. The idea was to mimic effector binding by narrowing the sizeable binding pocket, considered large enough to be able to accommodate both a steroid and ANF at the same time (e.g. [32]), through the introduction of bulkier residues. As a consequence, homotropic cooperativity for steroid hydroxylation was eliminated and a reduced response to stimulation by ANF was

observed. Further analysis of the model for residues that could affect cooperativity suggested that F304 (positioned on the highly conserved 1 helix and suggested experimentally [55] and from the model to play a role in substrate binding) was a likely candidate [56]. As with the L211F/D214E double mutant, the F304W enzyme was unable to fully mimic effector binding. However, the triple mutant L211F/D214E/F304W was much more effective.

Other residues whose mutation influenced stimulation of activity by ANF are I369, L373 (SRS 5) [57] and A305 (SRS 4) [55].

Related studies of *P*-450 3A4 probed aspects of substrate binding and specificity. It was shown through mutagenesis of S119 from SRS 1, a residue predicted from modeling to be involved in progesterone binding [32], that *P*-450 3A4 could be converted from a steroid 6 β -hydroxylase to a 2 β -hydroxylase [58]. This residue may occupy a similar position to F87 in *P*-450 BM3 [32,58], shown to be important in controlling regioselectivity of substrate oxidation (see Section 2.2). Cassette and site-directed mutagenesis were carried out on amino acids 364–377 in SRS 5 [57]. Two of these residues, 370 and 373, were predicted from the model to interact with progesterone when the substrate was docked in the 6 β -orientation [32]. Mutant enzymes I369V, A370V and L373H all exhibited altered progesterone metabolic profiles. I369V and A370V showed decreased and increased 16 α -hydroxylation activities, respectively, compared to the wild-type enzyme. However, mutant L373H, whilst retaining progesterone 6 β and 16 α activities, produced a new, unidentified, metabolite. Analysis of progesterone docked in the 16 α binding orientation in the model suggested that the effects observed with the I369V and A370V enzymes (involving substitution with a smaller and a larger residue, respectively) were due to changes in substrate mobility within the active site.

In addition to the above studies to probe substrate and effector binding, the structure-function relationship between *P*-450s 3A4 and 3A5 was investigated using differences in the regioselectivities of the two enzymes (which share >85% amino acid sequence identity) towards the biotransformation of the carcinogen aflatoxin B₁ [59]. The six, putative substrate recognition sites of the two enzymes were compared and non-conserved residues between the two enzymes

were replaced in *P*-450 3A4 with those of *P*-450 3A5. Two, individual, mutations in SRS 2 (N206S and L210F) had the greatest effect, conferring the phenotype of the 3A5 enzyme onto *P*-450 3A4.

Thus far, analysis of *P*-450 3A4 through the use of homology models and mutagenesis in the absence of a crystal structure has provided significant advances in the understanding of substrate and effector binding in this enzyme. Eventually it is hoped that these and further studies will allow prediction of drug/drug interactions with *P*-450 3A4 [56].

2.5. Chimeragenesis as a probe of substrate specificity

The absence (until recently) of crystal structures for mammalian *P*-450s limits solid understanding of the factors that confer substrate specificity. However, one approach to this problem that has proved successful is the use of chimeric constructs in combination with site-directed mutagenesis to identify structural determinants of substrate specificity within a *P*-450 subfamily. In most cases, two *P*-450s with high sequence identity but different substrate specificities have been investigated by substituting a region of one with the corresponding region from the other and analyzing for any change in substrate specificity. Once regions of interest have been elucidated, site-directed mutagenesis can be used to pinpoint key individual residues that are responsible for the particular substrate specificity. A number of such studies using *P*-450 chimeras have been published over the last 5 years, the majority concerning *P*-450 family 2. These include: 2C1 and 2C2 [60]; 2B1 and 2B2 [61]; 2B4 and 2B5 [62]; 2C9 and 2C19 [63–65]. For this reason, we have chosen to highlight this family in this section of the review, focusing on human *P*-450s 2C9 and 2C19. Other examples discussed are canine *P*-450s 3A12 and 3A26 [66] and *P*-450s Cm2 and Alk3A from the yeast *Candida maltosa* [67]. These studies demonstrate the power of the chimeragenesis approach in elucidating the controlling factors of substrate specificity.

2.5.1. Probing substrate specificity of cytochromes *P*-450 2C9 and 2C19

The *P*-450s of the 2C family comprise approx. 16% of the total hepatic *P*-450 content [68]. They are weakly inducible by phenobarbital, and are fre-

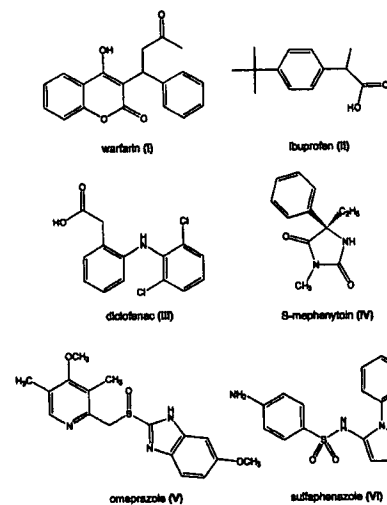


Fig. 7. Substrates for *P*-450s 2C9 and/or 2C19.

quently involved in hydroxylations of aromatic ring systems. Endogenous substrates for the 2C subfamily are usually steroids, although rabbit *P*-450 2C2 is known to hydroxylate laurate at the ω -1 position. Human *P*-450s 2C9 and 2C19 are closely related, with 92% sequence identity [69]. 2C9 is a testosterone 16 β -hydroxylase, but the physiological substrate for 2C19 is not clear. Both metabolize a number of clinically important drugs, an example common to both being the anti-coagulant warfarin (Fig. 7, I) [65]. However, the regio- and stereospecificities of 2C9 and 2C19 towards this substrate differ. The non-steroidal, anti-inflammatory drugs ibuprofen (II) and diclofenac (III) are principally metabolized by 2C9 [70]. 2C19 does not metabolize either of these compounds [71,72], but shows selectivity for 4'-hydroxylation of the anti-convulsant *S*-mephenytoin (IV) [73] and 5'-hydroxylation of omeprazole (V) [74] (an anti-ulcer drug). In general, 2C19 appears to have less stringent steric requirements than does 2C9 [65]. A further difference between the two is that 2C9 is inhibited by sulfaphenazole (VI) ($K_d < 1 \mu\text{M}$) whereas

2C19 is not inhibited by this compound at concentrations even up to 100 μM [75,76]. A detailed knowledge of the determinants of substrate specificity in these two *P*-450s could provide the basis for the design of drugs less dependent on metabolism by a specific isoform [65]. In other words, their metabolism would be less affected by genetic variation, an important factor considering, for example, that 15–20% of Orientals and 2–5% of Caucasians do not express 2C19 [77].

Using the substrate recognition sites identified by Gotoh [19], Ibeanu et al. [64] constructed 2C9/2C19 chimeras and site-directed mutant forms of 2C9 to elucidate the key determinants of omeprazole hydroxylation by 2C19. A 2C9 chimera containing residues 160–227 from 2C19 in combination with the point mutation I99H gives an engineered *P*-450 2C9 which displays greater omeprazole 5-hydroxylase activity than does 2C19. Further site-directed mutagenesis showed that three residues from 2C19 were found to confer omeprazole activity into 2C9. The I99H, S220T and P221T triple mutant of 2C9 hydroxylated omeprazole as efficiently as 2C19. Residue 99 is located within a predicted substrate recognition site (SRS 1) whereas 220 and 221 are not. According to the results of sequence analysis with *P*-450cam they are located on the turn between the F and G helices [19]. This region varies considerably in length between *P*-450s and may form a flexible cap over the active site, thereby forming part of the substrate access channel [26,64,78].

More recent studies [63] have determined the critical areas of *P*-450 2C9 which define the specificity for diclofenac and ibuprofen. Chimeras of both 2C9 and 2C19 were constructed with the emphasis on SRS 3 and 4. Replacing residues 228–340, containing SRS 3 and 4, of 2C19 with those of 2C9, generated a chimera that could hydroxylate both drugs. Interestingly, the regioselectivity for ibuprofen hydroxylation differs from that of wild-type 2C9, probably indicating that the orientations of the bound substrate are slightly different. The converse construct had little or no activity towards diclofenac or ibuprofen. Individual substitution of SRS 3 and 4 revealed that the latter was the most important region for conferring specificity. As the two isoforms differ in only five residues within SRS 4 (283–340), site-directed mutagenesis was carried out on a 2C19 chimera contain-

ing residues 228–282 of 2C9 (including SRS 3) to pinpoint the key residue(s). These studies showed that the I289N mutation confers specificity for diclofenac hydroxylation. The activity increased when a second mutation, N286S, was introduced. In addition it was shown that S286 in combination with N289 confers specificity for ibuprofen, the former residue appearing to be the major contributor. Both these residues are found in a highly conserved region corresponding to the I helix of structurally characterized cytochromes *P*-450.

The importance of residues N289 and S286 in *P*-450 2C9 was again underlined by Jung et al. [65] who investigated the amino acid residues that confer a high affinity for sulfaphenazole binding and a high catalytic efficiency for warfarin metabolism. Two substitutions of 2C9 residues into 2C19, N286S and I289N, were found to be sufficient to confer high affinity binding of the inhibitor sulfaphenazole ($K_d = 4 \mu\text{M}$). Interpretation of results was facilitated by the generation of a homology model of 2C9 with docked sulfaphenazole which indicated that it was unlikely that S286 and N289 contacted the inhibitor. However, it was considered that these residues could influence substrate access or active site packing. In combination with E241K (mutation of a residue located in the region corresponding to helix G), the 2C19 double mutant was able to hydroxylate both *R* and *S* enantiomers of warfarin with a higher catalytic efficiency than observed for wild-type 2C19 [65].

2.5.2. Substrate specificity in cytochromes *P*-450 3A12 and 3A26

Chimeragenesis has been used to determine residues responsible for differences in steroid hydroxylation catalyzed by two canine *P*-450s, 3A12 and 3A26 [66]. Although these enzymes have 96% amino acid sequence identity (differing by only 22 of 503 residues [45]) the former exhibits higher rates of steroid hydroxylation. The approach used was to monitor the loss of progesterone 6 β -hydroxylation activity in *P*-450 3A12 caused by the introduction of sequences from 3A26. Once regions responsible for the loss of activity had been identified, site-directed mutagenesis of non-identical residues within such regions was employed to restore activity of the chimera back to that of *P*-450 3A12. Three residues, at positions 187,

368 and 369 were identified as those mainly responsible for the differences in steroid 6 β -hydroxylation between the two proteins. When these three were mutated in *P*-450 3A26 to those of 3A12 (I187T, S368P and V369I), a 10–20-fold increase in the ability of 3A26 to hydroxylate steroids was observed. All the testosterone and androstenedione 6 β -hydroxylase activity of 3A12 was conferred to 3A26. These canine cytochromes *P*-450 are considered as models for human drug metabolism since residues identified in this study are also important for the function of human *P*-450 3A4 [57,66].

2.5.3. The substrate specificities of cytochromes *P*-450 Cm2 and Alk3A

Cytochromes *P*-450 Cm2 and Alk3A are CYP52A4 variants naturally occurring in the yeast *C. maltosa* [79]. The family 52 *P*-450s are alkane and fatty acid hydroxylases related to the mammalian *P*-450 4A and the bacterial *P*-450 BM3 (around 25% amino acid identity) [80]. Zimmer et al. [80] used chimeragenesis to transpose the substrate specificities of cytochromes *P*-450 Cm2 and Alk3A. Although both these enzymes show affinities for laurate and palmitate, *P*-450 Cm2 displays greater efficiency for the ω -hydroxylation of laurate. Five pairs of chimeric constructs were devised in order to investigate each of the seven amino acid differences between the two enzymes. The key residue was found to be at position 527 (a valine in *P*-450 Cm2 and a leucine in Alk3A). Analysis of an engineered enzyme pair in which V527 of Cm2 and L537 of Alk3A were exchanged showed a transposition of specificity, providing compelling evidence that position 527 was the key residue modulating fatty acid turnover. To show that this residue was acting independently it was changed to methionine in both *P*-450s to give enzymes with almost identical activities (more similar to that of Cm2). The fact that such subtle differences in side chain lengths between valine and leucine could have such effects suggested that residue 527 must be at the active site, and may even play a role in holding the terminal methyl group of the substrate at the correct position for monooxygenation.

In addition to this 'directed' chimeragenesis, an alternative random chimeragenesis approach [81,82] has been used in an attempt to map the active sites of

the distantly related *P*-450s soc and c27 [83]. It was concluded from this work that an amino acid identity of 25% or greater between *P*-450s is necessary for the successful application of this technique [83]. A more recent study used random chimeragenesis to probe species-specific biochemical differences between rat and human *P*-450c17, two proteins with 68% amino acid sequence identity [84]. However, the five chimeras generated did not exhibit activity patterns that equated to those of the parents, limiting the amount of useful structure/function information that could be obtained.

2.5.4. Bacterial/mammalian chimeric cytochromes *P*-450

To examine whether mammalian and bacterial enzymes are structurally related and if the bacterial structures provide a valid basis for building homology models of mammalian enzymes, Shimoji et al. [85] constructed a novel chimera from the cytosolic bacterial cytochrome *P*-450cam and the membrane-bound mammalian cytochrome *P*-450 2C9. These two cytochromes have less than 15% amino acid sequence identity. To ensure solubility the chimera was designed with the N-terminal 216 amino acids of *P*-450cam fused to a fragment of *P*-450 2C9 from residue 257 to the C-terminus. This accommodated the putative substrate recognition sites 1–3 of *P*-450cam and 4–6 of *P*-450 2C9. No mammalian amino acids prior to the random coil between the G- and H-helices were included to avoid any potential membrane interactions. The resultant chimera was soluble and correctly folded. Assays of catalytic activity (the oxidation of 4-chlorotoluene to 4-chlorobenzyl alcohol) demonstrated that the chimera was functionally active. The fact that the chimera folded correctly was considered indicative of conservation between the three-dimensional structures of these bacterial and mammalian *P*-450s. A further application suggested for such chimeragenesis was the construction of soluble *P*-450s with active site characteristics of mammalian forms, which could prove of use in crystallization studies and bioremediation [85]. Also of interest would be to further characterize such chimeras with different reductase components to delineate regions important in the two enzymes for protein/protein interactions and electron transfer.

3. Protein engineering to alter membrane binding

With the exception of *P*-450nor, all eukaryotic *P*-450s identified are membrane-bound. For the microsomal *P*-450s, which are bound to the endoplasmic reticulum (ER), the major determinant of membrane binding seems to be a hydrophobic stretch of amino acids at the N-terminus. The remaining polypeptide folds into a globular form that resides above the membrane. In most microsomal *P*-450s the N-terminal region contains a sequence of 16–20 non-polar side chains that are believed to provide the major hydrophobic interaction with the ER membrane. When the first 29 N-terminal residues of cytochrome *P*-450 2C1 were fused to a globular secretory protein (β -galactosidase), or to a soluble cytosolic protein (alkaline phosphatase) the resulting polypeptide was translocated to the ER [86]. Experiments on cytochrome *P*-450 21B have shown that removal of more than one third of the hydrophobic residues in the N-terminus result in the production of a cytosolic *P*-450 form [87]. Such studies demonstrate that N-terminal deletion or modification could facilitate heterologous expression of the *P*-450s, for the overproduction of soluble forms of microsomal *P*-450s for various applications. However, the overexpression of N-terminally truncated forms of several *P*-450s in *Escherichia coli* has shown that both the yield of soluble protein and the catalytic activity are highly variable and dependent on the *P*-450 in question [88]. For example, full-length *P*-450s 2E1 and 2B4 are both targeted to the bacterial inner membrane, but whereas deletion of residues 3–29 from 2E1 still locates the protein predominantly in the membrane fraction (65%), deletion of residues 2–20 from 2B4 locates 68% of the protein to the cytosol. Fusion of the N-termini from 2E1 and 2B4 to the heme domain of the soluble bacterial *P*-450 BM3 had the effect, in both cases, of locating only 20 and 27%, respectively, to the bacterial membrane fraction [89]. This indicates that there are different determinants of membrane binding between 2E1 and 2B4 on the globular domain distinct from the N-terminal anchor. Thus, the N-terminal portion of the eukaryotic *P*-450s is not the sole determinant of membrane binding. Further, isoform-specific, structural motifs on the surface of the globular *P*-450 domain must interact with the membrane. It has

been demonstrated by chemical labeling [90] and mutagenesis [91] experiments that sites even close to the C-terminus may be involved in membrane interactions.

Although recombinant eukaryotic *P*-450s often need to be purified in the presence of detergents (even after N-terminal modification) this is not always the case. For example, Sueyoshi et al. [92] were able to purify a modified form of *P*-450 2A4 from *E. coli* without the use of detergents. The hydrophobic N-terminal residues 2–19 were substituted for a sequence that forms an amphipathic helix, and although the modified form of the protein was initially localized to the membrane fraction, it could be readily freed by treatment with sodium carbonate. In another example a soluble form of cytochrome *P*-450 51 (*P*-450 sterol 14 α -demethylase) from *Candida albicans* has been engineered with a modified N-terminus containing a protease cleavage site [93]. Initial solubilization using detergent can be followed, after the cleavage reaction, by further purification without the use of detergent.

The recent breakthroughs in the expression of soluble domains of eukaryotic *P*-450s and *P*-450 reductases without their N-terminal membrane spanning domains have provided great hope that more crystal structures can be solved for mammalian *P*-450 systems. In addition, it has been shown that soluble *P*-450 domains heterologously expressed in *E. coli* can retain activity, and that this activity can be supported by the host enzymes flavodoxin and NADP⁺-flavodoxin oxidoreductase [94]. This has raised expectations that *E. coli* expressing different human *P*-450 isoforms and utilizing either the host redox system or co-expressed human *P*-450 reductase, can be used as a model to predict the metabolic fate of drugs and identify the *P*-450s responsible [95]. Yeast (*Saccharomyces cerevisiae*) is another attractive system for simultaneous expression of multiple human *P*-450s [96]. Systems of this type have great potential in mutagenicity testing and predictive metabolism [97].

Protein engineering studies to promote solubility of a *P*-450 and to prevent its oligomerization have seen their greatest success only this year. After intensive studies of rabbit progesterone hydroxylase *P*-450s 2C3 and 2C5, Eric Johnson and co-workers were able to generate a modified *P*-450 2C5 that

could be expressed in a soluble, monomeric form in *E. coli*. In initial studies, these workers showed that by deletion of the regions encoding the N-terminal membrane spanning sections and by incorporation of a 4-histidine tag at the proteins' C-terminus, the *P*-450s could be overexpressed in *E. coli* and solubilized from the membrane by high salt [34]. The *P*-450s could then be purified without use of detergents. However, the 2C3 and 2C5 enzymes formed dimers and tetramers, respectively, and these forms could not be crystallized. Subsequent studies of *P*-450 2C3/2C5 chimeras showed that replacement of selected amino acids in *P*-450 2C5 with those from 2C3 resulted in production of *P*-450 2C5 hybrids that retained catalytic activity and remained monomeric after solubilizing with salt [98]. The monomeric *P*-450 2C5 enzyme containing five substitutions from 2C3 (N202H, R206E, I270L, S209G and S210T) was crystallized successfully, leading to the determination of the first atomic structure of a mammalian *P*-450 [9].

4. Electron transfer

4.1. A thermodynamic switch

For the well-characterized bacterial *P*-450s cam and BM3, the binding of substrate (camphor and fatty acid, respectively) displaces the sixth heme ligand (water) and shifts the ferric heme iron from low to high spin. This results in a positive shift in heme reduction potential of some 130 mV. The magnitude of this change makes electron transfer from a redox partner thermodynamically favored [99,100]. The biological benefit of this thermodynamic 'switch' in electron transfer is an avoidance of the futile production of oxygen radicals and/or hydrogen peroxide in the absence of substrate. However, such control does not appear to be operative for all *P*-450s.

4.2. Probing the route of electron transfer

The analysis of the route of electron transfer in the *P*-450s has been intensively studied since the determination of the first *P*-450 crystal structure, *P*-450cam [11]. In this class I system (Fig. 1), NADH reduces the FAD containing putidaredoxin

reductase (PdR), which shuttles electrons one at a time through the iron-sulfur containing putidaredoxin (Pd) to the *P*-450 [2]. The system is analogous to the eukaryotic mitochondrial class I *P*-450s, such as that for *P*-450scc (partnered by adrenodoxin and adrenodoxin reductase) [101]. In this system, the interactions between the various redox components are thought to be mainly electrostatic [102,103]. Electrostatics are also thought to dominate redox partner binding in *P*-450cam and other class I systems. Stayton and co-workers defined the Pd docking site on *P*-450cam [104]. At least four basic residues on the proximal side of the *P*-450cam heme iron (R72, K344, R112, Q343 and, perhaps, R364) are involved in the interaction with residues of opposite charge on Pd (D58, E65, E67 and E72). It has been postulated that the three components of these class I *P*-450 systems can come together as a ternary complex for catalysis [105]. However, a more realistic model for the class I systems may be that the exposed iron-sulfur centers of the redoxin proteins shuttle electrons singly between the reductase and the *P*-450. The reaction between putidaredoxin and the *P*-450 is among the best studied of all biological electron transfer reactions. The first and second electron transfers from putidaredoxin to the heme iron are the two slowest steps in catalysis. At physiological concentrations of Pd, the second electron transfer is the overall rate limiting step [106]. The decrease in apparent affinity (elevated K_m value) for these redox partners observed with increasing ionic strength is consistent with an electrostatic interaction. However, what appears to be a straightforward set of electrostatic interactions between redox partners is in fact much more complex. This is demonstrated by the fact that *P*-450cam has completely different affinities for oxidized and reduced putidaredoxin [99,107]. The C-terminal tryptophan of putidaredoxin has been found to be a major determinant for the higher affinity for reduced Pd [108]. Much recent attention has focused on the role of arginine 112 in *P*-450cam – a surface residue which is hydrogen bonded to a heme propionate. Substitution to various neutral residues resulted in decreased electron transfer rates to the heme iron, and resulted in more negative heme reduction potentials. Mutation R112K had a less severe effect, but did show similar trends in reduction rate and heme potential [109]. These data are consis-

tent with the studies of Nakamura and co-workers, who also showed that heme content and *P*-450 stability were affected by mutation at this residue (R112Q and R112E mutant enzymes) [107]. Other recent studies on the *P*-450cam system have implicated Pd residue E72 in the stabilization of the Pd/PdR complex, and Pd residue V98 in hydrophobic interactions with *P*-450cam [110,111]. Through the application of electrostatic and electron transfer theories, and taking into account prior mutagenesis results, Roitberg and co-workers proposed an electron transfer pathway from the iron sulfur center of Pd to the heme of *P*-450cam involving R38 and C39 on Pd, and R112 on the *P*-450 as a conduit to the heme propionate group [112].

It appears that redox partner docking is similar in the prokaryotic and mammalian systems, in the sense that all interact with either ferredoxin or *P*-450 reductase partners and since the site of docking is at the proximal face of the heme. However, strong evidence for direct mediation of electron transfer by amino acid side chains has not been found. The involvement of a tryptophan at the C-terminus of putidaredoxin (W106) in electron transfer was considered likely, based on the fact that its removal led to a large decrease in the rate of electron transfer [113]. Furthermore, a highly conserved tryptophan residue throughout the *P*-450 enzyme superfamily, the equivalent to W96 in *P*-450 BM3, for example, is notably absent from *P*-450cam. It was therefore postulated that this aromatic residue is an obligatory electron transfer mediator in the *P*-450s, and that the *P*-450cam system is an unusual example in which the tryptophan is a component of the redox partner instead [114]. The role of W96 in *P*-450 BM3 was investigated, and it was found that mutant enzymes W96A, W96Y and W96F bound sub-stoichiometric amounts of heme, but were otherwise catalytically competent [115]. The subsequent solution of the crystal structure of the *P*-450 BM3 heme domain indicated that W96 is in hydrogen bonding distance to a heme propionate group [12], helping to explain the effects on heme content. In other studies on the *P*-450cam system, it was found that the removal of W106 from putidaredoxin resulted in a large increase in the K_d of the reduced form for *P*-450cam [108]. Thus the tryptophan residues in the *P*-450cam and *P*-450 BM3 systems are required for efficient redox

partner interaction and heme binding, respectively. A direct role in electron transfer has yet to be proven.

4.3. The role of cytochrome b_5

Cytochrome b_5 is involved in many mammalian $P-450$ reactions, particularly those catalyzing steps in steroid metabolism. It may donate the second electron to the oxyferrous $P-450$ during catalysis, but is known to act as a structural effector of $P-450$ function – as evidenced by the ability of apo (heme-free) b_5 to stimulate activity of cytochrome $P-450$ 3A4 [116]. Also, both holo- and apo-cytochrome b_5 augment the reaction profile of the human cytochrome $P-450$ c17 system in favor of the 17,20-lyase reaction (cleavage of the $C_{17}-C_{20}$ bond), while the b_5 -free enzyme system favors 17 α -hydroxylation [117]. These data indicate that b_5 has allosteric roles, but redox functions may also be operative and the precise role is probably dependent on the $P-450$ system involved. Cytochrome b_5 binding frequently perturbs the $P-450$ heme iron spin state equilibrium in favor of the high spin form, in similar fashion to the binding of substrates. However, its binding site is on the distal, not the proximal, face of the heme. Microsomal cytochrome b_5 has a highly charged surface and is also thought to bind electrostatically to $P-450$ s, with carboxylate groups important to the interaction. In elegant experiments, Stayton and co-workers modified bovine cytochrome b_5 by replacement of surface threonines with cysteines. This enabled the attachment (via the sulfhydryl groups) of the fluorophore acrylodan and the use of fluorescence as a tool to measure the binding of b_5 to $P-450$ cam. A K_d value of 1.1 μ M was thus determined, and Pd was shown to competitively inhibit the binding of b_5 [104,118]. These results indicate that both proteins bind at overlapping sites on the distal face of $P-450$ cam [119]. The fact that cytochrome b_5 binds tightly to $P-450$ cam is indicative that the bacterial cytochromes $P-450$ retain strong structural similarity to their mammalian counterparts. The incisive $P-450$ 2B4 mutagenesis studies of Waskell and co-workers have helped to define the binding site for cytochrome b_5 , demonstrating the importance of the $P-450$ C- and C'-helices in the b_5 interaction site [120]. There is extensive,

but not complete, overlap of the $P-450$ reductase and b_5 binding sites on the proximal surface of the $P-450$.

Until recently, the interaction between cytochrome b_5 and bacterial $P-450$ s ($P-450$ BM3 also binds b_5) was considered to reflect merely an evolutionary link between redox partner binding sites in prokaryotic and eukaryotic $P-450$ s, since b_5 was thought to be exclusively a eukaryotic redox protein. However, recent studies indicate that bacteria may also encode cytochromes b_5 , indeed the first three-dimensional structure of a bacterial cytochrome b_5 has been reported [121]. It may be the case, then, that certain bacterial $P-450$ s are also able to use b_5 as a redox partner.

4.4. Flavocytochrome $P-450$ BM3

The soluble flavocytochrome $P-450$ BM3 system is considered the best model for deconvoluting electron transfer in class II $P-450$ systems [122]. Genetic dissection of the enzyme has allowed the expression of its component domains. Initially, the $P-450$ domain (residues 1–472) and the diflavin reductase domain (residues 472–1048) were expressed independently in *E. coli* [123]. More recently, the subdomains of the diflavin domain have been overproduced in *E. coli*. These subdomains are ferredoxin reductase-like (residues 654–1048) and flavodoxin-like (residues 471–664), each binding a single flavin cofactor [124]. The ability to produce proteins with single redox cofactors has enabled the deconvolution of their otherwise overlapping spectral properties, and the determination of the reduction potentials for all the cofactors [124]. This study revealed that fatty acid substrate binding to the $P-450$ resulted in an approx. 130 mV increase in the reduction potential of the heme iron (from –368 to –239 mV on arachidonate binding), triggering electron transfer from the FMN (see Section 4.1).

The electron transfer pathway in $P-450$ BM3 has not been as intensively studied as that in $P-450$ cam, although W96 in the heme domain has been ruled out as an electron transfer mediator [115]. In studies of the reductase domain of the enzyme, Klein and Fulco demonstrated that W574 affected electron transport in the enzyme [125]. However, these defects may be explained by low incorporation of FMN, and

possibly by perturbation of the reduction potentials of the FMN. Recently, the crystal structure of the combined FMN and heme domains has been reported [126]. Unfortunately, the FMN domain of the protein was found to be proteolytically separated from the heme domain, and the stoichiometry of the domains was 1:2, not 1:1. An electron transfer pathway through the polypeptide chain was proposed, but is perhaps unlikely given the excessive length of the route. Indeed, the search for proteinaceous electron transfer pathways through $P-450$ systems may be a pointless one. A short, through-space route is much more likely in the class II system, with the possible involvement of a small number of amino acids that themselves are hydrogen-bonded or intimately associated with the FMN or heme cofactors, as postulated for the $P-450$ cam system [112]. The recently solved crystal structure of rat cytochrome $P-450$ reductase indicates that FAD-to-FMN electron transfer occurs between edges of the flavin ring systems and does not involve a protein pathway [127]. Rotation of the reduced FMN domain of the reductase away from its FAD/NADPH domain is probably necessary in order to expose the FMN for interaction at the heme proximal face and subsequent delivery of electrons to the heme.

In the $P-450$ BM3 heme domain, the cysteine-thiolate ligand to the heme iron (C400) is exposed to solvent at the distal face of the heme iron in the center of a region likely to represent a redox partner docking area. As such, it is accessible for direct electron transfer from FMN through to the heme iron [12,16].

4.5. Alternative reducing sources

All $P-450$ systems rely on NAD(P)H as the ultimate electron donor. However, this is not a cost-effective way to drive $P-450$ reactions, because NADPH is very expensive to produce commercially. There is much interest in developing alternative, cheaper means of driving $P-450$ reactions. These include the use of the 'peroxide shunt' mechanism to deliver oxygen and reducing equivalents simultaneously via an organic peroxide (e.g. cumene hydroperoxide) or hydrogen peroxide. However, such reactions are generally inefficient and result in gradual oxidative destruction of the heme macrocycle by

the peroxide. The future of such technology may rest with the design of mutant $P-450$ s selected for optimal reactivity with peroxides. The ground breaking study of Joo et al. [128] demonstrated that 'directed evolution' (i.e., successive rounds of random mutagenesis coupled to a selection screen for mutants with desired activity enhancement) could be used to select for mutants of $P-450$ cam able to hydroxylate naphthalene. In this study, mutants with hydrogen peroxide-driven activity greater than 20-fold that of wild-type were isolated. This was achieved by co-expression of a peroxidase enzyme that converted the hydroxylated product into easily detectable fluorescent derivatives. This technique is in its infancy, but there are clearly great possibilities for the generation of mutant $P-450$ s able to perform industrially or medically important processes that are driven by inexpensive chemicals.

Perhaps an even more exciting prospect is the use of an electrode to drive $P-450$ catalysis. This technique has been pioneered by Faulkner and co-workers in their study of the fatty acid hydroxylase $P-450$ 4A1 from rat [129]. The ω -hydroxylation of laurate in a system containing distinct or fused $P-450$ and $P-450$ reductase and the redox mediator cobalt(III) sepulchrate could be driven from an electrode poised at low potential (approx. –650 mV). The system could be run for up to 2 h without significant destruction of $P-450$ activity [130]. The presence of a flavoprotein is essential for transfer of electrons from cobalt sepulchrate, the reduced form of which is regenerated from the electrode. In studies with the progesterone hydroxylase $P-450$ c17, Estabrook and co-workers demonstrated that *E. coli* flavodoxin could substitute for $P-450$ reductase in the system, albeit with lower efficiency [131]. These studies demonstrate the potential for the bulk production of chemicals, and again have been greatly simplified by the breakthroughs in heterologous expression that have permitted the high level expression of eukaryotic $P-450$ s in *E. coli* (reviewed by Barnes [132]).

4.6. Genetic fusions

$P-450$ BM3 represents a natural fusion between a reductase and a $P-450$ and is the most catalytically efficient $P-450$ characterized to date. Another area of interest is the construction of 'artificial' fusions by

tween *P*-450 moieties and their electron transport accessory protein(s). The ultimate goal of such studies would be to reproduce the catalytic efficiency displayed by *P*-450 BM3. Failing that, self-sufficient enzymatic fusions could still be of great biotechnological potential, obviating the need to express and purify independently the component proteins of *P*-450 systems.

4.6.1. Fusions with NADPH-*P*-450 reductase

The first artificial *P*-450 fusion protein was reported by Murakami et al. in 1987 [133]. This group fused rat *P*-450 1A1 with rat NADPH-*P*-450 reductase to give a functionally active enzyme expressed in yeast. Following on from this success, fusions using the bovine *P*-450s 17A [134] and 21A [135] and yeast NADPH-*P*-450 reductase were generated by the same group. The development of heterologous expression systems for eukaryotic cytochromes *P*-450 in *E. coli* [136] allowed the overexpression of *P*-450 fusion proteins in this bacterium. Fisher et al. [137] reported the fusion of two mammalian *P*-450s, bovine 17A and rat 4A1, with rat liver NADPH-*P*-450 reductase and Shet et al. [138] generated a fusion between the human *P*-450 3A4 and the same reductase. The molecular biology involved in the construction of such fusions has been reviewed elsewhere [139]. The basic premise is that both cDNAs are modified and joined in a single reading frame. The stop codon of the *P*-450 is removed and replaced with a short polypeptide linker encoding a restriction endonuclease site (e.g. Ser/Thr dipeptide linker containing a *Sall* site [135]). This facilitates the fusing of the *P*-450 with the reductase. The latter is modified at its N-terminus to remove the major membrane binding region (e.g. first 56 residues of rat liver reductase deleted [133]).

In a more recent report, Chun et al. reported the construction of a human *P*-450 1A1/rat reductase fusion expressed in *E. coli* [140]. The study of human *P*-450 1A1 is of interest due to its potential role in activation of carcinogens and its inducibility by some environmental toxins [141,142]. The fused system was constructed essentially as described above, using a Ser/Thr linker (Fig. 8a). *P*-450 reductase from rat was used, since attempts to utilize the human reductase in fusions with human *P*-450s 3A4 and 3A5 had resulted in constructs in which the reductase portion

was not fully functional [46,143]. The fusion enzyme was expressed at high levels in *E. coli* and found to be catalytically active either in purified form or within the bacterial cells. Substrate turnover rates were comparable to those for the reconstituted system.

An example of a reported application of a fused rat *P*-450 1A1/yeast reductase protein was described by Shiota et al. [144]. The fusion was expressed in tobacco plants and although its expression level and activity were less than those observed in yeast, it conferred resistance to the herbicide chlortoluron to the plants.

A further demonstration of the usefulness of *P*-450/NADPH-*P*-450 reductase chimeras is seen from studies of a fusion between canine liver *P*-450 2B11 and rat liver NADPH-cytochrome *P*-450 reductase. This was constructed to expedite the analysis of mutated 2B11 enzymes [145]. The 2B11 fusion protein efficiently metabolized androstenedione when assayed as crude sonicated whole cell extracts. Activity and metabolic profiles were comparable with those of purified and reconstituted preparations. In this study, nine mutant forms of 2B11 were generated in the fusion protein and rapidly characterized using sonicated *E. coli* extracts.

4.6.2. Fusions with electron donors other than *P*-450 reductase

Sibbesen et al. [146] described the first heterologous, self-sufficient catalytic system for oxidation of *P*-450cam substrates. Fusions of the cDNAs of *P*-450cam and its electron donors PdR and Pd (both soluble) were generated and expressed in *E. coli*. The ordering of the components as well as the regions linking them were varied. Activities of the fusion proteins were compared by measuring oxygen consumption in the presence and absence of camphor. The most active of the constructs was that with *P*-450cam at the C-terminus: PdR-Pd-*P*-450cam (in contrast to the *P*-450 reductase fusions) (Fig. 8b), the order of the proteins in the fusion having more of an effect than the nature of the linkers between them. The limiting feature of catalytic turnover was found to be the interaction between *P*-450cam and Pd, most likely due to structural constraints. Evidence for this included the increase in catalytic activity of the fusion upon addition of both exogenous Pd and *P*-450cam and the high activity observed when

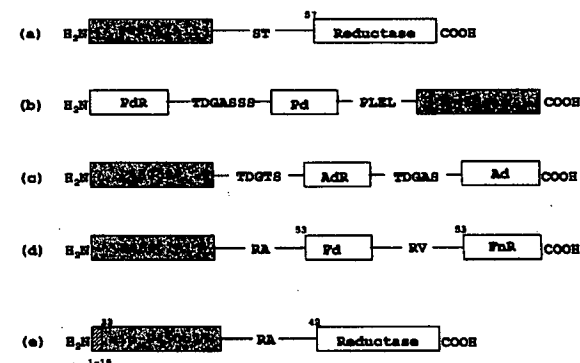


Fig. 8. Schematic representation of the different *P*-450 fusion constructs described showing the variation in linkers used and the ordering of the component proteins. The stop codons between protein pairs are deleted, fusing all components in a single, open reading frame. The amino acids in the linker regions are denoted by their single letter codes. (a) Fusion between human *P*-450 1A1 and (Δ 1-56)-rat NADPH-*P*-450 reductase [140]; (b) putidaredoxin reductase (PdR)/putidaredoxin (Pd)/*P*-450cam triple fusion [146]; (c) human *P*-450c27/mature adrenodoxin reductase (AdR)/mature adrenodoxin (Ad) triple fusion [147]; (d) triple fusion between rat microsomal *P*-450 1A1, mature maize ferredoxin I (Fd) and mature pea ferredoxin NADP⁺ reductase (FnR) [150]; (e) mitochondrially modified by deleting the mitochondrial targeting sequence (residues 1–32) and replacing it with the microsomal targeting sequence of *P*-450c17 (residues 1–15) (mic-*P*-450c27) fused to (Δ 1–41)-yeast NADPH-*P*-450 reductase [151].

P-450cam was incubated with fused PdR/Pd. Because the activity of the triple fusion increases linearly with its concentration the electron transfer from NADPH is considered to occur via an intramolecular pathway. Although this fusion protein is less efficient than the reconstituted wild-type system, the turnover is comparable to that of other reconstituted *P*-450 systems.

Similar fusions, expressed in mammalian COS-1 cells, have also been reported for the class I mitochondrial *P*-450s c27, soc and 11 β with their redox partners adrenodoxin and adrenodoxin reductase [147–149]. In the case of *P*-450c27, the fusion (Fig. 8c) was more efficient than the native reconstituted system in transfected mammalian cells.

4.6.3. Fusions with non-physiological electron donors

Whereas the above fusions describe *P*-450s in combination with their 'physiological' electron donors, Lacour and Ohkawa [150] have reported a fusion (expressed in yeast) in which rat *P*-450 1A1, a class II *P*-450 normally supplied with reducing equivalents

from NADPH-*P*-450 reductase, has been fused to ferredoxin (Fd) and ferredoxin NADP⁺ reductase (FnR) from plant chloroplasts to recreate an electron transfer chain resembling a class I system. The order of the proteins in the most efficient triple fusion generated was *P*-450-Fd-FnR (Fig. 8d) for all activities assayed. Not surprisingly, activities were lower when compared with *P*-450 1A1 fused to its physiological electron donor NADPH-*P*-450 reductase (e.g. the 1A1/reductase fusion was 5-fold more active with 7-ethoxycoumarin as the substrate than the triple fusion). It was concluded that electron transfer from FnR to Fd was not optimal in the triple fusion due to unfavorable redox potentials. The ultimate aim of generating such a system is to produce mammalian *P*-450s in plant chloroplasts to improve herbicide detoxification (to date, no *P*-450 monooxygenase system has been identified in plant chloroplasts) [150].

Sakaki et al. [151] describe the fusion of a modified class I *P*-450 with the class II microsomal yeast reductase (Fig. 8e). In modified *P*-450c27 (mic-*P*-450c27), the mitochondrial targeting signal was re-

placed by the microsomal targeting sequence of bovine P-450c17. This localized the protein to yeast microsomes where it appeared able to function as a microsomal P-450 by accepting electrons from NADPH-P-450 reductase. To study further electron transfer from NADPH-P-450 reductase to mic-P-450c27, a fusion between the two proteins was constructed. It was shown that the reductase in the fusion efficiently transferred electrons to the P-450, the rate of heme reduction being much faster than observed for the separate enzymes (similar results were obtained from studies with a fusion between rat P-450 1A1 and NADPH-P-450 reductase [152]). The rate of substrate hydroxylation was also 5-fold greater than that obtained when the two separate proteins were expressed simultaneously.

5. Conclusions

The cytochromes P-450 catalyze the monooxygenation of a vast array of substrate types. Some of these reactions have great medical or industrial importance with a huge potential for the application of protein engineering. This review demonstrates the attractive and realistic proposition that protein engineering approaches can be used to modulate cytochromes P-450 to catalyze the oxygenation of a molecule of choice. Protein engineering has also been shown to be a key tool for probing the role of active site residues and for dissecting the route of electron transfer through the protein. In addition, the manipulation of properties such as membrane binding and even the possibility of employing alternative reducing sources have been shown to be amenable to protein engineering methods.

Acknowledgements

We thank the Biotechnology and Biochemical Sciences Research Council (BBSRC) UK for support for CSM and MAN and for a studentship to TWBO. We are also grateful to the Leverhulme trust for financial support for this work. AWM wishes to thank the Royal Society of Edinburgh and Caledonian Research Foundation for the award of a re-

search fellowship. We also thank Dr. Simon Daff for helpful discussions.

References

- [1] D.R. Nelson, T. Kamatani, D.J. Waxman, F.P. Guengerich, R.W. Estabrook, R. Feyereisen, F.J. Gonzalez, M.J. Coon, I.C. Gunsalus, O. Gotoh, K. Okuda, D.W. Nebert, The P450 superfamily: update on new sequences, gene-mapping, accession numbers, early trivial names of enzymes, and nomenclature, *DNA Cell Biol.* 12 (1993) 1–51.
- [2] A.W. Munro, J.G. Lindsay, Bacterial cytochromes P450, *Mol. Microbiol.* 20 (1996) 1115–1125.
- [3] E.J. Mueller, P.J. Loida, S.G. Sligar, Twenty-five years of P450cam research, in: Ortiz de Montellano (Ed.), *Cytochrome P450: Structure, Mechanism and Biochemistry*, New York: Plenum Press; 1995, Ch. 3, pp. 473–535.
- [4] D.R. Nelson, L. Koymans, T. Kamatani, J.J. Stegeman, R. Feyereisen, D.J. Waxman, M.R. Waterman, O. Gotoh, M.J. Coon, R.W. Estabrook, I.C. Gunsalus, D.W. Nebert, P450 superfamily: update on new sequences, gene mapping, accession numbers and nomenclature, *Pharmacogenetics* 6 (1996) 1–42.
- [5] R.L. Wright, K. Harris, B. Solow, R.H. White, P.J. Kennelly, Cloning of a potential cytochrome P450 from the archaeon *Sulfolobus solfataricus*, *FEBS Lett.* 384 (1996) 235–239.
- [6] S.M. Park, H. Shimizu, S. Adachi, A. Nakagawa, I. Tanaka, K. Nakahara, H. Shoun, E. Obayashi, H. Nakamura, T. Iizuka, Y. Shiro, Crystal structure of nitric oxide reductase from denitrifying fungus *Fusarium oxysporum*, *Nat. Struct. Biol.* 4 (1997) 827–832.
- [7] I.A. Pikuleva, R.L. Mackman, R.L. Kagawa, M.R. Waterman, P.R. Ortiz de Montellano, Active site topology of bovine cholesterol side-chain cleavage cytochrome P450 sc and evidence for interaction of tyrosine 94 with cholesterol, *Arch. Biochem. Biophys.* 322 (1995) 189–197.
- [8] A.P. Koley, J.T.M. Buters, R.C. Robinson, A. Markowitz, F.K. Friedman, Interaction of polycyclic aromatic hydrocarbons with human cytochrome P450 1A1: a CO flash photolysis study, *Arch. Biochem. Biophys.* 336 (1996) 261–267.
- [9] P.A. Williams, J. Cosme, V. Sridhar, E.F. Johnson, D.E. McRee, Mammalian microsomal cytochrome P450 monooxygenase: structural adaptations for membrane binding and functional diversity, *Mol. Cell* 5 (2000) 121–131.
- [10] S.Y. Park, K. Yamane, S. Adachi, Y. Shiro, K.E. Weiss, S.G. Sligar, Crystallization and preliminary X-ray diffraction analysis of a cytochrome P450 (CYP119) from *Sulfolobus solfataricus*, *Acta Crystallogr. D Biol. Crystallogr.* 56 (2000) 1173–1175.
- [11] T.L. Poulos, B.C. Finzel, A.J. Howard, Crystal structure of substrate-free *Pseudomonas putida* cytochrome P450, *Biochemistry* 25 (1986) 5314–5322.
- [12] K.G. Ravichandran, S.S. Boddupalli, C.A. Hasemann, J.A.

Peterson, J. Deisenhofer, Crystal structure of hemoprotein domain of P450 BM3, a prototype for microsomal P450s, *Science* 261 (1993) 731–736.

- [13] C.A. Hasemann, K.G. Ravichandran, J.A. Peterson, J. Deisenhofer, Crystal structure and refinement of cytochrome P450terp at 2.3 Å resolution, *J. Mol. Biol.* 236 (1994) 1169–1185.
- [14] J.R. Cupp-Vickery, T.L. Poulos, Structure of cytochrome P450 eryF involved in erythromycin biosynthesis, *Nat. Struct. Biol.* 2 (1995) 144–153.
- [15] T.L. Poulos, B.C. Finzel, A.J. Howard, High resolution crystal structure of cytochrome P450cam, *J. Mol. Biol.* 195 (1987) 687–700.
- [16] H.Y. Li, T.L. Poulos, The structure of the cytochrome P450 BM3 heme domain complexed with the fatty acid substrate, palmitoleic acid, *Nat. Struct. Biol.* 4 (1997) 140–146.
- [17] S. Ito, T. Matsuoka, I. Watanabe, T. Kagasaki, T. Seriwaza, T. Hata, Crystallisation and preliminary X-ray diffraction analysis of P450 sc2 from *Streptomyces carbophilus* involved in production of pravastatin sodium, a tissue-selective inhibitor of HMG-CoA reductase, *Acta Crystallogr. D Biol. Crystallogr.* 55 (1999) 1209–1211.
- [18] R. Raag, H.Y. Li, B.C. Jones, T.L. Poulos, Inhibitor-induced conformational change in P450cam, *Biochemistry* 32 (1993) 4571–4578.
- [19] O. Gotoh, Substrate recognition sites in cytochrome P450 family 2 (CYP2) proteins inferred from comparative analyses of amino acid and coding nucleotide sequences, *J. Biol. Chem.* 267 (1992) 83–90.
- [20] M. Iwasaki, T.A. Darden, L.G. Pedersen, D.G. Davis, R.O. Juvonen, T. Sueyoshi, M. Negishi, Engineering mouse P450coh to a novel corticosterone 15- α -hydroxylase and modelling steroid binding orientation in the substrate pocket, *J. Biol. Chem.* 268 (1993) 759–762.
- [21] J. Liu, Y.A. He, J.R. Halpert, Role of residue 480 in substrate specificity of cytochrome P450 2B5 and 2B11, *Arch. Biochem. Biophys.* 327 (1996) 167–173.
- [22] M.-H. Hsu, K.J. Griffin, Y. Wang, B. Kemper, E.F. Johnson, A single amino acid substitution confers progesterone 6 β -hydroxylase activity to rabbit cytochrome P450 2C3, *J. Biol. Chem.* 268 (1993) 6939–6944.
- [23] M.J.J.M. Zvebil, C.R. Wolf, M.J.E. Sternberg, A predicted 3-D structure of human cytochrome P450-implications for substrate specificity, *Protein Eng.* 4 (1991) 271–282.
- [24] G.D. Szklarz, R.L. Orstein, J.R. Halpert, Application of 3-Dimensional homology modelling of cytochrome P450 2B1 for interpretation of site-directed mutagenesis results, *J. Biomol. Struct. Dyn.* 12 (1994) 61–78.
- [25] S. Vijayakumar, J.C. Salerno, Molecular modelling of the 3-D structure of cytochrome P450sc, *Biochim. Biophys. Acta* 1160 (1992) 281–286.
- [26] C.A. Hasemann, R.G. Kurumbail, S.S. Boddupalli, J.A. Peterson, J. Deisenhofer, Structure and function of cytochromes P450: a comparative analysis of three crystal structures, *Structure* 2 (1995) 41–62.
- [27] D.F.V. Lewis, M. Dickens, B.G. Lake, P.J. Eddershaw,

M.H. Tarbit, P.S. Goldfarb, Molecular modelling of the human cytochrome P450 isoform CYP2A6 and investigations of CYP2A substrate selectivity, *Toxicology* 133 (1999) 1–33.

- [28] D.F.V. Lewis, B.G. Lake, Molecular modelling of CYP4A subfamily members based on sequence homology with CYP102, *Xenobiotica* 29 (1999) 763–781.
- [29] S. Graham-Lorence, B. Amarnesh, R.E. White, J.A. Peterson, E.R. Simpson, A three-dimensional model of aromatase cytochrome P450, *Protein Sci.* 4 (1995) 1065–1080.
- [30] G.D. Szklarz, Y.A. He, J.R. Halpert, Site-directed mutagenesis as a tool for molecular modelling of cytochrome P450 2B1, *Biochemistry* 34 (1995) 14312–14322.
- [31] R.K. Dai, M.R. Pincus, F.K. Friedman, Molecular modeling of cytochrome P450 2B1: mode of membrane insertion and substrate specificity, *J. Protein Chem.* 17 (1998) 121–129.
- [32] G.D. Szklarz, J.R. Halpert, Molecular modeling of cytochrome P450 3A4, *J. Comp.-Aided Mol. Des.* 11 (1997) 265–272.
- [33] R.L. Haining, J.P. Jones, K.R. Henne, M.B. Fisher, D.R. Koop, W.F. Trager, A.E. Rettie, Enzymatic determinants of the substrate specificity of CYP2C9: role of the B'-C loop residues in providing the n-stacking anchor site for warfarin binding, *Biochemistry* 38 (1999) 3285–3292.
- [34] J. Cosme, E.F. Johnson, Engineering microsomal P-450 2C5 to be a soluble, monomeric enzyme: mutations that alter aggregation, phospholipid dependence of catalysis, and membrane binding, *J. Biol. Chem.* 275 (2000) 2545–2553.
- [35] P.J. Loida, S.G. Sligar, Molecular recognition in cytochrome P450: mechanism for the control of uncoupling reactions, *Biochemistry* 32 (1993) 11530–11538.
- [36] J.A. Stevenson, A.C.G. Westlake, C. Whitlock, L.-L. Wong, The catalytic oxidation of linear and branched alkanes by cytochrome P450cam, *J. Am. Chem. Soc.* 118 (1996) 12846–12847.
- [37] P.A. England, C.F. Harford-Cross, J.-A. Stevenson, D.A. Rouch, L.-L. Wong, The oxidation of naphthalene and pyrene by cytochrome P450cam, *FEBS Lett.* 424 (1998) 271–274.
- [38] S.M. Fowler, P.A. England, A.C.G. Westlake, D.R. Rough, D.P. Nickerson, C. Blunt, D. Braybrook, S. West, L.L. Wong, S.L. Flitsch, Cytochrome P450cam monooxygenase can be redesigned to catalyze the regioselective aromatic hydroxylation of diphenylmethane, *J. Chem. Soc. Chem. Commun.* 24 (1994) 2761–2762.
- [39] J.A. Stevenson, J.P. Jones, L.L. Wong, Mutations of phenylalanine 193 in the putative substrate access channel alter the substrate specificity of cytochrome P450 cam, *Isr. J. Chem.* 40 (2000) 55–62.
- [40] C.F. Oliver, S. Modi, W.U. Primrose, L.-Y. Lian, G.C.K. Roberts, Engineering the specificity of *Bacillus megaterium* P450 BM3: hydroxylation of alkyl triammonium compounds, *Biochem. J.* 327 (1997) 537–544.
- [41] M.A. Noble, C.S. Miles, S.K. Chapman, D.A. Lysek, A.C. Mackay, G.A. Reid, R.P. Hanzlik, A.W. Munro, Roles of key active-site residues in flavocytochrome P450 BM3, *Biochem. J.* 339 (1999) 371–379.

- [42] C.F. Oliver, S. Modi, M.J. Sutcliffe, W.U. Primrose, L.Y. Lian, G.C.K. Roberts, A single mutation in cytochrome P450 BM3 changes substrate orientation in a catalytic intermediate and the regioselectivity of hydroxylation, *Biochemistry* 36 (1997) 1567–1572.
- [43] S. Modi, M.J. Sutcliffe, W.U. Primrose, L.-Y. Lian, G.C.K. Roberts, The catalytic mechanism of cytochrome P450 BM3 involves a 6 angstrom movement of the bound substrate upon reduction, *Nat. Struct. Biol.* 3 (1996) 414–417.
- [44] E.A. Dierks, S.C. Davis, P.R. Ortiz de Montellano, Glu-320 and Asp-323 are determinants of the CYP4A1 hydroxylation regioselectivity and resistance to inactivation by 1-aminobenzotriazole, *Biochemistry* 37 (1998) 1839–1847.
- [45] D.F. Fraser, R. Feyereisen, G.R. Harlow, J.R. Halpert, Isolation, heterologous expression and functional characterisation of a novel cytochrome P450 3A enzyme from a canine cDNA library, *J. Pharmacol. Exp. Ther.* 283 (1997) 1425–1432.
- [46] F.P. Guengerich, Human cytochrome P450 enzymes, in: Ortiz de Montellano (Ed.), *Cytochrome P450: Structure, Mechanism and Biochemistry*, New York: Plenum Press; 1995, Ch. 14, pp. 473–535.
- [47] D.J. Waxman, C. Attisano, F.P. Guengerich, D.P. Lapenson, Human liver microsomal steroid metabolism-identification of the major microsomal steroid-hormone 6-beta-hydroxylase cytochrome P450 enzyme, *Arch. Biochem. Biophys.* 263 (1988) 424–436.
- [48] T. Shimada, F.P. Guengerich, Evidence for cytochrome P450NF, the nifedipine oxidase, being the principal enzyme involved in the bioactivation of aflatoxins in human liver, *Proc. Natl. Acad. Sci. USA* 86 (1989) 462–465.
- [49] L.Z. Benet, D.L. Kroetz, L.B. Sheiner, in: J.G. Hardman, L.E. Limbird, P.B. Molinoff, R.W. Ruddon, A.D. Gilman (Eds.), *Goodman and Gilman's The Pharmacological Basis of Therapeutics*, 9th edn., McGraw-Hill, New York, pp. 3–27.
- [50] G.E. Schwab, J.L. Raucy, E.F. Johnson, Modulation of rabbit and human hepatic cytochrome P450 catalysed steroid hydroxylations by α -naphthoflavone, *Mol. Pharmacol.* 33 (1988) 493–499.
- [51] Y.F. Ueng, T. Kuwabara, Y.J. Chun, F.P. Guengerich, Cooperativity in oxidations catalysed by cytochrome P450 3A4, *Biochemistry* 36 (1997) 370–381.
- [52] G.R. Harlow, J.R. Halpert, Alanine-scanning mutagenesis of a putative substrate recognition site in human cytochrome P450 3A4, *J. Biol. Chem.* 272 (1997) 5396–5402.
- [53] D.F.V. Lewis, P.J. Eddershaw, P.S. Goldfarb, M.H. Tarbit, Molecular modelling of CYP3A4 with an alignment with CYP102: identification of key interactions between putative active site residues and CYP3A-specific chemicals, *Xenobiotica* 26 (1996) 1067–1086.
- [54] G.R. Harlow, J.R. Halpert, Analysis of human cytochrome P450 3A4 cooperativity: construction and characterisation of a site-directed mutant that displays hyperbolic steroid hydroxylation kinetics, *Proc. Natl. Acad. Sci. USA* 95 (1998) 6636–6641.
- [55] T.L. Domanski, J. Liu, G.R. Harlow, J.R. Halpert, Analysis of four residues within substrate recognition site 4 of cytochrome P450 3A4: role of steroid hydroxylase activity and α -naphthoflavone stimulation, *Arch. Biochem. Biophys.* 350 (1998) 223–232.
- [56] T.L. Domanski, Y.-A. He, G.R. Harlow, J.R. Halpert, Dual role of human cytochrome P450 3A4 residue Phe-304 in substrate specificity and cooperativity, *J. Pharmacol. Exp. Ther.* 293 (2000) 585–591.
- [57] Y.A. He, Y.Q. He, G.D. Szklarz, J.R. Halpert, Identification of three key residues in substrate recognition site 5 of human cytochrome P450 3A4 by cassette and site-directed mutagenesis, *Biochemistry* 36 (1997) 8831–8839.
- [58] F. Roussel, K.K. Khan, J.R. Halpert, The importance of SRS-1 residues in catalytic specificity of cytochrome P450 3A4, *Arch. Biochem. Biophys.* 374 (2000) 269–278.
- [59] H. Wang, R. Dick, H. Yin, E. Licad-Coles, D.L. Kroetz, G. Szklarz, G. Harlow, J.R. Halpert, M.A. Correia, Structure-function relationships of human liver cytochromes P450 3A: aflatoxin B1 metabolism as a probe, *Biochemistry* 37 (1998) 12536–12545.
- [60] M.K. Ramarao, P. Straub, B. Kemper, Identification by in vitro mutagenesis of the interaction of two segments of C2MstC1, a chimera of cytochromes P450 2C2 and P450 2C1, *J. Biol. Chem.* 270 (1995) 1873–1880.
- [61] I.H. Hanna, E.S. Roberts, P.F. Hollenberg, Molecular basis for the differences in lidocaine binding and regioselectivity of oxidation by cytochrome P450 2B1 and 2B2, *Biochemistry* 37 (1998) 311–318.
- [62] G.D. Szklarz, Y.Q. He, K.M. Kedzie, J.R. Halpert, V.L. Burnett, Elucidation of amino acid residues critical for unique activities of rabbit cytochrome P450 2B5 using hybrid enzymes and reciprocal site-directed mutagenesis with rabbit cytochrome P450 2B4, *Arch. Biochem. Biophys.* 327 (1996) 308–318.
- [63] T.S. Klose, G.C. Ibeanu, B.I. Ghanayem, L.G. Pedersen, L. Li, S.D. Hall, J.A. Goldstein, Identification of residues 286 and 289 as critical for conferring substrate specificity of human CYP2C9 for diclofenac and ibuprofen, *Arch. Biochem. Biophys.* 357 (1998) 240–248.
- [64] G.C. Ibeanu, B.I. Ghanayem, P. Linko, L. Li, L.G. Pedersen, J.A. Goldstein, Identification of residues 99, 220 and 221 of human cytochrome P450 2C19 as key determinants of omeprazole hydroxylase activity, *J. Biol. Chem.* 271 (1996) 12496–12501.
- [65] F. Jung, K.J. Griffin, W. Song, T.H. Richardson, M. Yang, E.F. Johnson, Identification of amino acid substitutions that confer a high affinity for sulfaphenazole binding and a high catalytic efficiency for warfarin metabolism to P450 2C19, *Biochemistry* 37 (1998) 16270–16279.
- [66] D.J. Fraser, Y.Q. He, G.R. Harlow, J.R. Halpert, Use of chimeric enzymes and site-directed mutagenesis for identification of three key residues responsible for differences in steroid hydroxylation between canine cytochromes P450 3A12 and 3A26, *Mol. Pharmacol.* 55 (1999) 241–247.
- [67] T. Zimmer, U. Scheller, M. Takagi, W.-H. Schunk, Mutual conversion of fatty-acid substrate specificity by a single amino acid exchange at position 527 in P450Cm2 and P450Alk3A, *Eur. J. Biochem.* 256 (1998) 398–403.
- [68] T. Shimada, H. Yamazaki, M. Mimura, Y. Inui, F.P. Guengerich, Inter-individual variations in human liver cytochrome P450 enzymes involved in the oxidation of drug, carcinogens and toxic chemicals, *J. Pharmacol. Exp. Ther.* 270 (1994) 414–423.
- [69] M. Romkes, M.B. Faletto, J.A. Blaisdell, J.L. Raucy, J.A. Goldstein, Cloning and expression of complementary DNAs for multiple members of the human cytochrome P450lic cub-family, *Biochemistry* 30 (1991) 3247–3255.
- [70] J.A. Goldstein, S.M.F. de Moraes, *Biochemistry and molecular biology of the human CYP2C subfamily*, *Pharmacogenetics* 4 (1994) 285–299.
- [71] M.A. Hamman, G.A. Thompson, S.D. Hall, Regioselective and stereoselective metabolism of ibuprofen by human cytochrome P4502C, *Pharmacology* 54 (1997) 33–41.
- [72] T.S. Klose, B.I. Ghanayem, J.A. Goldstein, G.C. Ibeanu, Abstracts of 17th International Congress of Biochemistry and Molecular Biology, San Francisco, CA, 1997, p. A794.
- [73] J.A. Goldstein, M.B. Faletto, M. Romkes-Sparks, T. Sullivan, S. Kitarewan, J.L. Raucy, J.M. Lasker, B.I. Ghanayem, Evidence that CYP2C19 is the major (S)-mephenytoin 4'-hydroxylase in humans, *Biochemistry* 33 (1994) 1743–1752.
- [74] B.I. Ghanayem, W.G. Karam, J.A. Goldstein, Sixth North American International Society for the Study of Xenobiotics Meeting, 23–27 October 1994, Raleigh, NC, p. 50 (abstr.).
- [75] M.E. Veronesi, P.J. Mackenzie, C.J. Doeck, M.E. McManus, J.O. Miners, D.J. Birkett, Tolbutamide and phenytoin hydroxylations by cDNA-expressed human liver cytochrome P4502C9, *Biochem. Biophys. Res. Commun.* 175 (1991) 1112–1118.
- [76] A. Mancy, S. Dijols, S. Poli, F.P. Guengerich, D. Mansuy, Interaction of sulfaphenazole derivatives with human liver cytochromes P450 2C: molecular origin of the specificity inhibitory effects of sulfaphenazole on CYP2C9 and consequences for the substrate binding site topology of CYP2C9, *Biochemistry* 35 (1996) 16205–16212.
- [77] J.A. Goldstein, T. Ishizaki, K. Chiba, S.M. de Moraes, D. Bell, P.M. Krahn, D.A. Evans, Frequencies of the defective CYP2C19 alleles responsible for the mephenytoin poor metabolizer phenotype in various Oriental, Caucasian, Saudi Arabian and American black populations, *Pharmacogenetics* 7 (1997) 59–64.
- [78] D.F.V. Lewis, H. Moerels, The sequence homologies of cytochromes P450 and active-site geometries, *J. Comp.-Aided Mol. Des.* 6 (1992) 235–252.
- [79] W.-H. Schunck, F. Vogel, B. Gross, E. Kärger, S. Mauersberger, K. Köpke, C. Gengnagel, H.-G. Müller, Comparison of two cytochromes P450 from *Candida maltosa*: primary structure, substrate specificities and effects of their expression in *Saccharomyces cerevisiae* on the proliferation of the endoplasmic reticulum, *Eur. J. Cell Biol.* 55 (1991) 336–345.
- [80] T. Zimmer, U. Scheller, M. Takagi, W.-H. Schunck, Mutual conversion of fatty acid substrate specificity by a single amino acid exchange at position 527 in P450Cm2 and P450Alk3A, *Eur. J. Biochem.* 256 (1998) 398–403.
- [81] J.-Y. Kim, P.N. Devreotes, Random chimeragenesis of G-protein-coupled receptors-mapping the affinity of the cAMP chemoattractant receptors in Dictyostelium, *J. Biol. Chem.* 269 (1994) 28724–28731.
- [82] L.R. Levin, R.R. Reed, Identification of functional domains of adenylyl-cyclase using in-vivo chimeras, *J. Biol. Chem.* 270 (1995) 7573–7579.
- [83] I.A. Pikuleva, I. Bjorkhem, M.R. Waterman, Studies of distant members of the P450 superfamily (P450csc and P450c27) by random chimeragenesis, *Arch. Biochem. Biophys.* 334 (1996) 183–192.
- [84] B.J. Brock, M.R. Waterman, The use of random chimeragenesis to study structure/function properties of rat and human P450c17, *Arch. Biochem. Biophys.* 373 (2000) 401–408.
- [85] M. Shimoi, H. Yin, L.-A. Higgins, J.P. Jones, Design of a novel P450: a functional bacterial-human cytochrome P450 chimera, *Biochemistry* 37 (1998) 8848–8852.
- [86] K. Ahn, E. Szczesna-Skorupa, B. Kemper, The amino-terminal 29 amino acids of cytochrome P450 2C1 are sufficient for retention in the endoplasmic reticulum, *J. Biol. Chem.* 268 (1993) 18726–18733.
- [87] L.-C. Hsu, M.-C. Hu, H.-C. Cheng, J.-C. Lu, B. Chung, The N-terminal hydrophobic domain of P450c21 is required for membrane insertion and enzyme stability, *J. Biol. Chem.* 268 (1993) 14682–14686.
- [88] S.J. Pernecky, M.J. Coon, N-terminal modifications that alter P450 membrane targeting and function, *Methods Enzymol.* 272 (1996) 25–34.
- [89] S.J. Pernecky, J.R. Larson, M.J. Coon, Cytosolic localisation of NH₂-terminal-modified microsomal P450 in *E. coli*, *FASEB J.* 7 (1994) A1200.
- [90] V.Y. Uvarov, A.I. Sotnichenko, E.L. Vodovozova, J.G. Molotkovsky, E.F. Kolesanova, Y.A. Lyulkin, A. Stier, V. Krueger, A.I. Archakov, Determination of membrane-bound fragments of cytochrome P450 2B4, *Eur. J. Biochem.* 222 (1994) 483–489.
- [91] B. Doray, C.D. Chen, B. Kemper, Substitutions in the C-terminal portion of the catalytic domain partially reverse assembly defects introduced by mutations in the N-terminal linker sequence of cytochrome P450 2C2, *Biochemistry* 38 (1999) 12180–12186.
- [92] T. Sueyoshi, L.J. Park, R. Moore, R.O. Juvonen, M. Negishi, Molecular engineering of microsomal P450 2A4 to a stable, water-soluble enzyme, *Arch. Biochem. Biophys.* 322 (1995) 265–271.
- [93] D.C. Lamb, D.E. Kelly, K. Venkateswarlu, N.J. Manning, H.F.J. Bligh, W.-H. Schunck, S.L. Kelly, Generation of a complete, soluble, and catalytically active sterol 14 α -demethylase-reductase complex, *Biochemistry* 38 (1999) 8733–8738.
- [94] C.M. Jenkins, M.R. Waterman, NADPH-flavodoxin reductase and flavodoxin from *Escherichia coli*: characteristics and

- a soluble microsomal P450 reductase, *Biochemistry* 37 (1998) 6106–6113.
- [95] M. Kranendonk, F. Carreira, P. Theisen, A. Lairens, C.W. Fisher, J. Rueff, R.W. Estabrook, N.P.E. Vermeulen, *Escherichia coli* MTC, a human NADPH P450 reductase competent mutagenicity tester strain for the expression of human cytochrome P450 isoforms 1A1, 1A2, 2A6, 3A4 or 3A5: catalytic activities and mutagenicity studies, *Mutat. Res. Genet. Toxicol. Environ. Mutagen.* 441 (1999) 73–83.
- [96] S. LeCoeur, J.-C. Gautier, C. Belloc, A. Gaultre, P.H. Beaune, Use of heterologous expression systems to study autoimmune drug-induced hepatitis, *Methods Enzymol.* 272 (1996) 76–85.
- [97] R.W. Estabrook, J.M. Trant, P.A. Mathew, J.I. Mason, M.R. Waterman, Designer membranes-construction of a cell containing multiple membrane-bound cytochromes P450, *Curr. Top. Cell Regul.* 33 (1992) 419–431.
- [98] C. von Wachenfeldt, T.H. Richardson, J. Cosme, E.F. Johnson, Microsomal P450 2C3 is expressed as a soluble dimer in *Escherichia coli* following modifications of its N-terminus, *Arch. Biochem. Biophys.* 339 (1997) 107–114.
- [99] S.G. Sligar, I.C. Gunsalus, A thermodynamic model of regulation: modulation of redox equilibria in camphor monooxygenase, *Proc. Natl. Acad. Sci. USA* 73 (1976) 1078–1082.
- [100] S.N. Daff, S.K. Chapman, K.L. Turner, R.A. Holt, S. Govindaraj, T.L. Poulos, A.W. Munro, Redox control of the catalytic cycle of flavocytochrome P450 BM3, *Biochemistry* 36 (1997) 13816–13823.
- [101] J.D. Lambeth, S.E. Kitchen, A.A. Farooqui, R. Tuckey, H. Kamin, Cytochrome P450_{sec}-substrate interactions: studies of binding and catalytic activity using hydroxycholesterols, *J. Biol. Chem.* 257 (1982) 1876–1884.
- [102] J.D. Lambeth, H. Kamin, Adrenodoxin reductase-adrenodoxin complex: flavin to iron-sulfur electron transfer as the rate-limiting step in the NADPH-cytochrome c reductase reaction, *J. Biol. Chem.* 254 (1979) 2766–2774.
- [103] J.D. Lambeth, S. Kriensiri, Cytochrome P-450_{sec}-adrenodoxin interactions: ionic effects on binding, and regulation of cytochrome reduction by bound steroid substrates, *J. Biol. Chem.* 260 (1985) 8810–8816.
- [104] P.S. Stayton, T.L. Poulos, S.G. Sligar, Putidaredoxin competitively inhibits cytochrome b₅-cytochrome P450 cam electron transfer complex, *Biochemistry* 28 (1989) 7381–7386.
- [105] T. Kido, T. Kimura, The formation of binary and ternary complexes of cytochrome P450_{sec} with adrenodoxin and adrenodoxin reductase-adrenodoxin complex, *J. Biol. Chem.* 254 (1979) 11806–11815.
- [106] C.B. Brewer, J.A. Peterson, Single turnover kinetics of the reaction between oxy-cytochrome P450 cam and reduced putidaredoxin, *J. Biol. Chem.* 263 (1986) 791–798.
- [107] K. Nakamura, T. Horiuchi, T. Yasukochi, K. Sekimizu, T. Hara, Y. Sagara, Significant contribution of arginine 112 and its positive charge of *Pseudomonas putida* P450 cam in the electron transport from putidaredoxin, *Biochim. Biophys. Acta* 1207 (1994) 40–48.
- [108] M.D. Davies, S.G. Sligar, Genetic variants in the putidaredoxin-cytochrome P450 cam electron transfer complex: identification of the residue responsible for redox-state-dependent conformers, *Biochemistry* 31 (1992) 11383–11389.
- [109] M. Unno, H. Shimada, Y. Toba, R. Makino, Y. Ishimura, Role of Arg 112 of cytochrome P450 cam in the electron transfer from reduced putidaredoxin-analyses with site-directed mutants, *J. Biol. Chem.* 271 (1996) 17869–17874.
- [110] M. Aoki, K. Ishimori, I. Morishima, Roles of negatively charged surface residues of putidaredoxin in interactions with redox partners in P450cam monooxygenase system, *Biochim. Biophys. Acta* 1386 (1998) 157–167.
- [111] M. Aoki, K. Ishimori, I. Morishima, Y. Wada, Roles of valine 98 and glutamic acid 72 of putidaredoxin in the electron transfer complexes with NADH-putidaredoxin reductase and P450 cam, *Inorg. Chim. Acta* 272 (1998) 80–88.
- [112] A.E. Roitberg, M.J. Holden, M.P. Mayhew, I.V. Kurnikov, D.N. Beratan, V.L. Vilker, Binding and electron transfer between putidaredoxin and cytochrome P450 cam. Theory and experiments, *J. Am. Chem. Soc.* 120 (1998) 8927–8932.
- [113] S.G. Sligar, P.G. Debrunner, J.D. Lipscomb, M.J. Namtvedt, I.C. Gunsalus, A role for putidaredoxin COOH-terminus in P450 cam (cytochrome m) hydroxylations, *Proc. Natl. Acad. Sci. USA* 71 (1974) 10.
- [114] J.E. Baldwin, G.M. Morris, W.G. Richards, Electron transport in cytochromes P450 by covalent switching, *Proc. R. Soc. London Ser. B* 245 (1991) 43–51.
- [115] A.W. Munro, K. Malarkey, J. McKnight, A.J. Thomson, S.M. Kelly, N.C. Price, J.G. Lindsay, J.R. Coggins, J.S. Miles, The role of tryptophan 97 of cytochrome P450 BM3 from *Bacillus megaterium* in catalytic function. Evidence against the 'covalent switching' hypothesis of P450 electron transfer, *Biochem. J.* 303 (1994) 423–428.
- [116] H. Yamazaki, W.W. Johnson, Y.F. Ueng, T. Shimada, P.P. Guengerich, Lack of electron transfer from cytochrome b₅ in stimulation of catalytic activities of cytochrome P450 3A4-characterization of a reconstituted cytochrome P450 3A4 NADPH-cytochrome P450 reductase system and studies with apo-cytochrome b₅, *J. Biol. Chem.* 271 (1996) 27438–27444.
- [117] R.J. Achus, T.C. Lee, W.L. Miller, Cytochrome b₅ augments the 17, 20-lyase activity of human P450 c17 without direct electron transfer, *J. Biol. Chem.* 273 (1998) 3158–3165.
- [118] P.S. Stayton, M.T. Fisher, S.G. Sligar, Determination of cytochrome b₅ association reactions: Characterization of metmyoglobin and cytochrome P450 cam binding to genetically engineered cytochrome b₅, *J. Biol. Chem.* 263 (1988) 13544–13548.
- [119] P.S. Stayton, S.G. Sligar, The cytochrome P450 cam binding surface as defined by site-directed mutagenesis and electrostatic modelling, *Biochemistry* 29 (1990) 7381–7384.
- [120] A. Bridges, L. Gruenke, Y.-T. Chang, I.A. Vasker, G. Loew, L. Waskell, Identification of the binding site on cytochrome P450 2B4 for cytochrome b₅ and cytochrome P450 reductase, *J. Biol. Chem.* 273 (1998) 17036–17049.
- [121] V. Kostanjevecki, D. Leys, G. Van Driessche, T.E. Meyer, M.A. Cusanovich, U. Fischer, Y. Guisez, J. Van Beeumen, Structure and characterization of *Ecotiorhodospira vacuolata* cytochrome b₅₅₈, a prokaryotic homologue of cytochrome b₅, *J. Biol. Chem.* 274 (1999) 35614–35620.
- [122] L.O. Narhi, A.J. Fulco, Identification and characterization of two functional domains in cytochrome P450 BM3, a catalytically self-sufficient monooxygenase induced by barbiturates in *Bacillus megaterium*, *J. Biol. Chem.* 262 (1987) 6683–6690.
- [123] J.S. Miles, A.W. Munro, B.N. Rospendowski, W.E. Smith, J. McKnight, A.J. Thomson, Domains of the catalytically self-sufficient cytochrome P450 BM3-genetic construction, overexpression, purification and spectroscopic characterization, *Biochem. J.* 288 (1992) 503–509.
- [124] S. Govindaraj, T.L. Poulos, The domain architecture of cytochrome P450 BM3, *J. Biol. Chem.* 272 (1997) 7915–7921.
- [125] M.L. Klein, A.J. Fulco, Critical residues involved in FMN binding and catalytic activity in cytochrome P450 BM3, *J. Biol. Chem.* 268 (1993) 7553–7561.
- [126] J.F. Sevrioukova, H.-Y. Li, H. Zhang, J.A. Peterson, T.L. Poulos, Structure of a cytochrome P450-redox partner electron-transfer complex, *Proc. Natl. Acad. Sci. USA* 96 (1999) 1863–1868.
- [127] M. Wang, D.L. Roberts, R. Paschke, T.M. Shea, B.S.S. Masters, J.J.P. Kim, Three-dimensional structure of NADPH-cytochrome P450 reductase: prototype for FMN- and FAD-containing enzymes, *Proc. Natl. Acad. Sci. USA* 94 (1997) 8411–8416.
- [128] H. Joo, Z.L. Lin, F.H. Arnold, Laboratory evolution of peroxide-mediated cytochrome P450 hydroxylation, *Nature* 399 (1999) 670–673.
- [129] K.M. Faulkner, K.M. Shet, C.W. Fisher, R.W. Estabrook, Electro-catalytically driven omega-hydroxylation of fatty acids using cytochrome P450 4A1, *Proc. Natl. Acad. Sci. USA* 92 (1995) 7705–7709.
- [130] R.W. Estabrook, K.M. Faulkner, M.S. Shet, C.W. Fisher, Application of electrochemistry for P450-catalyzed reactions, *Methods Enzymol.* 272 (1996) 44–51.
- [131] R.W. Estabrook, M.S. Shet, C.W. Fisher, C.M. Jenkins, M.R. Waterman, The interaction of NADPH-P450 reductase with P450: an electrochemical study of the role of the flavin mononucleotide-binding domain, *Arch. Biochem. Biophys.* 333 (1996) 308–315.
- [132] H.J. Barnes, Maximizing expression of eukaryotic cytochrome P450s in *Escherichia coli*, *Methods Enzymol.* 272 (1996) 3–14.
- [133] H. Murakami, Y. Yabusaki, T. Sakaki, M. Shibata, H. Ohkawa, A genetically engineered P450 monooxygenase: construction of the functional fused enzyme between rat cytochrome P450c and NADPH-cytochrome P450 reductase, *DNA* 6 (1987) 189–197.
- [134] M. Shibata, T. Sakaki, Y. Yabusaki, H. Murakami, H. Ohkawa, Genetically engineered P450 monooxygenases: construction of bovine P450c17_{sec} reductase fused enzymes, *DNA Cell Biol.* 9 (1990) 27–36.
- [135] T. Sakaki, M. Shibata, Y. Yabusaki, H. Murakami, H. Ohkawa, Expression of bovine cytochrome P450c21 and its fused enzymes with yeast NADPH-cytochrome P450 reductase in *Saccharomyces cerevisiae*, *DNA Cell Biol.* 9 (1990) 603–614.
- [136] H.J. Barnes, M.P. Arlotto, M.R. Waterman, Expression and enzymatic activity of recombinant cytochrome P450 17 α -hydroxylase in *E. coli*, *Proc. Natl. Acad. Sci. USA* 88 (1991) 5597–5601.
- [137] C.W. Fisher, M.S. Shet, D.L. Caudle, C.A. Martin-Wirtz, R.W. Estabrook, High-level expression in *Escherichia coli* of enzymatically active fusion proteins containing the domains of mammalian cytochromes P450 and NADPH-P450 reductase flavoprotein, *Proc. Natl. Acad. Sci. USA* 89 (1992) 10817–10821.
- [138] M.S. Shet, C.W. Fisher, P.L. Holmans, R.W. Estabrook, Human cytochrome P450 3A4: enzymatic properties of a purified recombinant fusion protein containing NADPH-P450 reductase, *Proc. Natl. Acad. Sci. USA* 90 (1993) 11748–11752.
- [139] C.W. Fisher, M.S. Shet, R.W. Estabrook, Construction of plasmids and expression in *E. coli* of enzymatically active fusion proteins containing the heme domain of a P450 linked to NADPH-P450 reductase, *Methods Enzymol.* 272 (1996) 15–25.
- [140] Y.-J. Chun, T. Shimada, P.P. Guengerich, Construction of a human cytochrome P4501A1:ratNADPH-cytochrome P450 reductase fusion cDNA and expression in *Escherichia coli*, purification and catalytic properties of the enzyme in bacterial cells and after purification, *Arch. Biochem. Biophys.* 330 (1996) 48–58.
- [141] D.W. Nebert, The AH locus-genetic differences in toxicity, cancer, mutation, and birth-defects, *Crit. Rev. Toxicol.* 20 (1989) 153–174.
- [142] P.J. Wedlund, S. Kimura, F.J. Gonzalez, D.W. Nebert, I462V mutation in the human CYP1A1 gene-lack of correlation with either the Msp I 1.9 kb (m2) allele or CYP1A1 inducibility in a 3-generation family of east Mediterranean descent, *Pharmacogenetics* 4 (1994) 21–26.
- [143] P.P. Guengerich, Cytochrome-P450 enzymes, *Am. Sci.* 81 (1993) 440–447.
- [144] N. Shiota, A. Nagasawa, T. Sakaki, Y. Yabusaki, H. Ohkawa, Herbicide-resistant tobacco plants expressing the fused enzyme between rat cytochrome P4501A1 (CYP1A1) and yeast NADPH-cytochrome P450 oxidoreductase, *Plant Physiol.* 106 (1994) 17–23.
- [145] G.R. Harlow, J.R. Halpert, Mutagenesis study of Asp-290 in cytochrome P450 2B11 using a fusion protein with rat NADPH-cytochrome P450 reductase, *Arch. Biochem. Biophys.* 326 (1996) 85–92.
- [146] O. Sibbesen, J.J. de Voss, P.R.O. de Montellano, Putidaredoxin reductase-putidaredoxin-cytochrome P450cam tri-

- ple fusion protein, *J. Biol. Chem.* 271 (1996) 22462–22469.
- [147] F.J. Dilworth, S.M. Black, Y.-D. Guo, W.L. Miller, G. Jones, Construction of a P450c27 fusion enzyme: a useful tool for analysis of vitamin D₃ 25 hydroxylase activity, *Biochem. J.* 320 (1996) 267–271.
- [148] J.A. Harikrishna, S.M. Black, G.D. Szklarz, W.L. Miller, Construction and function of fusion enzymes of the human cytochrome-P450c27 system, *DNA Cell Biol.* 12 (1993) 371–379.
- [149] P. Cao, H. Bulow, B. Dumas, R. Bernhardt, Construction and characterisation of a catalytic fusion protein system: P450 11 β -adrenodoxin reductase-adrenodoxin, *Biochim. Biophys. Acta* 1476 (2000) 253–264.
- [150] T. Lacour, H. Ohkawa, Engineering and biochemical characterisation of the rat microsomal cytochrome P4501A1 fused to ferredoxin and ferredoxin-NADP⁺ reductase from plant chloroplasts, *Biochim. Biophys. Acta* 1433 (1999) 87–102.
- [151] T. Sakaki, S. Kominami, K. Hayashi, M. Akiyoshi-Shibata, Y. Yabusaki, Molecular engineering study on electron transfer from NADPH-P450 reductase to rat mitochondrial P450c27 in yeast microsomes, *J. Biol. Chem.* 271 (1996) 26209–26213.
- [152] T. Sakaki, S. Kominami, S. Takemori, H. Okhawa, M. Akiyoshi-Shibata, Y. Yabusaki, Kinetic studies on a genetically engineered fused enzyme between rat cytochrome P450 1A1 and yeast NADPH-P450 reductase, *Biochemistry* 33 (1994) 4933–4939.
- [153] J. Kraulis, *J. Appl. Crystallogr.* 24 (1991) 946–950.

Phenylalanine 393 Exerts Thermodynamic Control over the Heme of Flavocytochrome P450 BM3

Tobias W. B. Ost, Caroline S. Miles, Andrew W. Munro, Jane Murdoch, Graeme A. Reid, and Stephen K. Chapman

Department of Chemistry, University of Edinburgh, West Mains Road, Edinburgh, EH9 3JJ, U.K., Institute of Cell and Molecular Biology, University of Edinburgh, Mayfield Road, Edinburgh, EH9 3JT, U.K., and Department of Biochemistry, The Adrian Building, University of Leicester, University Road, Leicester, LE1 7RH, U.K.

Biochemistry[®]

Reprinted from
Volume 40, Number 45, Pages 13421–13429

Phenylalanine 393 Exerts Thermodynamic Control over the Heme of Flavocytochrome P450 BM3[†]

Tobias W. B. Ost,^{*,‡} Caroline S. Miles,[§] Andrew W. Munro,^{||} Jane Murdoch,[§] Graeme A. Reid,[§] and Stephen K. Chapman[‡]

Department of Chemistry, University of Edinburgh, West Mains Road, Edinburgh, EH9 3JJ, U.K., Institute of Cell and Molecular Biology, University of Edinburgh, Mayfield Road, Edinburgh, EH9 3JT, U.K., and Department of Biochemistry, The Adrian Building, University of Leicester, University Road, Leicester, LE1 7RH, U.K.

Received April 9, 2001; Revised Manuscript Received September 4, 2001

ABSTRACT: Site-directed mutants of the phylogenetically conserved phenylalanine residue F393 were constructed in flavocytochrome P450 BM3 from *Bacillus megaterium*. The high degree of conservation of this residue in the P450 superfamily and its proximity to the heme (and its ligand Cys400) infers an essential role in P450 activity. Extensive kinetic and thermodynamic characterization of mutant enzymes F393A, F393H, and F393Y highlighted significant differences from wild-type P450 BM3. All enzymes expressed to high levels and contained their full complement of heme. While the reduction and subsequent treatment of the mutant P450s with carbon monoxide led to the formation of the characteristic P450 spectra in all cases, the absolute position of the Soret absorption varied across the series WT/F393Y (449 nm), F393H (445 nm), and F393A (444 nm). Steady-state turnover rates with both laurate and arachidonate showed the trend WT > F393Y ≫ F393H > F393A. Conversely, the trend in the pre-steady-state flavin-to-heme electron transfer was the reverse of the steady-state scenario, with rates varying F393A > F393H ≫ F393Y ≈ wild-type. These data are consistent with the more positive substrate-free [−312 mV (F393A), −332 mV (F393H)] and substrate-bound [−151 mV (F393A), −176 mV (F393H)] reduction potentials of F393A and F393H heme domains, favoring the stabilization of the ferrous-form in the mutant P450s relative to wild-type. Elevation of the heme iron reduction potential in the F393A and F393H mutants facilitates faster electron transfer to the heme. This results in a decrease in the driving force for oxygen reduction by the ferrous heme iron, so explaining lower overall turnover of the mutant P450s. We postulate that the nature of the residue at position 393 is important in controlling the delicate equilibrium observed in P450s, whereby a tradeoff is established between the rate of heme reduction and the rate at which the ferrous heme can bind and, subsequently, reduce molecular oxygen.

The cytochromes P450¹ are a superfamily of heme *b*-containing monooxygenase enzymes (1). They are widespread in all life forms (from bacteria through to man) and are notable for their diversity in substrate selectivity. The best understood P450 systems are the bacterial P450cam (camphor hydroxylase from *Pseudomonas putida*) and P450 BM3 (fatty acid hydroxylase from *Bacillus megaterium*) (2, 3). Study of the crystal structures (4, 5) of these soluble enzymes has enabled the design of site-directed mutants, allowing the roles of several key amino acids to be determined. Despite similar tertiary structure, these two enzymes belong to two different classes of P450. P450cam is a class I (or B-class) P450, receiving electrons from a

two component reductase system (ferredoxin and NADH-ferredoxin reductase) (6). P450 BM3 is a class II (or E-class) P450, receiving electrons from a eukaryotic-like diflavin NADPH-cytochrome P450 reductase fused to the P450 in one continuous polypeptide (7). This fused arrangement of its redox partners correlates with the high catalytic activity of P450 BM3 and makes the system very convenient as a model for mechanistic studies of P450s and P450-related enzymes (such as the nitric oxide synthases) (8).

Comparisons of the amino acid sequences of all P450s reveal only a few residues which are implicitly conserved throughout the superfamily. One of these is the cysteine that provides the thiolate ligand to the heme iron (Cys400 in P450 BM3) (Figure 1). In addition there are several residues, located close to this ligand, which display high conservation within what is termed the "heme binding" motif (9). A phenylalanine residue (F393 in P450 BM3) is almost totally conserved within this region, with a small number of exceptions, including the dehydratase P450 74 (an allene oxide synthase from flax seed) and P450 10 from the pond snail *Lymnaea stagnalis*, with potential involvement in steroid synthesis (10, 11). The analogous residues are proline and tryptophan, respectively. This high level of conservation

[†] The research was performed with support from the Edinburgh Protein Interaction Centre (EPIC), the BBRSC (studentship to T.W.B.O. and Postdoctoral funding to C.S.M. and J.M.), The Royal Society of Edinburgh and the Leverhulme Trust (A.W.M.).

* To whom correspondence should be addressed. Phone: +44 131 6507386. Fax: +44 131 6504760. E-mail: skc03@holyrood.ed.ac.uk.

[‡] Department of Chemistry.

[§] Institute of Cell and Molecular Biology.

^{||} Department of Biochemistry.

¹ Abbreviations: P450, cytochrome P450 monooxygenase; PMSF, phenylmethanesulfonyl fluoride; SHE, standard hydrogen electrode; ΔG, Gibbs' free-energy; NOS, nitric oxide synthase.

Cyp101 (cam)	345	V	S	H	T	T	<u>E</u>	G	H	G	S	H	L	<u>C</u>	L	G	Q	H	L	362
Cyp102 (BM3)	388	H	A	F	K	P	<u>E</u>	G	N	G	Q	R	A	<u>C</u>	I	G	Q	Q	F	405
Cyp6A1 (Housefly)	437	L	D	W	L	G	<u>E</u>	G	D	G	P	R	N	<u>C</u>	I	G	M	R	F	444
Cyp2E1 (Rabbit)	425	D	Y	F	K	P	<u>E</u>	S	A	G	K	R	V	<u>C</u>	V	G	E	G	L	442
Cyp11A1 (Human)	450	F	R	N	L	G	<u>E</u>	G	W	G	V	R	Q	<u>C</u>	L	G	R	R	I	467
Cyp74 (flaxseed)	477	P	E	T	E	T	<u>P</u>	S	V	A	N	K	Q	<u>C</u>	A	G	K	D	F	494
Cyp10 (snail)	481	T	S	Q	L	V	<u>W</u>	G	H	G	A	R	M	<u>C</u>	L	G	R	R	I	499

FIGURE 1: Sequence alignment within the heme-binding region of selected P450s (2, 26–29). The alignment shows the implicitly conserved cysteine residue which provides the sixth ligand to the heme iron of all P450s (dotted box). Seven residues downstream is located the highly conserved phenylalanine, corresponding to Phe 393 of P450 BM3 (grey box). Two of the known P450s lacking this phenylalanine are also shown, where the phenylalanine is replaced by a tryptophan (10) or a proline (11) (solid box).

highlights the importance of this residue, yet, to date, no satisfactory explanation as to its role has been made. Previously, the aromatic side chain of the corresponding phenylalanine in P450 cam (F350) was proposed to participate directly in electron transfer to the P450 heme in a cytochrome *b₅*/P450 complex (12). Mutagenesis of this phenylalanine in rat liver P450 1A2 (F449) and rabbit P450 2E1 (F429) and subsequent characterization of the mutant enzymes led the investigators to different conclusions (with respect to P450 cam) regarding its role. In P450 1A2, F449 mutants showed diminished catalytic capacity and were affected in heme binding (13). In P450 2E1, only an effect on heme binding was observed in F429 mutants (14). However, neither study has conclusively resolved the question as to the conserved phenylalanine's importance in the catalytic competence of P450s. To elucidate its role, we describe here a series of comprehensive studies, characterizing both the kinetic and thermodynamic properties of site-directed mutants at phenylalanine 393 in flavocytochrome P450. Our results indicate that F393 is not essential for heme incorporation, but does have a key role in controlling the electronic properties of the heme system. We postulate that the interaction between this residue and the heme iron–sulfur bonding system is central to the control of the reactivity of oxygen with the ferrous heme.

EXPERIMENTAL PROCEDURES

Escherichia coli Strains and Plasmid Vectors. *Escherichia coli* TG1 [*supE*, *hsdΔ5*, *thi*, Δ (*lac-proAB*), *F'* [*traΔ36*, *proAB*⁺, *lacI*^q, *lacZΔM15*]] was used for all cloning work and for overexpression of intact P450 BM3 and its component cytochrome domain. The preparation of plasmids for the overexpression of intact P450 BM3 (pBM23) and heme domain (P450, residues 1–472; pBM20) has been described in previous publications (15, 16). Mutants F393A, F393H, and F393Y (intact) and F393A-HD, F393H-HD, and F393Y-HD (HD denotes heme domain) were constructed by oligonucleotide-directed mutagenesis of pBM23 and pBM20 respectively, using the Kunkel method (17, 18). Single-stranded DNA was prepared using the helper phage M13K07. Oligonucleotide primers used in the mutagenesis procedures were as follows (mismatches are indicated by the underlined bases and the names of the resulting expression plasmids are in parentheses): F393A and F393A-HD (pCM36, pCM80), 5'CTGACCGTTTCCAGCCGGTTTAAACGC 3'; F393H and F393H-HD (pCM 37, pCM81), 5' CTGACCGTTTCCATGCGGTTTAAACGC 3'; F393Y, and F393Y-HD (pCM 109, pCM125), 5' CCGTTTCCATACGGTTTAAAC 3'.

To ensure that no secondary mutations had occurred, pCM 36, pCM37, and pCM109 were sequenced by the dideoxy chain termination method. These plasmids were digested with restriction enzymes *Sna*BI and *Spe*I, generating a 3 kbp fragment containing the required mutation. The *Sna*BI/*Spe*I fragment was then ligated with the 4 kbp band liberated from a similar digestion of pBM23 (containing the WT P450 BM3 coding sequence under the control of the native CYP102 promoter) generating pJM1, pJM2, and pJM3, respectively.

Mutants were overexpressed in *E. coli* strain TG1 in an identical fashion to the wild-type clone.

Enzyme Preparations. All flavocytochromes P450 (wild-type and mutants) were purified from *E. coli* TG1 transformants (which express the P450 to high levels in the stationary phase under the control of the authentic promoter from *Bacillus*) by growth of transformant cultures (2–5 L of Luria-Bertani medium at 37 °C with shaking at 200 rpm) for ~36 h after entry into the stationary phase. For the heme domains of wild-type and mutants, cells were induced (1 mM IPTG) at an *A*₆₀₀ = 1, and growth was continued for 6–12 h prior to harvesting cells. Cells were disrupted by sonication. A similar purification protocol was employed for all enzymes using ion-exchange chromatography on DEAE-Sephacel and hydroxyapatite, as described previously (19). A final step (HiLoad 26/10 Q-Sepharose high performance column attached to a Pharmacia FPLC system, with protein elution gradient 0 to 500 mM KCl in 50 mM Tris·HCl/1 mM EDTA, pH 7.4) was employed to maximize the final purity of all the proteins. PMSF (1 mM) was added to all buffers to minimize proteolysis. All pure proteins were concentrated to >500 μM by ultrafiltration and were stored at –20 °C after dialysis against two successive 500-fold volumes of buffer A (50 mM Tris HCl, pH 7.4) containing 50% (v/v) glycerol. Enzymes were used within 1 month of isolation.

Spectrophotometric Analysis of Fatty Acid and Carbon Monoxide Binding to P450s. UV–vis absorption spectra were recorded over the 300–800 nm range using a Shimadzu 2101 spectrophotometer and quartz cuvettes of 1 cm path length. Typically, the concentration of wild-type or mutant P450 BM3 used was 1–5 μM in 1 mL of assay buffer (20 mM MOPS/100 mM KCl pH 7.4) at 30 °C.

Fatty Acid Binding Titrations. For enzyme titrations with arachidonic acid, aliquots (0.1–0.5 μL; not exceeding 3 μL total addition) of a 33 mM solution (in ethanol) were added to the enzyme solution (1–5 μM in assay buffer). For enzyme titrations with sodium laurate, 10 μL aliquots of P450 BM3 (1–5 μM in assay buffer) were withdrawn and replaced with aliquots of a solution of enzyme at identical concentration in the same buffer, but containing in addition 1 mM

sodium laurate. Spectra were recorded after each addition of substrate. Difference spectra were generated by subtraction of each spectrum recorded from the substrate-free spectrum. Dissociation constant (K_d) values were determined by plotting the maximal absorbance changes calculated from each difference spectrum against the concentration of substrate, and fitting the data to a rectangular hyperbola using Origin software (Microcal).

Carbon Monoxide Binding. Fe–CO complexes of wild-type and the mutant enzymes were prepared in the same fashion. Proteins were reduced by the addition of a few grains of sodium dithionite and were converted to the P450-complex by slow bubbling of the solutions with carbon monoxide gas for one minute.

Steady-State Kinetics. All steady-state kinetic measurements were performed at 30 °C in assay buffer using 1 cm path-length quartz cuvettes. Initial rates of fatty acid (arachidonate and laurate) oxidation were measured as described previously (20), by monitoring the oxidation of NADPH at 340 nm (ϵ_{340} 6.21 mM⁻¹ cm⁻¹) with 10–100 nM enzyme and NADPH at saturating concentration (200 μ M). The initial arachidonate concentration was varied by addition of small volumes (<2.0 μ L) from a 33 or 3.3 mM ethanolic stock using a 10 μ L Hamilton gastight syringe (Hamilton, Reno, NV), and the initial laurate concentration was varied by dilution of a 1 mM aqueous stock. Rate measurements were converted into activity units, s⁻¹ (mol of NADPH oxidized/s per mol of P450) and plotted against fatty acid concentration. Data were fitted to the Michaelis–Menten equation using Origin software.

Determination of Enzymatic Coupling Efficiency. The coupling efficiencies of wild-type and the F393A, F393H, and F393Y mutant holoenzymes were determined by negative-ion electrospray mass spectrometry. Turnover assays were performed on each P450 under limiting concentrations of NADPH and excess arachidonate and oxygen (980 μ L of 20 mM MOPS, pH 7.4, 4 μ L of 33 mM arachidonate, 5 μ L of 19.7 mM NADPH, and 10 μ L of 4 μ M P450). Reactions were initiated by addition of P450. The air-saturated concentration of oxygen in aqueous solution was \sim 260 μ M (21). Under these conditions, NADPH consumption can only be coupled to product formation or oxygen reduction (due to the absence of other electron acceptors in the assay and with both [substrate] and [oxygen] in excess of [NADPH]). Samples of each reaction mixture were injected into the mass spectrometer (Micromass Platform electrospray mass spectrometer) and analyzed under the following conditions: ESI-ve, cone voltage = 35 V, acquired range 150–500 Da. The concentration of unreacted substrate (m/z 303) and hydroxylated substrate (m/z 319) in each reaction mixture was evaluated from the total ion current for each peak (MassLynx software). The concentration of NADPH was calculated from its absorption spectrum (ϵ_{340} = 6.21 mM⁻¹ cm⁻¹). All appropriate controls were run, and under these conditions, no interfering signals from NADPH, buffer, or enzyme were observed, with monohydroxylated arachidonate being the only observable product. The reactions were performed at 30 °C and conditions were optimized so that each reaction proceeded to completeness (total consumption of NADPH) within 30 s of initiation by addition of the catalytic concentration of enzyme. The quoted percent coupling was calculated from the relative stoichiometries of NADPH

consumed to product formed, and is an average of four separate experiments for each P450.

Pre-Steady-State Kinetics of Heme Reduction. Measurement of the rate of the first flavin-to-heme electron transfer step was performed at 30 °C as described previously (16) using CO-saturated buffers and monitoring the formation of the ferrous-CO adduct at 450 nm using an Applied Photo physics stopped-flow spectrophotometer (SX. 17MV). One syringe contained NADPH (200 μ M) and the second syringe contained intact wild-type or mutant P450 BM3 (1–5 μ M). Both syringes contained assay buffer of identical substrate concentration (arachidonate or laurate), previously deoxygenated (by bubbling extensively with oxygen-free nitrogen) and saturated with CO by bubbling for 5 min. Rates for each substrate concentration were obtained by fitting the progress curves obtained to a double exponential function using the Applied Photophysics. The k_{lim} values were calculated by plotting the observed rates (k_{obs}) at a variety of substrate concentrations against fatty acid concentration, and fitting the data to the Michaelis–Menten equation using Origin software.

Generation of the Oxy-Ferrous Complex. All experiments were conducted within a Belle Technology glovebox under a nitrogen atmosphere ([O₂] < 5 ppm). Samples of wild-type HD, F393A-HD, F393H-HD, and F393Y-HD (\sim 2 μ M) were prereduced by addition of a few grains of sodium dithionite. Excess dithionite was removed by elution of the protein through an anaerobic Biorad Econo-pac 10DG gel-filtration column, pre-equilibrated with degassed 100 mM MOPS, pH 7.0, ensuring no direct reduction of oxygen by dithionite. Generation of the oxy-ferrous complex was attempted by addition of 2.6 μ M O₂ (addition of a 10 μ L aliquot of air-saturated buffer) to 1 mL of reduced P450 (2 μ M). The reaction was monitored at 424 nm over a 300 s time period, using a Shimadzu Multispec 1501 diode array UV–vis spectrophotometer. Experiments were conducted at 15 °C.

Potentiometric Titrations. All redox titrations were conducted within a Belle Technology glovebox under a nitrogen atmosphere, with the oxygen concentration maintained at less than 5 ppm. Degassed, concentrated enzyme samples (WT-HD, F393A-HD, F393H-HD, and F393Y-HD) were eluted through an anaerobic Bio-Rad Econo-pac 10DG gel filtration column, pre-equilibrated with 100 mL of degassed buffer (100 mM potassium phosphate, pH 7.0) immediately upon admission of the sample to the glovebox. This ensured removal of all traces of oxygen. Enzyme solutions (\sim 20 μ M in 10 mL total volume) were titrated electrochemically according to the method of Dutton (22) using sodium dithionite (from a 34 mM stock) as reductant and potassium ferricyanide (from a 18 mM stock) as oxidant. Mediators were added to facilitate electrical communication between enzyme and electrode, prior to titration. Typically, 7.0 μ M 2-hydroxy-1,4-naphthoquinone, 0.3 μ M methyl viologen, and 1.0 μ M benzyl viologen were included in the 10 mL sample volume (to mediate in the range –95 to –195 mV, –380 to –480 mV, and –260 to –360 mV, respectively). After a sufficient equilibration period (typically 10–15 min) following each reductive/oxidative addition, visible spectra were recorded over a 300–800 nm range using a Shimadzu 2101 UV–vis spectrophotometer contained within the anaerobic environment. The electrochemical potentials of the equilibrated

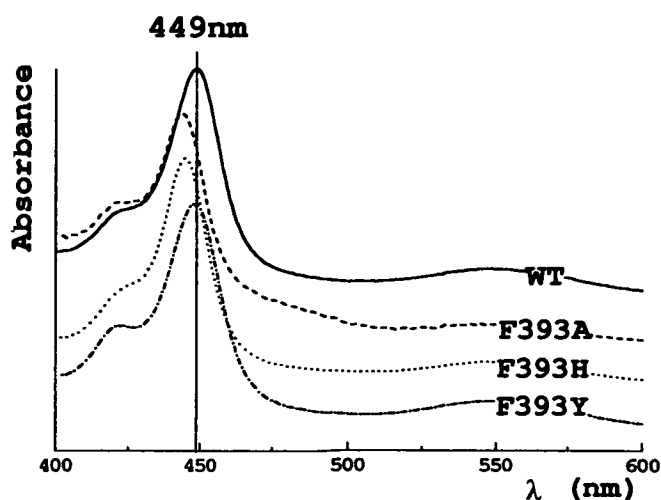


FIGURE 2: UV-vis spectra of the ferrous-CO complexes of wild-type P450 BM3 and F393A, F393H, and F393Y mutant forms. The spectra highlight the deviation in the position of the Soret absorption maximum. The spectra have been offset along the absorbance axis in the order indicated, for clarity. The Soret peak positions were blue-shifted by 4 nm (F393H), 5 nm (F393A), and 0 nm (F393Y) relative to that of wild-type ($A_{\max} = 449$ nm, vertical line).

sample solutions were monitored using a CD740 meter (WPA) coupled to a Pt/calomel combination electrode (Russell pH Ltd.) at 25 ± 2 °C. The electrode was calibrated using the $\text{Fe}^{3+}/\text{Fe}^{2+}$ EDTA couple as a standard (+108 mV). A factor of +242 mV was employed to correct relative to the standard hydrogen electrode. For substrate-bound redox titrations, arachidonate was added to the sample prior to the titration. Conversion to the high-spin form was observed spectrophotometrically as a shift from 418 to 390 nm. The K_M values for arachidonate for all the enzymes studied were much lower than $10 \mu\text{M}$. Therefore, $33 \mu\text{M}$ arachidonate was sufficient in all cases to saturate the P450 (no further spin-state shift was observed upon further additions of substrate).

RESULTS

Overexpression and Purification of Mutant Enzymes. The successful overexpression and subsequent purification of the holoenzymes F393A, F393H, and F393Y, along with the heme domains (HD) F393A-HD and F393H-HD, immediately negated the previous assumption that phenylalanine 393 (Phe393) was essential for heme incorporation and stability. All mutant enzymes expressed to high levels, similar to wild-type, and remained stable when stored at -20 °C. All of the enzymes generated a native-like P450 absorbance spectrum, with no P420 contribution. An absorption peak at 420 nm would indicate the presence of enzyme with non-cysteine heme ligation.

Spectrophotometric Analysis of Carbon Monoxide Binding. Typically, treatment of a sample of reduced P450 with carbon monoxide will generate the characteristic P450-CO Soret absorption at 450 nm. This was the case for both wild-type P450 BM3 ($A_{\max} = 449$ nm) and the most conservative mutant F393Y. However, a ~ 5 nm blue-shift in the P450-CO Soret absorption for mutants F393A ($A_{\max} = 444$ nm) and F393H ($A_{\max} = 445$ nm) was observed (Figure 2). This indicates a change in the strength, and hence the vibrational energy, of the CO bond, induced by changes in the degree

Table 1: Substrate Dissociation Constants (K_d) for Wild-Type and F393 Mutants of P450 BM3^a

	K_d (μM)			
	wild-type	F393A	F393H	F393Y
arachidonate	3.6 ± 0.3	2.6 ± 0.3	7.6 ± 0.5	4.2 ± 0.3
laurate	241 ± 9	230 ± 11	525 ± 10	520 ± 9

^a Parameters were determined as described in the Experimental Procedures.

of back-bonding from the ferrous heme iron to the CO antibonding orbitals. This is indicative of changes in the electron density at the iron. High electron density increases the degree of back-bonding to the CO antibonding orbitals, effectively weakening the CO bond, accompanied by a decrease in the $\text{Fe}^{\text{II}}-\text{CO}$ vibrational energy (absorption would be red-shifted). A blue shift in the $\text{Fe}^{\text{II}}-\text{CO}$ absorption is indicative of an increase in the strength of the CO bond (less back-bonding) as a direct result of a decrease in the electron density at the heme iron. Substitution of phenylalanine by either histidine or alanine appears to decrease the electron density of the heme iron, providing evidence that stabilization of the ferrous forms of mutants F393A and F393H is favored more so than in wild-type. The nature of the residue at position 393 appears to have an influence over this fundamental property of the heme. The most conservative substitution of phenylalanine (by tyrosine) does not appear to affect significantly the heme environment as its spectral properties are identical to wild-type.

Fatty Acid Binding. The values for the dissociation constants for arachidonate and laurate binding to wild-type P450 BM3 and the mutant enzymes F393A, F393H, and F393Y are shown in Table 1. The major observation is that changing the nature of the side chain of residue 393 does not significantly alter the fatty acid-binding properties of the enzyme. This is intuitive considering the fact that the mutation is on the opposite side of the heme to the substrate-binding channel. Although mutations of Phe393 appeared to have little effect on substrate binding, differences in the degree of spin state shift (low- to high-spin) associated with the dehydration of the ferric iron center are apparent. For wild-type P450 BM3, there is a correlation between the degree of spin-state conversion and both the K_d and chain length of saturated fatty acid substrates. Fatty acids of chain length C_{15} and C_{16} (pentadecanoic and palmitic acids) have the lowest K_d values, and induce the largest degree of spin-state change. However, these substrates are highly insoluble in water. Lauric acid has better solubility in aqueous media (to approximately 1.2 mM) and has a K_d of $\sim 250 \mu\text{M}$. A much better substrate for P450 BM3 than any of the saturated fatty acids is the C_{20} , tetra-unsaturated arachidonic acid ($K_d \approx 4 \mu\text{M}$), which also has acceptable water solubility. Arachidonate induces a much greater spin-state shift than laurate (>95 and <40%, respectively). Comparisons between the mutants and wild-type P450 BM3 show differences in the degree of spin-state conversion with lauric acid. The arachidonate-induced ($33 \mu\text{M}$) spin-state shift for wild-type and all mutants was >95%, whereas the laurate-induced (1.0 mM) spin-state shift varies across the series $\text{F393A} > \text{F393Y} > \text{WT} > \text{F393H}$, with F393A giving $\sim 12\%$ higher proportion of the high-spin form than wild-type P450 BM3 (Figure 3).

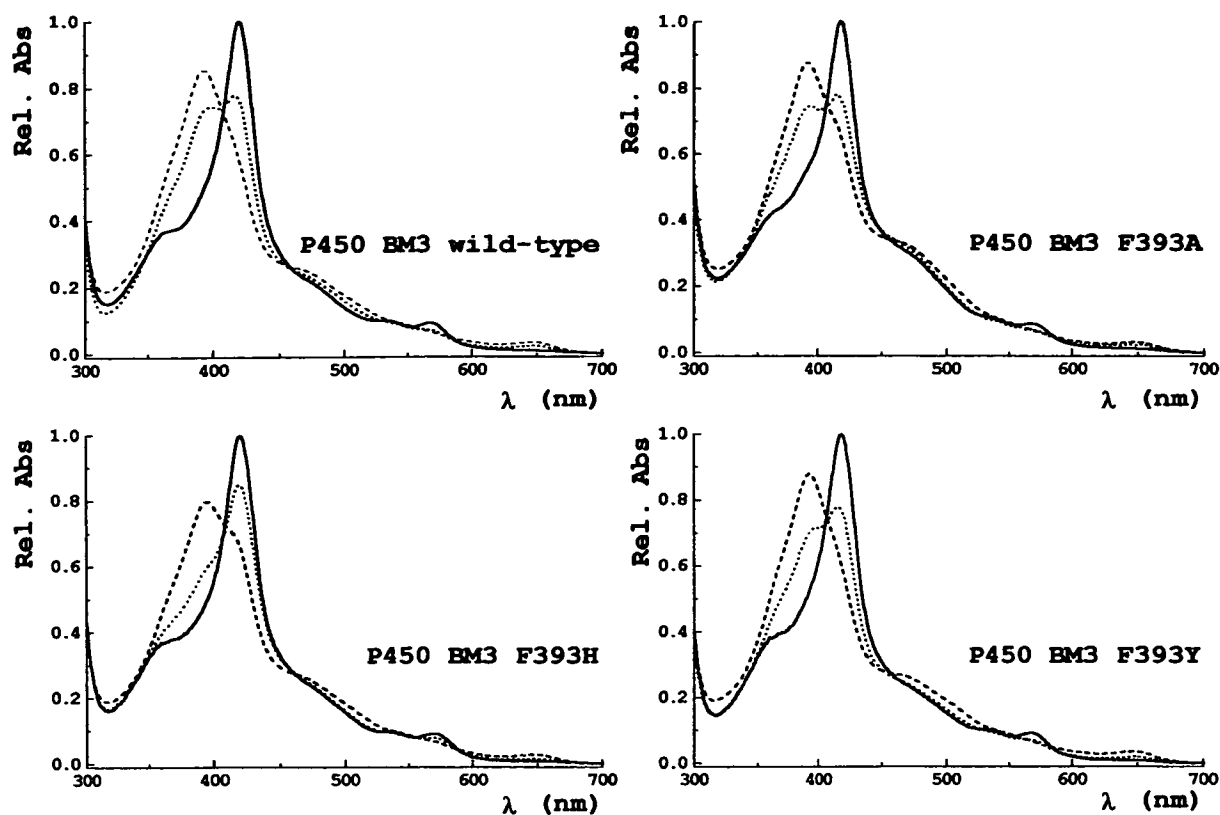


FIGURE 3: UV-vis spectra of the ferric (solid line), laurate (dotted line)-, and arachidonate-saturated (dashed line) forms of wild-type P450 BM3 and the F393A, F393H, and F393Y mutants. Rel. Abs. = relative absorbance compared to ferric Soret absorption maximum in each case. Arachidonate (33 μ M) induces near-complete shift in spin-state in all forms. Laurate induces a much lower degree of spin-state shift in all enzymes, with F393H showing the smallest proportion of high-spin ferric heme at saturation with laurate (1 mM).

Table 2: Steady-State Kinetics of Fatty Acid (arachidonate and laurate)-Stimulated NADPH Oxidation by Wild-Type and F393 Mutant Flavocytochrome P450 BM3^a

	wild-type		F393A		F393H		F393Y	
	K_M (μ M)	k_{cat} (s^{-1})	K_M (μ M)	k_{cat} (s^{-1})	K_M (μ M)	k_{cat} (s^{-1})	K_M (μ M)	k_{cat} (s^{-1})
arachidonate	4.7 \pm 0.3	285 \pm 3	2.7 \pm 0.3	21 \pm 1	3.8 \pm 0.5	33 \pm 1	9.5 \pm 1.1	143 \pm 8
laurate	288 \pm 15	86 \pm 2	18.5 \pm 2.7	29 \pm 1	60 \pm 5	37 \pm 1	274 \pm 20	65 \pm 2

^a Parameters were determined as described in the Experimental Procedures.

Kinetics of Fatty Acid Oxidation. Although binding of the fatty acids was essentially unaffected by the nature of the residue at position 393, steady-state kinetic analysis shows significant differences in the rates of turnover of the mutant flavocytochromes compared to wild-type (Table 2). For both arachidonate and laurate oxidation, the observed trend in k_{cat} was WT > F393Y \gg F393H > F393A. The differences in turnover are most obvious when arachidonate is the substrate, with 14-, 8-, and 2-fold decreases in k_{cat} for F393A, F393H, and F393Y, respectively, compared to wild-type P450 BM3. Although the magnitude of the difference between wild-type P450 BM3 and the mutants is smaller when laurate is the substrate, the trend is the same. Clearly some step in the catalytic cycle, other than substrate binding, has been perturbed and has become rate-limiting in the mutant enzymes.

The coupling efficiencies for wild-type, F393Y, and F393H (\sim 90%) for arachidonate hydroxylation are all within experimental error of each other (Table 3) and suggest near exclusive coupling of NADPH oxidation to product formation. While the coupling of the F393A mutant is lower than the other P450s studied, this decrease cannot fully account

Table 3: Coupling Efficiency of the Wild-Type and F393 Mutant Holoenzymes in the Presence of Arachidonate, as Determined by Electrospray Mass Spectrometry^a

	[unreacted substrate] (mM)	[product] (mM)	% coupling
wild-type	43 \pm 3	89 \pm 7	91 \pm 11
F393A	77 \pm 6	55 \pm 5	56 \pm 8
F393H	53 \pm 4	79 \pm 6	81 \pm 10
F393Y	39 \pm 3	93 \pm 7	95 \pm 11

^a The concentrations of unreacted substrate and product were calculated from the total ion count for the negative ion of each relevant species in the mass spectrum, as outlined in the Experimental Procedures. In each case, the starting concentrations of arachidonate and NADPH were 132 and 99 μ M, respectively. Percent coupling was determined from the relative stoichiometries of NADPH consumed to product generated.

for the order of magnitude difference observed between the steady-state parameters for the F393A mutant with respect to wild-type.

This indicates that all enzymes are catalytically functional, and that the lowered catalytic activity observed for all the F393 mutants is due to decreased rate(s) of steps in the

Table 4: Pre-Steady-State Kinetics of Heme Reduction in Wild-Type and F393 Mutant Flavocytochromes P450 BM3^a

	wild-type		F393A		F393H		F393Y	
	K_d (μM)	k_{lim} (s^{-1})	K_d (μM)	k_{lim} (s^{-1})	K_d (μM)	k_{lim} (s^{-1})	K_d (μM)	k_{lim} (s^{-1})
arachidonate	13.8 ± 2.0	348 ± 17	19.3 ± 3.5	1176 ± 78	13.3 ± 2.9	832 ± 53	6.4 ± 0.8	366 ± 11
laurate	300 ± 65	172 ± 14	124 ± 13	468 ± 11	291 ± 37	439 ± 20	400 ± 42	215 ± 10

^a Rates were determined in the presence of both arachidonate and laurate substrates as described in the Experimental Procedures.

catalytic cycle after substrate binding and not as a result of the uncoupled reduction of oxygen.

Kinetics of Heme Reduction. To investigate whether the kinetics of flavin-to-heme electron transfer in the F393 mutants was affected, we undertook stopped-flow experiments to determine the rate of this process. The rate of the first electron-transfer step from the reductase FMN to the substrate-bound P450 BM3 heme can be conveniently measured using CO-saturated buffer, monitoring the formation of the ferrous iron-CO adduct at 450 nm (16). For each of the mutant flavocytochromes (F393A, F393H, and F393Y), the rate of flavin-to-heme electron transfer at 30 °C was measured by rapid mixing of CO-saturated solutions of (a) NADPH (200 μM) and substrate (either arachidonate at concentrations between 0 and 80 μM , or laurate at concentrations between 0 and 1000 μM) and (b) wild-type or mutant flavocytochrome (1–5 μM) and substrate (equal concentration to mixture a). The observed initial fast-phase rate constants (k_{obs}) for heme reduction were plotted against substrate concentration and fitted to a rectangular hyperbola. From these data, maximal apparent rates of first electron transfer to the heme iron (k_{lim}) and apparent dissociation constants for the substrates (K_d) were obtained and are shown in Table 4. The trend in k_{lim} F393A > F393H \gg F393Y \approx WT was the reverse of that observed for the steady-state turnover of both laurate and arachidonate. Thus, although steady-state experiments suggest an overall decrease in the turnover rates of these F393 mutant enzymes, the first flavin-to-heme electron transfer reaction is actually faster in all the mutant enzymes than in wild-type. In the wild-type P450 BM3, the apparent rate of flavin-to-heme electron transfer (as measured by the formation rate of the ferrous-CO adduct) is 348 s^{-1} , where the overall turnover rate of the enzyme is 285 s^{-1} (in the presence of arachidonate). Clearly, this microscopic rate is the major determinant of catalytic turnover rate, as observed previously (19). However, with the F393A and F393H mutants, the situation is markedly different. For instance, in F393A, the flavin-to-heme rate is 1176 s^{-1} but the steady-state rate is only 21 s^{-1} . Evidently, a step after the first electron transfer to the heme iron has become rate limiting in these mutants.

Generation of the Oxy-Ferrous Complex of F393A-HD. Binding of oxygen to the ferrous wild-type heme domain and F393Y-HD was too transient to be monitored on a macroscopic time scale. Addition of oxygenated buffer to the prereduced protein led to immediate oxidation to the ferric resting state, without noticeable formation of any oxyferrous intermediate. This was unsurprising considering that the oxyferrous intermediate has only been transiently observed for wild-type P450 BM3 at cryogenic temperatures (23). However, the formation of the oxyferrous complex for the F393A-HD and F393H-HD was observed (Figure 4) and had a half-life of approximately 30 s. This result provides evidence that the reaction between oxygen and the ferrous

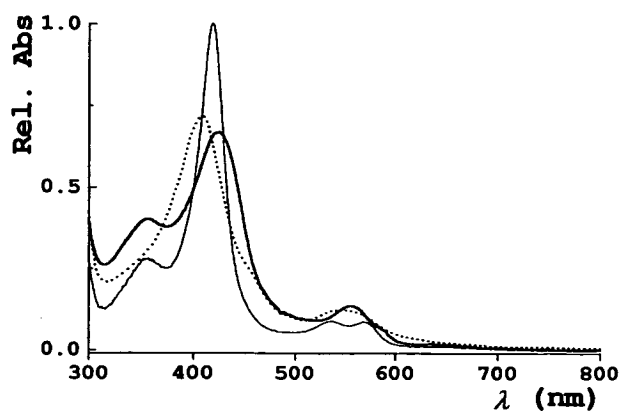


FIGURE 4: UV-vis spectra showing formation of the stable oxyferrous intermediate of P450 BM3 F393A mutant. The spectra were generated prior to (ferrous, dotted line), immediately after (oxyferrous, heavy solid line), and 300 s after (low-spin ferric, light solid line) addition of 2.6 μM oxygenated buffer to a sample of prereduced protein.

iron is significantly faster in wild-type and F393Y than in either F393A or F393H. It also suggests an increase in the stability of the ferrous-form of the F393A and F393H mutants with respect to wild-type, allowing the stable binding of oxygen to the heme for a appreciable period prior to eventual reoxidation of the heme. This supports the idea that the substitution of phenylalanine 393 alters considerably the reactivity of the P450 heme with molecular oxygen.

Heme Domain Potentiometric Titrations. The substrate-free and arachidonate-saturated (33 μM) reduction potentials of wild-type HD, F393A-HD, F393H-HD, and F393Y-HD were measured in an attempt to establish effects of the mutations on the thermodynamic properties of these variants. Figure 5 shows the spectral shifts observed during the course of these potentiometric titrations. At the high P450 concentration ($\sim 20 \mu\text{M}$) required for efficient communication between the P450/mediators/electrode, the absorption at the Soret maximum is much too high for accurate spectrophotometric measurement. A convenient part of the spectrum that reflects accurately the change in reduction state of the heme iron at this P450 concentration is the region between 460 and 470 nm. Therefore, data for the substrate-free titrations at 465 nm were plotted against measured potential (mV vs SHE). Due to the spectral differences generated upon addition of substrate to the enzymes, substrate-saturated titrations were evaluated differently, plotting the difference in absorbance $A_{484} - A_{730}$ against measured potential (Figure 6). Data were fitted to a one-electron Nernst function, and values obtained are presented in Table 5. The first observation is that the reduction potential of the wild-type P450 BM3 heme iron has been more accurately re-determined in light of improved experimental techniques. The more negative reduction potential determined fits better to the proposed redox organization within P450 BM3. At this potential, the substrate-induced redox switch (24) can still operate, since

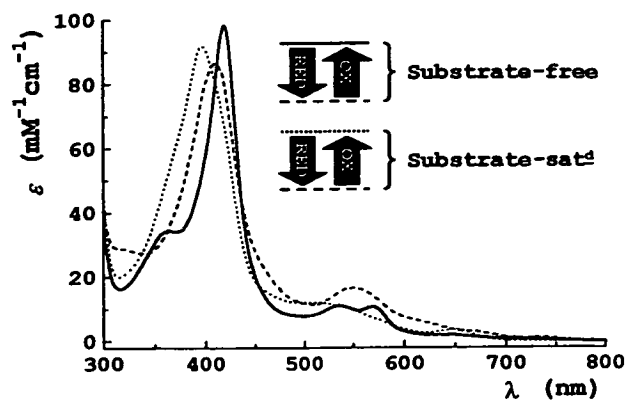


FIGURE 5: UV-vis spectra showing spectral changes associated with reduction of substrate-free (low-spin) and substrate (arachidonate)-saturated P450 BM3 (high-spin) heme domain. For the wild-type ferric enzyme (solid line), the substrate-free Soret maximum is at 418 nm, and for the substrate-bound form (dotted line) it is located at 390 nm. In both cases, the fully reduced ferrous form (dashed line) has its Soret maximum at approximately 410 nm. The millimolar extinction coefficients of the different species are indicated. The reduction of all heme domains was freely reversible (reduction by dithionite, oxidation by ferricyanide) with minimal hysteresis. Complete reoxidation of the ferrous-form results in the regeneration of the initial starting spectra (ferric low- or high-spin).

binding of substrate increases the reduction potential by 138 mV (to -289 mV) allowing electron transfer from NADPH, through the reductase and ultimately to the heme. However, there is tighter control than previously imagined over uncoupling by virtue of the fact that the substrate-free heme potential is considerably more negative than that of the physiological electron donor NADPH (-320 mV) in the low-spin ferric form of wild-type P450 BM3. The midpoint potentials of the two mutants F393A and F393H are considerably more positive than wild-type (-312 and -332 mV, respectively) and both display similar magnitudes of reduction potential shift upon substrate binding to wild-type (~ 140 – 160 mV shift). The more positive heme reduction potentials of these two mutants are also consistent with the higher rates of flavin-to-heme electron transfer observed. A thermodynamic consequence of the more positive reduction potentials of the heme iron is an increase in the stabilization of the ferrous form. This is borne out by the ability to generate the ferrous form ($A_{\max} = 410$ nm) for the F393H and F393A mutant P450s aerobically, whereas this is achievable only under strictly anaerobic conditions for the wild-type P450 BM3. It is notable that the increase in reduction potential correlates to the relative size of the side chain at position 393. As the steric bulk is decreased (Phe/Tyr \rightarrow His \rightarrow Ala), the reduction potential increases accordingly (-427 / $-418 \rightarrow -332 \rightarrow -312$ mV).

DISCUSSION

Phenylalanine 393 of P450 BM3 is one of only a small number of residues highly conserved throughout the P450 superfamily. While previous mutagenesis studies have been performed to characterize mutants at this position in other P450s (e.g., 2E1, 1A2) (13, 14) no satisfactory explanation has been offered as to why this residue should be a phenylalanine or how this residue may influence P450 mechanism. What is clear (in the case of P450 BM3 as well as those P450s studied previously) is that changing the nature

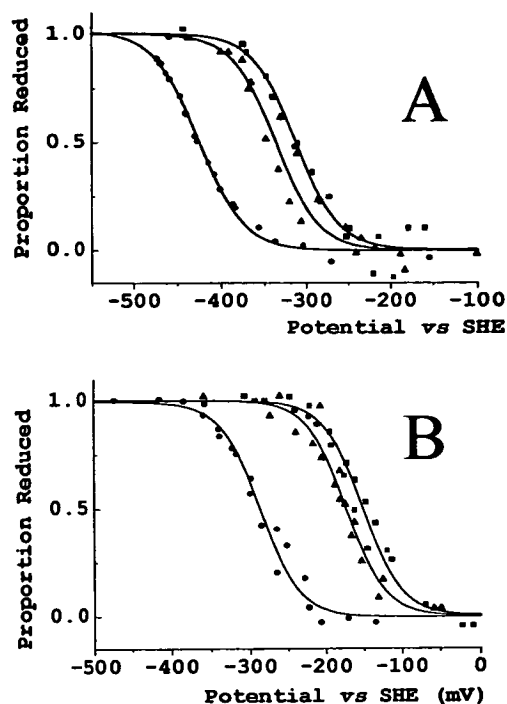


FIGURE 6: Heme-domain reduction potentials of wild-type and mutant P450s BM3. Overlaid, normalized one-electron Nernst curves showing the changes in the proportion of reduced species with reduction potential (vs standard hydrogen electrode) are presented. The data for F393Y-HD is essentially identical to WT-HD, and has been omitted for clarity. From these, the midpoint potentials of the substrate-free (A) and arachidonate-saturated (B) wild-type heme domain (circles), F393A-HD (squares), and F393H-HD (triangles) were determined (Table 5). The measured heme reduction potentials of both the F393A-HD and F393H-HD (substrate-free and substrate-saturated) mutants are considerably more positive than wild-type heme domain (between 95 and 138 mV) suggesting stabilization of their ferrous forms. The substrate-induced redox shift, observed for wild-type (24), still operates in the F393A, F393H mutants (whereby addition of substrate causes a 138–161 mV increase in the reduction potential), suggesting that substrate binding exerts the same type of control over the heme reduction potential as observed in wild-type. The nature of the residue at position 393 appears to control the thermodynamic properties of the heme.

Table 5: Midpoint Heme Reduction Potentials for Substrate-Free and Arachidonate-Saturated Wild-Type and F393 Mutant P450s BM3

	midpoint potential (mV)			
	WT-HD ^a	F393A-HD	F393H-HD	F393Y-HD
substrate-free	-427 ± 4	-312 ± 4	-332 ± 6	-418 ± 6
arachidonate-sat ^d	-289 ± 5	-151 ± 4	-176 ± 4	-295 ± 6

^a HD denotes heme domain.

of this residue has severe implications on the catalytic competence of the resultant mutants compared with native forms. The purpose of our study was to attempt to resolve the role of this conserved phenylalanine using the flavocytochrome P450 BM3 system. Certain parallels can be drawn between our data and those reported previously for mutants of P450 1A2 (e.g., similar blue-shifts in the ferrous-CO spectra) (13) and P450 2E1 (slower turnover kinetics) (14). However, in the light of our studies, it is clear that previous assumptions made as to the role of the phenylalanine (decreased enzyme stability and alteration of electron flow) are unlikely to fully account for the observed decreases in

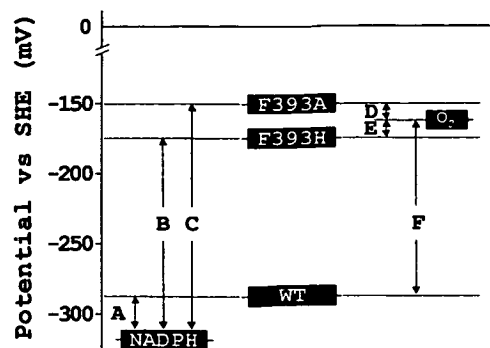


FIGURE 7: Diagrammatic representation of relevant reduction potentials in the P450 BM3 system. The reduction potentials of NADPH (-320 mV), the arachidonate-saturated heme domains of wild-type (-289 mV), F393A (-151 mV), F393H (-176 mV), and the one electron reduction potential of oxygen to superoxide (-160 mV) are presented. A much greater driving force is associated with heme reduction for the mutants F393A/H (B, C) compared to wild-type (A), while the gap in reduction potential associated with oxygen reduction is much smaller for the mutants F393A/H (D, E) compared to wild-type (F).

catalytic activity. It is clear that F393 plays a much more important and fundamental role—by controlling the ability of P450 BM3 to bind and activate molecular oxygen.

The successful overexpression of F393A, F393H, and F393Y mutants demonstrates the lack of a requirement for a phenyl ring to stabilize heme binding. Also, the kinetic profiles of these mutant enzymes dismisses the argument that this residue is essential in facilitating electron transfer to the heme. We have shown that while the F393A and F393H enzymes are less catalytically competent (lower turnover rate), the study of individual steps in the catalytic cycle reveals that the rate of heme reduction is actually faster for these mutants than for wild-type. Thus, replacement of the phenylalanine can actually elevate the rate of heme reduction. Hence, contrary to previous suggestions, the residue is non-essential for mediation of electron transfer, either directly or indirectly, to the heme. It is not required absolutely for electron transfer, but instead plays a vital role in the control of the process. The question is then one of how this control is achieved. The most convenient starting point for discussion is with the thermodynamic data obtained from the potentiometric titrations. All other results are consistent with, and can be explained in light of, data from these experiments.

Substitution of phenylalanine 393 by either histidine or alanine results in an increase of the heme iron reduction potential with respect to wild-type P450 BM3, whereas the reduction potential is unchanged upon substitution by tyrosine. This explains the apparent contradiction in effects on steady state (decreased) and heme reduction (increased) kinetic rates observed for the mutants relative to wild-type P450 BM3. Creating a large positive gap in reduction potential between the electron donor [NADPH at -320 mV ultimately providing the electron(s) to the FMN semiquinone at -213 ± 5 mV] and the substrate-bound heme (e.g., -151 ± 4 mV for F393A) increases the driving force (ΔG) for heme reduction in this system (Figure 7). The observed increase in pre-steady-state flavin-to-heme electron-transfer kinetics ($k_{\text{lim}} = 1180$ s $^{-1}$ cf. 348 s $^{-1}$ for wild-type P450 BM3) is totally consistent with the more positive reduction potentials of heme iron (suggesting stabilization of the ferrous form) in the F393A and F393H mutants. However, the fact

that F393A and F393H mutants give much lower steady-state rates of fatty acid-dependent NADPH oxidation is explained by the concomitant decrease in driving force for molecular oxygen to superoxide (-160 mV, Figure 7). Thus, whereas having alanine or histidine at position 393 facilitates faster electron transfer to the heme iron, the rate at which the ferrous iron can then reduce bound molecular oxygen is much lowered, with a net large decrease in enzyme turnover rate.

Substrate affinity for these mutant enzymes is not significantly perturbed compared to wild-type, and the rate of substrate-induced spin-state change is known to be rapid from previous studies (16). For wild-type P450 BM3, the rate of first electron transfer to the ferric heme (348 s $^{-1}$ with arachidonate) is similar to the steady-state k_{cat} for turnover of this substrate (285 s $^{-1}$), indicating that the sequence of events leading to the first electron transfer to the heme plays a major role in turnover rate limitation. In contrast, in the F393A and F393H mutants, not only are the rates of heme reduction elevated (1176 and 832 s $^{-1}$, respectively, with arachidonate), but the steady-state turnover rates are diminished (21 and 33 s $^{-1}$, respectively). Obviously, there is a new major factor in overall rate limitation that occurs after the first heme reduction and, presumably, does not involve substrate binding. This factor almost certainly reflects the increased stability of the oxy-ferrous form in the mutants. The elevated reduction potential of their hemes results in decreased driving force for reduction of bound dioxygen, leading to the oxy-ferrous form being considerably more stable than the superoxy-ferric form. This is borne out by the observation that in the mutants with the most positive heme reduction potential (F393A and F393H), the substrate-saturated, oxy-ferrous form is not only observable ($A_{\text{max}} = 424$ nm), but also has a long half-life (~ 30 s) at 15 °C. Under similar conditions, the decay of the oxy-ferrous form of wild-type P450 BM3 is virtually instantaneous, and even at cryogenic temperatures, the species can be observed only transiently (23). The consequence of the elevated heme reduction potential in F393A and F393H is that oxygen activation is disfavored and that the stabilized oxy-ferrous intermediate becomes a thermodynamic trap, which decreases the rate of overall catalysis. It appears likely that, in these mutants, oxygen reduction replaces heme reduction as the overall rate-limiting step.

In conclusion, we have established for flavocytochrome P450 BM3 that the phylogenetically conserved phenylalanine residue F393 has an important role in control of the reduction potential of the P450 heme iron. As evidenced by a combination of steady-state and stopped-flow studies, we have shown that the ability to poise the heme potential appropriately is critical for efficient catalysis. The physical origin of these catalytic modifications is still unclear and are presently under investigation. In ongoing studies, we are characterizing site-directed mutant F393W. In the nitric oxide synthases (NOSs), a tryptophan residue is conserved in place of the phenylalanine (25). Analysis of this mutant may allow a clearer understanding of the differences in catalytic properties of NOS and the P450s.

ACKNOWLEDGMENT

The authors wish to thank Dr. S. N. Daff for his useful and constructive discussions.

REFERENCES

1. Munro, A. W., and Lindsay, J. G. (1996) *Mol. Microbiol.* **20**, 1115–1125.
2. Unger, B. P., Gunsalus, I. C., and Sligar, S. G. (1986) *J. Biol. Chem.* **261**, 1158–1163.
3. Narhi, L. O., and Fulco, A. J. (1986) *J. Biol. Chem.* **261**, 7160–7169.
4. Poulos, T. L., Finzel, B. C., and Howard, A. J. (1986) *Biochemistry* **25**, 5314–5322.
5. Ravichandran, K. G., Boddupalli, S. S., Hasemann, C. A., Peterson, J. A., and Deisenhofer, J. (1993) *Science* **261**, 731–736.
6. Mueller, E. J., Loida, P. J., and Sligar, S. G. (1995) Twenty five years of P450 cam research. in *Cytochrome P450: Structure, Mechanism and Biochemistry* (Ortiz de Montellano, P. R., Ed.) pp 83–124, Plenum Press, New York.
7. Narhi, L. O., and Fulco, A. J. (1987) *J. Biol. Chem.* **262**, 6683–6690.
8. Li, H. Y., Raman, C. S., Glaser, C. B., Blasko, E., Young, T. A., Parkinson, J. F., Whitlow, M.; Poulos, T. L. (1999) *J. Biol. Chem.* **274**, 21276–21284.
9. Nelson, D. R., Koymans, L., Kamataki, T., Stegeman, J. J., Feyereisen, R., Waxman, D. J., Waterman, M. R., Gotoh, O., Coon, M. J., Estabrook, R. W., Gunsalus, I. C., and Nebert, D. W. (1996) *Pharmacogenetics* **6**, 1–42.
10. Song, W.-C., Funk, C. D., and Brash, A. R. (1993) *Proc. Natl. Acad. Sci. U.S.A.* **90**, 8519–8523.
11. Teunissen, Y., Geraerts, W. P. M., van Heerikhuizen, H., Planta, R. J., Joosse, J. (1992) *J. Biochem.* **112**, 249–252.
12. Stayton, P. S., Poulos, T. L., and Sligar, S. G. (1989) *Biochemistry* **28**, 8201–8205.
13. Shimizu, T., Hirano, K., Takahashi, M., Hatano, M., and Fujii-Kuriyama, Y. (1988) *Biochemistry* **27**, 4138–4141.
14. Porter, T. D. (1994) *Biochemistry* **33**, 5942–5946.
15. Miles, J. S., Munro, A. W., Rospendowski, B. N., Smith, W. E., McKnight, J., and Thomson, A. J. (1992) *Biochem. J.* **288**, 503–509.
16. Munro, A. W., Daff, S., Coggins, J. R., Lindsay, J. G., and Chapman, S. K. (1996) *Eur. J. Biochem.* **239**, 403–409.
17. Kunkel, T. A. (1985) *Proc. Natl. Acad. Sci. U.S.A.* **82**, 488–492.
18. Zoller, M. J., and Smith, M. (1983) *Methods Enzymol.* **100**, 468–500.
19. Noble, M. A., Miles, C. S., Chapman, S. K., Lysek, D. A., Mackay, A. C., Reid, G. A., Hanzlik, R. P., and Munro, A. W. (1999) *Biochem. J.* **339**, 371–379.
20. Munro, A. W., Noble, M. A., Miles, C. S., Daff, S. N., Green, A. J., Quaroni, L., Rivers, S., Ost, T. W. B., Reid, G. A., and Chapman, S. K. (1999) *Biochem. Soc. Trans.* **27**, 190–196.
21. Abu-Soud, H. M., Ichimori, K., Presta, A., and Stuehr, D. J. (2000) *J. Biol. Chem.* **275**, 17349–17357.
22. Dutton, P. L. (1978) *Methods Enzymol.* **54**, 411–435.
23. Bec, N., Anzenbacher, P., Anzenbacherova, E., Gorren, A. C. F., Munro, A. W., and Lange, R. (1999) *Biochem. Biophys. Res. Commun.* **266**, 187–189.
24. Daff, S. N., Chapman, S. K., Turner, K. L., Holt, R. A., Govindaraj, S., Poulos, T. L., and Munro, A. W. (1997) *Biochemistry* **36**, 13816–13823.
25. Adak, S., Crooks, C., Wang, Q., Crane, B. R., Tainer, J. A., Getzoff, E. D., and Stuehr, D. J. (1999) *J. Biol. Chem.* **38**, 26907–26911.
26. Wen, L. P., and Fulco, A. J. (1987) *J. Biol. Chem.* **262**, 6676–6682.
27. Feyereisen, R., Koener, J. F., Farnsworth, D. E., and Nebert, D. W. (1989) *Proc. Natl. Acad. Sci. U.S.A.* **86**, 1465–1469.
28. Andersson, S., Davis, D. L., Dahlbäck, H., Jörnvall, H., and Russell, D. W. (1989) *J. Biol. Chem.* **264**, 8222–8229.
29. Chung, B., Matteson, K. J., Voutilainen, R., Mohandas, T. K., and Miller, W. L. (1986) *Proc. Natl. Acad. Sci. U.S.A.* **83**, 8962–8966.

BI010716M

Structural and Spectroscopic Analysis of the F393H Mutant of Flavocytochrome P450 BM3

**Tobias W. B. Ost, Andrew W. Munro, Christopher G. Mowat,
Paul R. Taylor, Antonio Pesseguiro, Armand J. Fulco,
Arthur K. Cho, Myles A. Cheesman, Malcolm D. Walkinshaw, and
Stephen K. Chapman**

Department of Chemistry, University of Edinburgh, West Mains
Road, Edinburgh, EH9 3JJ, U.K., Department of Biochemistry, The
Adrian Building, University of Leicester, University Road, Leicester
LE1 7RH, U.K., ICMB, University of Edinburgh, Mayfield Road,
Edinburgh, EH9 3JR, U.K., Department of Biological Chemistry, UCLA
School of Medicine, P.O. Box 951737, Los Angeles, California
90095-1737, Department of Molecular and Medical Pharmacology,
UCLA School of Medicine, P.O. Box 951735, Los Angeles, California
90095-1735, School of Chemical Sciences, University of East Anglia,
Norwich, NR4 7TJ, U.K.

Biochemistry[®]

Reprinted from
Volume 40, Number 45, Pages 13430-13438

Structural and Spectroscopic Analysis of the F393H Mutant of Flavocytochrome P450 BM3[†]

Tobias W. B. Ost,^{*‡} Andrew W. Munro,[§] Christopher G. Mowat,^{‡||} Paul R. Taylor,^{||} Antonio Pesseguiero,[‡] Armand J. Fulco,[‡] Arthur K. Cho,[#] Myles A. Cheesman,[∇] Malcolm D. Walkinshaw,^{||} and Stephen K. Chapman[‡]

Department of Chemistry, University of Edinburgh, West Mains Road, Edinburgh, EH9 3JJ, U.K., Department of Biochemistry, The Adrian Building, University of Leicester, University Road, Leicester LE1 7RH, U.K., ICMB, University of Edinburgh, Mayfield Road, Edinburgh, EH9 3JR, U.K., Department of Biological Chemistry, UCLA School of Medicine, P.O. Box 951737, Los Angeles, California 90095-1737, Department of Molecular and Medical Pharmacology, UCLA School of Medicine, P.O. Box 951735, Los Angeles, California 90095-1735, School of Chemical Sciences, University of East Anglia, Norwich, NR4 7TJ, U.K.

Received April 9, 2001; Revised Manuscript Received September 4, 2001

ABSTRACT: In the preceding paper in this issue [Ost, T. W. B., Miles, C. S., Munro, A. W., Murdoch, J., Reid, G. A., and Chapman, S. K. (2001) *Biochemistry* 40, 13421–13429], we have established that the primary role of the phylogenetically conserved phenylalanine in flavocytochrome P450 BM3 (F393) is to control the thermodynamic properties of the heme iron, so as to optimize electron-transfer both to the iron (from the flavin redox partner) and onto molecular oxygen. In this paper, we report a detailed study of the F393H mutant enzyme, designed to probe the structural, spectroscopic, and metabolic profile of the enzyme in an attempt to identify the factors responsible for causing the changes. The heme domain structure of the F393H mutant has been solved to 2.0 Å resolution and demonstrates that the histidine replaces the phenylalanine in almost exactly the same conformation. A solvent water molecule is hydrogen bonded to the histidine, but there appears to be little other gross alteration in the environment of the heme. The F393H mutant displays an identical ferric EPR spectrum to wild-type, implying that the degree of splitting of the iron *d* orbitals is unaffected by the substitution, however, the overall energy of the *d*-orbitals have changed relative to each other. Magnetic CD studies show that the near-IR transition, diagnostic of heme ligation state, is red-shifted by 40 nm in F393H relative to wild-type P450 BM3, probably reflecting alteration in the strength of the iron-cysteinate bond. Studies of the catalytic turnover of fatty acid (myristate) confirms NADPH oxidation is tightly coupled to fatty acid oxidation in F393H, with a product profile very similar to wild-type. The results indicate that gross conformational changes do not account for the perturbations in the electronic features of the P450 BM3 heme system and that the structural environment on the proximal side of the P450 heme must be conformationally conserved in order to optimize catalytic function.

The cytochromes P450¹ are a family of monooxygenase enzymes implicated in a wide variety of biosynthetic and degradative pathways in organisms throughout nature (1–3). One essential feature shared by all P450s is a cysteine-ligated *b*-type heme (protoporphyrin IX) cofactor (4). Replacement of this cysteine residue results in a lack of heme

incorporation yielding catalytically inactive enzyme (5). Sequence comparisons of P450s clearly illustrate the implicit conservation of this cysteine throughout the P450 superfamily. It has been proposed that the electron-donating character of this residue facilitates the stabilization of the putative Fe^{IV}=O oxyferryl reactive species (6, 7) and, hence, is considered as an integral structural and mechanistic feature required by P450s.

Although overall topology is common to all of the structurally characterized P450s, the degree of sequence identity is often quite low between members (<25% amino acid identity) (8). However, investigations into a number of highly conserved residues over a range of P450s (primarily those of P450 cam—the camphor hydroxylase from *Pseudomonas putida*, and P450 BM3—the fatty acid hydroxylase from *Bacillus megaterium*) indicate their necessity for controlling aspects of the P450 catalytic cycle. For example, residues homologous to Thr252 of P450cam are implicated in providing a hydrogen bond to ferrous-bound molecular oxygen, participating in oxy-ferrous complex stabilisation (9). Also, a tryptophan residue (Trp96 in P450 BM3)

[†] This work is a contribution from the Edinburgh Protein Interaction Centre (EPIC) funded by the Wellcome Trust and the BBSRC (T.W.B.O.). The authors would like to thank Prof. A. J. Thomson for the use of the MCD and EPR facilities at the School of Chemical Sciences, U.E.A., with support from the BBSRC and EPSRC through core funding to the Centre for Metalloprotein Spectroscopy and Biology (CMSB) under Grant BO1727.

* To whom correspondence should be addressed. Phone: +44 131 6507386. Fax: +44 131 6504760. E-mail: skc03@holyrood.ed.ac.uk.

[‡] Department of Chemistry.

[§] Department of Biochemistry.

^{||} ICMB.

[∇] Department of Biological Chemistry.

[#] Department of Molecular and Medical Pharmacology.

[∇] School of Chemical Sciences.

¹ Abbreviations: P450, cytochrome P450 monooxygenase; MCD, magnetic circular dichroism; GC/MS, gas chromatography/mass spectrometry; NOS, nitric oxide synthase.

interacting with the heme-propionates encourages heme binding and has been shown to have a controlling influence over the spin-state of the heme (10). The fact that the number of implicitly conserved residues common to all P450s constitutes only a small proportion of a "typical" P450 polypeptide infers that they are essential for catalytic competence and, hence, an evolutionary prerequisite.

Our previous study (11) has shown that substitution of one of these highly conserved residues, phenylalanine 393 (by alanine or histidine), in P450 BM3 results in a mutant form with appreciably different catalytic characteristics to wild-type. We have postulated this residue to be vital in controlling the reaction of the heme iron with molecular oxygen. The few examples in which this phenylalanine is not conserved fall into a small group of P450s which do not have to activate molecular oxygen. Examples of these are allene oxide synthase (Cyp74) (12), divinyl ether synthase (Cyp74) (13), prostacyclin synthase (Cyp8) (14), and thromboxane synthase (~Cyp3) (15). In all cases, the phenylalanine is substituted by either proline or tryptophan. Unlike typical P450s, these enzymes do not function as monooxygenases and do not require molecular oxygen or NAD(P)H-dependent P450 reductase for activity. These enzymes catalyze rearrangement or isomerization reactions, for which the activation of molecular oxygen is non-essential. This provides additional, yet unsubstantiated, evidence that this phenylalanine residue is intimately involved in steps in the P450 catalytic cycle, concerned with the binding and activation of molecular oxygen. The focus of our previous study (11) identified and characterized the catalytic differences of a series of F393-mutant enzymes, relative to wild-type. In this paper, we have attempted to resolve the origin of these perturbations to the kinetic and thermodynamic profile of wild-type P450 BM3 by focusing on spectroscopic and structural inspection of the mutant enzyme P450 BM3 F393H.

EXPERIMENTAL PROCEDURES

Escherichia coli Strains and Protein Preparation. Plasmids encoding the intact wild-type (pBM23), F393H (pCM37), and the heme domain of wild-type (pBM20) and F393H (pCM81) mutant enzymes were used to transform *Escherichia coli* strain TG1 (11). Cell growth and the extraction and purification of protein followed the same protocol as described previously (16).

Product Characterization. The products of the catalytic turnover of myristic acid (tetradecanoic acid) by wild-type P450 BM3 and F393H mutant were determined using gas chromatography/mass spectrometry according to the following methodology. A Hewlett-Packard 5971A GC/MS utilizing electron impact ionization (70 eV) instrument was used to determine structural information on the monohydroxylated metabolites of myristic acid. Metabolites were generated by incubation of 120 μ M myristate in the presence of 5 mM NADPH and a catalytic amount of P450 (ca. 1 nM) in 2 mL samples of 100 mM K_2HPO_4/KH_2PO_4 , pH 8. The metabolites were extracted into diethyl ether and converted to their methyl ester derivatives using diazomethane, before analysis by GC/MS. Chromatography of the samples was performed on a HP-35 capillary column (30 m \times 0.25 mm id \times 0.25 μ M film thickness) with a thermal gradient beginning at 100

Table 1: Characteristic Retention Times and Fragmentation Patterns of Myristate Metabolites Used to Identify the Site of Substrate Hydroxylation^a

position of hydroxylation retention time (min)	$\omega-1$ 24.66	$\omega-2$ 24.54	$\omega-3$ 24.23
fragment	<i>m/z</i>	<i>m/z</i>	<i>m/z</i>
M - CH ₃ (CH ₂) _{<i>n</i>-1}	243	229	215
M - CH ₃ (CH ₂) _{<i>n</i>-1} CH ₂ OH	211	197	183
M - CH ₃ (CH ₂) _{<i>n</i>-1} CHO	214	200	186

^a The conditions under which these data were generated is described in the Experimental Procedures.

°C for 0.5 min and increasing to 200 °C at a rate of 5 °C/min for 5 min and then to a final temperature of 250 °C at a rate of 10 °C/min. Injector temperature was set to 250 °C and the GC/MS transfer line was set at 280 °C. Column flow rate was set at 0.76 mL/min.

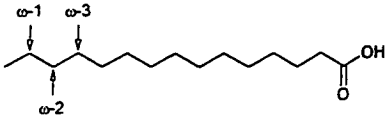
The mass spectra of the products from the control run (wild-type P450 BM3) were used to identify each GC peak. Monohydroxylated products were identified by their characteristic fragmentation pattern as shown in Table 1. The distribution of products was based on the relative peak area of the gas chromatogram, in which the total ion current was used to assess quantity.

UV-Vis Spectroscopy of Exogenous Ligand-Binding. The binding characteristics of azide, cyanide, imidazole, and pyridine (all from Aldrich and to the highest purity possible) to P450 BM3 wild-type and the F393H mutant were investigated. Protein concentrations in all cases were <5 μ M and were made up to 1 mL of total volume (100 mM MOPS, pH 7.0) in a 1 mL quartz cuvette (10 mm path length). Final ligand concentrations were no greater than 1.0 mM. The visible spectra of the ligand-bound P450s were taken in both the ferric- and ferrous-forms. Reduction was achieved by the addition of a few grains of dithionite to the cuvette. All spectrophotometric measurements were conducted using a Shimadzu 2101 Spectrophotometer at 25 °C.

MCD and EPR Spectroscopy. EPR spectra were recorded on an EPR spectrometer comprising an ER-200D electromagnet and microwave bridge interfaced to an EMX control system (Brüker Spectrospin) and fitted with a liquid helium flow cryostat (ESR-9, Oxford Instruments) and a dual-mode X-band cavity (Brüker, type ER4116DM). MCD spectra were recorded using circular dichrographs, JASCO models J-500D and J-730 for the UV-vis and near-infrared regions, respectively. An Oxford Instruments superconducting solenoid with a 25 mm ambient temperature bore was used to generate a magnetic field of 6 T for the room temperature MCD measurements. Room temperature MCD intensities are linearly dependent on magnetic field and are plotted normalized to magnetic field as $\Delta\epsilon/H$ ($M^{-1} cm^{-1} T^{-1}$).

Crystallography and Determination of the Crystal Structure of the F393H Heme Domain. Crystallization of F393H-HD (heme domain) was carried out by hanging drop vapor diffusion at 4 °C in Linbro plates. Crystals were obtained with a well solution comprising 100 mM sodium PIPES (piperazine-*N,N'*-bis[2-ethanesulfonic acid]), pH 6.5, 40 mM MgSO₄, 18–21% PEG 8000. Hanging drops of 4 μ L were prepared by adding 2 μ L of 41.7 mg/mL protein (in 50 mM TrisHCl/1 mM EDTA, pH 7.4) to 2 μ L of well solution. Plates of up to 1 \times 0.3 \times 0.3 mm were formed after about 1 week.

Table 2: Relative Proportions of Different Hydroxylated Metabolites from the Reactions of Wild-Type and F393H Mutant Flavocytochromes P450 BM3 with Myristic Acid^a



ENZYME	Product distribution (%)			Unreacted
	ω-1	ω-2	ω-3	
P450 BM3 WT	53.6	24.5	20.0	1.9
P450 BM3 F393H	57.7	22.5	15.0	4.8

^a Products were determined as described in the Experimental Procedures.

Crystals were immersed in well solution containing 22% glycerol as a cryoprotectant, before being mounted in nylon loops and flash-cooled in liquid nitrogen. A data set was collected to 2.0 Å ($\lambda = 1.3$ Å) on station 9.5 at Daresbury synchrotron source using a MAR CCD detector. The crystals are isomorphous with those of the hemoprotein domain of wild-type flavocytochrome P450 BM3, with space group $P2_1$ and cell dimensions $a = 58.8$ Å, $b = 153.0$ Å, $c = 61.4$ Å, and $\beta = 94.7^\circ$ and have two molecules in the asymmetric unit. This compares with unit cell dimensions of $a = 59.4$ Å, $b = 154.0$ Å, $c = 62.2$ Å, and $\beta = 94.7^\circ$ obtained for crystals of wild-type heme domain (17).

Data processing was carried out using the HKL package (18). The wild-type flavocytochrome P450 BM3 heme domain structure (2HPD), stripped of water, was used as the initial model. Electron density fitting was carried out using the program O (19). Restraints for the heme group were calculated from the CNS parameter file. Structure refinement was carried out using SHELX-97 (20). The atomic coordinates have been deposited in the Protein Data Bank (1JME).

RESULTS

Product Characterization. It is well established that wild-type P450 BM3 displays strict substrate-specificity for long-chain fatty acids, performing hydroxylation in a highly regio-specific manner. For wild-type enzyme, the sole hydroxylation products of palmitic acid are the ω -1, ω -2, and ω -3 hydroxy derivatives (21, 22). The same trend has been demonstrated here for the hydroxylation of myristate (Table 2) by the F393H mutant.

Previously reported substrate-binding characteristics of the F393H mutant enzyme indicated that its affinity for long-chain fatty acids was insensitive to the nature of the residue at position 393 (11). This mutant shows comparable affinity toward laurate and arachidonate as wild-type ($K_d = \sim 250$ and ~ 4 μ M, respectively). Characterization of the F393H-mediated turnover of myristate reveals an identical product profile to wild-type, indicating that both the substrate specificity and the regio-specificity of hydroxylation is unaffected by the F393H substitution. There is a virtually identical product profile to wild-type, although there appears to be a slightly higher proportion of the ω -1 metabolite with respect to the ω -3 product for F393H compared to wild-type. Notwithstanding this, the trend in regio-specificity between wild-type and the F393H mutant is the same (ω -1: ω -2: ω -3:unreacted = 28:13:11:1 (12:5:3:1), respectively). There is a slightly higher proportion of unreacted

myristate in the case of F393H turnover, resulting from the lower overall catalytic activity in this mutant, i.e., the F393H mutant turns over less myristate in the same time period as wild-type.

The important result is that the substitution of phenylalanine 393 by histidine results in a mutant-form that retains the same selectivity for long-chain fatty acids and displays the same regio-specificity of hydroxylation as wild-type P450 BM3.

Ligand Binding. Figure 1 shows the spectral characteristics of azide, cyanide, imidazole, and pyridine binding to wild-type (Figure 1a) and the F393H mutant (Figure 1b). The key features of the ferric, ferric ligand-bound and ferrous ligand-bound spectra are shown in Table 3.

For the F393H mutant, the ferrous spectrum in the presence of azide is identical to the ferrous, ligand-free spectra, the generation of which (in aerobic conditions) is only feasible due to its increased reduction potential. A similar argument can be made when pyridine is ligated. The F393H mutant displays a 19 nm red-shift (423 \rightarrow 442 nm) in the Soret absorption upon reduction of the ferric-pyridine complex. The wild-type ferric-pyridine complex can also be generated, but addition of dithionite fails to form the ferrous-pyridine form. This reflects the very negative wild-type heme reduction potential (-427 mV) compared to the more positive value (-332 mV) for the F393H mutant. This is substantiated by the ferrous-cyanide complex, where a shift in the Soret absorption peak (440 \rightarrow 437 nm) is observed (100% conversion) for F393H, yet incomplete conversion is observed ($\sim 50\%$) for wild-type. The ferrous-cyanide complex of wild-type seems to be intermediate between the ferric and ferric-cyanide complex, probably as a consequence of incomplete heme reduction.

Magnetic Circular Dichroism (MCD) Spectroscopy. The room-temperature UV-vis electronic spectrum of the F393H mutant is shown in Figure 2a, with its visible MCD spectrum in Figure 2b. Features at wavelengths 300–600 nm are due to π - π^* transitions of the porphyrin ring. Mixing of porphyrin- π with iron- d levels occurs to the extent that the spectra become diagnostic of the spin- and oxidation-state of the metal ion. This is especially so in the MCD where the spectroscopic changes are most pronounced (23, 24). At these wavelengths, the room-temperature MCD of F393H is almost identical in form to that of the WT P450 BM3 heme-domain (25).

The most informative low-spin ferric heme MCD feature is a positive-signed porphyrin (π)-to-ferric (d) charge transfer transition, the exact energy of which varies systematically with changes in axial ligation (26). In the room temperature near-infrared MCD of F393H (Figure 2c), this charge-transfer band is at ~ 1085 nm, a red-shift of ~ 40 nm relative to the WT heme-domain.

Electron Paramagnetic Resonance (EPR) Spectroscopy. Figure 3 shows the perpendicular-mode X-band EPR spectrum of F393H, recorded at 10 K using 2.01 mW microwave power. The g -values of features discussed are indicated on the figure. Minor signals at $g \approx 5.8$ and 4.3 are due to trace amounts of high-spin ferric heme and adventitious Fe^{III} ion, respectively. The three major features at $g = 2.43$, 2.25, and 1.92 are characteristic of a low-spin ferric heme and are virtually identical to those reported for the wild-type protein. These g -values are typical of native low-spin ferric P450s

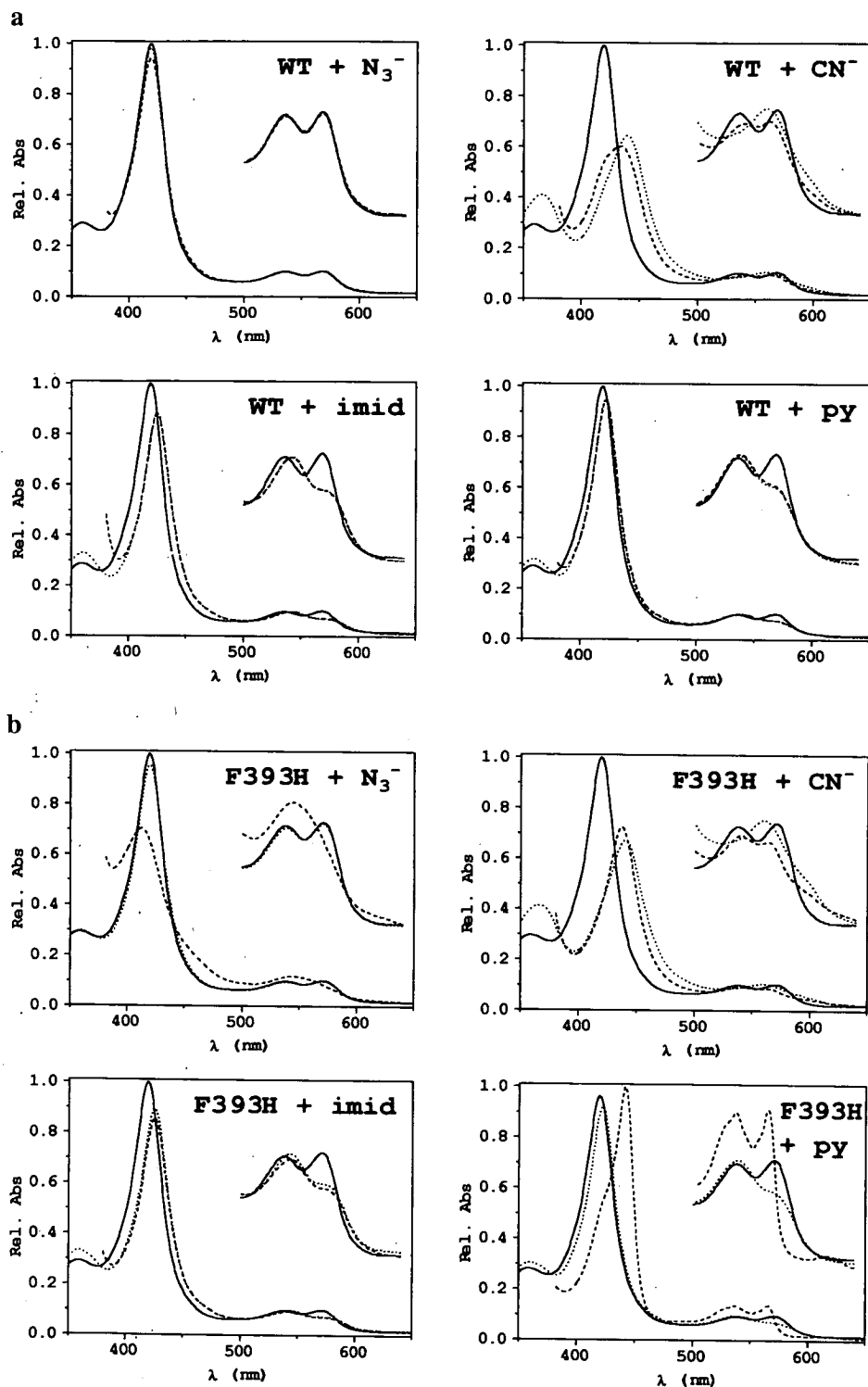


FIGURE 1: Visible spectra of azide (N_3^-), cyanide (CN^-), imidazole (imid), and pyridine (py) binding to wild-type P450 BM3 (Figure 1a) and to the F393H mutant (Figure 1b) in their oxidized (dotted line) and reduced (dashed line) ligand-bound forms. The spectra have been corrected to the same relative absorbance. The ligand-free, oxidized spectrum is also shown for each case (solid line) as a comparison.

and nitric oxide synthases (NOS) in which the heme is bound axially by cysteinate and water and also match those of adducts in which the water is displaced by a range of oxygen-donor ligands (27–31).

Determination of the F393H Crystal Structure. A data set to a resolution of 2.0 Å was used to refine the structure to a final *R*-factor of 17.9% (Table 4). The final model consists of two protein molecules, A and B, each containing residues Lys3–Leu188 and Asn201–Leu455, 1 heme, and a total of

1182 water molecules. For both molecules, the electron density for the first two N-terminal residues and the loop region containing residues Gln189–Glu200 was uninterpretable, so these have been omitted from the model. The rmsd fits [using the Dali server (32)] of all remaining C α atoms for the wild-type and F393H-HD enzymes have been calculated using all possible combinations of molecules A and B in either model. The smallest difference (0.3) is found by comparing F393H-HD chain A with wild-type chain A,

Table 3: Spectral Characteristics of Ligand Binding to Wild-Type and F393H Mutant Cytochromes P450 BM3^a

	absorption maxima (nm)					
	P450 BM3 wild-type			P450 BM3 F393H		
	Soret	α	β	Soret	α	β
Fe ^{III}	419	569	536	419	571	538
Fe ^{III} -N ₃ ⁻	419	569	536	419	571	538
Fe ^{III} -CN ⁻	440	560*		440	560*	
Fe ^{III} -imidazole	425	573	543	426	576	543
Fe ^{III} -pyridine	422	568	538	423	572	538
Fe ^{II}	407	550*		413	554*	
Fe ^{II} -N ₃ ⁻	419	569	536	413	554*	
Fe ^{II} -CN ⁻	434	563	541	437	564	540
Fe ^{II} -imidazole	425	573	543	426	576	543
Fe ^{II} -pyridine	422	568	538	442	565	538

^a The table illustrates the positions of the major heme absorption bands [α , β , and γ (or Soret)] for ferric- and ferrous-forms of the enzymes in the absence and presence of exogenous ligands azide, cyanide, imidazole and pyridine. Asterisks denote fused absorbance bands whose components cannot be resolved into two separate contributions. Spectra were collected as described in the Experimental Procedures.

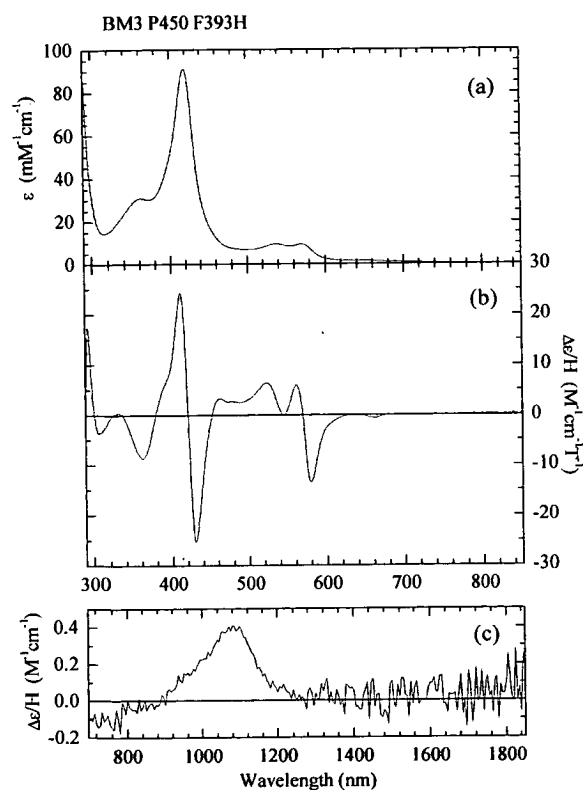


FIGURE 2: Spectral characteristics of P450 BM3 F393H heme domain, (a) electronic absorption spectrum, (b) UV-vis region MCD spectrum, (c) NIR-region MCD spectrum. MCD were recorded using a magnetic field of 6 T. MCD Sample concentration was 218 μ M.

and the largest (0.8) is found by comparison of F393H-HD chain A with wild-type chain B, indicating no significant structural differences. The regions surrounding residue 393 in the two structures is shown in Figure 4. Superposition of the phenyl ring of Phe393 from wild-type P450 BM3 onto His393 of F393H-HD molecule A is shown in Figure 5, and the comparison shows that the substitution causes little difference in the conformation of the residue side chain.

The only significant difference between the wild-type heme domain structure and the F393H-HD structure is the

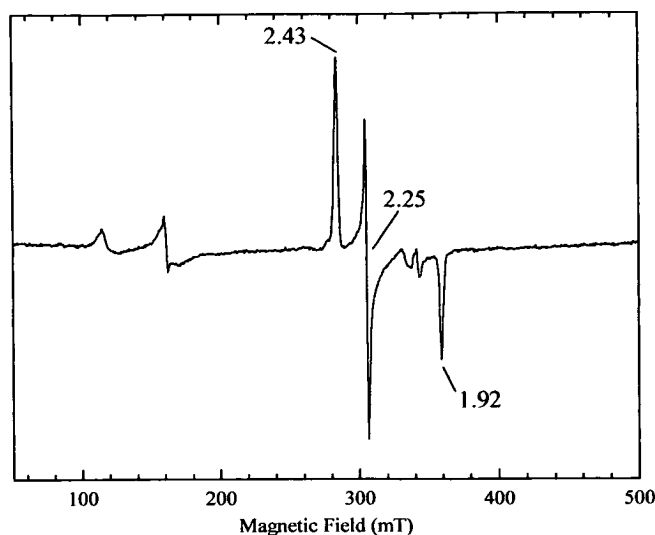


FIGURE 3: EPR spectrum of ferric P450 BM3 F393H heme domain. The spectrum was recorded at 10 K, using a 1 mT modulation and 2.01 mW microwave power. Sample concentration was 218 μ M. The g -values of 2.43, 2.25, and 1.92 are typical of low spin, ferric heme. Signals at $g \approx 5.8$ and 4.3 are due to small amounts of high spin ferric heme and adventitious iron.

Table 4: Crystallographic Data Statistics for the Crystal Structure of P450 BM3 Heme Domain Mutant F393H

refinement (\AA)	40.0–2.0
total no. of reflections	480 222
unique reflections	73 016
completeness (%)	96.9
$\langle I \rangle / \langle \sigma(I) \rangle$	19.4
R_{merge} (%) ^a	5.4
R_{merge} in outer shell (2.07–2.00) (%)	13.8
R_{cryst} (%) ^b	17.93
R_{free} (%) ^b	23.12
rmsd from restraint values	
bond length (\AA)	0.006
bond angle distance (\AA)	1.8
Ramachandran analysis	
most favored (%)	90.8
additionally allowed (%)	8.8

^a $R_{\text{merge}} = \sum |I - \langle I \rangle| / \sum I$ over all reflections. ^b $R_{\text{cryst}} = \sum |F_o - F_c| / F_o$; R_{free} calculated with 5.2% data withheld from refinement.

replacement of phenylalanine by histidine (Figure 5). The side chain of residue 393 is in a very similar position in both structures, sandwiched between the side chains of Pro392 and Gln403, with no major conformational changes of surrounding residues as a result of the mutation (Figure 6).

In the structure of the substrate-free wild-type heme domain, the distance of closest contact between Phe393 and Cys400 (the thiolate ligand to the heme iron) is 3.67 \AA , while in the structure of F393H-HD, the closest contact is between C δ 2 of the histidine side chain and C β of Cys400, a distance of 3.50 \AA (resulting from a slight tilt in the imidazole ring of H393, toward the heme ligand).

A possibility as to why the thermodynamic properties of the heme of the F393H mutant differ so much from wild-type is the ability for this histidine to be protonated and to form a hydrogen bond with Cys400 (analogous to the Trp...Cys hydrogen bond observed in NOS) (33). It can be seen from the structure of the mutant enzyme that there is a solvent water molecule (X526 in molecule A) positioned on the opposite side of His393 to the heme, which is hydrogen

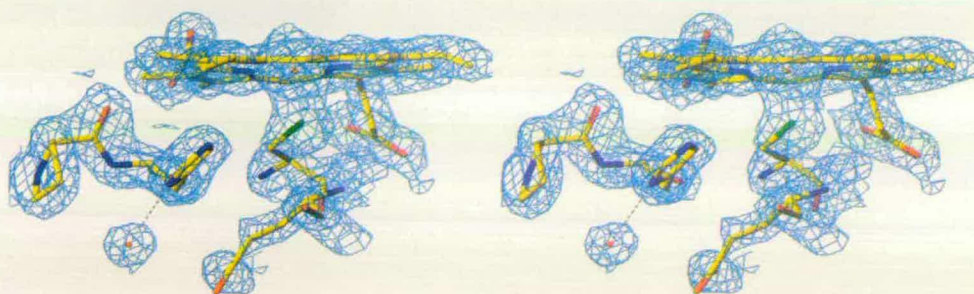


FIGURE 4: A stereoview of the heme binding region of the F393H mutant. Electron density is shown in cyan, while the heme macrocycle and peptide are shown in atom-type colors (red = oxygen, blue = nitrogen, and green = sulfur), the heme iron is depicted in orange. This figure clearly shows electron density for water molecule X and the likelihood of an intermolecular hydrogen bond to histidine 393. The electron density map was calculated using Fourier coefficients ($2F_o - F_c$), where F_o and F_c are the observed and calculated structure factors, respectively. The contour level is 1.5σ , where σ is the rms electron density. This diagram was generated using TURBO-FRODO (46).

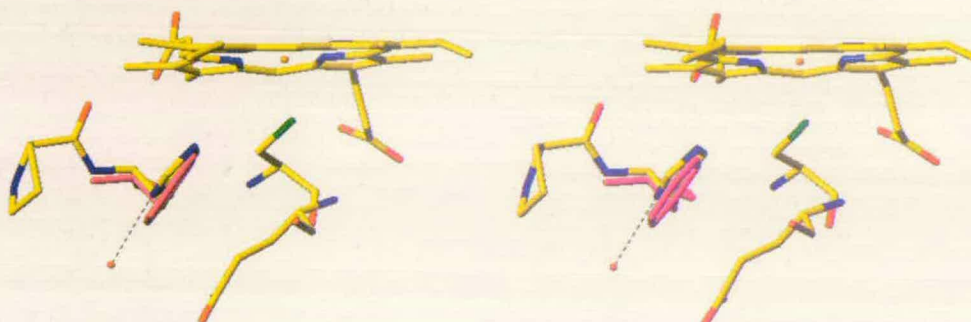


FIGURE 5: Superposition of phenylalanine 393 of wild-type P450 BM3 (magenta) onto histidine 393 of the F393H mutant. This clearly illustrates the minimal perturbation caused to the heme binding region by substitution of phenylalanine by histidine.

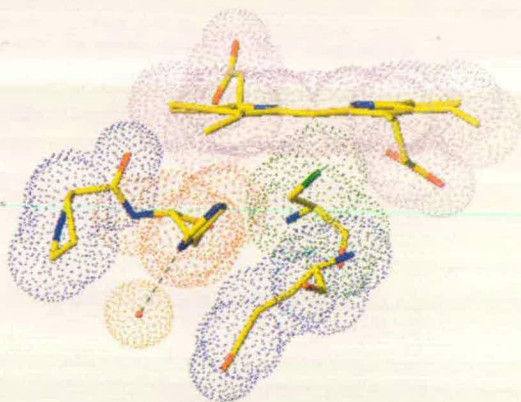


FIGURE 6: Constrained conformation of Phe393 in P450 BM3. The dotted regions describe the van der Waals surfaces of residues and the heme macrocycle surrounding histidine 393. The proximity of Pro392 and Gln403 prevents rotation of the imidazole ring of H393, precluding the possibility of the formation of an intramolecular H393...Cys400 hydrogen bond.

bonded to N δ 1 of the histidine side chain (N...O = 2.77 Å). The apparent protonation state of this histidine and the presence of an intermolecular hydrogen bond to water appears to preclude the formation of an intramolecular His393...Cys400 hydrogen bond.

DISCUSSION

Analysis of the F393H mutant of flavocytochrome P450 BM3 highlights the sensitivity of this enzyme to the nature of the residue at this position. Induced changes in the catalytic properties of the enzyme by substitutions at F393 suggest an important role for this residue, and have been discussed in detail in the previous paper (11). While the

effects on kinetic and thermodynamic properties have been experimentally substantiated, the physical process (i.e., the precise cause) by which these differences have occurred remained unresolved.

The product profile characterization of the F393H mutant confirmed the kinetics of NADPH oxidation described in the previous paper, with NADPH consumption being almost exclusively coupled to substrate turnover (~90% coupling) (11). Product analysis of the F393H mutant-catalyzed myristate-turnover was essentially identical to wild-type, with ω -1 hydroxylation predominating. No unusual oxidation products, suggestive of a change in the specificity of the mutant, were observed. From this we can conclude that F393 does not influence significantly the regio- and substrate-specificity of the enzyme. This is an important observation, confirming that F393H is able to act as a P450, yet is catalytically impaired relative to wild-type.

The EPR spectrum of the F393H mutant is identical to that of the wild-type enzyme. This infers that the iron in the ferric form is in a similar environment (no change in g values) in both enzymes and that they share a common ferric resting state. The form of the EPR spectrum is determined mainly by the relative splitting of the ferric d -orbitals, and if all five are moved in energy together by a process that does not substantially alter the iron geometry, then the spectrum would remain the same. It is surprising, therefore, that the elevation in the reduction potential of the heme does not induce a significant change in the EPR spectrum. This is our observation, which implies that the positive shift in the reduction potential of the F393H mutant relative to wild-type [reported previously (11)] is due to a difference in the energy of their ferrous-forms, relative to this common ferric ground state (Figure 7). Electrons are more easily introduced

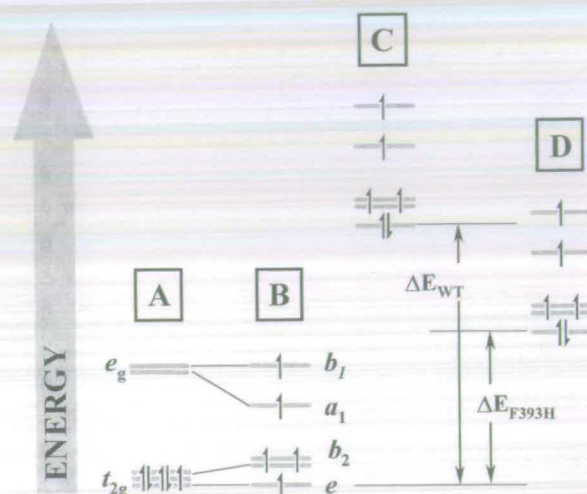


FIGURE 7: Diagrammatic representation of the proposed perturbation in the iron *d*-orbital energies between the ferric-resting state (A), the substrate-bound state (B), and the one-electron reduced forms of wild-type (C), and F393H mutant (D), caused by the substitution of phenylalanine 393 by histidine. The energy difference (ΔE) between the ferric- and ferrous-*d*-orbitals (related to the $\text{Fe}^{\text{III}}/\text{Fe}^{\text{II}}$ reduction potential by the Nernst equation, $\Delta G = -nF\Delta E$) is smaller for the F393H mutant (ΔE_{F393H}) than wild-type (ΔE_{WT}). This is consistent with the elevated reduction potential of the F393H mutant compared to the wild-type enzyme. The similarity of the ferric-EPR spectra for the F393H and wild-type enzymes suggest that the magnitude of the crystal field splitting parameter (Δ_0) is unchanged by the mutation.

to the iron frontier orbitals of the F393H mutant as a consequence of the difference in the energy (ΔE) between the ferric- and ferrous-forms being smaller than for wild-type. This is reflected in the $\text{Fe}^{\text{III}}/\text{Fe}^{\text{II}}$ couple for the F393H mutant being more positive than wild-type (reduction requires less energy). While this is an unusual observation, it is not unique. It has been demonstrated that loading the core of the bacterioferritin from *Azotobacter vinelandii* drops the reduction potential of its heme group by ~ 250 mV, without changes being observed in the EPR and MCD spectra of the loaded and unloaded forms (34). However, the most informative difference between wild-type and the F393H mutant is seen as a ~ 40 nm shift in the NIR charge transition in the MCD spectrum. This absorption has been assigned to a porphyrin (π) \rightarrow ferric (*d*) ligand to metal charge transition. The position of this band has been shown to vary greatly with axial ligation, for example a shift of ~ 350 nm is observed between a bis-his ligated (e.g., cytochrome *c*₃, *Desulfovibrio vulgaris*) and met-his ligated (e.g., cytochrome *b*₅₆₂, *E. coli*) heme (26). Although we are concerned with a six coordinate cys-aqua ligated heme in P450s, a similar interpretation can be employed, whereby the shift in the NIR-CT band arises not as a result of a change in the nature of the ligation, but due to a change in the strength (as a consequence of a change in length) of the Fe-Cys bond. Although our observed shift is considerably smaller than that observed for a ligand change, it is large enough to be significant and consistent with a change in axial bond strength rather than bond type. Whether the change in the strength of the Fe-S bond is equivalent to the same magnitude of shift in the reduction potential observed between wild-type and the F393H mutant, is questionable.

The crystal structure of the F393H-HD mutant (solved to 2.0 Å) clearly shows the presence of the five-membered

imidazole ring of histidine, in place of the six membered phenyl ring of phenylalanine. This appears to be the only significant difference in the heme-binding region between the F393H mutant- and wild-type structures. Unfortunately, this does not help to explain how the presence of a histidine in place of a phenylalanine can so severely change the physical properties of the heme. No obvious conformational change is observed, and so the modification to the catalytic properties must be due to a more subtle, yet significant change in the protein superstructure or the way in which it interacts with the heme.

While inspection of the crystal structure does not immediately answer the question of how the reduction potential in the F393H mutant is being modulated, it does provide a structural context for discussion. The two dominant factors which influence reduction potentials in proteins are (a) the dielectric environment of the heme and (b) bonding interactions at, and to, the redox center (35). Both of these factors will be discussed in the context of the F393H mutant and in comparison with wild-type.

The study of the F393H mutant enzyme allows us to qualitatively evaluate how, or even if, changes in size, hydrophobicity, and electrostatics (due to the substitution of phenylalanine to histidine), affects the heme reduction potential. The Phe \rightarrow His substitution does not grossly increase the exposure of the heme to solvent, or dramatically change the hydrophobicity of the heme binding pocket. While the N δ 1 of the His393 is solvent exposed [formation of a His \cdots H₂O H-bond (Figure 4)], the steric bulk of the histidine residue is sufficient to prevent the penetration of water which would alter the dielectric environment at the iron, and hence the redox properties, of the heme. The crystal structure was determined at pH 6.5, a pH at which His may be expected to be partially protonated, with the resulting imidazolium interacting with Cys400. Redox titrations of both wild-type and the F393H mutant have been performed over a pH range 6–8 (data not shown) and neither show a significant (<15 mV) deviation from the value of the reduction potential determined at pH 7.0. Since the redox potential of the F393H mutant is not pH dependent, one must conclude that His393 remains in the same protonation state through the pH range 6–8. How the His-water hydrogen bond affects the pK_a of this residue is unquantifiable, but if, for example, it is dramatically increased (i.e., toward the pK_a of free imidazole, $pK_a = 9$), it is plausible that the residue would have mainly imidazolium character within the range pH 6–8. The presence of a positive charge so close to the heme-ligand would introduce a significant electrostatic interaction between His393 and Cys400. This increase in Lewis acidity would destabilize the Fe-S bond, probably by drawing electron density away from the iron and toward His393 and have the concomitant effect of lengthening, hence weakening, the Fe-S bond.

On the basis of structural evidence, there is little conformational difference in the heme binding region between the F393H mutant and wild-type. In fact, this region of the F393H mutant is the most well-defined (conformationally) stretch of polypeptide compared to wild-type. It seems unlikely that the substitution of phenylalanine by histidine would cause a large enough change in the hydrophobicity or dielectric environment of the heme to account for the dramatic differences observed in the reduction potentials. The

comparison of cytochrome *c* with the octapeptide (methionine) complex (formed by the hydrolysis of cytochrome *c*) is the classic study of how heme solvation and the change in the dielectric environment of the heme affects redox properties (36). Here a heme reduction potential shift of 300 mV is observed between the semiexposed, partially solvated heme of cytochrome *c*, with the fully exposed and solvated heme of the octapeptide (hence, the difference in solvation being substantial and influential). It is also interesting to note that the reduction potential in a series of F82 mutants of cytochrome *c* (a highly conserved phenylalanine in cytochrome *c*, in a similar environment to F393 in P450 BM3) shift only slightly (by 43 mV) upon substitution of phenylalanine by glycine (37). Previously, the minor redox potential changes of these cytochrome *c* Phe82 mutants had been rationalized by assuming the removal of the steric bulk of phenylalanine was compensated for by a refolding of the peptide. While this resulted in a change in the dielectric environment of the heme (increased the number of polar amide backbone groups in the hydrophobic heme pocket, due to the refolding), no overall increase in the degree of heme solvation was observed compared to wild-type cytochrome *c* (38, 39). The fact the F393H mutant involves such a slight steric substitution suggests that the changes in hydrophobicity and heme-exposure, would be minimal compared to wild-type P450 BM3.

Distortions to the heme-plane would cause perturbations in the energy levels of the porphyrin macrocycle, leading to modifications of the thermodynamic properties of heme. Residue 393 is within van der Waals contact of the heme plane, so any increase or decrease in steric bulk at this position would have an impact on the degree of this interaction. How this change would manifest itself is unclear, but it is conceivable that the energy levels in the porphyrin could be perturbed. Direct comparison of heme planes is difficult, as the degree of distortion depends highly upon the constraints placed on the heme during refinement of the structure. Neither heme looks particularly distorted with no significant difference in the *b*-factor of the hemes between the two structures.

More plausible reasons for the modification of the redox properties observed are the factors affecting the bonding interactions of the redox center. The iron–cysteine bond is central to the reactivity of P450s. It has been suggested that the cysteinate ligand provides a “push” effect, whereby the strong electron donating nature of the thiolate pushes electron density toward the heme iron. This increases the heme electronegativity (40, 41), facilitating the stabilization of high iron oxidation states, and also helping the heterolytic cleavage of the O₂ bond. Therefore, it is likely that factors affecting the nature of the Fe–S bond are likely to have significant implications on the P450 catalytic cycle. In nitric oxide synthases (NOSs), there is a highly conserved tryptophan residue six residues downstream of the cysteine ligand, which forms an intramolecular hydrogen-bond with the heme ligand (33). The formation of such a bond in the F393H mutant would have the effect of removing electron density from the Fe–S bond, reducing the ability of the thiolate to stabilize high oxidation states. Alternatively, this thiolate can be considered as being more highly tuned to stabilizing low oxidation states [e.g., nNOS, E_{1/2} = –239 mV (42)]. Wild-type P450 BM3 does not have the potential to form a

Phe393···Cys400 hydrogen-bond, yet the F393H mutant does. The F393H mutant has an elevated reduction potential, which equates to as a more stable ferrous-form. The question is whether this increase in the reduction potential is due to His393 forming an intramolecular hydrogen bond to the cysteine or not. Our results suggest this might not be the case, for three different reasons. First, the His393···Cys400 distance is too long (3.5 Å) for an efficient hydrogen bond. Second, a region of electron density is observed between Nδ1 of His393 and a solvent water molecule, indicative of a protein–solvent hydrogen-bond. This does not immediately preclude the presence of an intramolecular hydrogen-bond, as the nature of the His393···H₂O bond is dependent on whether His393 is acting as the hydrogen-donor or hydrogen-acceptor, a feature undeterminable at the resolution of the crystal structure. Third, it would appear that the available sulfur lone pair is pointing in an orientation unsuitable for efficient hydrogen-bonding geometry with respect to His393. Such a hydrogen bond, if formed, would be severely strained.

Porphyrin complexes with sulfur donors as axial ligands have been studied as a method of modeling features specific to P450s, such as control of their spin-state, reduction potential, and activity (43). For these types of complexes, the length of the ferric Fe–S bond is in excess of 2.3 Å and can be assumed as the equilibrium length of an Fe–S bond (44, 45). In P450cam and BM3, this distance is significantly shortened to 2.17 and 2.05 Å, respectively. It is clear that the protein superstructure in these P450s forces this distance to a nonequilibrium value, holding the sulfur closer to the iron. This is likely to be a key to P450 reactivity. The artificially short and strained (unfavorable interaction with pyrrole nitrogens of the porphyrin) Fe–S bond exaggerates the electron donating nature of the sulfur, increasing the electronegativity of the heme iron. In wild-type P450 BM3, Phe393 is sandwiched between Gln403 and Pro392 which prevents rotation of the phenyl ring. In the F393H structure, His393 adopts the same sandwiched orientation but is slightly tilted toward Cys400. As a result of this, the imidazole ring moves closer to Cys400 [distance of closest contact F393-(H393)···Cys400 = 3.67 Å (3.50 Å)]. The increased steric interaction between His393 and Cys400 could lengthen the Fe–S bond, causing a decrease in the electronegativity of the iron. A comparison of the substrate-free heme-domain crystal structures of wild-type and the F393H mutant may lend some support to this suggestion. The Fe–S distances of wild-type and the F393H mutant are 2.05 and 2.13 Å, respectively, suggesting a slight increase in the bond length induced by the substitution of phenylalanine by histidine. However, at the resolution to which these structures have been solved (2.0 Å), the difference in the Fe–S bond lengths falls within the error associated with each bond (±0.2 Å). Clearly, further investigation of this hypothesis is required before a formal conclusion can be drawn as to whether this increase in bond length is genuine. However, if it were, such a lengthening would account for the observed increased in redox potential.

CONCLUSION

The spectroscopic and structural comparison of wild-type and the F393H mutant of P450 BM3 has provided important information pertaining to the thermodynamic control exerted over the heme by phenylalanine 393. Our investigations have

shown that this control is achieved not by a gross conformational change in the heme binding region of the polypeptide. Rather, it arises as a consequence of a combination of a number of subtle, intimately linked factors. These include the close proximity of Phe393 to the heme porphyrin and to the cysteine ligand and their unavoidable interaction, its electrochemical neutrality, hydrophobicity, and ability to prevent exposure of the heme or the cysteine ligand to solvent.

ACKNOWLEDGMENT

Thanks is also due to Dr. S.N. Daff and L.J. Yellowlees for useful discussions and intellectual contributions.

REFERENCES

- Bower, S., Perkins, J. P., Yocum, R. R., Howitt, C. L., Rainham, P., and Pero, J. (1996) *J. Bacteriol.* 178, 4122–4130
- Chung, B.-C., Matteson, K. J., Voutilainen, R., Mohandas, T. K., and Miller, W. L. (1986) *Proc. Natl. Acad. Sci. U.S.A.* 83, 8962–8966
- Guengerich, F. P. (1995) Human Cytochrome P450 enzymes. In *Cytochrome P450: Structure, Mechanism and Biochemistry* (Ortiz de Montellano, P. R. O., Ed.) 2nd ed., pp 473–535, Plenum Press, New York.
- Chapman, S. K., Daff, S. N., and Munro, A. W. (1997) *Struct. Bonding* 88, 39–70.
- Shimizu, T., Hirano, K., Takahashi, M., Hatano, M., and Fujii-Kuriyama, Y. (1988) *Biochemistry* 27, 4138–4141.
- Sono, M., Roach, M. P., Coulter, E. D., and Dawson, J. H. (1996) *Chem. Rev.* 96, 2841–2887.
- Sono, M., Andersson, L. A., and Dawson, J. H. (1982) *J. Biol. Chem.* 257, 8308–8320.
- Miles, C. S., Ost, T. W. B., Noble, M. N., Munro, A. W., and Chapman, S. K. (2000) *Biochim. Biophys. Acta* 1543, 383–407.
- Gerber, N. C., and Sligar, S. G. (1994) *J. Biol. Chem.* 269, 4260–4266.
- Munro, A. W., Malarkey, K., McKnight, J., Thomson, A. J., Kelly, S. M., Price, N. C., Lindsay, J. G., Coggins, J. R., and Miles, J. S. (1994) *Biochem. J.* 303, 423–428.
- Ost, T. W. B., Miles, C. S., Munro, A. W., Murdoch, J., Reid, G. A., and Chapman, S. K. (2001) *Biochemistry* 40, 13421–13429.
- Song, W.-C., Funk, C. D., and Brash, A. R. (1993) *Proc. Natl. Acad. Sci. U.S.A.* 90, 8519–8523.
- Itoh, A., and Howe, G. A. (2001) *J. Biol. Chem.* 276, 3620–3627.
- Hara, S., Miyata, A., Yokoyama, C., Inoue, H., Brugger, R., Lottspiech, F., Ullrich, V., and Tanabe, T. (1994) *J. Biol. Chem.* 269, 19897–19903.
- Ohashi, K., Ruan, K.-H., Kulmacz, R. J., Wu, K. K., and Wang, L.-H. (1992) *J. Biol. Chem.* 267, 789–793.
- Miles, J. S., Munro, A. W., Rospendowski, B. N., Smith, W. E., McKnight, J., and Thompson, J. A. (1992) *Biochem. J.* 288, 503–509.
- Ravichandran, K. G., Boddupalli, S. S., Hasemann, C. A., Peterson, J. A., and Deisenhofer, J. (1993) *Science* 261, 731–736.
- Otwinowski, Z., and Minor, W. (1997) *Methods Enzymol.* 276, 307–326.
- Jones, T. A., Zou, J. Y., Cowan, S. W., and Kjeldgaard, M. (1991) *Acta Crystallogr., Sect. A* 47, 110–119.
- Sheldrick, G. M., and Schneider, T. R. (1997) *Methods Enzymol.* 277, 319–343.
- Ho, P. P., and Fulco, A. J. (1976) *Biochim. Biophys. Acta* 431, 249–256.
- Boddupalli, S. S., Estabrook, R. W., and Peterson, J. A. (1990) *J. Biol. Chem.* 265, 4233–4239.
- Williams, R. J. P. (1956) *Chem. Rev.* 5, 299–328.
- Cheesman, M. R., Greenwood, C., and Thomson, A. J. (1991) *Adv. Inorg. Chem.* 36, 201–255.
- Seward, H. S. (2000) Ph.D. Thesis, University of East Anglia.
- Gadsby, P. M. A., and Thomson, A. J. (1990) *J. Am. Chem. Soc.* 112, 5003–5011.
- Dawson, J. H., Andersson, L. A., and Sono, M. (1982) *J. Biol. Chem.* 257, 3606–3617.
- Berka, V., Palmer, G., Chen, P.-F., and Tsai, A. L. (1998) *Biochemistry* 37, 6136–6144.
- McKnight, J., Cheesman, M. R., Thomson, A. J., Miles, J. S., and Munro, A. W. (1993) *Eur. J. Biochem.* 213, 683–687.
- Salerno, J. C., Frey, C., McMillan, K., Williams, R. F., Masters, B. S. S., and Griffith, O. W. (1995) *J. Biol. Chem.* 270, 27423–27428.
- Tsai, A.-L., Berka, V., Chen, P.-F., and Plamer, G. (1996) *J. Biol. Chem.* 271, 32563–32571.
- Holm, L., and Sander, C. (1996) *Science*, 273, 595–602.
- Adak, S., Crooks, C., Wang, Q., Crane, B. R., Tainer, J. A., Getzoff, E. D., and Stuehr, D. J. (1999) *J. Biol. Chem.* 274, 26907–26911.
- Watt, G. D., Frankel, F. H. A., Al-Basheet, J., Al-Massad, F., Farrar, J., Greenwood, C., Thomson, A. J., and Moore, G. R. (1986) *Biochemistry* 85, 4330–4336.
- Moore, G. R., Pettigrew, G. W., and Rogers, N. K. (1986) *Proc. Natl. Acad. Sci. U.S.A.* 83, 4998–4999.
- Churg, A. K., and Warshel, A. (1986) *Biochemistry* 25, 1675–1681.
- Rafferty, S. P., Guillemette, J. G., Berghuis, A. M., Smith, M., Brayer, G. D., and Mauk, A. G. (1996) *Biochemistry* 35, 10784–10792.
- Louie, G. V., and Brayer, G. D. (1989) *J. Mol. Biol.* 209, 313–322.
- Rafferty, S. P., Pearce, L. L., Braker, P. D., Guillemette, J. G., Kay, C. M., Smith, M., and Mauk, A. G. (1990) *Biochemistry* 29, 9365–9369.
- Crane, B. R., Arvai, A. S., Gachhui, R., Wu, C., Ghosh, D. K., Getzoff, E. D., Stuehr, D. J., and Tainer, J. A. (1997) *Science* 278, 425–431.
- Ghosh, D. K., Wu, C., Pitters, E., Moloney, M., Werner, E. R., Mayer, B., and Stuehr, D. J. (1997) *Biochemistry* 36, 10609–10619.
- Presta, A., Weber-Main, A. M., Stankovich, M. T., and Stuehr, D. J. (1998) *J. Am. Chem. Soc.* 120, 9460–9465.
- Tani, F., Matsu-ura, M., Nakayama, S., Ichimura, M., Nakamura, N., and Naruta, Y. (2001) *J. Am. Chem. Soc.* 123, 1133–1142.
- Hahn, J. E., Hodgson, K. O., Andersson, L. A., and Dawson, J. H. (1982) *J. Biol. Chem.* 257, 10934–10941.
- Schappacher, M., Ricard, L., Fischer, J., Weiss, R., Bill, E., Montiel-Montoya, R., Winkler, H., and Trautwein, A. X. (1987) *Eur. J. Biochem.* 168, 419–429.
- Roussel, A., and Cambillau, C. (1991) *Silicon Graphics Geometry Partners Dictionary* 86, Silicon Graphics, Mountain View, CA.

BI010717E